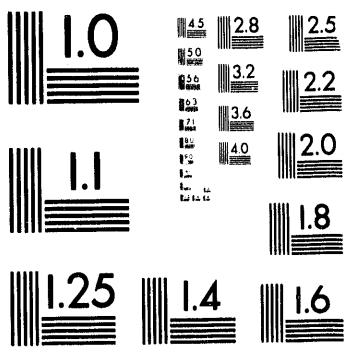
1.0
1.1
1.25
1.4
1.6
1.8
2.0
2.2
2.5
2.8
3.2
3.6
4.0
4.5
5.0
5.6
6.3
7.1

1 of 3

APPENDIX 1

ADVANCED PARTICLE FILTER

Technical Progress Report No. 11
January through March 1993

Prepared by

Westinghouse Science and Technology Center
Pittsburgh, Pennsylvania

For

American Electric Power Service Corporation
Columbus, Ohio

AEPSC Contract No. C8014

TIDD ADVANCED PARTICLE FILTER

1.0 RETROFIT WORK

1.1 APF Vessel Head

Numerous vendor visits were made during January 1993 to verify APF vessel head retrofit work. The stainless steel liner was removed and modified to eliminate subsequent thermal distortion which could induce a flow path for hot gas suspected of causing a local hot spot on the carbon steel dome. All insulation was removed from the dome interior, all acid liner (Plasite), was removed by sandblasting, Plasite was reapplied and Z-blok insulation was reinstalled.

Holes for back pulse pipe feedthrough in the stainless steel dome liner had previously been sealed by stainless steel collars tack welded in place. Lateral thermal expansion of the liner relative to the fixed back pulse pipes caused distortion of the collars and breaking of their tack welds (See Figure 1). A floating collar was designed that did not require tack welds (See Figure 2). These collars were fabricated and reinstalled with the dome liner. The assembled dome has been returned to site.

1.2 APF Internals

Distortion was noted in stainless steel liner plates covering insulation beneath the tubesheet. All covers were removed, flattened, cut to prevent thermal impingement, stiffened with radial ribs, and reconfigured with lap joints to accommodate thermal expansion. The liners have been reinstalled (See Figure 3).

Thorough inspection of all candle filters has been completed and is documented separately in the report attached. Ash was cleaned from all internal components, and candle filters have been replaced in all three bottom plenums. An improved top gasket and filter holder ring has been designed and procured to reduce the potential for gasket slippage during back pulsing (See Figure 4). Installation of this hardware is scheduled for May 1993.

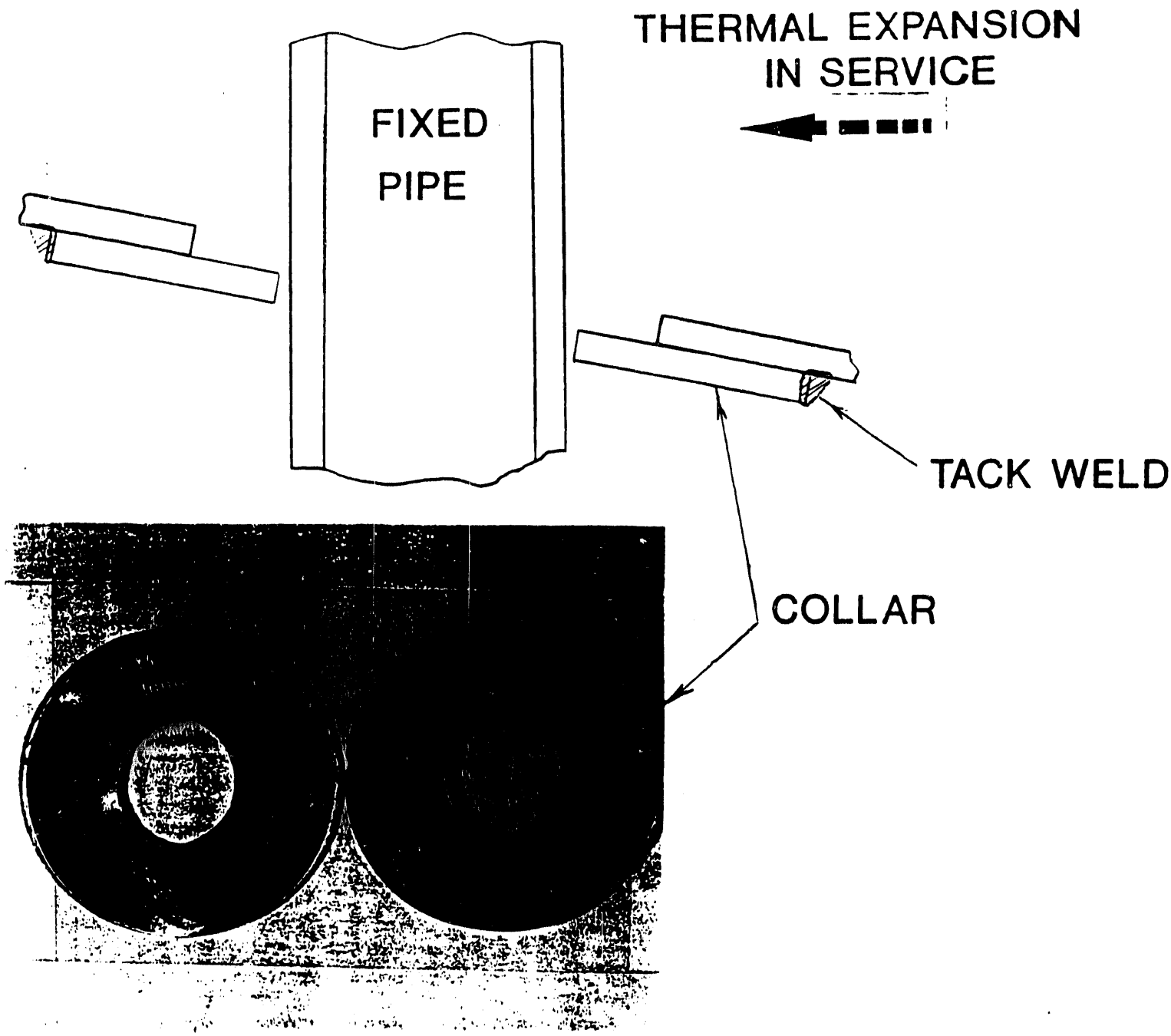

Figure 1 - Breakage of Collar Tack Welds Due to Thermal Expansion

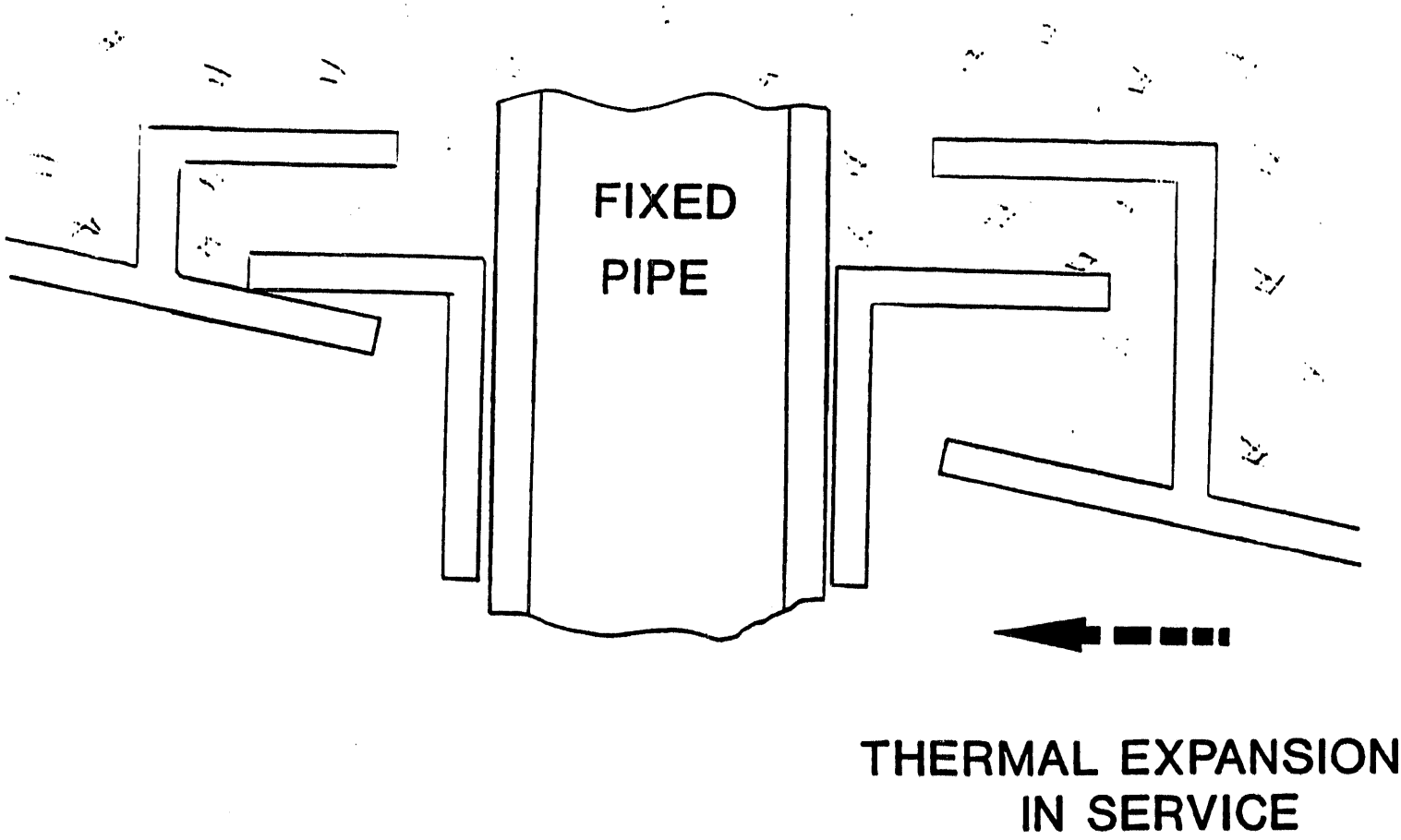

Figure 2 - Floating Collar Design to Accommodate Thermal Expansion

Enhancement of ash discharge from the conical APF vessel bottom has been studied. A liner vibration device has been identified that can be installed in the vessel manway.

1.2.1 Vibrator Test

A pneumatic vibrator has been tested inside the APF manway in an attempt to aide ash flow during operation. A vibrator, manufactured by the Cleveland Vibrator Company, was bolted to a 1 inch thick steel bar which was clamped to the liner inside the manway. The design operating pressure range for this vibrator is 20 to 80 psig. The test was successful in producing vibration at the ash outlet. The test data is as follows:

Air Pressure to Vibrator, psig	Vibration Acceleration on the Liner at the ash outlet, g
30	1.8
40	3.6
50	5.0
60	6.0
70	7.3
80	7.3

After the above data was measured, the clamps securing the bar/vibrator assembly to the liner were tightened and an 8.7 g vibration was measured with a 70 psig air supply to the vibrator. Work on a permanent installation of the vibrator inside the manway is underway.

1.2.2 Vibrator Air Supply/Exhaust Hose Test

A pressure test was performed on a Swagelok, 0.5 inch ID, 48 inch long TFE lined 304 SST braided hose by pressurizing the outside of the hose to 200 psig while maintaining the internal pressure at one atmosphere. A schematic and photograph of the

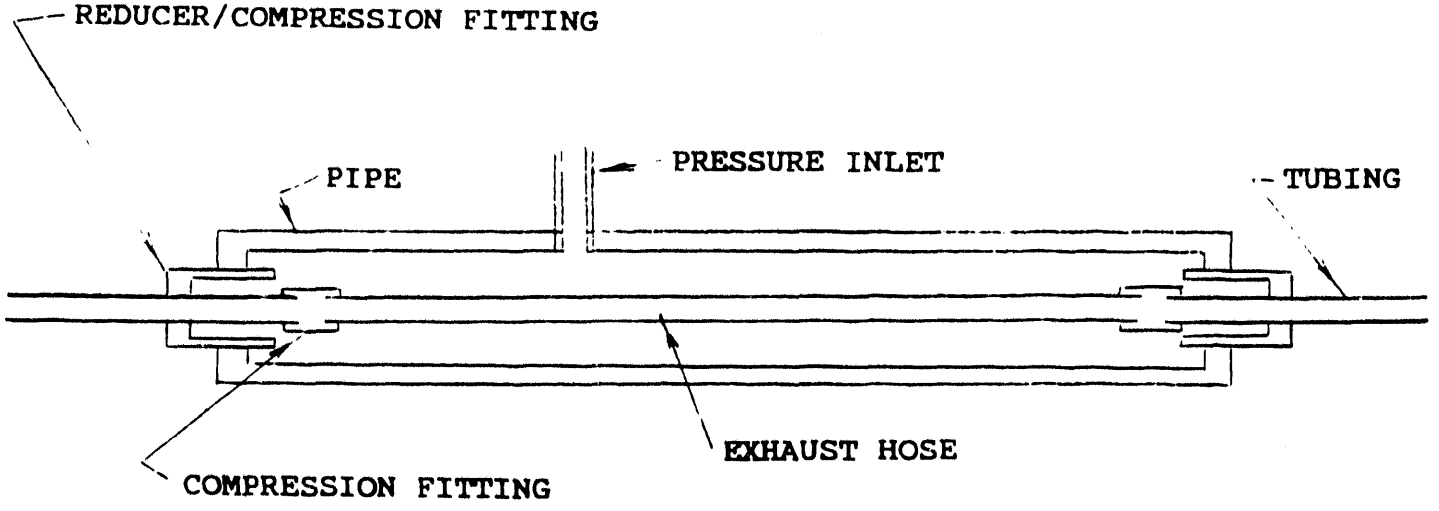

Figure 5 - Schematic Illustration and Photograph of Exhaust Hose Pressure Test

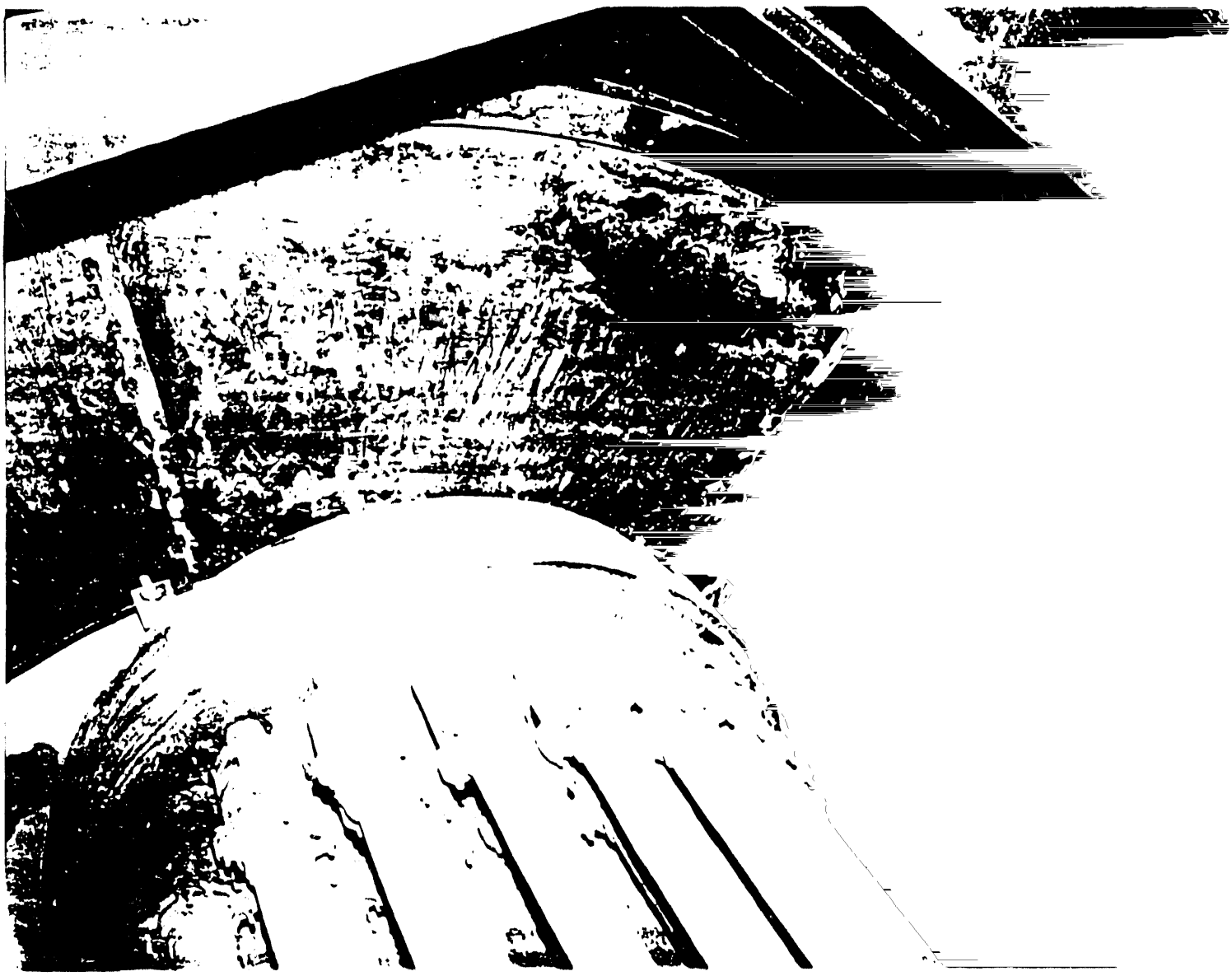

Figure 3 - View of Insulation Liner Plates After Straightening, Lap Joint Modification and Reinstallation

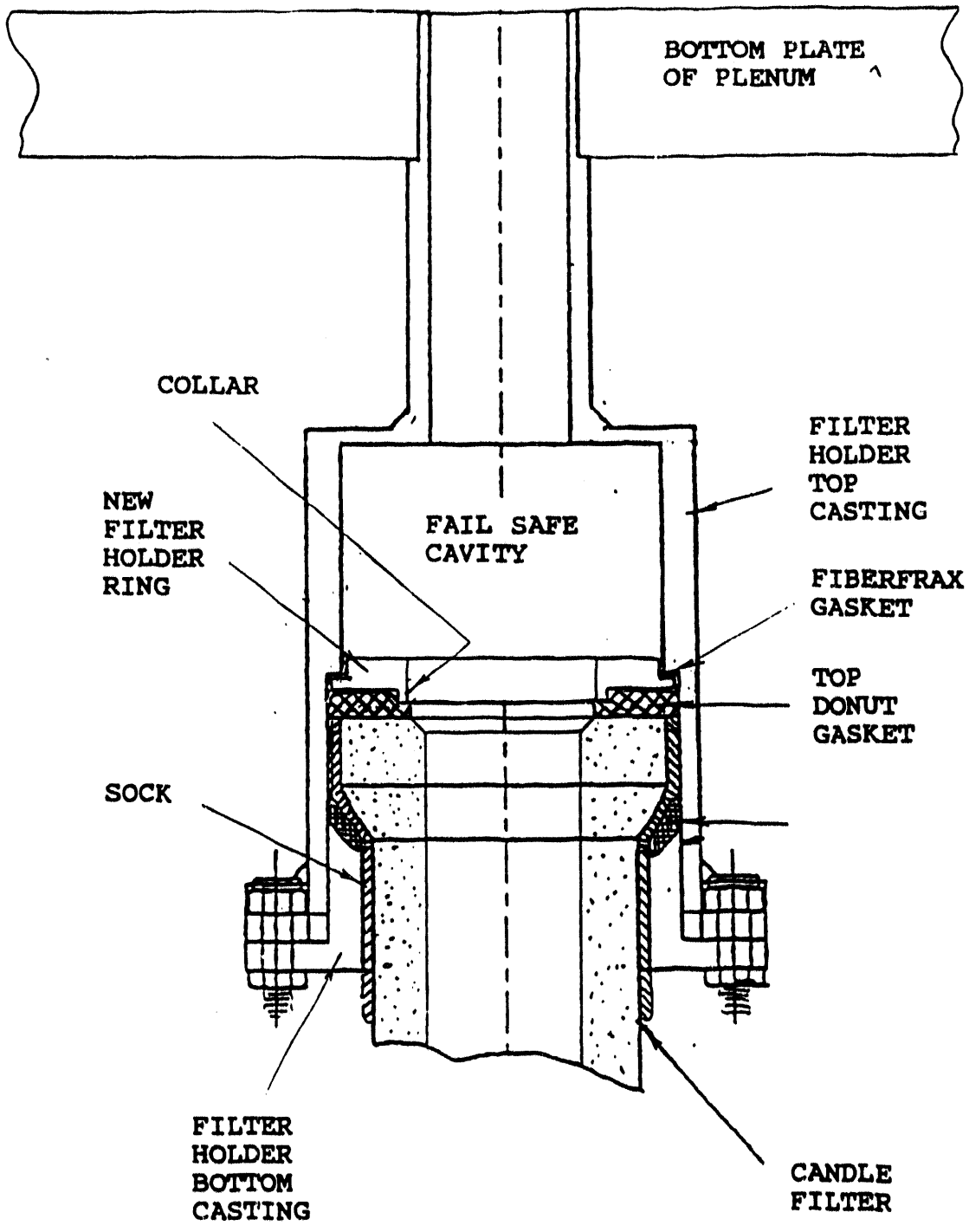

Figure 4 - Modified Filter Holder Ring with Gasket Containment Collar - Shown Installed

experimental arrangement is shown in Figure 5. Visual examination through the bore of this assembly confirmed that the hose maintained its shape. Two identical hoses will be used to supply and exhaust air to the pneumatic vibrator inside the Tidd APF manway. The capability to withstand external pressure is necessary when the APF vessel is pressurized to 150 psig and the air supply to the vibrator is shut off.

Liner brackets for the vibration device have been fabricated. Design details for the vibrator attachment are under review by AEP. Installation is scheduled for May/June 1993.

1.3 Back Pulse Control

Extended flexibility of back pulse control has been recommended to and is being implemented by site personnel. Improved capabilities include pulse sequence logic and broadened ranges of permissives.

Back pulse valve and pressure regulator manufacturers have provided hardware design improvements. Components have been retrofitted and site personnel are currently installing the improved components.

1.4 Pulse Air Supply

The pulse air supply compressor has been repaired and corrected with improved lubrication hardware and improved discharge valving. A performance test has been conducted. AEP is making provision for backup pulse air supply at the time of APF system restart.

2.0 SURVEILLANCE INSPECTION AND TESTING

2.1 Pulse Pipe Inspection

The nine Incoloy 800 HT back pulse pipes were 100% dye penetrant inspected on their outside surface at site and prior to installation in the head of the APF. No relevant indications were detected.

Following shutdown in December 1992, after 500 hours of filter operation, one of these pipes was removed and returned to Westinghouse STC for inspection. Dye penetrant inspection was attempted but was assessed to be inconclusive due to significant background bleed out from oxides which coated both outside and inside surfaces of the pipe. Alternatively, thru-pipe radiography was performed on the bottom-most 16 inches of the pipe. Two x-ray exposures were taken at 90 degrees to one another. No relevant indications were detected. This limited sample check of back pulse pipe integrity suggests that the Incoloy 800 HT pipe is performing satisfactorily for the service exposure thus far accumulated.

2.2 Weldability Test

AEP expressed a need to check design and to retrofit as required the cluster assemblies such that they would function for tubesheet differential pressures of 10 psi. Finite element stress analysis was performed and concluded that reinforcement of the bottom plates of the bottom plenums would be appropriate to satisfy performance requirements. Reinforcing bars and weldments depicted in Figure 6 were designed to fit across two major chords of each of the three bottom plenums (6 bars total).

The material of construction for the cluster assemblies, type 310 S stainless steel, is known to progressively embrittle due to sigma phase formation upon prolonged exposure at elevated temperatures that are typical for APF service. It was

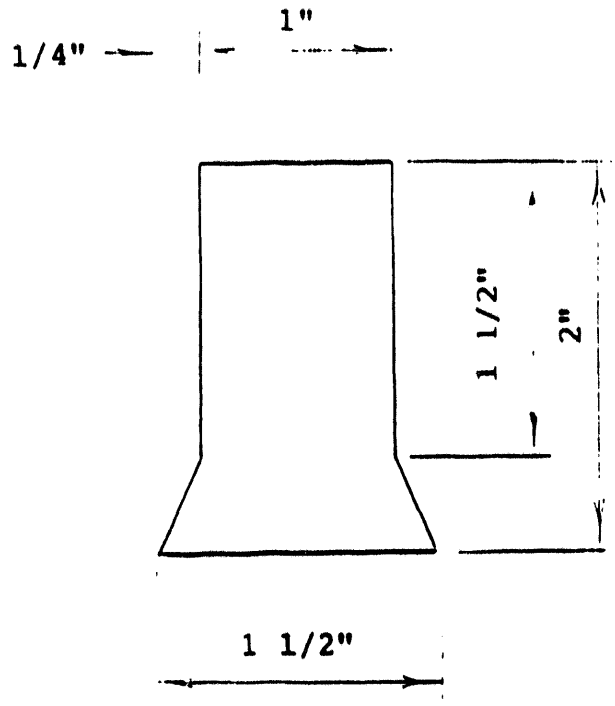

Figure 6 - Reinforcing Bar Configuration

therefore considered appropriate to weldability test a sample of type 310 S surveillance material (that had been stored in the vessel head) prior to weld installation of reinforcing bars on the bottom plenums.

Weld restraint is known to influence weldability of embrittled materials. Base metal thickness affects weld restraint. The surveillance sample was of 1/2-inch section thickness. The bottom plenum's bottom plate is of 1-9/16 inch section thickness. For the weldability test, simulation of the plenum plate restraint was achieved by prewelding the relatively thin surveillance sample to a heavy section backing plate.

A T-joint configuration was then welded to simulate the reinforcing bar to plenum plate configuration as shown in Figure 7. Type E310-15 electrode was used to shielded metal arc weld an unexposed sample of 310 S material to the 310 S surveillance sample. A cross section of the weldability test sample, shown in Figure 8, revealed no evidence of heat affected zone cracking due to possible sigma phase embrittlement.

The centerline of the surveillance sample showed some evidence of lamellar tearing. This indication is attributable to the severe restraint imposed on this sample by the test configuration. It is possible that similar tearing could occur in the cluster plate material, if it contained elongated segregations in similar proximity to the material surface. However, no evidence of lamellar tearing was encountered during cluster fabrication which involved many heavy section structural welds. Therefore, the probability of such lamellar tearing during reinforcement bar attachment was projected to be small.

Welding of the reinforcing bars to plenum plates was conducted at site without evidence of visually detectable defects (See Figure 9). Additional type 310 S surveillance material will be secured in the APF vessel head to continue monitoring property changes in this material.

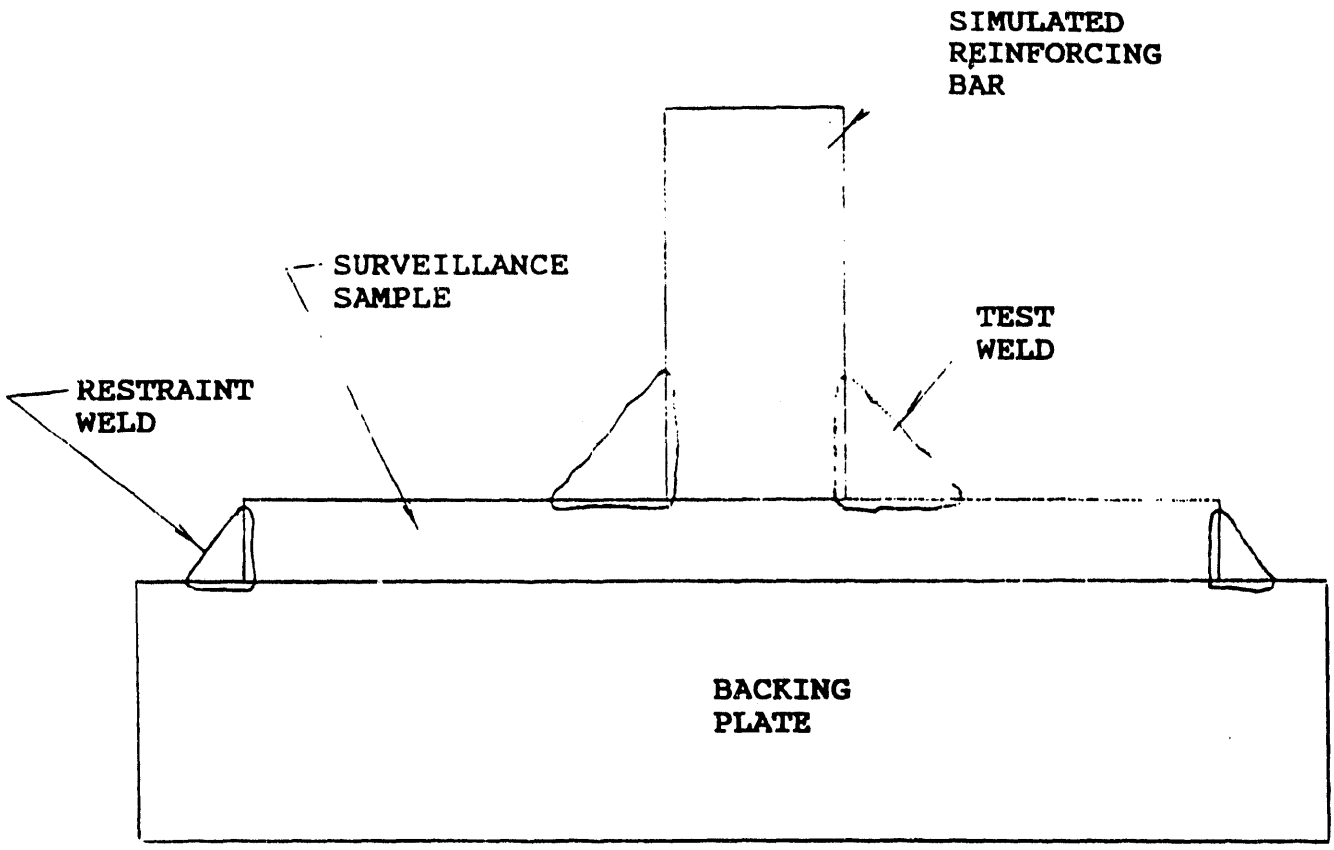

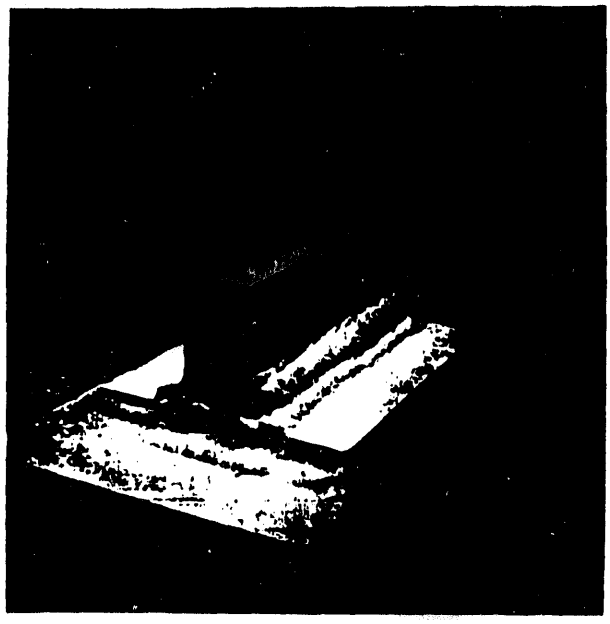

Figure 7 - T-Joint Configuration Prepared to Test Weldability of Plenum Plate Material

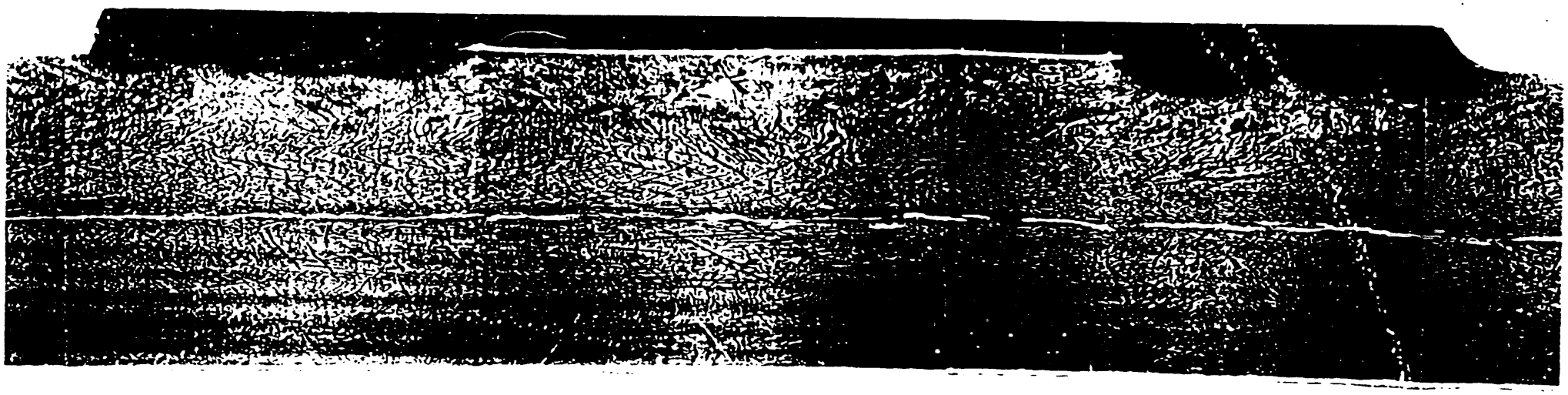

Figure 8 - Cross Section of T-Joint Test Weld

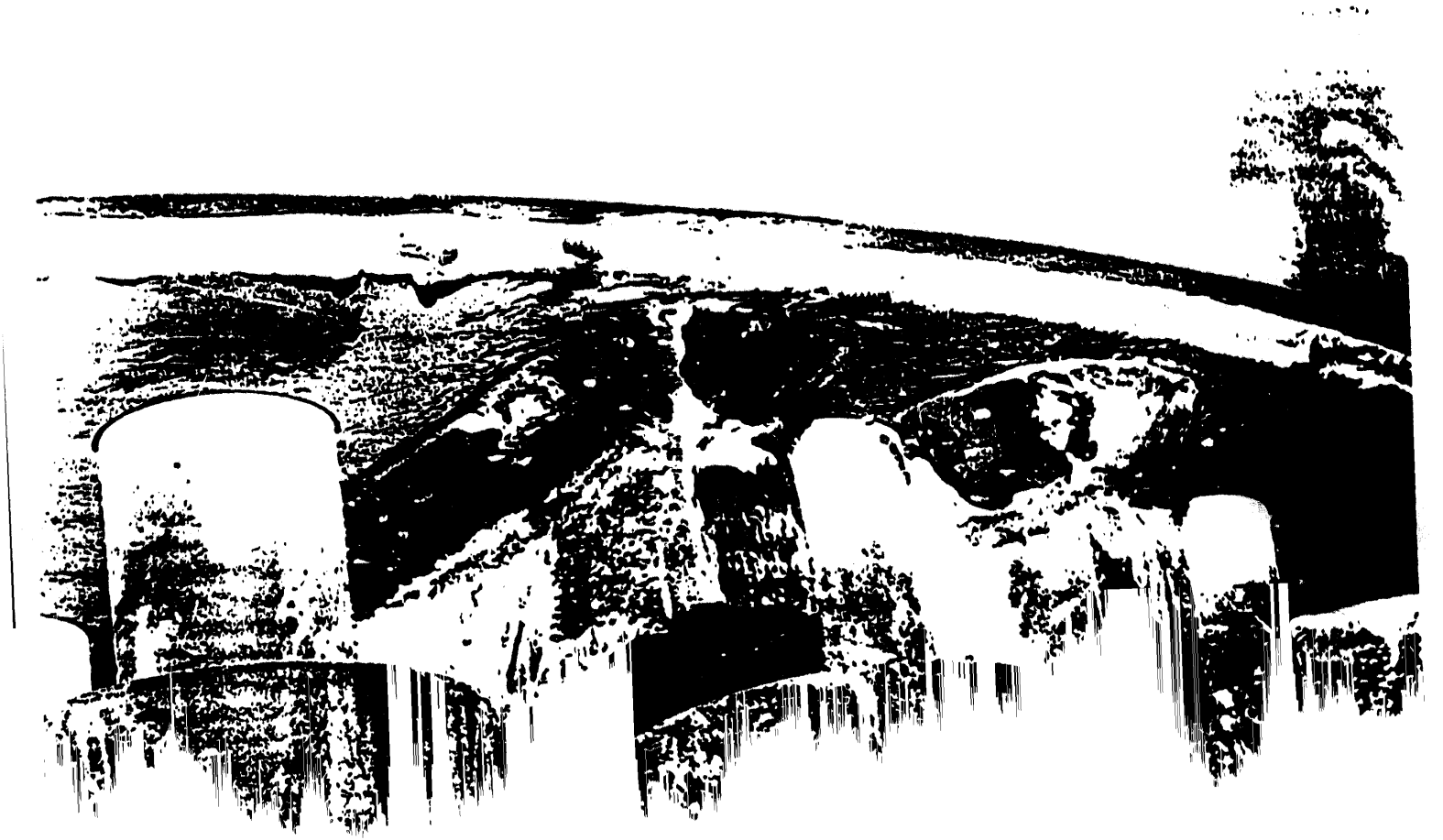

KARHULA PARTICLE FILTER TESTING

1.0 INTRODUCTION

A report of Karhula particle filter testing covering December '92 thru February '93 has been submitted previously. The present report summarizes difficulties encountered in the CHUBU test run during March 1993. Preliminary results of a late March/early April inspection are also included.

2.0 SCOPE OF TEST RUN AND DUST OUTPUT

Two coals - Newland and Kentucky, and three load levels - 50, 75 and 100%, were run during this test period. Figure 1 shows the flue gas dust concentration in milligrams per normal cubic meter that was encountered during the test. It is evident that dust levels generally increased as the test progressed.

3.0 PRELIMINARY PERFORMANCE EVALUATION

Preliminary evaluation of filter performance statistics included accumulator tank pulse cycle pressure drop, pulse intensities, filter differential pressure, temperatures, and venturi flows. Two events are noteworthy. First, during the transition from Newland coal to Kentucky coal on March 12 thru March 13, 1993, mixing problems were encountered and rapid temperature transients resulted from unstable combustion. This is shown in Figure 2. Transients of approximately 40 ° C per minute were encountered. Flue gas dust concentration increased from 16 to 40 mg/m3n over this period. Second, increase in top plenum flow relative to middle and bottom plenum flows occurred approximately 8:15 a.m. on March 17, 1993. This is shown in Figure 3. Relatively high dust concentrations were also measured subsequent to this occurrence.
(Ref. Figure 1).

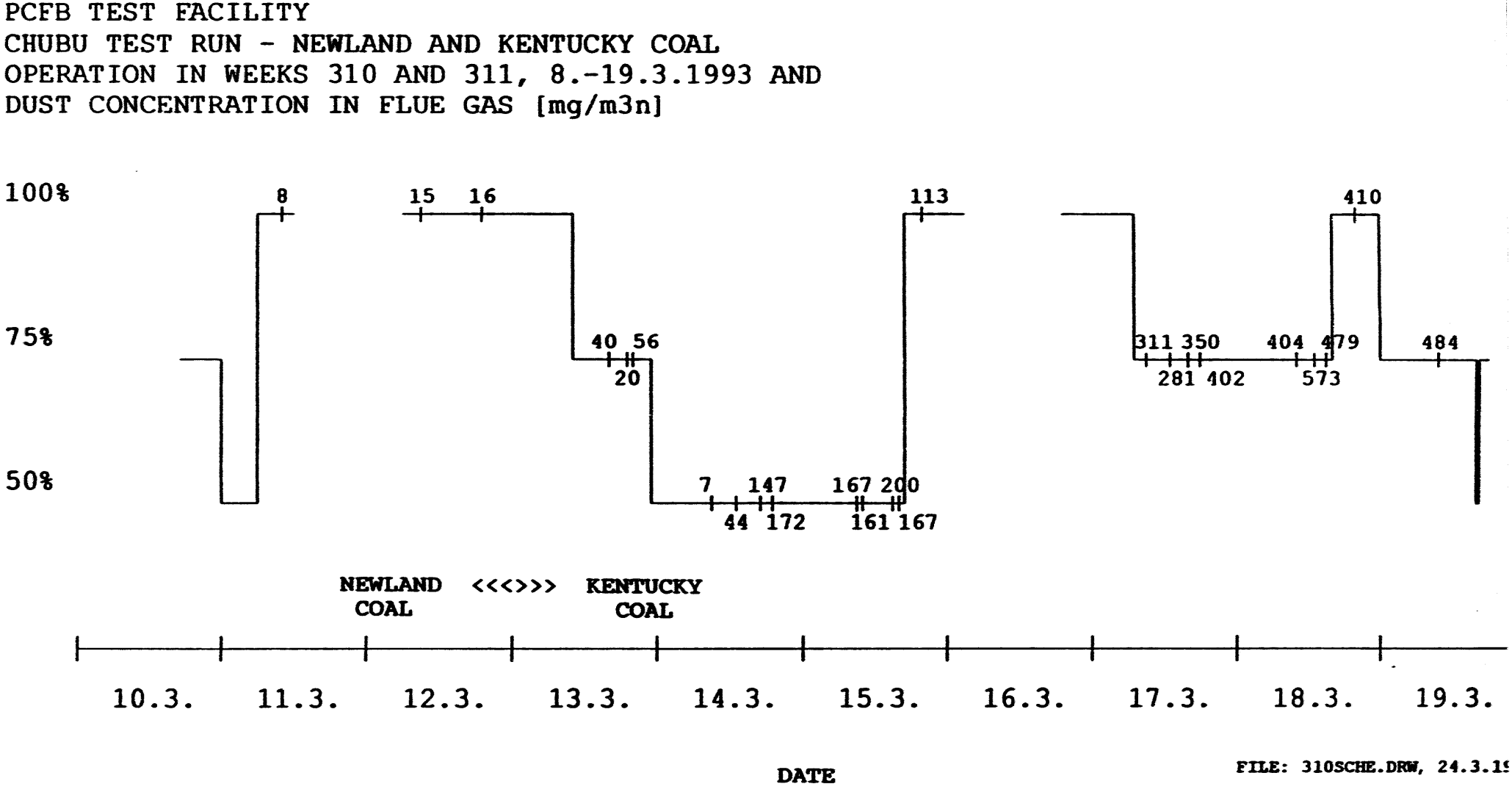

Figure 1 - Flue Gas Dust Concentration on Load Versus Date Plot (Data from Ahlstrom)

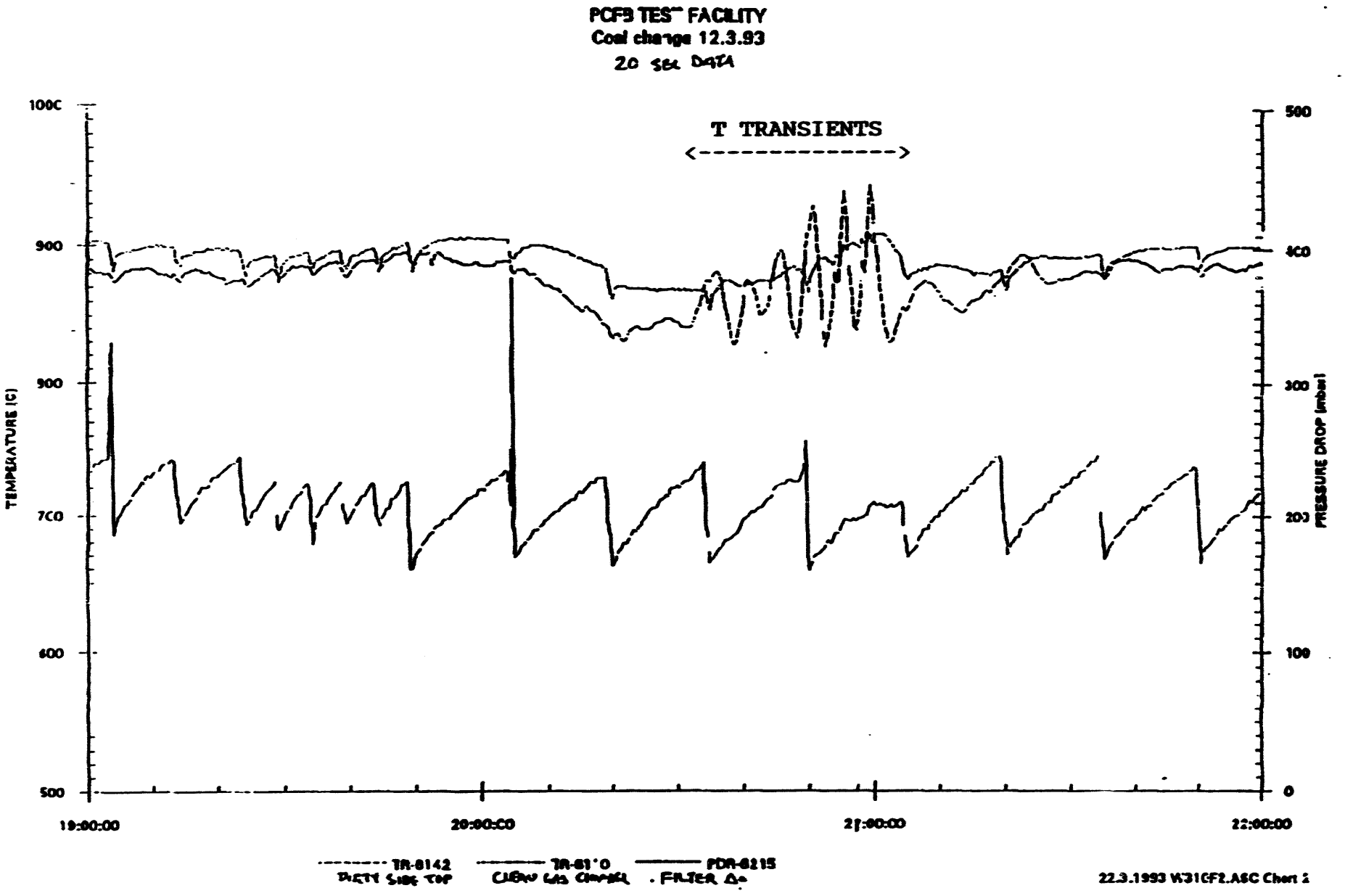

Figure 2 - Transients in Dirty Side Top Temperature Encountered During Change in Coals (Data from Ahlstrom)

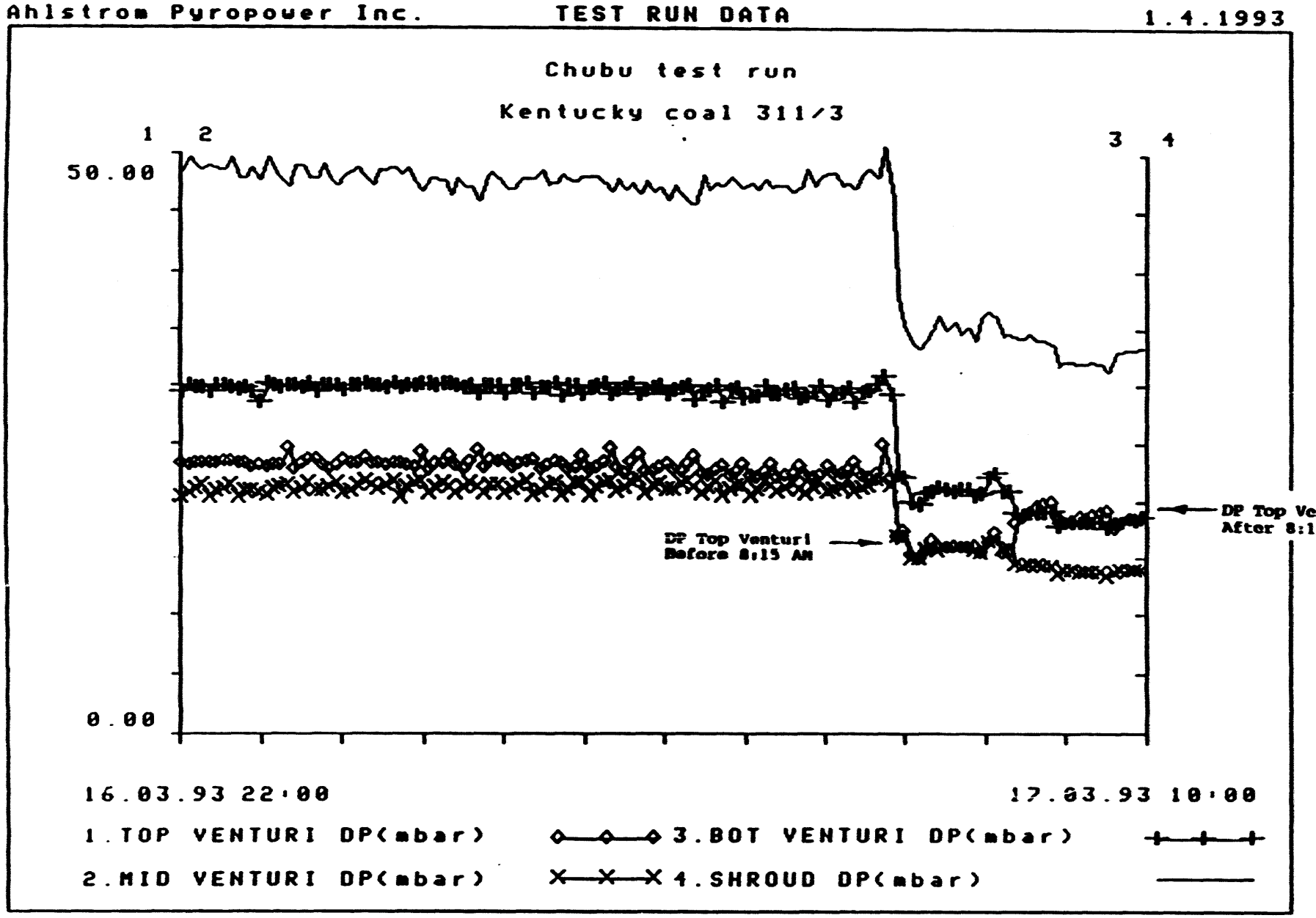

Figure 3 - Abrupt Change in Top Venturi Differential Pressure (Data from Ahlstrom)

4.0 PRELIMINARY INSPECTION

Post shutdown inspection revealed 8 broken top plenum filter elements. Dismantling of internals subsequently resulted in breakage of 15 additional top plenum filter elements. No middle or bottom plenum candles were broken prior to or during disassembly.

Predisassembly inspection revealed:

(P1) top plenum outer row candles were displaced radially outward
(P2) top plenum inner row candles were relatively plumb
(P3) top plenum ash bridging was evident between candles and between center support tube and inner row candles.
(P4) middle plenum candles were relatively plumb
(P5) middle plenum ash bridging was not evident
(P6) bottom plenum candles were not all plumb
(P7) bottom plenum ash bridging occurred in some areas
(P8) all candles showed considerable ash cake buildup

Candle filter disassembly revealed:

(D1) top plenum candles were loosely secured
(D2) middle plenum candles were rigidly secured
(D3) bottom plenum candles were rigidly secured

Candle filter fracture surface inspection revealed:

(F1) eight fracture surfaces were relatively dirty with ash
(F2) fracture orientations were primarily transverse to the candle axis
(F3) 22 out of 23 candles were broken within approximately 4 inches of the upper flange of the filter elements
(F4) 15 out of 23 candles showed a break somewhat angled to the candle axis
(F5) the low/high point of 14 angled breaks was oriented in line with a radius thru the candle/cluster center lines (See Figure 4)

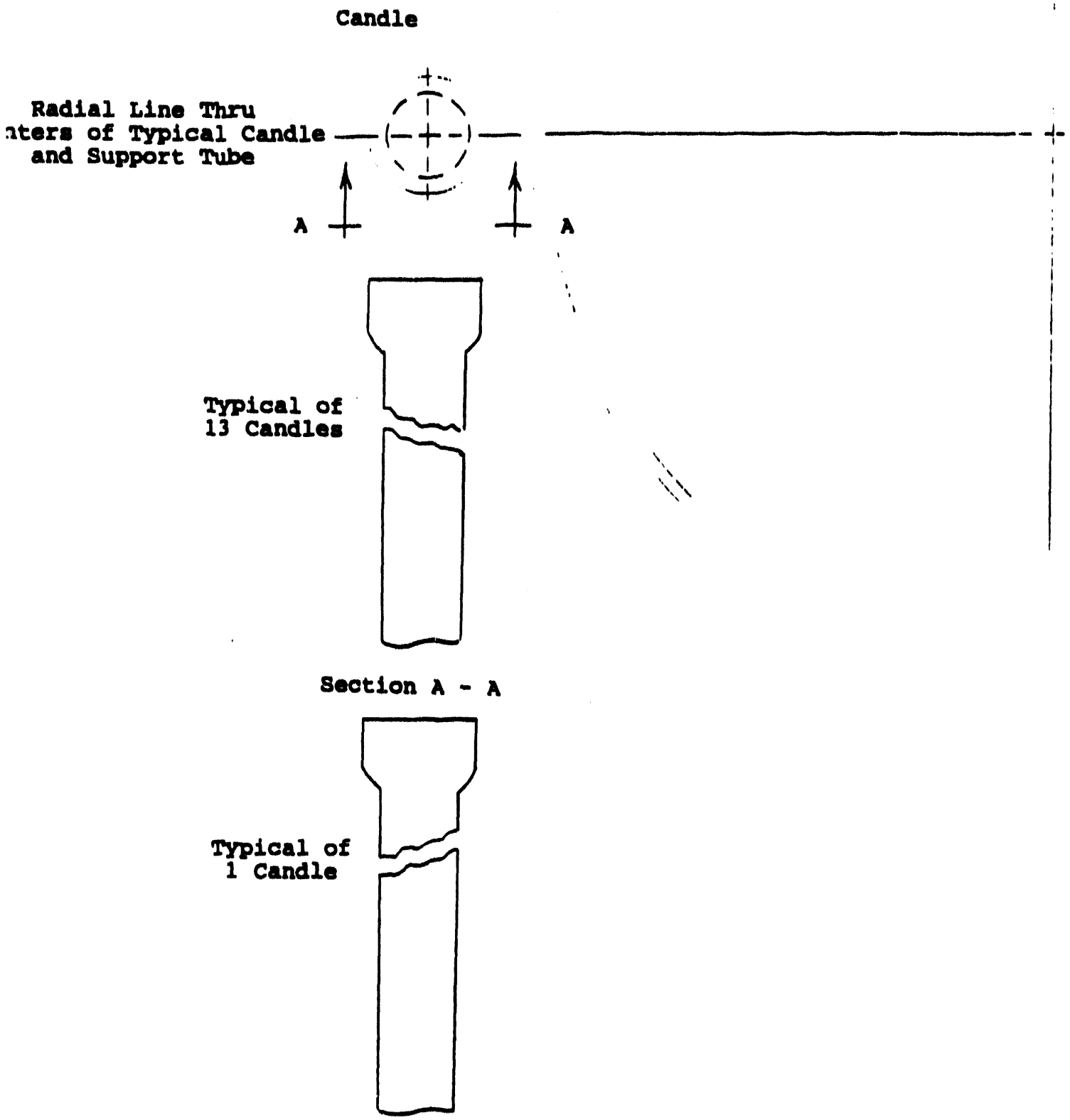

Figure 4 - Orientation of Plane of Fracture Surface with Respect to Candle/Support Tube Radial Line

Candle filter gasket inspection revealed:

(G1) bottom gaskets were generally clean on all surfaces

(G2) top gaskets were

(G2.1) virtually all clean on their bottoms (candle sides)

(G2.2) sometimes dirty on their tops (filter holder ring sides)

(G3) gaskets were generally centered, intact and in place

Miscellaneous findings include:

(M1) filter holder bolts were not elongated prior to disassembly

(M2) filter holder nuts were not unthreaded prior to disassembly

5.0 DISCUSSION

The transverse orientation of fractures (ref. F2) suggests a mechanical rather than thermal source of candle damage. Radially outward displacement of top plenum candles (ref. P1) and radial orientation of many fracture surfaces (ref. F5) suggest radial outward loading as the cause of mechanical damage. One possible breakage scenario could be the following:

> Flow/vibration-induced candle displacement loosened candles, gasket dust leakage and insufficient pulse cleaning resulted, ash cake continued to build until bridging occurred to the nearest-neighbor adjacent material component (candle or support tube) and continued vibration promoted further displacement away from solid bridges (radial) until bending stresses near filter holder constraints (ref. F3) exceeded candle strength.

While other explanations may be forthcoming (eg. inherently difficult to clean ash, gasket relaxation, etc.) it was deemed prudent to take certain corrective or preventive measures at this time and before further filter testing. Modifications currently in process include:

(1) Replacement of all top gaskets
(2) Replacement of all filter holder rings with a built-in gasket containment collar
(3) Inclusion of solid spacers between filter holder bottom castings and main filter holder housings to rigidize the assembly
(4) Elimination (blanking off) of the top plenum inner row candle locations (15) to eliminate nearest-neighbor bridge points
(5) Inclusion of regenerator (heat exchanger) devices in each filter holder housing to minimize possible back pulse-induced thermal stress effects

Reassembly is ongoing. Resumption of filter testing at Karhula is scheduled to begin May 3, 1993.

DOE/MC/26042--3449

PFBC HGCU Test Facility
Technical Progress Report

First Quarter, CY 1993

DISCLAIMER

Prepared by:

American Electric Power Service Corporation
Columbus, Ohio 43215

Prepared for:

The United States Department of Energy
Under DOE Instrument No. DE-FC21 89MC-26042

April, 1993

I. INTRODUCTION

This is the fourteenth Technical Progress Report submitted to the Department of Energy (DOE) in connection with the cooperative agreement between the DOE and Ohio Power Company for the Tidd PFBC Hot Gas Clean Up Test Facility. This report covers the period of work completed during the First Quarter of CY 1993.

On February 9, 1993, the Tidd gas turbine sustained severe damage due to a thrown turbine blade. The Tidd PFBC Plant and HGCU system are now expected to return to service in July or August 1993. The extended outage is a result of long lead replacement parts for the gas turbine.

II. WORK ACCOMPLISHED DURING THE REPORTING PERIOD

2.1 Detailed Design-Engineering

The laboratory analysis of the expansion joint bellows which developed a leak in the inner ply confirmed that the leak was due to acid dew point corrosion. Even Hastelloy C22 cannot withstand this type of corrosion. Consequently, it was decided to heat trace and insulate all expansion joint bellows. Considerable engineering effort was spent optimizing the design and selecting the best materials. A sketch of the design is attached, Figure 1. In order to monitor the bellows for possible hot spots, continuous thermocouple line detectors will be wrapped around each bellows. Additional thermocouples will be used for controlling the heating elements. All materials were purchased this quarter and will be installed prior to the next start-up.

In order to reduce the likelihood of ash accumulating in the APF hopper, a vibrator will be installed before the next start-up. The vibrator will be powered by compressed air and be installed in the hopper manway nozzle (See Figure 2). It will be mechanically linked to the hopper liner and used only during backpulsing.

Preliminary testing performed using the vibrator at Tidd on February 9, 1993, revealed that the vibrator should be effective in keeping ash from sticking to the hopper walls.

A method of detuning the primary cyclone upstream of the APF was devised. The method involves injecting air from the sorbent system upwards into the cyclone dip leg, thereby reducing the cyclone efficiency. The purpose of cyclone detuning is to increase dust loading and the proportion of larger dust particles to the APF in order to improve filter cleaning and/or ash removal and transport, should either become necessary. An analysis was performed to determine the proper air line size to obtain the required air velocity in the cyclone. The system will include a manual globe valve and flow metering orifice outside the combustor to allow the detuning air flow to be adjusted or shut off. The system will be installed prior to the next start-up.

2.3 Westinghouse Engineering & Design

See Appendix 1. NOTE: The Westinghouse report on the candle filter analysis referred to on Page 1 of Appendix 1 will be forwarded as soon as it is received.

3.0 Test Plan

In the Fourth Quarter of 1992, the Cooperative Agreement was amended to include testing of the Tidd HGCU System for Hazardous Air Pollutants (HAP). During the First Quarter of 1993, proposals were received from four vendors for implementing this testing. The proposals were reviewed by DOE, and are currently being evaluated by AEPSC. A contract should be awarded during the Second Quarter of 1993.

III. MANPOWER REPORT AND COST DATA

As of March 31, 1993, the AEPSC Engineering, Design and Project Support cumulative work-hours were 63,299 or 91.6% of the total 69,097 revised work-hours projected for the project. Figure 3 compares the actual work-hours expended versus the current estimate. For the reporting period, a total of 2,565 hours were charged to the project by AEPSC personnel.

The actual DOE's cost expenditures during the First Quarter 1993 were $780,122. As of March 31, 1993, the cumulative DOE's cost expenditures were $15,047,001. Figure 4 depicts the cumulative expenditure forecast for the project which includes Westinghouse cost share. During the First Quarter 1993, Westinghouse was paid a total of $52,006. Total payments to Westinghouse through March 31, 1993 were $5,261,602. Major contractual commitments during this reporting period totalled $204,400 and are summarized as follows:

Contract/ Purchase Order	Description (Contractor)	Contracted Costs
28041-071-3	Backup Compressors for HGCU Backpulse Compressor (Air Power of Ohio Co.)	$150,000
03341-071-3	Recorders for Expansion Joint Heaters (Westronics)	$ 14,900
28058-071-3	Expansion Joint Heaters (Big Chief Supply, Inc.)	$ 25,700
28223-071-3	Continuous Thermocouples and Lead Wire for Expansion Joint Heat Tracing (High Tech Systems)	$ 13,800
	TOTAL	$204,400

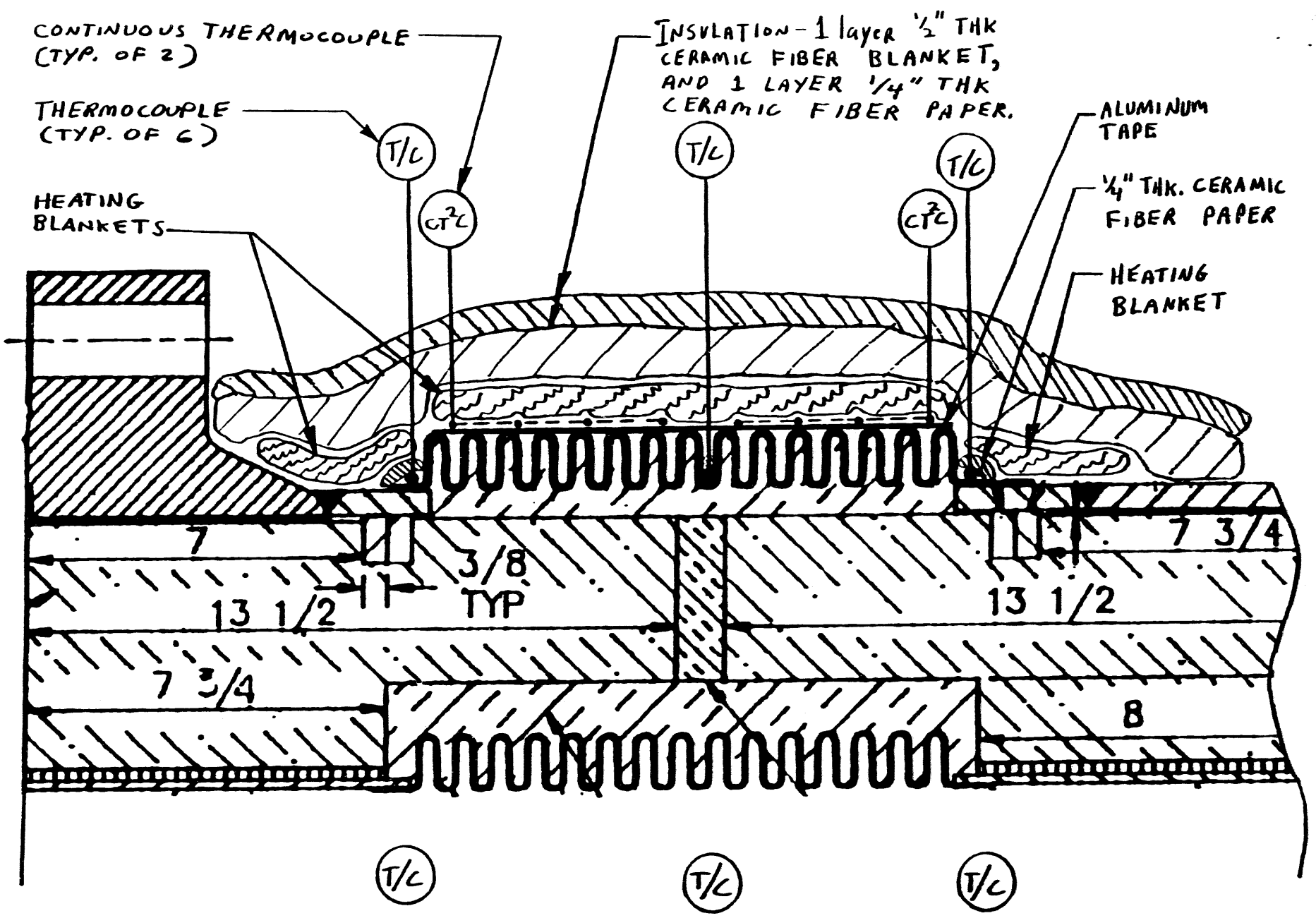

FIGURE 1

TYPICAL EXPANSION JOINT HEAT TRACING ARRANGEMENT

Figure 3

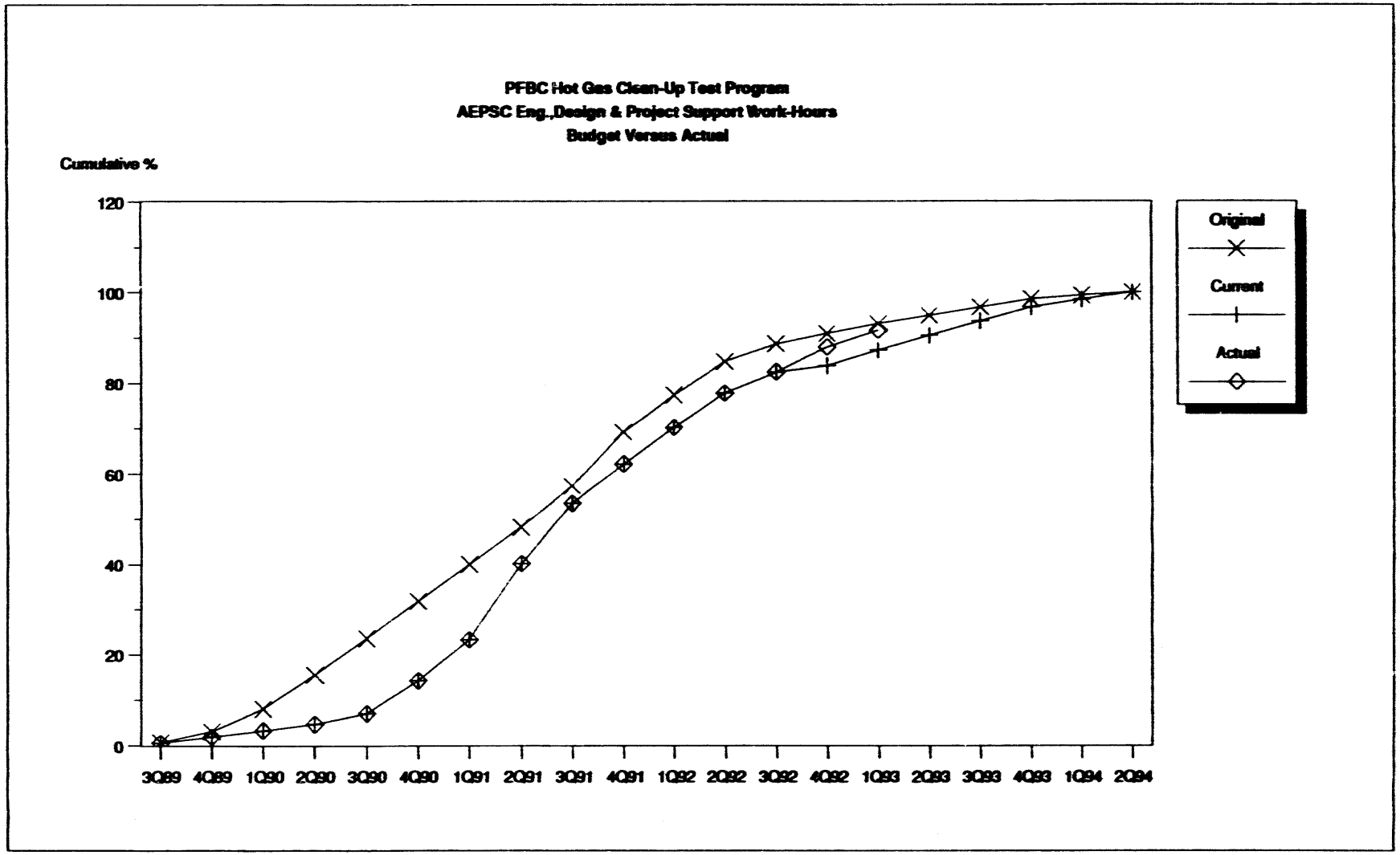

	3Q89	4Q89	1Q90	2Q90	3Q90	4Q90	1Q91	2Q91	3Q91	4Q91	1Q92	2Q92	3Q92	4Q92	1Q93	2Q93	3Q93	4Q93	1Q94	2Q94
Original	0.8	3.2	8.1	15.6	23.6	31.8	40.0	48.2	57.3	69.2	77.4	84.7	88.6	90.9	93.1	94.9	96.7	98.6	99.3	100.0
Current	0.6	2.0	3.4	4.8	7.1	14.3	23.3	40.2	53.4	62.2	70.2	77.8	82.5	83.8	87.2	90.5	93.7	96.7	98.4	100.0
Actual	0.6	2.0	3.4	4.8	7.1	14.3	23.3	40.2	53.4	62.2	70.2	77.8	82.5	87.9	91.6					

Figure 4

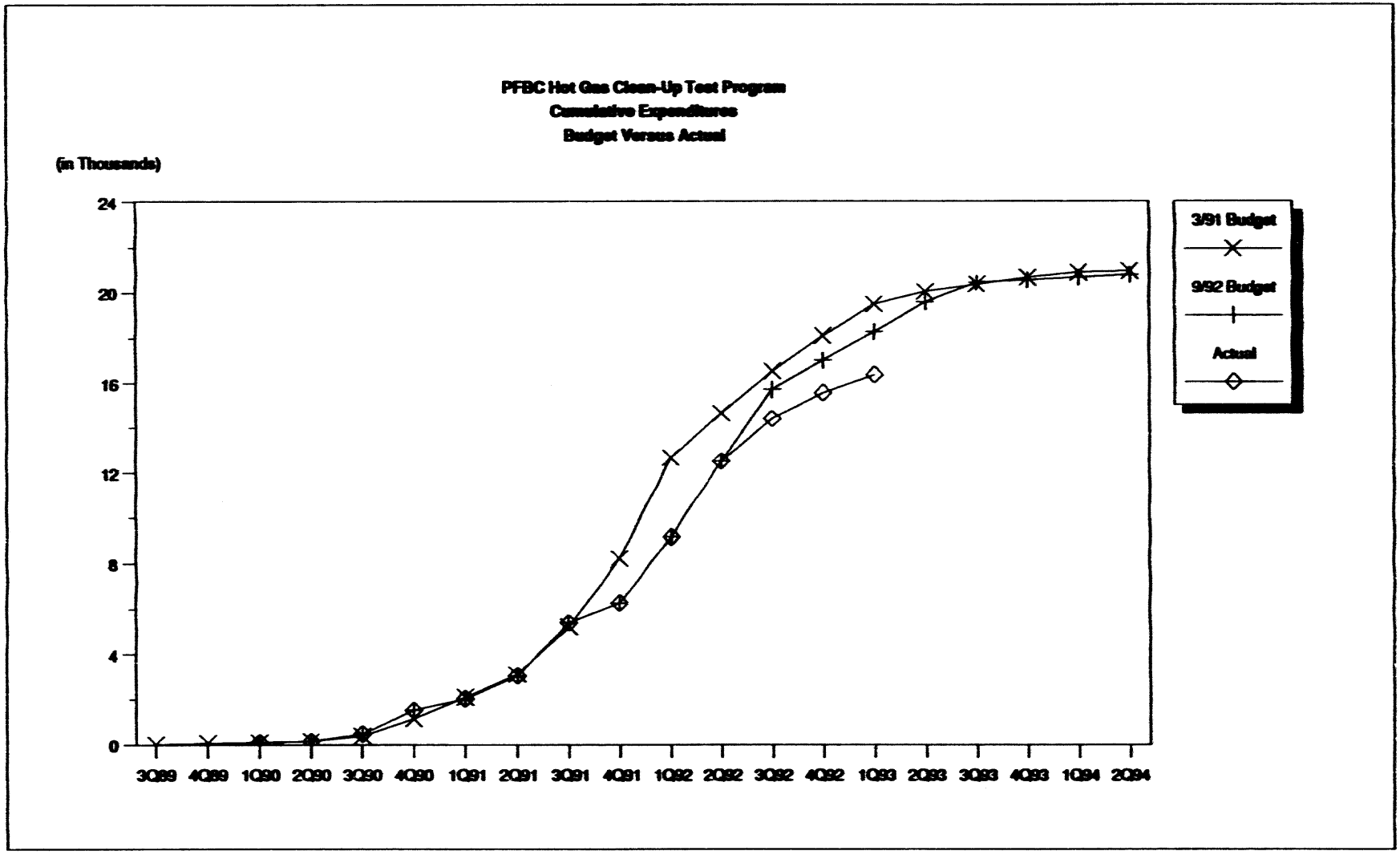

($000)	3Q89	4Q89	1Q90	2Q90	3Q90	4Q90	1Q91	2Q91	3Q91	4Q91	1Q92	2Q92	3Q92	4Q92	1Q93	2Q93	3Q93	4Q93	1Q94	2Q94
3/91 Budget	18.7	70.1	106.3	152.3	383.1	1142.4	2108.4	3120.3	5213.0	8220.2	12883.5	14656.2	16524.3	18106.5	19483.3	20039.8	20372.3	20672.6	20898.9	20855.5
9/92 Budget			90.5	146.7	477.6	1531.3	2040.6	3059.1	5387.9	6280.4	9162.2	12522.0	15711.7	18998.3	18284.9	19571.4	20453.8	20567.8	20881.8	20796.5
Actual			90.5	146.7	477.6	1531.3	2040.6	3059.1	5387.9	6280.4	9162.2	12522.0	14397.6	15569.3	16362.4					

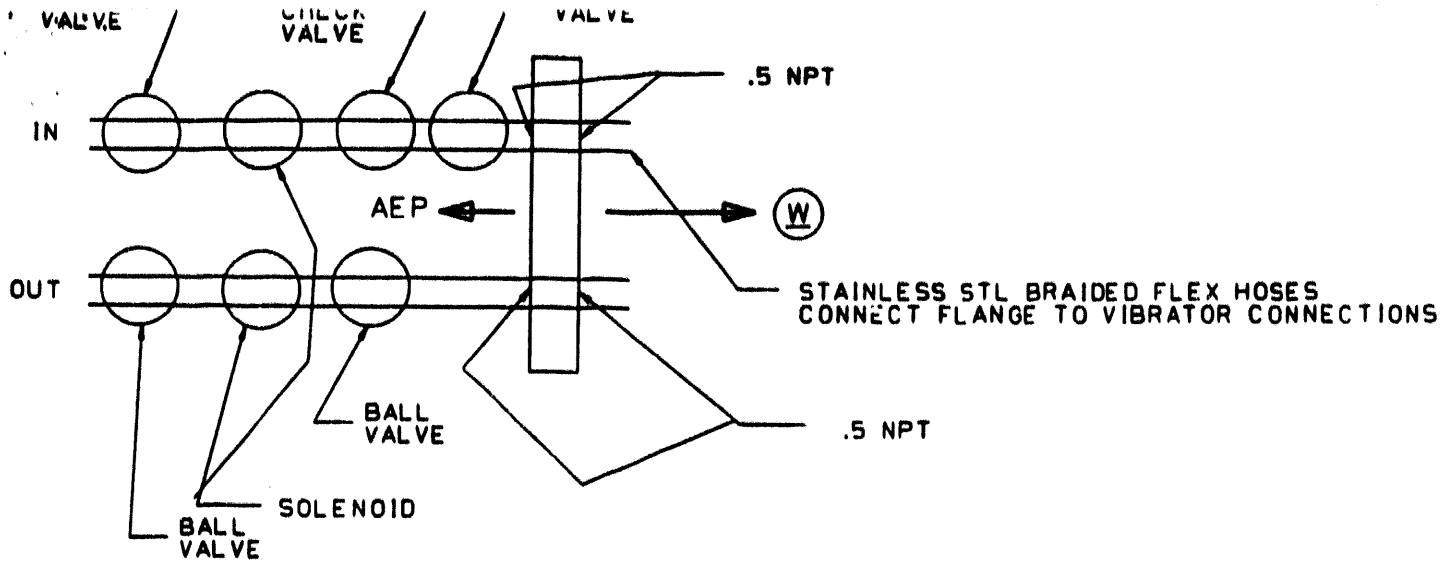
VALVE
VALVE
.5 NPT
IN
AEP
W
OUT
STAINLESS STL BRAIDED FLEX HOSES
CONNECT FLANGE TO VIBRATOR CONNECTIONS
BALL
VALVE
.5 NPT
SOLENOID
BALL
VALVE

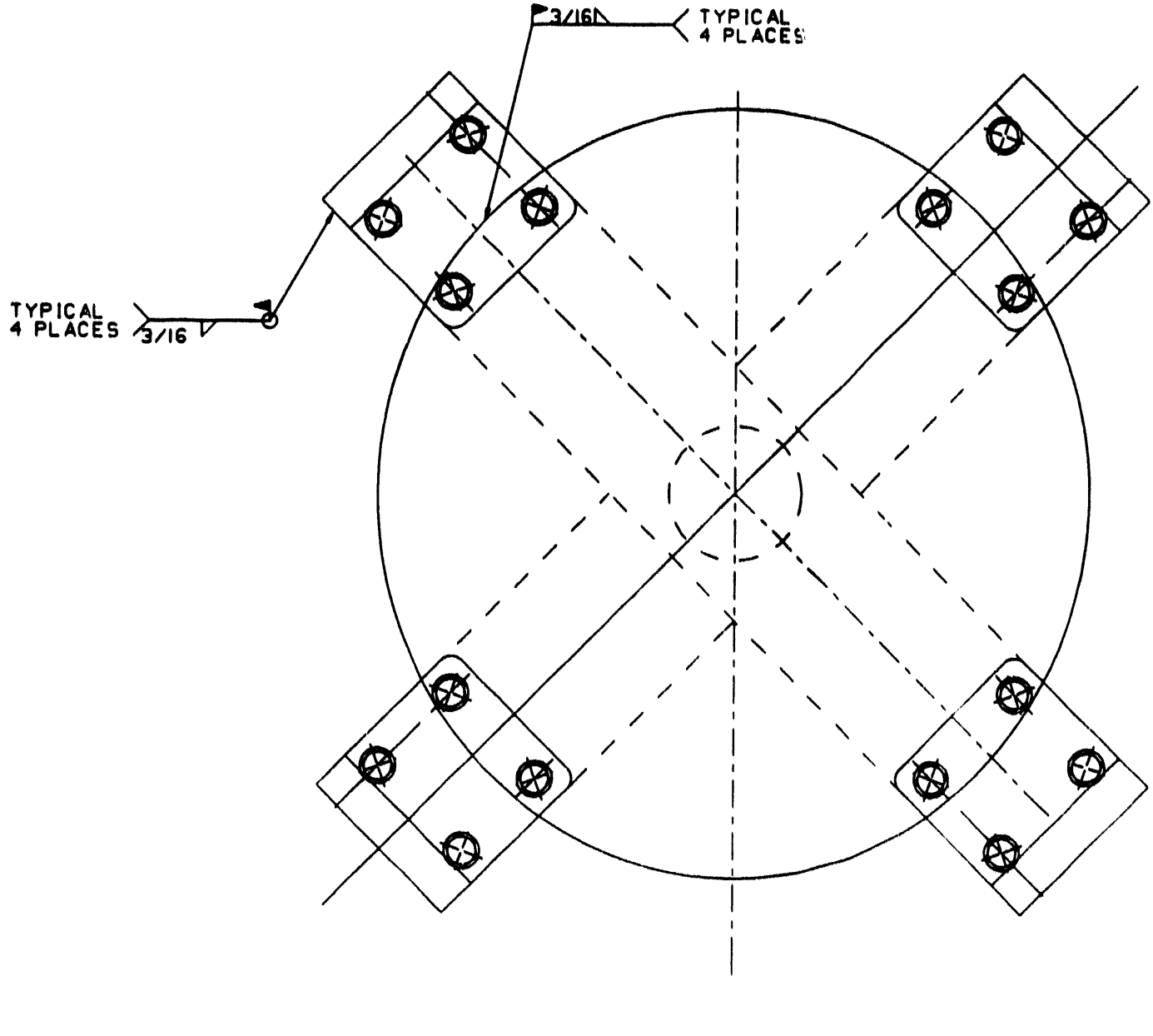
3/16
TYPICAL
4 PLACES
TYPICAL
4 PLACES
3/16

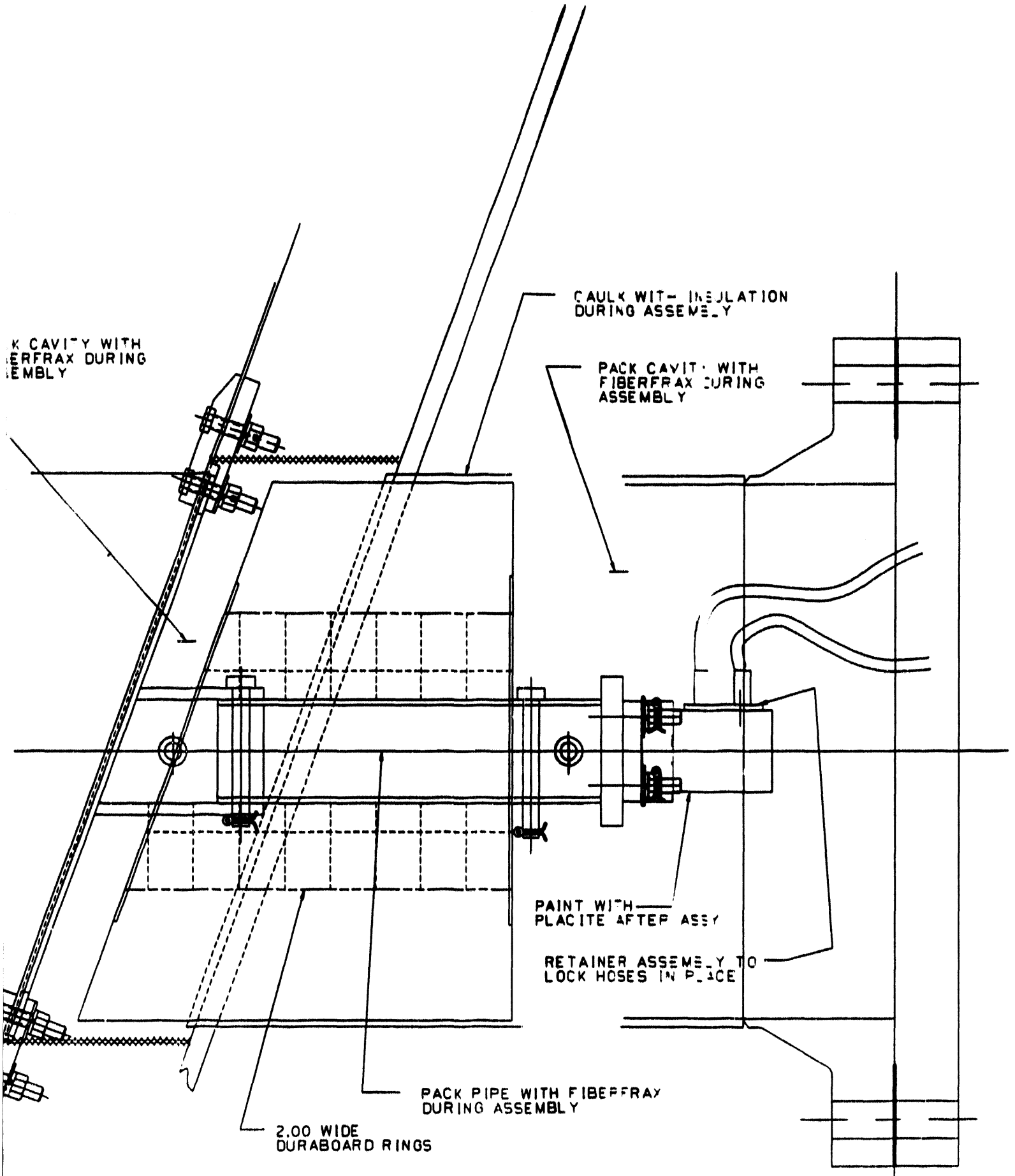
K CAVITY WITH
ERFRAX DURING
EMBLY
CAULK WIT- INSULATION
DURING ASSEMBLY
PACK CAVITY WITH
FIBERFRAX DURING
ASSEMBLY
PAINT WITH
PLACITE AFTER ASSY
RETAINER ASSEMBLY TO
LOCK HOSES IN PLACE
PACK PIPE WITH FIBERFRAX
DURING ASSEMBLY
2.00 WIDE
DURABOARD RINGS

FIGURE 2

Appendix To
ADVANCED PARTICLE FILTER
Technical Progress Report No. 11
January through March, 1993
AEPSC Contract No. C8014

Material Characterization of the Clay Bonded Silicon Carbide Candle Filters and Ash Formations in the W-APF System after 500 Hours of Hot Gas Filtration at AEP

M. A. Alvin
Westinghouse Science and Technology Center
Pittsburgh, Pennsylvania

April 5, 1993

Material Characterization of the Clay Bonded Silicon Carbide Candle Filters and Ash Formations in the W-APF System after 500 Hours of Hot Gas Filtration at AEP

M. A. Alvin
Westinghouse Science and Technology Center
Pittsburgh, Pennsylvania

April 5, 1993

CONTENTS

CONTENTS (continued)

MATERIAL CHARACTERIZATION OF THE CLAY BONDED SILICON CARBIDE CANDLE FILTERS AND ASH FORMATIONS IN THE W-APF SYSTEM AFTER 500 HOURS OF HOT GAS FILTRATION AT AEP

M. A. Alvin

April 5, 1993

ABSTRACT

This report details the results of the material characterisation efforts that were performed on the clay bonded silicon carbide candle filters that experienced 500 hours of operation in Westinghouse's Advanced Particulate Filtration (APF) system under pressurised fluidised-bed combustion gas (PFBC) conditions at the American Electric Power (AEP) plant in Brilliant, Ohio. Phase changes were identified along the clay binder surface in the ceramic filter material. A uniform loss of material strength (i.e., 10-15%) was also observed in the candle filter elements throughout the vessel. The analyses presented in this report support the fracture analyses which indicated that the failure of 21 bottom plenum candles resulted from ash bridging, and not substantial loss of strength or degradation of the ceramic candle matrix. Ash bridged between adjacent candles, providing a sustained bending load along the filter body at temperature. The sustained load ultimately caused a delayed fracture, and typically resulted in a failure below or near the fine-to-coarse grain transition section in the clay bonded silicon carbide filter elements.

After 500 hours of exposure in the PFBC gas environment, dumpling and scale-like cake layers were observed along the outer surface of each candle filter. Characterisation through the dumplings

and scale-like ash cake layers provided insight in terms of plant operation and carryover of fines into the Westinghouse APF vessel during the 500 hours of hot gas filtration. For example, during plant shutdown, carryover of sorbent fines, particularly from the primary cyclone occurred, depositing a sorbent but ash-free dust cake layer. Similarly characterisation of the ash removed from various levels in the Westinghouse APF ash hopper identified significant compositional changes within the dolomitic fraction of the ash. Residual cement-like ash material found in the bottom of the Westinghouse AFP ash hopper was typically uncharacteristic of the ash-sorbent composition found throughout the vessel.

1. INTRODUCTION

Westinghouse initially received 450 clay bonded silicon carbide Schumacher Dia Schumalith candle filters. Each candle filter was inspected in terms of appearance and evaluated on the basis of dimensional specifications prior to the selection and installation of 384 candles in the Westinghouse Advanced Particulate Filtration (APF) system. Of the 384 candles, 40 candles were identified as surveillance candles, and were placed in specified locations throughout the Westinghouse APF system. Each of these elements was characterised on the basis of time-of-flight (TOF) to provide nondestructive baseline data on the initial strength of all 40 surveillance candle filters.

After 500 hours of exposure in the pressurised fluidised-bed combustion (PFBC) gas environment, 21 candle filters in the bottom plenums had fractured. Typically 17 of the failed candles fractured near or below the fine-to-coarse grain transition section (i.e., 101 to 165 mm from the flange top) of the filter elements. Four candles fractured near the bottom closed end section of the filter elements (i.e., 1105 to 1270 mm). These candles were in close proximity to the filter vessel wall.

Characterisation of candles that were removed from the bottom plenum, as well as reconstructed candle filter segments indicated that bowing of the clay bonded silicon carbide candle filter elements resulted during hot gas filtration. The primary fracture in each candle contained transverse breaks with shear lips, typical of a beam breaking in a bending mode. There was no evidence of longitudinal fractures in any of the failed filters, and all secondary cracks consisted of additional transverse breaks. The results of the fracture analysis

indicated that a sustained bending load (i.e., bridged ash at temperature) caused bowing of the candle filter elements, and typically failure resulted near or below the fine-to-coarse grain transition zone of each filter element.

This report details the post-test results of the material analyses that were performed on either the intact filters or failed candle filter segments which experienced 500 hours of exposure in the AEP PFBC slipstream. Initially all 23 bottom surveillance candles (originally 24 surveillance candles were positioned in the bottom arrays, but one had broken during installation), as well as five additional candles throughout the nine cluster arrays were subjected to nondestructive TOF measurements. Each candle was subjected to length and bow measurements, as well as as-received and vacuum brushed permeability measurements. Five candles were selected for C-ring compression room temperature and high temperature strength measurements, as well as burst strength characterization. Extensive scanning electron microscopy/energy dispersive x-ray analyses (SEM/EDAX) were performed on intact candle sections and segments from failed candles that were recovered from the ash hopper. Elemental microprobe analysis was utilized to detail the presence of silicon (Si), oxygen (O), sulfur (S), carbon (C), sodium (Na), etc., within the binder and grain of the clay bonded silicon carbide candle filter matrix. Auger analysis was utilized to quantitatively detail microscopic changes that resulted within the binder and binder-grain interface of the 500 hour PFBC exposed clay bonded silicon carbide candle filter matrix. In an attempt to identify the total silicate content within the as-fabricated and 500 hour PFBC exposed candle filters, an acid leach (i.e., HF oxidation) was performed. This information provides insight into the potential stability of the silicon carbide grain under a high temperature, oxidizing environment.

To complement the material analysis, characterization of the ash materials formed throughout the vessel was also performed. Extensive SEM/EDAX characterization was used to detail the morphology and composition of ash that deposited in the dumpling- and scale-like formations along the candle OD surface. Ash fusion, ultimate and proximate analysis, and x-ray diffraction (XRD) analyses were also performed on select ash materials (i.e., candle wall, hopper ash, bottom hopper ash, etc.).

The results of both the ceramic filter material and ash analyses are presented in Sections 3 through 7 of this report. Currently quantitative elemental analyses [i.e., silicon (Si), aluminum (Al), calcium (Ca), magnesium (Mg), iron (Fe), sodium (Na), potassium (K), sulfur (S)] are being performed on various ash materials to detail compositional variations which resulted throughout the filter vessel (i.e., candle wall, candle ID, hopper ash, bottom hopper ash). The results of these analyses will be reported at a later date. This information will provide insight into the acidic and basic characteristics of the various ash materials, as well as insight into the total alkali concentration retained within the filter ash cake or filter element relative to the concentration of either sodium or potassium released during coal combustion.

2. SUMMARY

- After 500 hours of operation in the pressurized fluidized-bed combustion gas environment, the fibrous outer membrane along the clay bonded silicon carbide Schumacher Dia Schumalith candles remained intact. The fibrous outer membrane did not permit penetration of fines through the filter wall.

- An approximate 10-15% loss of material strength occurred within the intact candle clay bonded silicon carbide matrix after 500 hours of exposure to the PFBC gas environment. A relatively uniform strength change resulted within the intact candles throughout the vessel (i.e., top to bottom plenums), as well as within the various cluster ring positions (i.e., outer versus inner ring candle filters). A somewhat higher loss of material strength, i.e., 25% was detected in fractured candle segments removed from the W-APF ash hopper.

- Sulfur which is present in the pressurized fluidized-bed combustion gas system induced phase changes along the surface of the binder which coats the silicon carbide grains in the Schumacher Dia Schumalith candle filter matrix.

- Mullitization of the binder surface phase was evident in the Schumacher Dia Schumalith candle filter matrix in areas where micron and submicron sulfur-enriched aerosol droplets or particles deposited.

- Negligible oxidation of the silicon carbide grain resulted in the Schumacher Dia Schumalith candle filters after 500 hours of hot gas filtration testing under pressurized fluidized-bed combustion gas conditions.

- The clay bonded silicon carbide Schumacher Dia Schumalith candle filters bowed at PFBC process temperatures when ash bridges formed between adjacent filter elements. Transverse primary fractures typically resulted below or near the fine-to-coarse grain transition section in the filter elements. This was considered to have resulted from a sustained load (i.e., ash) being applied along the candle filter body during high temperature operation. Thermal fatigue was not evident in the clay bonded silicon carbide matrix (i.e., longitudinal fractures were not observed). C-ring tension strength testing will be performed to identify whether change has occurred within the matrix along the candle ID, which may be indicative of thermal fatigue.

- Ash analyses indicated the presence of a high concentration of sulfated dolomite within the various ash formations.

3. CLAY BONDED SILICON CARBIDE CANDLE FILTER SURVEILLANCE AND POST-TEST INSPECTION

3.1 INITIAL CERAMIC CANDLE FILTER SURVEILLANCE EFFORT

A candle filter surveillance and characterisation effort was initiated prior to assembly of the candle filter clusters in the Westinghouse Advanced Particle Filtration (APF) system at the Tidd plant. The purpose of the surveillance effort was to:

- Evaluate any physical and/or chemical changes that may have occurred within the clay bonded silicon carbide (SiC) Schumacher Dia Schumalith F40 candle filters during operation in the pressurised fluidised-bed combustion (PFBC) system.

- Identify whether all candle filters experienced similar process conditions throughout the entire filter vessel.

Forty-two (42) of the 450, 1.5 m clay bonded silicon carbide Schumacher Dia Schumalith F40 candles were selected for use in the surveillance effort. Forty of the 42 surveillance candles were installed at pre-determined locations within the Westinghouse APF system. Two of the original 42 surveillance candles were retained at Westinghouse STC as controls, representing the as-manufactured clay bonded silicon carbide candle matrix that was specifically used in our Advance Particle Filter (APF) program (AEPSC Contract No. C8014).

The 40 surveillance candle filter elements represented ~10% of the 384 candles that were installed in all nine filter plenums in the APF vessel. The 10% surveillance candle quantity was selected on the basis of paralleling the 10% destructive characterisation effort performed at Schumacher for filter production lot qualification testing.

All of the candle filter elements that were installed at Tidd had undergone vigorous manufacturing quality assurance testing both at Schumacher, as well as at Westinghouse. Qualification testing at Schumacher and an initial Westinghouse inspection of each received candle filter included a visual inspection of the outer membrane coating, flange, and closed end cap section; and an assessment of perpendicularity and bow. In addition Schumacher conducted dimensional tolerance measurements (i.e., length; outer and inner candle filter body diameters; flange diameter); individual candle filter weights; time-of-flight (TOF); ΔP at 6 ± 2 mbar of air at 200 m/hr (volume flow: 52 m^3/h); particle collection efficiency; and bubble testing. In Schumacher's 10% destructive qualification testing, candle filters were randomly selected for burst pressure analysis; O-ring room temperature strength testing; porosity; and determination of Young's modulus using grindosonic techniques.

At Westinghouse all 42 candle filters were subjected to a second nondestructive evaluation (NDE) using state-of-the-art TOF equipment. Time-of-flight was performed at Westinghouse in an attempt to replicate the TOF values that were originally generated by Schumacher, as well as to assure that our TOF techniques would be acceptable for future use when candles were returned for characterization after field testing.

At Westinghouse TOF data were generated using an Ultran BR-640A broad band receiver and a BR-9400A burst pulser (Figure 3.1). Each candle was supported on two V-blocks which rested on a roller bearing plate that permitted free lateral movement during pressure contact with the transmitting and receiving transducers.

Dry couplant urethane membranes (Figure 3.2) were placed on the surface of both transmitting and receiving 50 Khz Panametrics X-1021 transducers. The suspended transmitting transducer was pushed against the bottom closed end section of the candle filter via a spherical

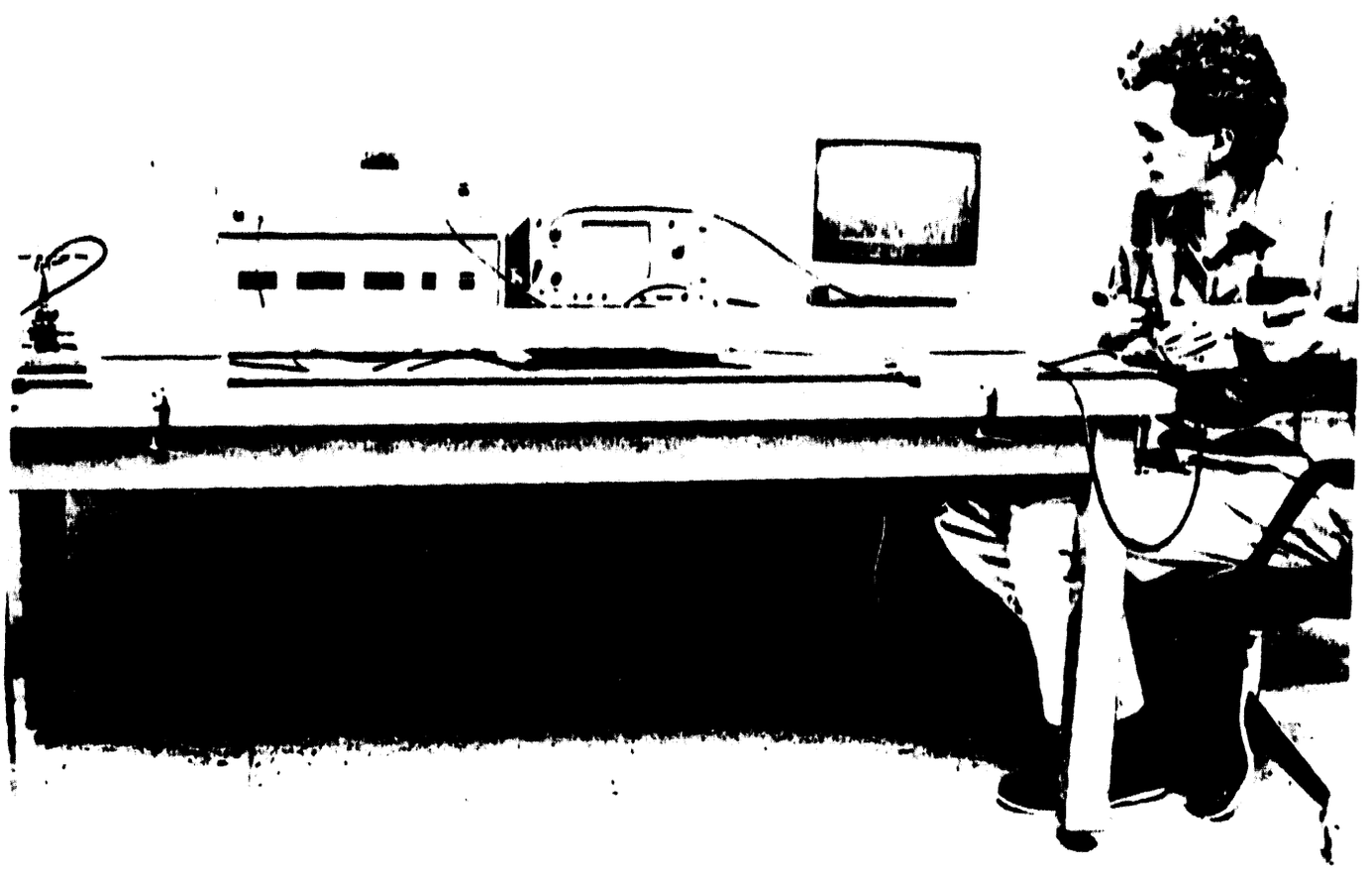

Figure 3.1 - Ultran Time-Of-Flight Testing of 1.5 m Surveillance Candle Filters

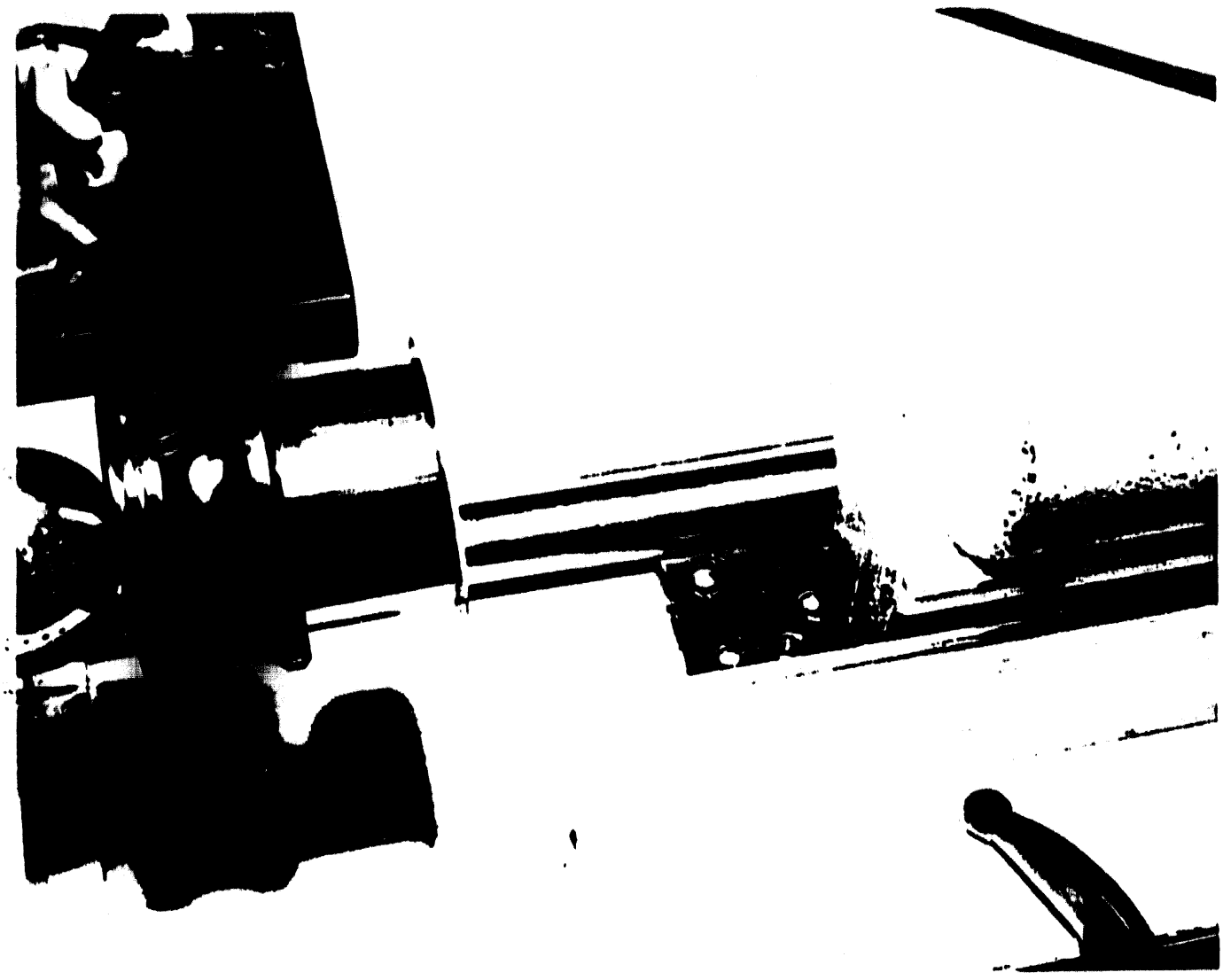

Figure 3.2 - Configuration of Closed End Section of the Candle Filter Prior to Contact With the Urethane Membrane Covered Dry Couplant Transmitting Transducer

support to ensure flat contact with the candle surface. The receiving transducer was mounted in a spring loaded holder for contact with the candle flange. Spring deflection at contact was adjusted to transmit 10.04 lb force (45 N). The equipment was periodically calibrated using a two-step plexiglas standard which consisted of a 4 x 4 x 4 inch cube with a 2 x 4 x 6 inch extension. TOF values through the urethane membrane and plexiglas standard are presented in Table 3.1. A 2 μs correction factor was identified for zero time transmission.

The Ultran equipment that was used for this effort was connected to an oscilloscope, as well as a Sonix digital acquisition system. Time-of-flight data that were generated for each surveillance candle filter were digitally logged and stored in a computer file. For select candle filters, FFT (Fast Fourier Transformation) waveforms were also generated and stored for possible further analyses.

Each TOF measurement was obtained using a 6.25 Mhz digitising rate where a threshold of one was used for data obtained between 280 and 362.24 μs. The collection accuracy of the equipment was established at $\pm$0.7 μs. The resulting TOF data generated for the 42 surveillance candles are presented in Table 3.2. Thirty-seven of the 42 candle filters were identified to be within 5 μs of the TOF values that were generated by Schumacher. The remaining five candle filters had TOF values that exceeded Schumacher's values by 14 to 29 μs. Each of the five candles exceeded the maximum TOF tolerance (345 μs) that was specified by Westinghouse for candle filter qualification and acceptance. Note that Westinghouse continuously recalibrated the Ultran equipment during conduct of the TOF measurements, while Schumacher calibrated their Pundit equipment only on a daily basis. Any discrepancy between Westinghouse and Schumacher's data was considered to result primarily from equipment recalibration frequency (i.e., the possibility of drift during a 24 hour period).

TABLE 3.1

PLEXIGLAS CALIBRATION SENSITIVITY

Contact (With Membranes Touching)	1.92 μs
2" Plexiglas	21.12 μs
4" Plexiglas	40.16 μs
6" Plexiglas	59.04 μs

TABLE 3.2

COMPARISON OF TIME-OF-FLIGHT DATA

Candle	Candle Identification #	Schumacher TOF, μs	(W) Raw Data	After -2 μs Correction for Urethane Membrane (W) TOF μs	Difference (W)-Schumacher
1	S/APF-2	339	339	337	-2
2	S/APF-19	340	340	338	-2
3	S/APF-38	341	343	341	0
4	S/APF-56	344	346	344	0
5	S/APF-65	345	348	346	1
6	S/APF-75	343	343	341	-2
7	S/APF-83	334	339	337	3
8	S/APF-89	334	350	348	14
9	S/APF-97	331	351*	349	18
10	S/APF-115	333	335	333	0
11	S/APF-129	343	347*	345	2
12	S/APF-150	340	360	358	18
13	S/APF-164	338	338	336	-2
14	S/APF-173	345	343	340	-5
15	S/APF-176	334	333	331	-3
16	S/APF-193	325	323+	321	-4
17	S/APF-213	323	323	321	-2
18	S/APF-228	339	336	334	-5
19	S/APF-238	332	331	329	-3
20	S/APF-253	336	335	333	-3
21	S/APF-263	337	336	334	-3
22	S/APF-277	330	361	359	29
23	S/APF-297	331	334	332	1
24	S/APF-314	329	332	330	1
25	S/APF-328	334	339	337	3
26	S/APF-348	344	345*	343	-1
27	S/APF-355	338	338	336	-2
28	S/APF-367	330	332	330	0
29	S/APF-374	343	345*	343	0
30	S/APF-393	337	339	337	0
31	S/APF-399	334	337	335	1
32	S/APF-418	327	348*+	346	19
33	S/APF-436	333	336	334	1
34	S/APF-443	328	331	329	1
35	S/APF-458	326	329+	327	1
36	S/APF-473	327	330	328	1
37	S/APF-493	328	330	328	0
38	S/APF-504	331	332	330	-1
39	S/APF-521	332	333	331	-1
40	S/APF-528	325	327	325	0
41	S/APF-6	336	(Control)	335	-1
42	S/APF-469	330	(Control) 329	327	-3

* Cannot lower time of flight with pressure
+ FFT taken

The TOF data presented in Table 3.2 were pressure sensitive in most cases. For several of the candle filters with high TOF values, application of a force that was greater than the spring load pressure brought the TOF value to within 2 μs of Schumacher's data. This was considered to be principally due to the seating of the urethane membrane on the relatively rough candle filter surface. Conversely, no significant change in the TOF value could be detected in several candles when additional pressure was applied. We suspect that material property variations (i.e., density, porosity, strength, possible flaws, etc.) produced the resulting high TOF values.

Failure of clay bonded silicon carbide candle filters has frequently been associated with material flaws that were generated during filter fabrication in the fine-to-coarse grain transition area of the Schumacher candle. Within the first 76 to 100 mm (3 to 4 inches) from the top of the flange, the Schumacher candle consists of fine silicon carbide grains that are held together with an aluminosilicate clay binder. Below the dense grain region is the remainder of the 1.5 m candle filter body which consists of coarse silicon carbide support grains. The coarse grains are also held together via the aluminosilicate clay binder phase. An external aluminosilicate fiber-silicon carbide grain membrane is applied to the candle body to prevent particle penetration into the support matrix. In an attempt to determine if fabrication flaws could be detected within the fine-to-coarse silicon carbide transition zone, through-thickness time-of-flight (TOF) measurements were performed.

An Ultran BR-640A broad band receiver and BR-9400A burst pulser were used to determine the through-thickness TOF measurement of six surveillance candle filters (Figure 3.3). A 1.5 Mhz Ultran 143067 transmitting transducer with a delay line contoured to the candle OD, and a 1.5 Mhz Ultran 143068 receiving transducer with a delay line contoured to the candle ID, were held in a spring loaded scissors-like fixture (Figure 3.4).

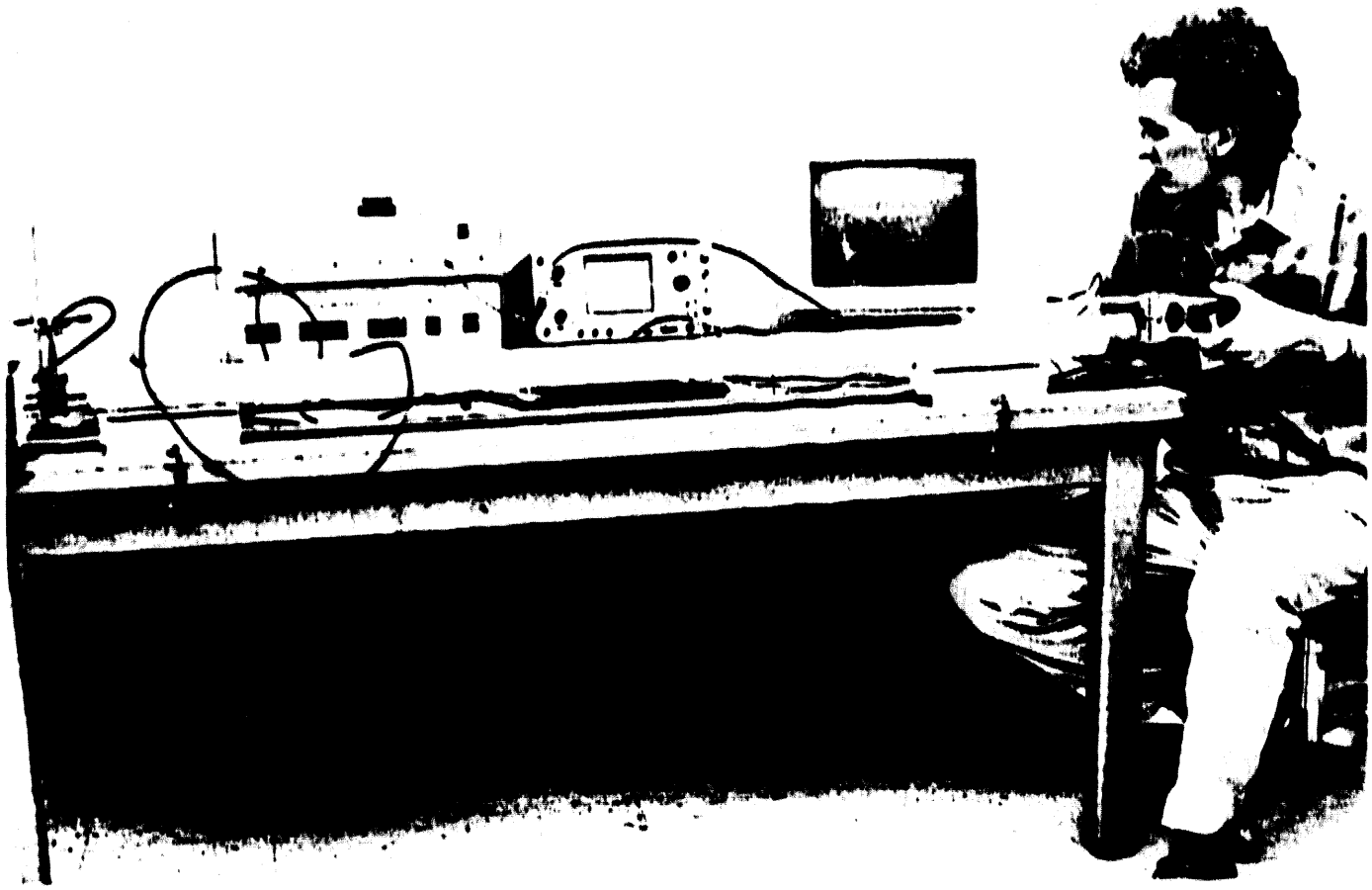

Figure 3.3 - Ultran Time-Of-Flight Testing for Through-Thickness Measurement on 1.5 m Surveillance Candle Filters

Figure 3.4 - Through-Thickness TOF Transducer Fixture for Measurement along the Coarse-to-Fine Grain Transition Section of the Surveillance Candles

The fixture was placed at various locations along the candle wall below the flange with the transmitting transducer positioned along the candle OD, and the receiving transducer along the candle ID. The spring deflection at contact with the candle body was adjusted to obtain a 12.1 μs TOF delay. A plexiglas cylindrical standard which had a TOF value of 13.1 μs (including delay time) was used for calibration. A 100 Mhz digitizing rate with a threshold of eight was used for data gate positioned between 0 and 20 μs. The collection accuracy of the unit was identified at $\pm$0.7 μs.

The six surveillance candles that were selected for the through-thickness TOF characterizations represented both the low and high range full length TOF values that were reported in Table 3.2. Candles which had significantly different TOFs (Schumacher's vs Westinghouse's data) were included. The resulting through-thickness TOF data for the six surveillance candles are presented in Table 3.3. Through-thickness data were generated at three locations within the fine grain structure at ~76 mm (~3 inches) below the top of the flange, as well as within the coarse grain region at ~115 mm (~4.5 inches) below the top of the flange.

The resulting through-thickness TOF values generated for the coarse region at 1.5 Mhz indicated good correlation with the full length TOF data. In particular, all 50 Khz full length TOF values that were reported as high values in Table 3.2, exhibited corresponding through-thickness values that exceeded 5 μs/in. Since a relatively small set of data was generated in this effort, final conclusions will not be made at this time with regard to the integrity of the fine-to-coarse grain transition section, nor to what effect the fine-to-coarse grain transition area had on the overall TOF value generated for each candle filter.

TABLE 3.3

ULTRAN 1.5 MHz Through-Thickness Transmission - Dry Coupled on Candle Thickness

Note: Delay - 12.1 μs; Thickness = 0.525 μs

Sample #	Full Length 50 Khz TOF μs Sch	(W)	Fine Grain 1.5 MhzTOF	Fine Grain TOF-Delay	Fine Grain TOF/in.	Coarse Grain 1.5Mhz TOF	Coarse Grain TOF-Delay	Coarse Grain TOF/in.
Broken Piece	--	--	14	1.9	3.36	15	2.9	5.13
469	330	329	24.3	2.2	3.89	14.8	2.7	4.77
277	330	361	13.9	1.8	3.18	14.7	2.6	4.60
97	331	351	14.7	2.6	4.60	15.1	3.0	5.30
343	345	343	14.1	2.0	3.54	15.3	3.2	5.66
418	327	348+	14.33[a]	2.23	3.94	15.01	2.91[b]	5.15
458	326	327+	13.92[c]	1.82	3.22	14.70	2.60[d]	4.60

+ - FFT's available for full length 50 KHz

a - FFT for 1.5 MHz (File CA418ND)

b - FFT for 1.5 MHz (File CA418NC)

c - FFT for 1.5 MHz (File CA458ND)

d - FFT for 1.5 MHz (File CA458NC)

3.2 SURVEILLANCE CANDLE FILTER POSITIONS

The surveillance candle filters were initially positioned at various locations in the Westinghouse APF system as shown in Figure 3.5. Nine surveillance candles were located in the top plenum clusters in positions A/T-1, A/T-16, A/T-19, A/T-35, A/T-36, B/T-1, B/T-16, B/T-19, and C/T-1; seven were located in the middle plenum clusters in positions A/M-1, A/M-16, A/M-19, B/M-1, B/M-16, B/M-19, and C/M-1; and twenty-four were located in the bottom plenum clusters in positions A/B-1, A/B-5, A/B-6, A/B-7, A/B-8, A/B-16, A/B-17, A/B-18, A/B-19, A/B-35, A/B-36, B/B-1, B/B-5, B/B-6, B/B-7, B/B-8, B/B-16, B/B-17, B/B-18, B/B-19, C/B-6, C/B-7, C/B-17, and C/B-18.

The positions of the surveillance candles provided for ease of access to the various bottom plenum cluster candles via the manway entrance. Note that candles located in the top and middle plenum clusters would only be accessible if the dome and tubesheet cluster assembly of the APF were removed. Candles were positioned so that a direct assessment of filter element and material life could be made for candles located at comparable positions in the top, middle, and bottom plenum arrays. All arrays within a common plenum level also contained surveillance candles at comparable locations, so that a direct comparison of the filter element and material life could be made for candles within the various arrays of a common plenum level. And finally, surveillance candles were positioned within a given array to reflect any change that may have occurred in the filter elements or material life along the inner and outer candle ring positions.

3.3 Candle Filter Inspection After 500 Hours Of Hot Gas Filtration

Between October and December 1992, the Westinghouse APF system operated for ~500 hours in the PFBC environment filtering fly ash fines that were generated from the combustion of Pittsburgh #8 coal. Plum Run dolomite was used as the sulfur sorbent during this segment of testing.

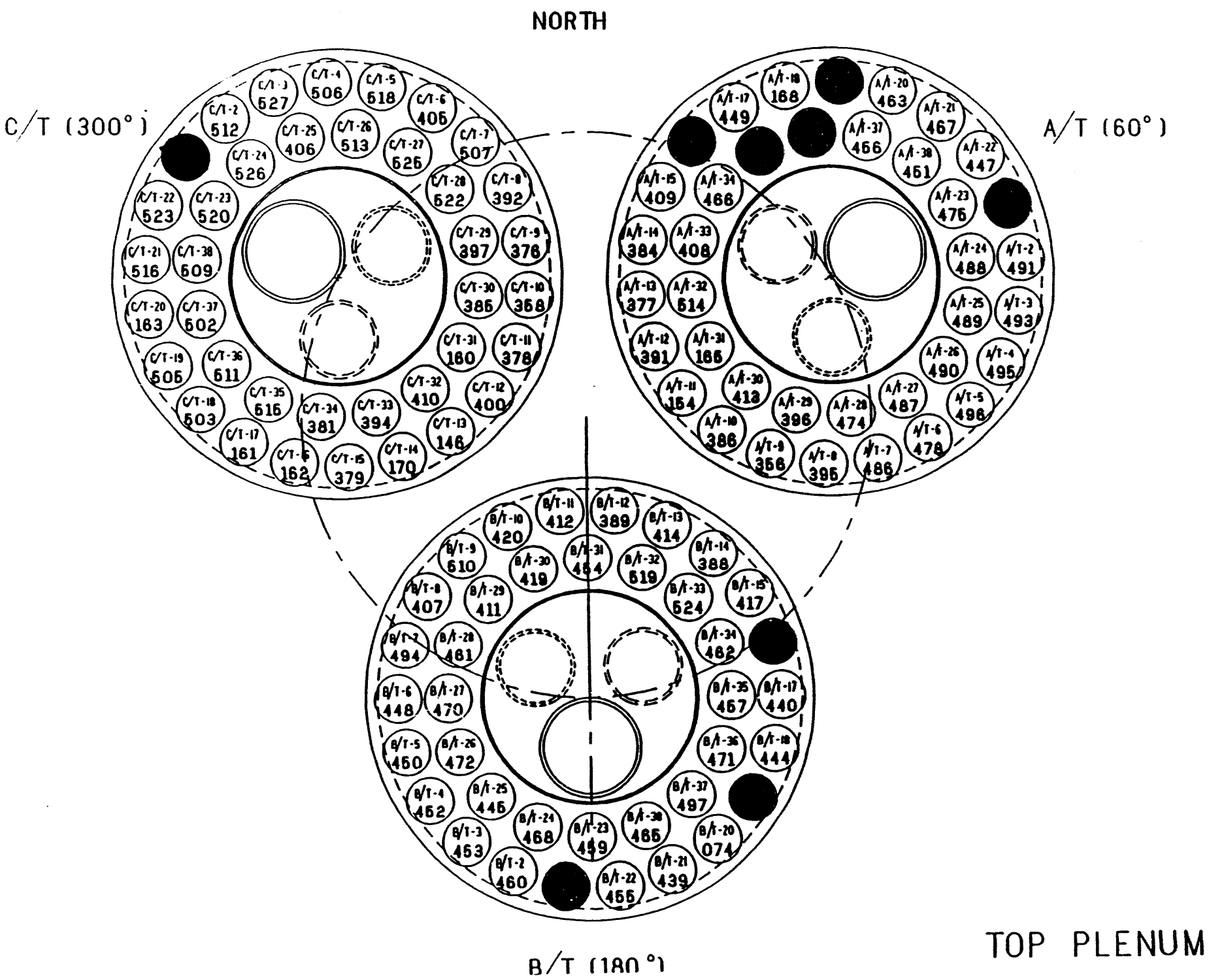

Figure 3.5 - Surveillance Candle Filter Locations

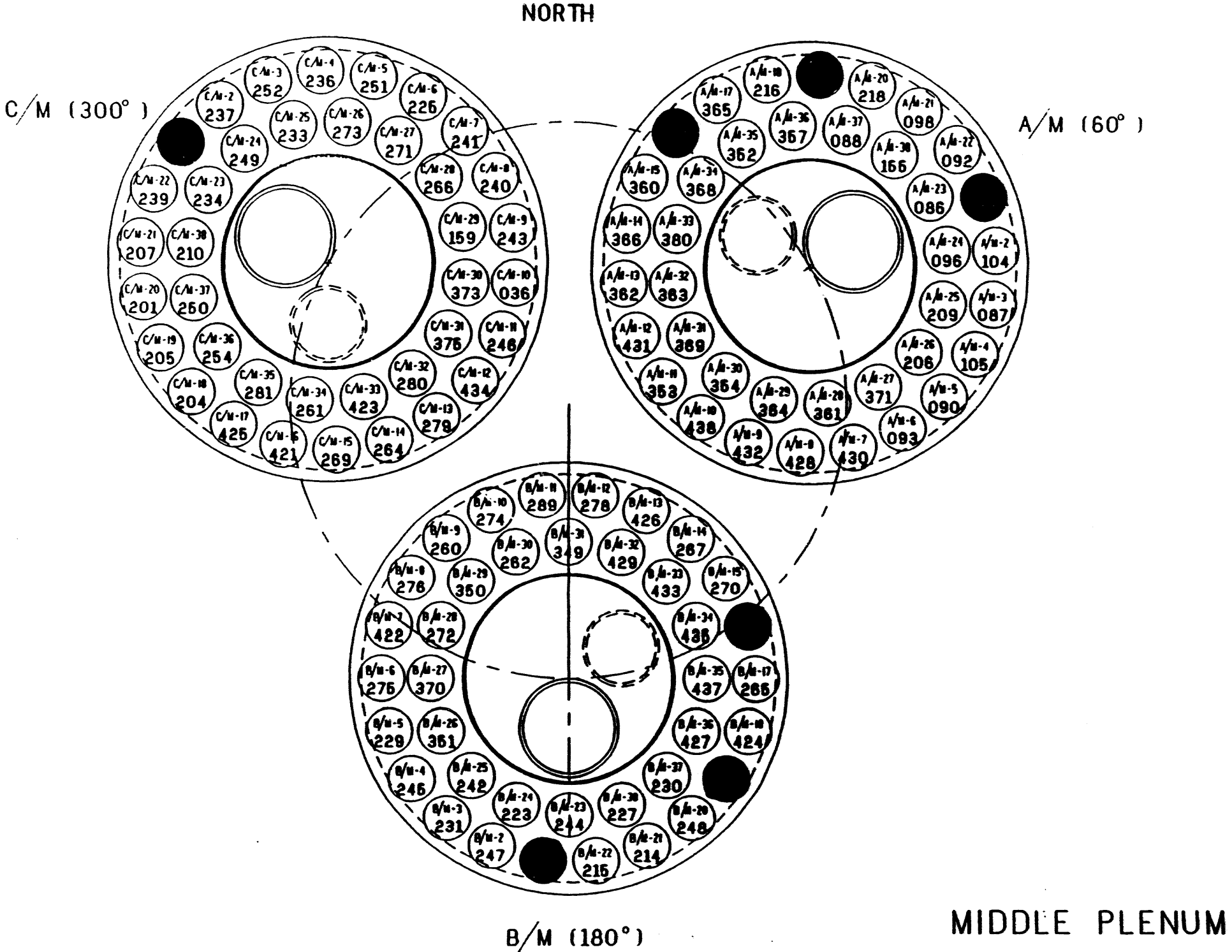

Figure 3.5 - Surveillance Candle Filter Locations

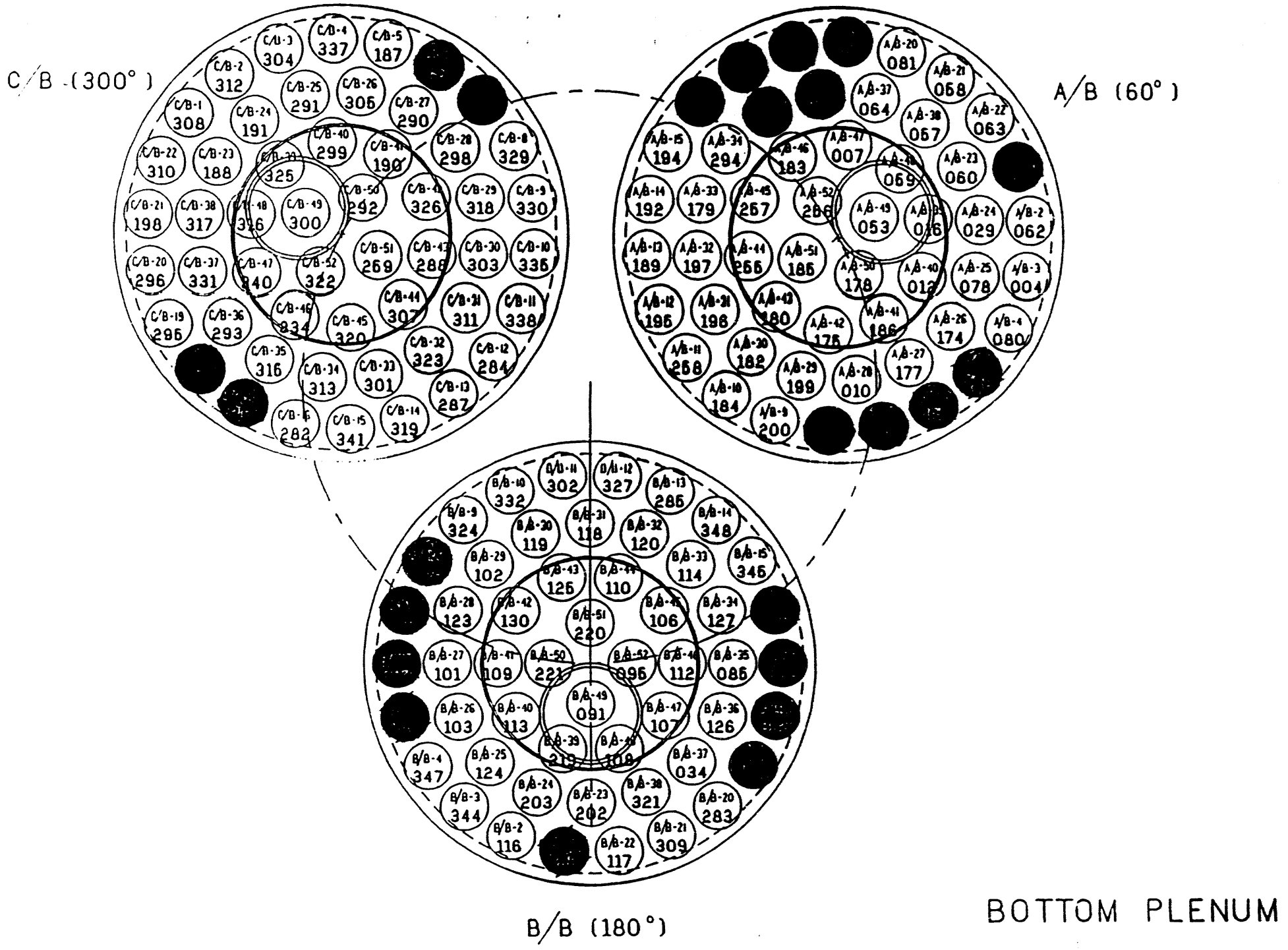

Figure 3.5 - Surveillance Candle Filter Locations

As shown in Table 3.4, the maximum temperature that the clay bonded silicon carbide candle filters experienced was 790-810°C (1450-1490°F) for a period of 45 hours. The first indication of dust in the off-gas stream was detected during this time period. The plant, however, continued to operate until a combustor trip occurred, which subsequently terminated hot gas filtration testing.

After cooling and prior to lifting the candle clusters out of the filter vessel, dust was removed from the APF ash hopper. Broken candle sections were encountered during the ash removal effort (Figure 3.6). Initial inspection of the three bottom plenum candle arrays via the manway entrance on December 16, 1992 indicated that candles had broken in each candle filter array. Fifteen candles had broken in the bottom plenum of Cluster A, four in Cluster B, and two in Cluster C (Figure 3.7).[1] Segments of these twenty-one failed candles were initially considered to have fallen into the ash hopper in the Westinghouse APF vessel. In the bottom plenum of Cluster B, one candle was identified as hanging below the bottom level of the attached candles, indicating that it had also fractured, but was supported in the array via the packed ash which was bridged between adjacent candles.

When viewed from the manway, severe bridging of ash was evident in the bottom plenum of Cluster B (Figure 3.8), while only marginal ash bridging was identified along the bottom to the mid-section of candles located in the bottom plenum of Cluster C (Figure 3.9). The bottom plenum of Cluster A (Figure 3.10) was virtually free of ash buildup, but had the greatest number of candles that failed during testing at Tidd.

---

(1) Bottom segment of candle AEP/APF-150 located at position A/B-1 failed between the time of the manway inspection and the filter lift, producing a fresh fracture near the transition section of the candle filter. Similarly during transfer of the APF system from the vessel to the stationary support structure, candle filter AEP/APF-125 located at position B/B-43 dropped onto the support structure floor boards, again producing a fresh fracture near the transition section of the candle.

TABLE 3.4

WESTINGHOUSE APF SYSTEM OPERATING TEMPERATURES

Test	Date	Time, Hrs	Temperature, °C (°F)	
1	10/28/92-	20	620-650 (1150-1200)	
	11/2/92	16	730-760 (1350-1400)	
		62	650-660 (1200-1225)	(a)
2	11/21/92-	12	540-620 (1000-1150)	
	11/25/92	24	760-790 (1400-1450)	
		30	650 (1200)	(b)
3	11/25/92-	32	705-730 (1300-1350)	
	12/7/92	46	720-745 (1325-1370)	
		27	760-790 (1400-1450)	
		45	790-810 (1450-1490)	
		60	725-730 (1335-1350)	(a)

(a) Followed By APF Inspection.
(b) Followed By Trip Restart.

Figure 3.6 - Candle Filter Segments Removed From The Ash Hopper

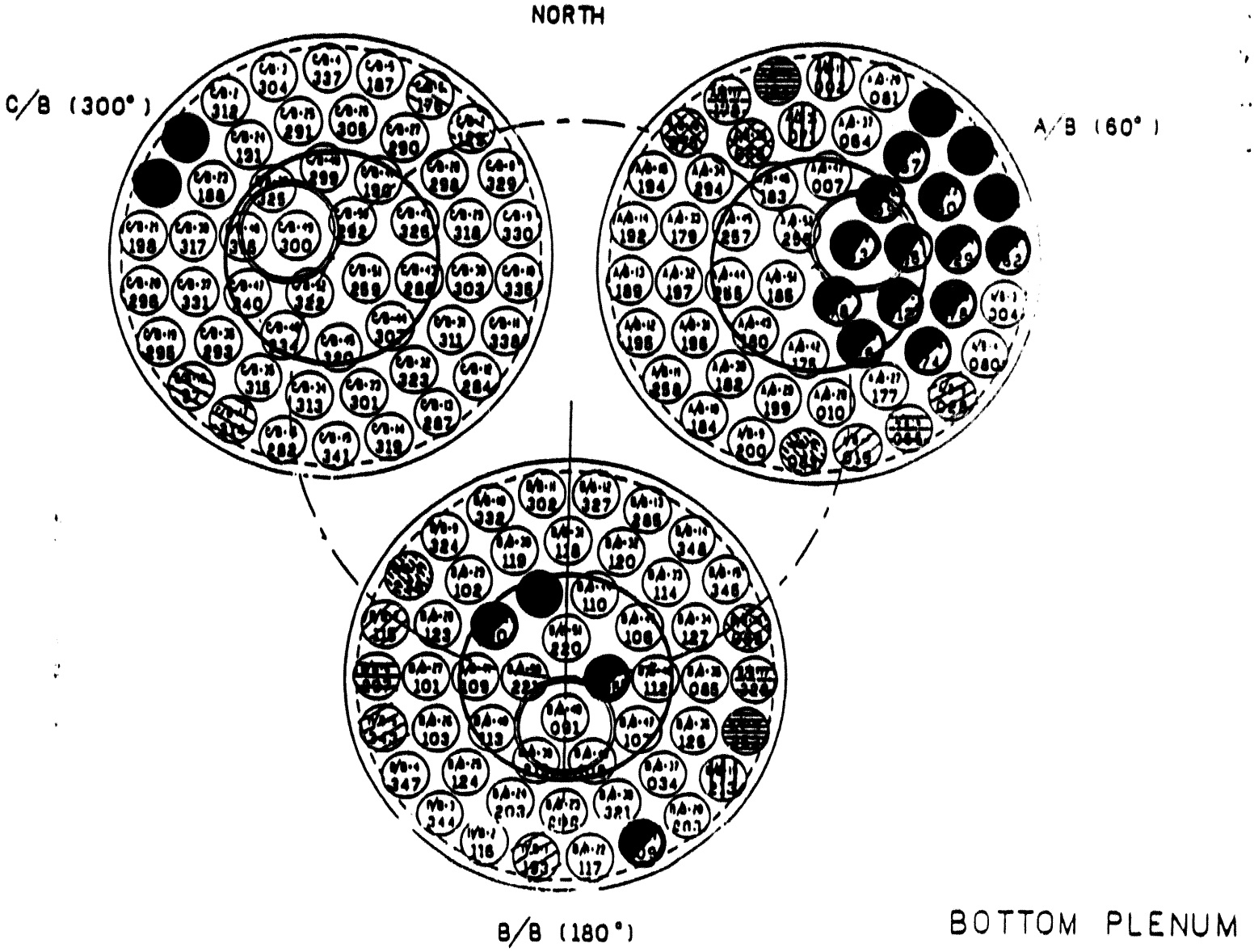

Figure 3.7 - Location of the Fractured Candles in the Bottom Clusters of the W-APF System

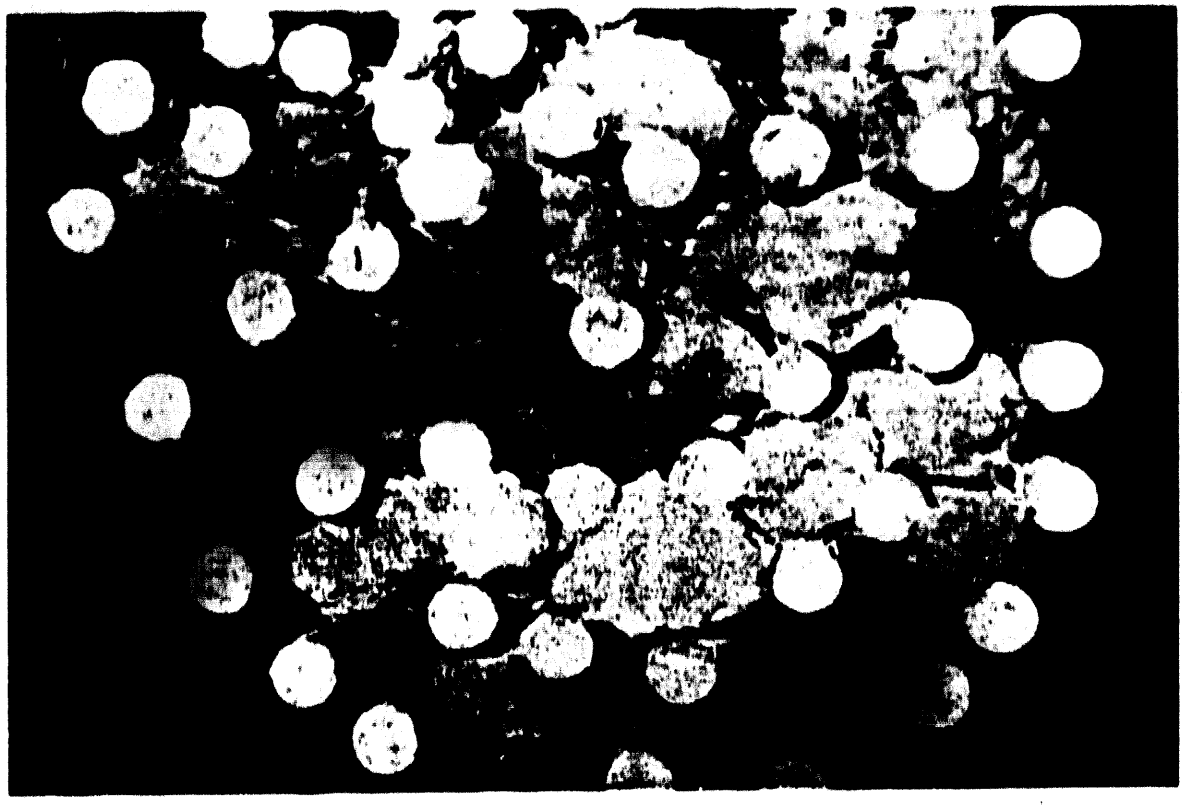

Figure 3.8 - Photo Of Bottom Cluster B In The Westinghouse APF System During The December 16, 1992 Manway Inspection

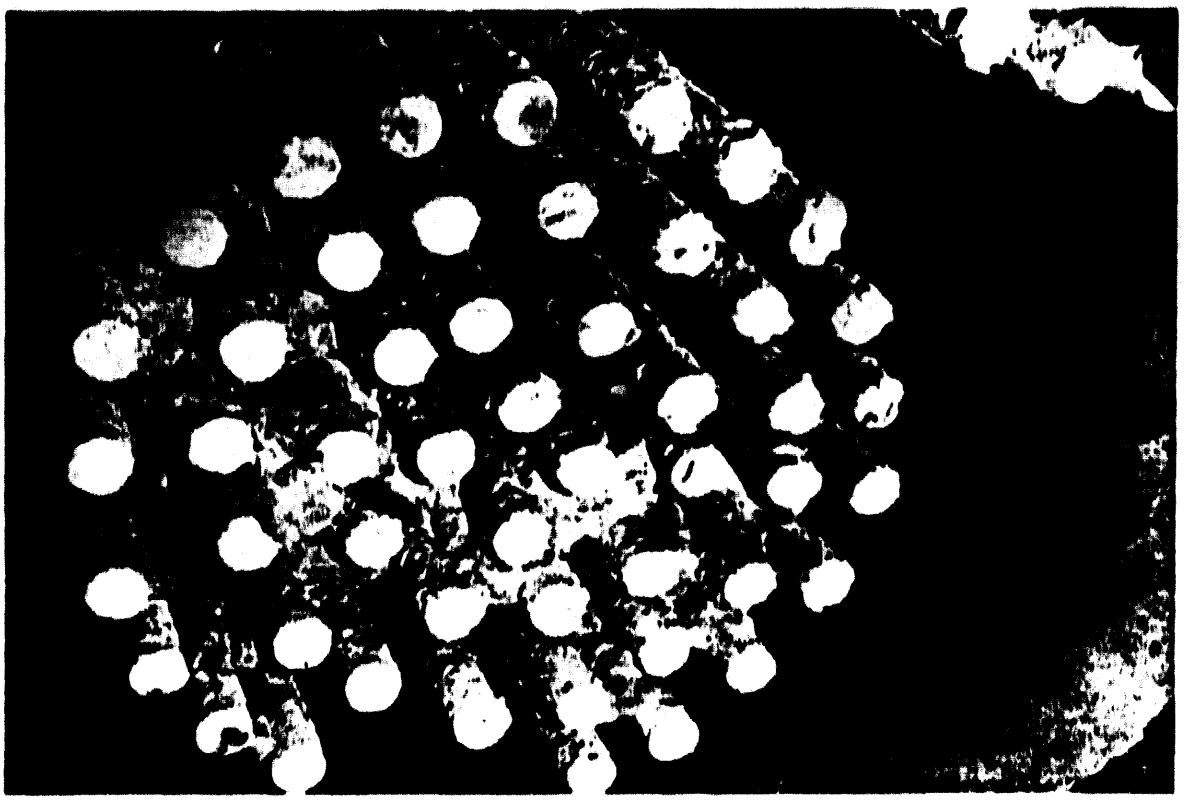

Figure 3.9 - Photo Of Bottom Cluster C In The Westinghouse APF System During The December 16, 1992 Manway Inspection

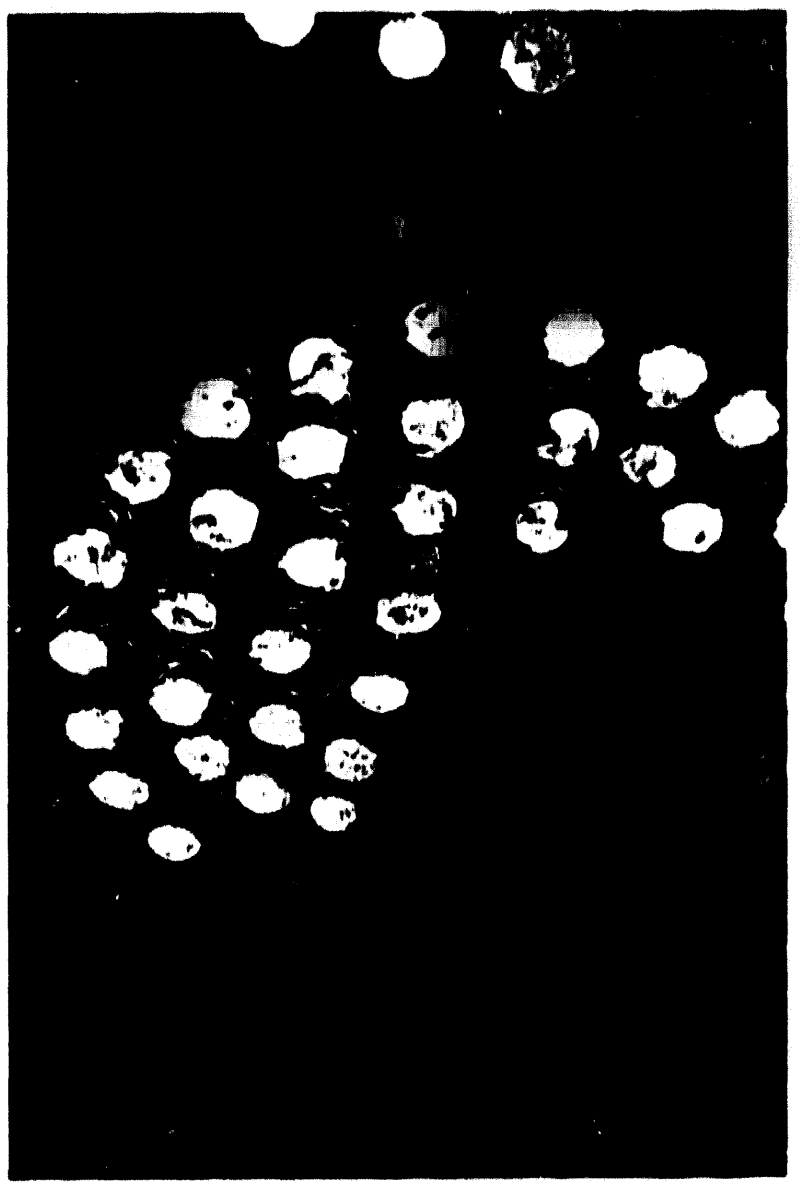

Figure 3.10 - Photo Of Bottom Cluster A In The Westinghouse APF System During The December 16, 1992 Manway Inspection

Forty-nine candle filter segments were retrieved during removal of the ash from the Westinghouse APF filter vessel, as well as during the lift of the filter cluster array from the pressure shell. The length of the retrieved candle filter segments ranged from ~75 mm to ~985 mm (3 inches to ~40 inches) (Table 3.5). The average length was 439 mm (17.28 inches; 1σ = 9.64 inches). Twelve of the collected candle filter segments were between 255 and 305 mm (10 and 12 inches) in length.

Chips and surface scratches were evident along many candle segments. During retrieval of the broken candle segments, the various pieces were stacked into a large pile. Based on the virtually clean surface of the chips (i.e., dark silicon carbide grains evident; absence of dust), we suspected that these chips occurred during stacking and were not the result of candle segments breaking during filter operation which collided into an adjacent candle(s), causing a cascade of falling candle sections to occur. If the in situ failure had occurred, the surface of the candle filter segments would be chipped, but a dust layer would blanket the chip, similar to many of the fractured candle surfaces.

What was interesting to note was that 13 candle sections were entirely caked with ash on both ends (7 with closed end tips and an exposed fractured surface; 6 with both fractured surfaces exposed). Alternately, 25 candle segments had only one end caked with dust, while the opposite fractured surface was virtually free of ash (9 with closed end tips and an exposed fractured surface; 14 with both fracture surfaces exposed). In addition 11 candle filter segments were removed from the ash hopper which appeared to have both relatively clean fractured surfaces (2 with closed end tips and an exposed fractured surface; 9 with both fractured surfaces exposed).

TABLE 3.5

LENGTHS OF BROKEN CANDLE FILTER SECTIONS RETRIEVED DURING ASH REMOVAL FROM THE WESTINGHOUSE APF SYSTEM

Open Ended Fractured Sections, mm				Fractured Closed Bottom Sections, mm	
(1)	305	(21)	690	(1)	330
(2)	~305	(22)	890	(2)	343
(3)	~305	(23)	876	(3)	318
(4)	438	(24)	984	(4)	267
(5)	311	(25)	699	(5)	457
(6)	184	(26)	254	(6)	394
(7)	260	(27)	254	(7)	362
(8)	305	(28)	165	(8)	260
(9)	254	(29)	127	(9)	222
(10)	254	(30)	229	(10)	146
(11)	305	(31)	76	(11)	533
(12)	216			(12)	845
(13)	311			(13)	787
(14)	191			(14)	590
(15)	350			(15)	648
(16)	813			(16)	781
(17)	635			(17)	533
(18)	521			(18)	457
(19)	940				
(20)	622				

After removal of the candle filters from the bottom plenums, post-test inspection of the 21 failed candle segments was conducted. Seventeen of the 21 candle segments were relatively short (i.e., ~100 to 165 mm), while four were relatively long sections (i.e., 1105 to 1143 mm) (Table 3.6). The 17 short segments had circumferentially fractured the dense clay bonded silicon carbide matrix below the fine-to-coarse transition section of the candle filter (Figures 3.11 through 3.13). Four of the 17 failed short candle segments had fresh fractured surfaced (A/B-1, A/B-21, A/B-22, and B/B-43), implying that the final fracture which removed the bottom section of the candle occurred after termination of the hot gas filtration test in the APF vessel. Alternately, actual failure of the candles prior to test termination may have occurred, only if the severed candle had not slipped, but was tightly held in the cluster array via the surrounding dust bridge (i.e., B/B-43).

Photographs of the four relatively long failed candle segments (A/B-2, B/B-21, C/B-1, and C/B-22) are shown in Figures 3.14 through 3.21. A fresh fracture surface was detected on C/B-1 #308 and C/B-22 #310. These candles were located along the outer ring of the bottom plenum of Cluster C, closest to the filter vessel wall. Note that A/B-2 #062 and B/B-21 #309 were positioned along the outer ring of the bottom plenums of Clusters A and B, respectively, again close to the filter vessel wall. Both A/B-2 and B/B-21 candles had a heavy deposit of ash along their fractured surfaces implying that failure of these candles had occurred at an earlier point in time in comparison to failure of either candle C/B-1 or C/B-22.

Two additional, near full length candle segments were also found in the ash-laden candle cluster after lifting the APF internals from the filter vessel and transporting it to the support structure. These near full length candle segments fractured below the flange transition section (Figure 3.22 through 3.25). As shown in these photos, ash-like

TABLE 3.6

LENGTH OF FAILED CANDLES THAT REMAINED IN THE FILTER MOUNT
(12/92)

Candle	Position	ID	Length, mm*	Comment
1	A/B-1	150	120.65	Fresh Fracture
2	A/B-2	062	1143	
3	A/B-21	098	120.65	Fresh Fracture
4	A/B-22	092	114.3	Fresh Fracture
5	A/B-23	475	107.95	
6	A/B-24	029	120.65	
7	A/B-25	078	139.7	
8	A/B-26	174	107.95	
9	A/B-39	016	120.65	
10	A/B-40	012	114.3	
11	A/B-38	451	120.65	
12	A/B-41	186	127.0	
13	A/B-48	059	165.1	
14	A/B-49	053	114.3	
15	A/B-50	178	114.3	
16	B/B-21	309	1270.0	
17	B/B-43	125	101.6	Fresh Fracture
18	B/B-42	130	139.7	
19	B/B-52	095	133.1	
20	C/B-1	308	1193.8	Fresh Fracture
21	C/B-22	310	1104.9	Fresh Fracture

* Top Of Flange To Fracture Surface.

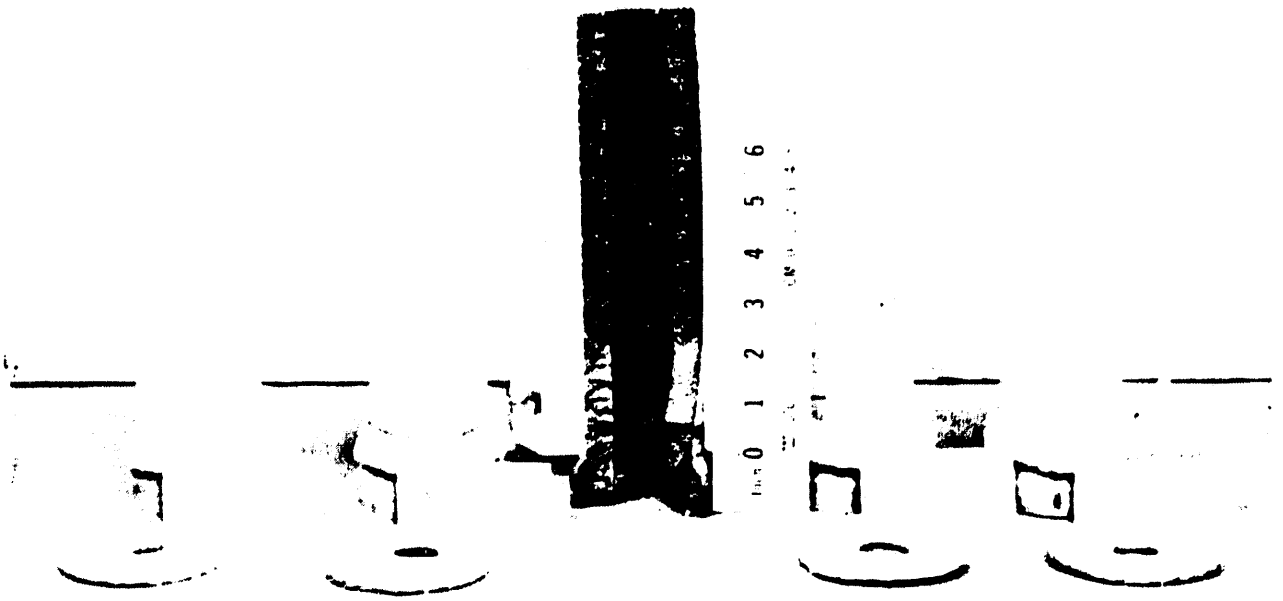

Figure 3.11 - Photograph Illustrating The Length Of The Fresh Fractured Candle Sections That Remained In The Filter Holders

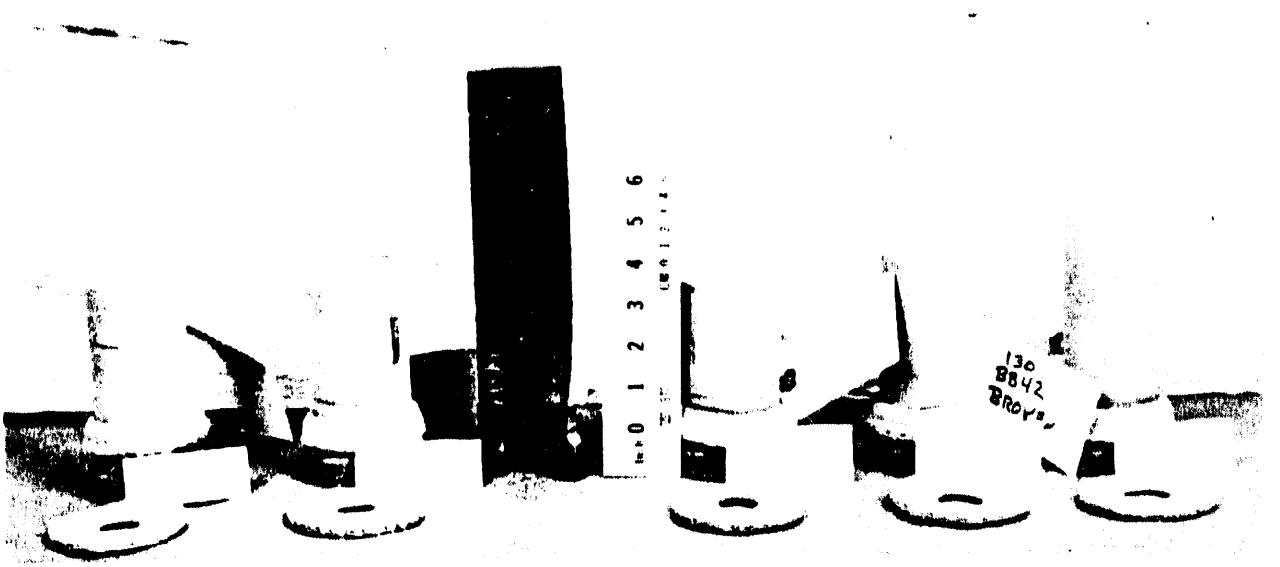

Figure 3.12 - Photograph Illustrating The Length Of The Fractured Candle Sections That Remained In The Filter Holders. A Heavy Deposit Of Ash Is Seen To Coat The Fractured Surfaces.

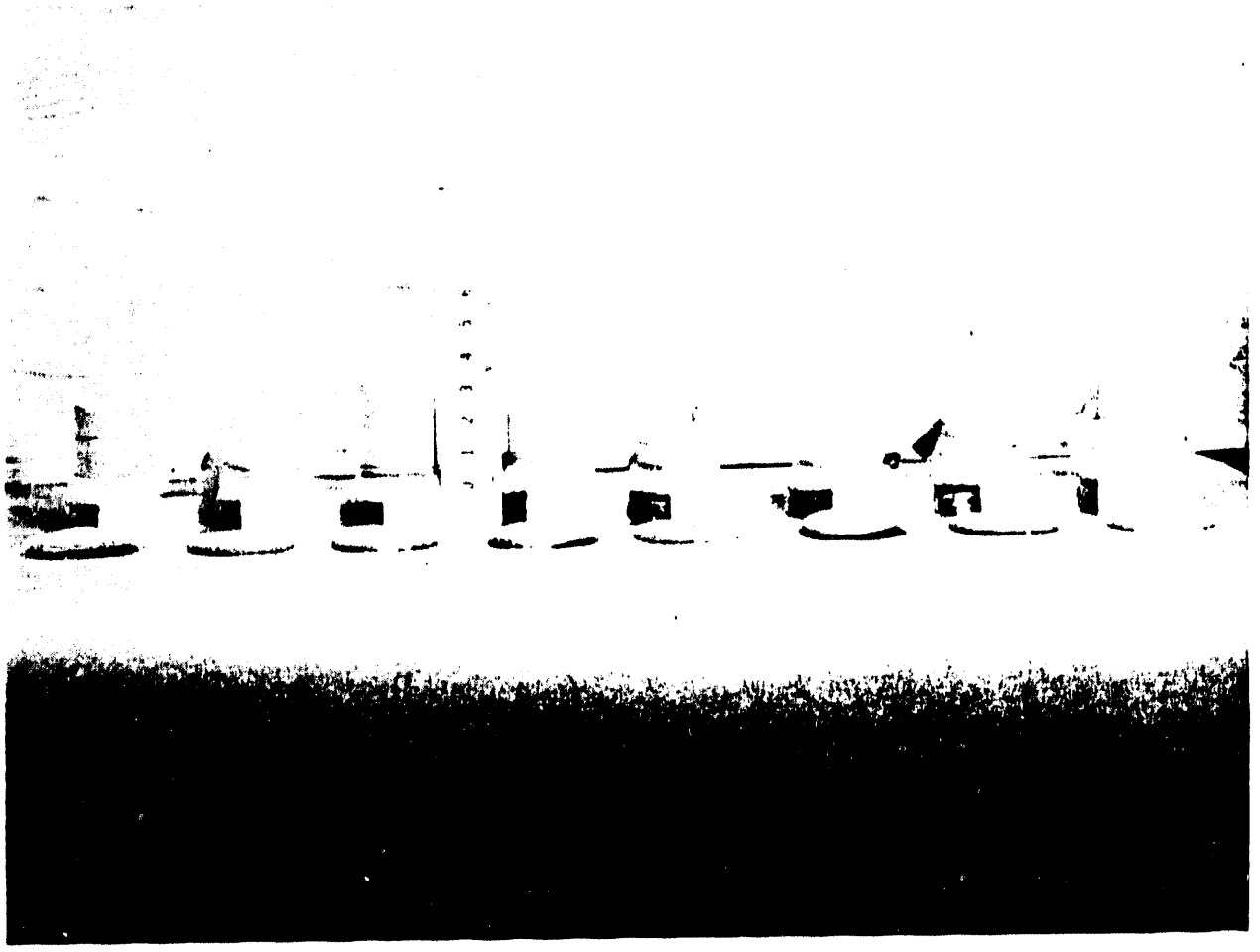

Figure 3.13 - Additional Photograph Illustrating The Length Of The Fractured Candle Sections That Remained In The Filter Holders. A Heavy Deposit Of Ash Is Seen To Coat The Fractured Surfaces.

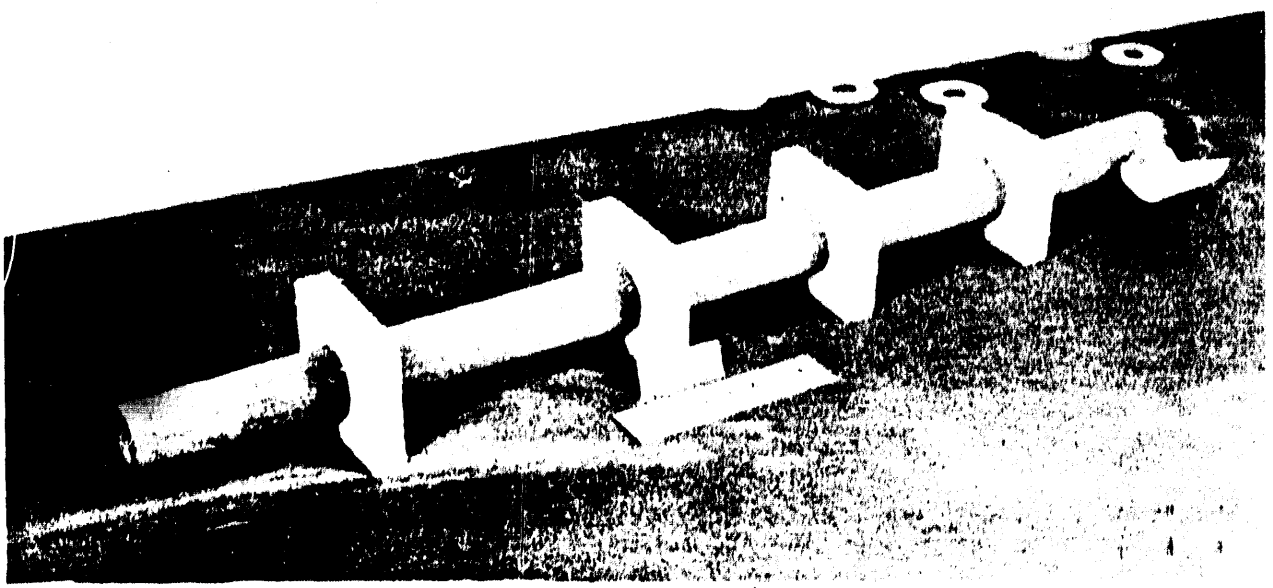

Figure 3.14 - Fractured Candle #062 (A/B-2)

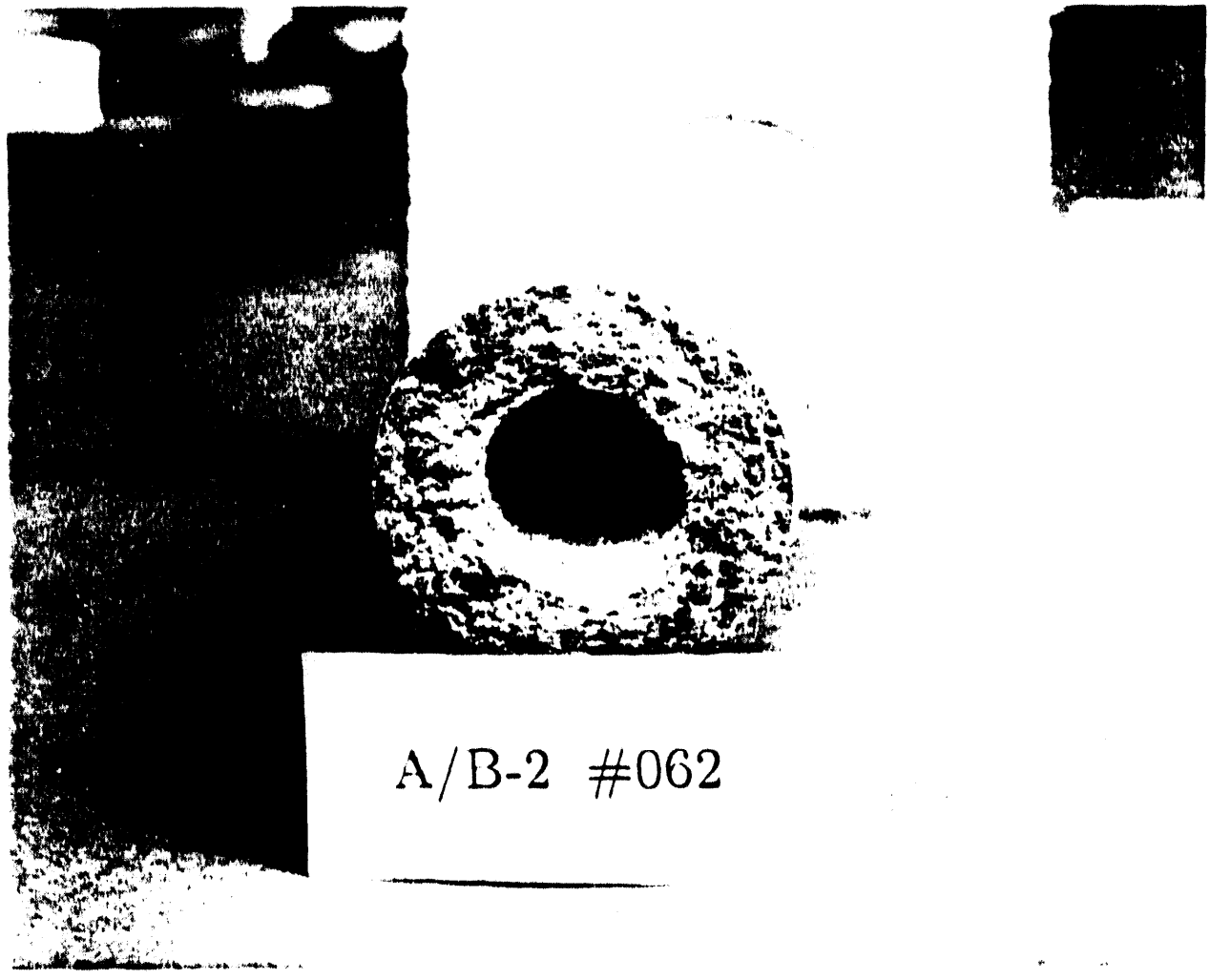

Figure 3.15 - Heavy Deposit Of Ash Along The Fractured Surface Of Candle #062 (A/B-2)

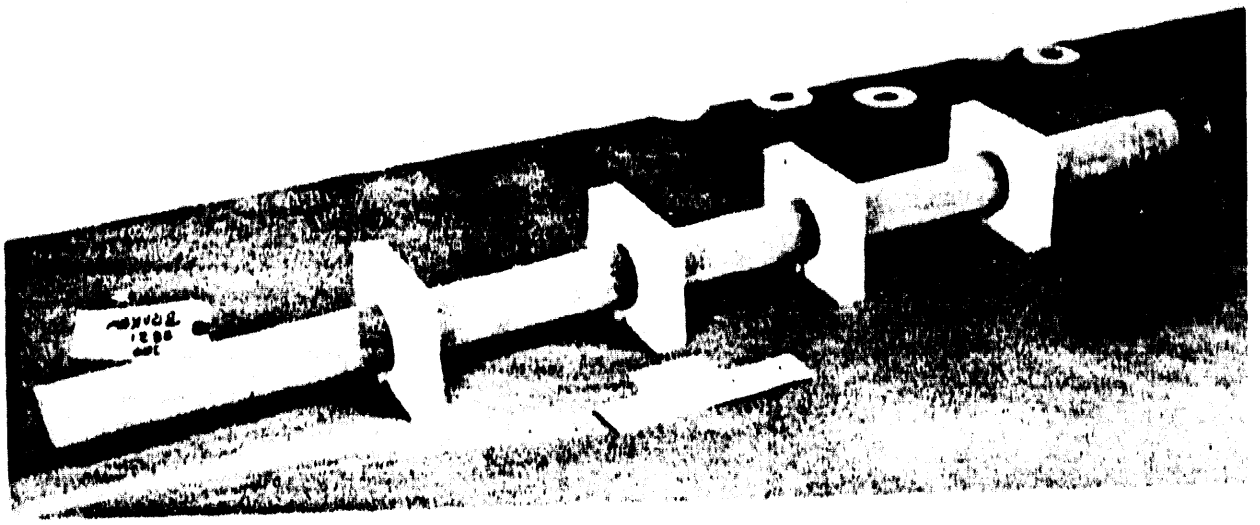

Figure 3.16 - Fractured Candle #309 (B/B-21)

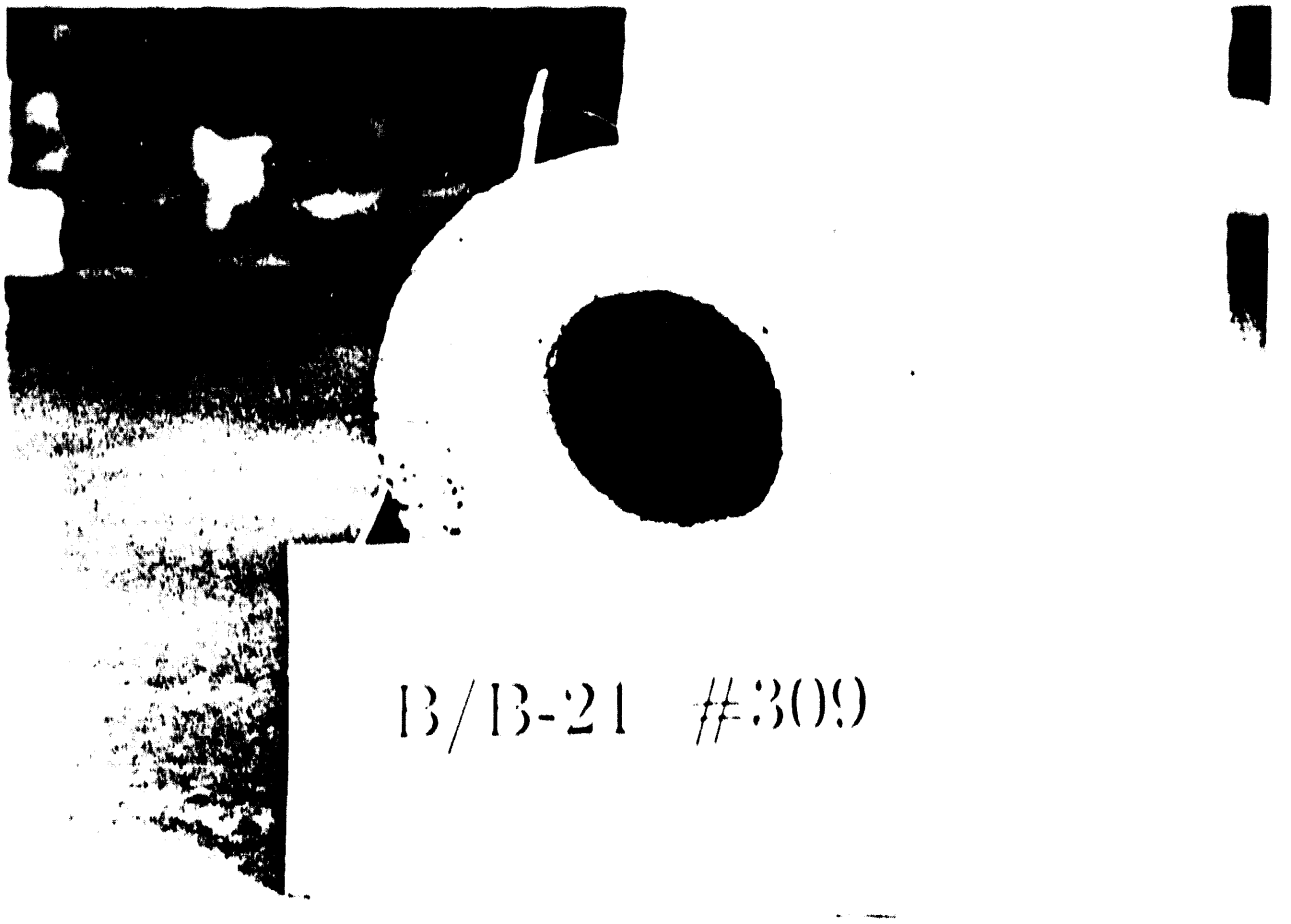

Figure 3.17 - Heavy Deposit Of Ash Along The Fractured Surface Of Candle #309 (B/B-21)

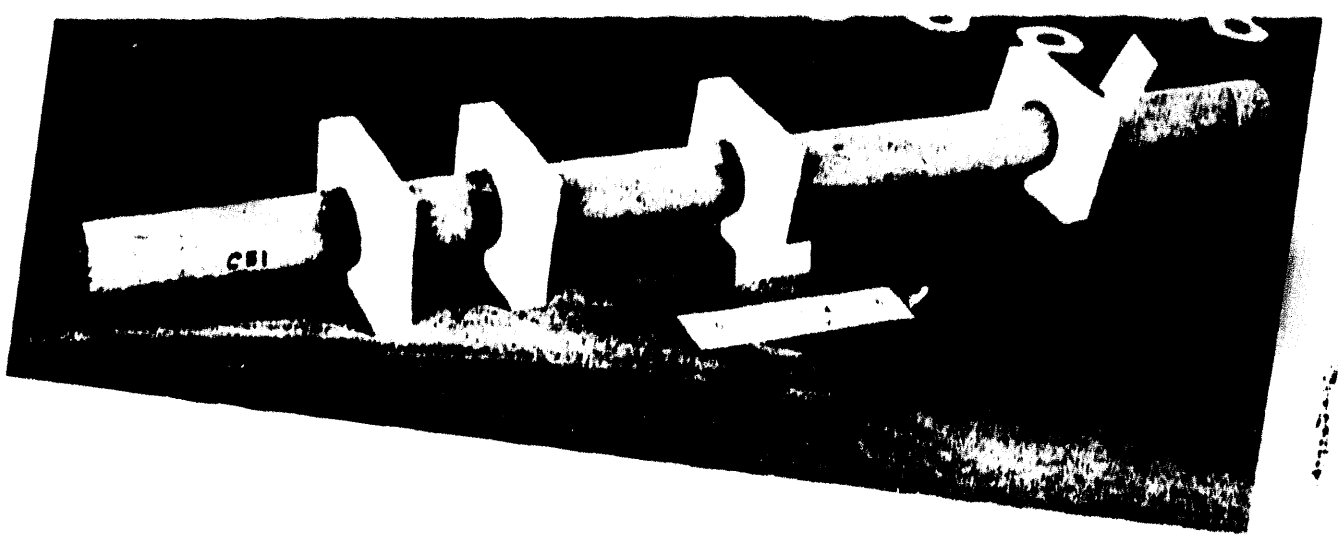

Figure 3.18 - Fractured Candle #308 (C/B-1)

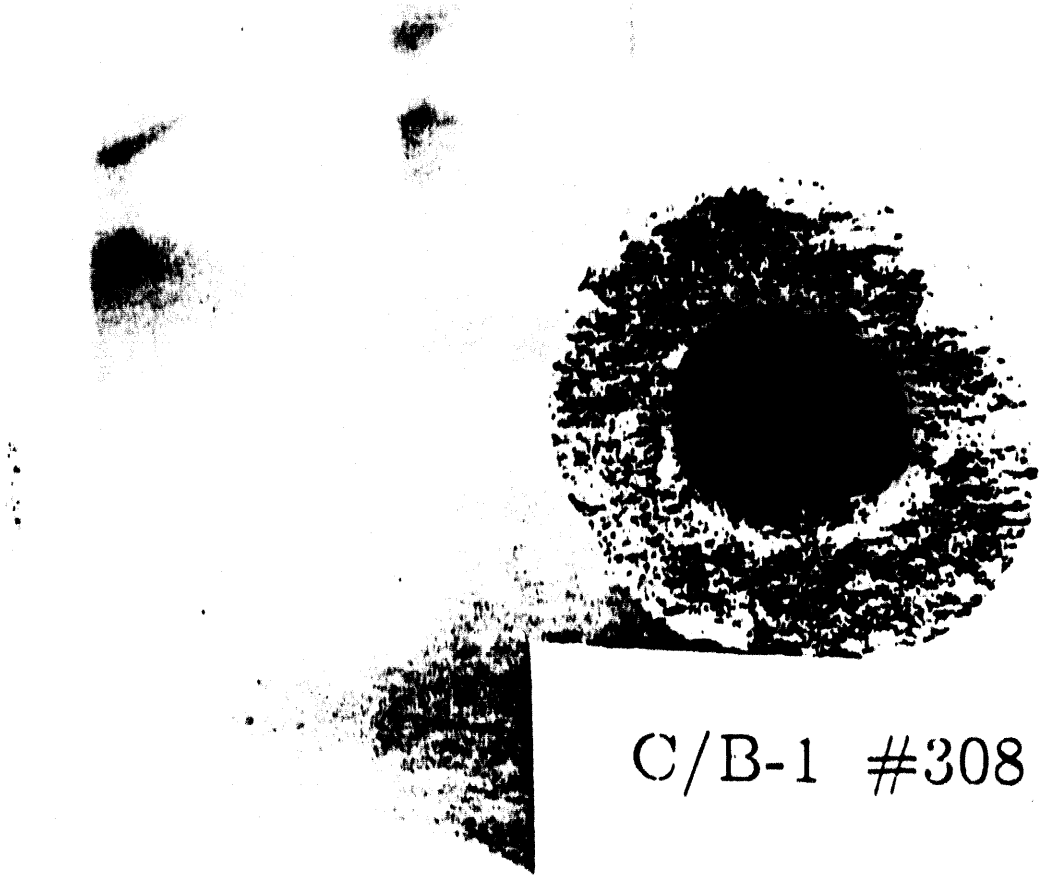

Figure 3.19 - Fresh Fractured Surface Of Candle #308 (C/B-1)

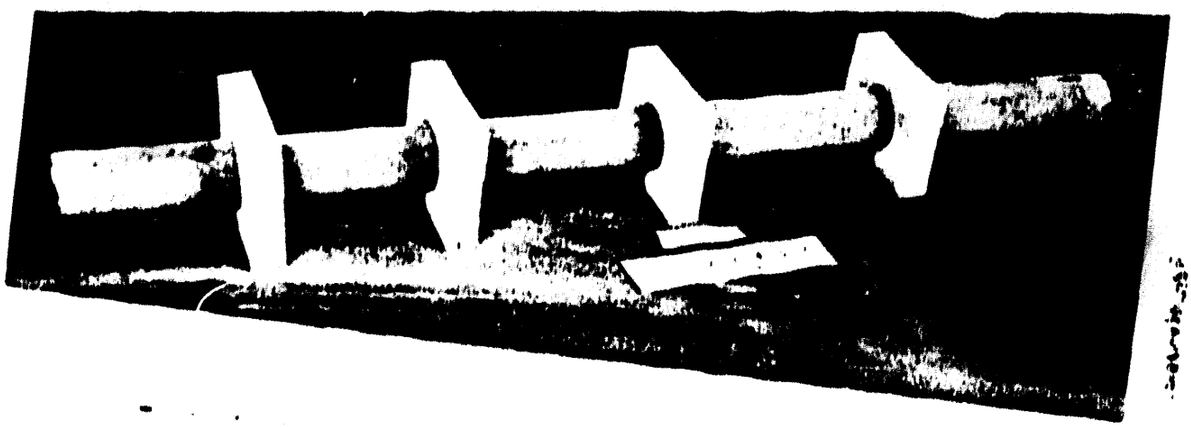

Figure 3.20 - Fractured Candle #310 (C/B-22)

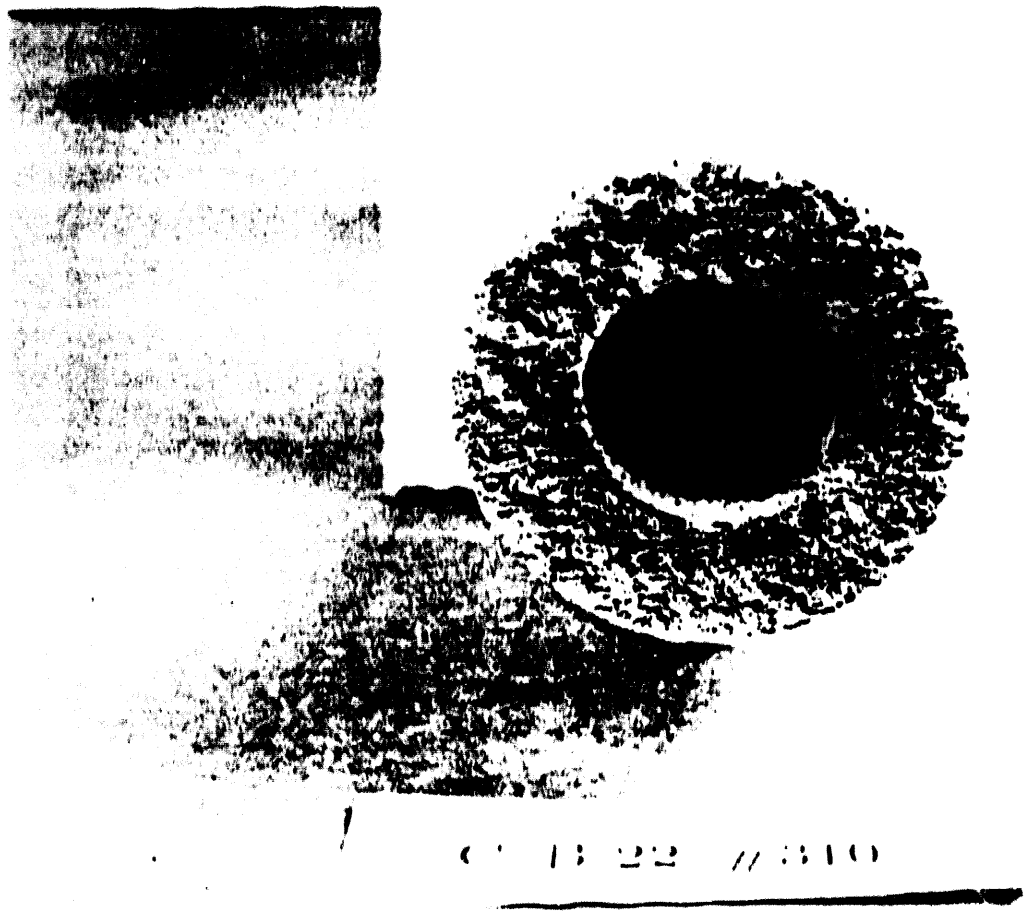

Figure 3.21 - Fresh Fractured Surface Of Candle #310 (C/B-22)

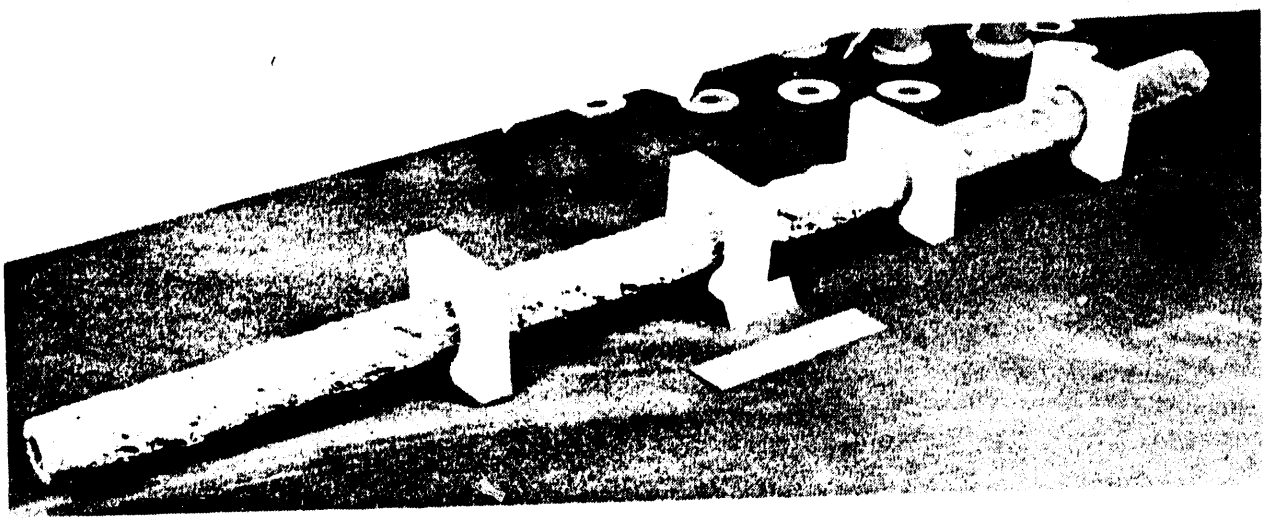

Figure 3.22 - Bottom Section Of Candle Filter #125 (B/B-43). Note The Dumpling-Like Ash Formations Along The Candle Filter Surface.

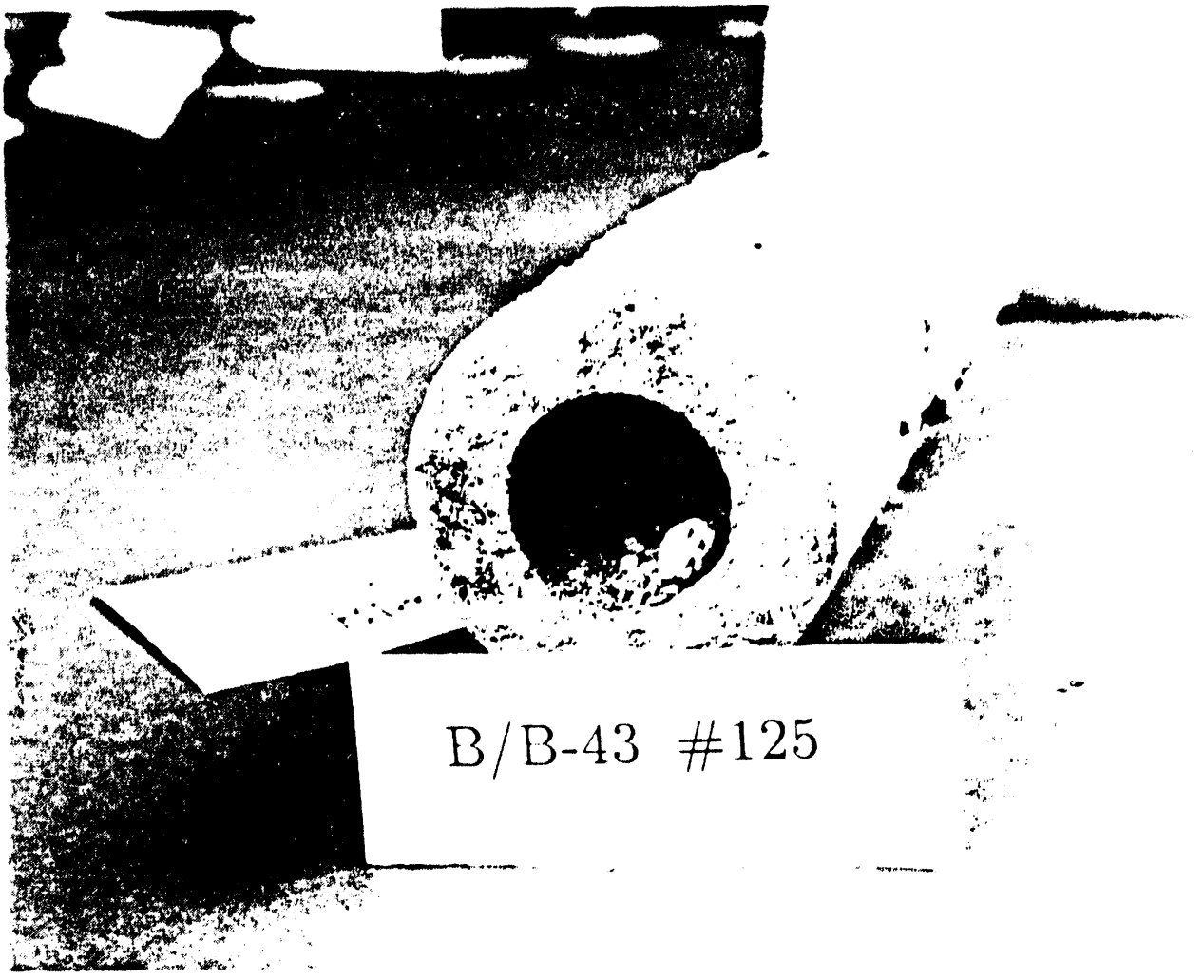

Figure 3.23 - Light Coating Of Ash Along The Fresh Fractured Surface Of Candle #125 (B/B-43)

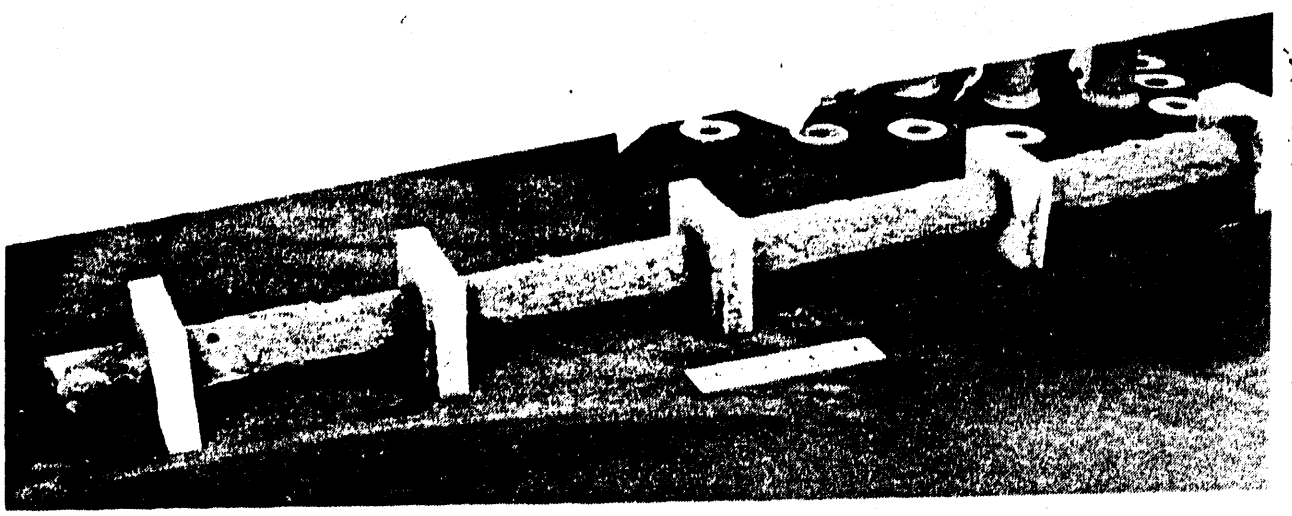

Figure 3.24 - Bottom Section Of An Unidentified Candle Filter. Note The Dumpling-Like Ash Formations Along The Candle Filter Surface.

Figure 3.25 - Heavy Coating Of Ash Along The Fractured Surface Of The Unidentified Candle

dumpling deposits were evident along the length of the candle body, typical of the ash deposits that remained along each candle at termination of the hot gas filtration test (Figures 3.8 through 3.10). The candle located in B/B-43 (#129) had a fresh fractured surface, indicating that the fracture either occurred during the hot gas filtration test whereby the bridged ash held the fractured section firmly in the candle array, or more likely at test termination during transfer of the candle array from the vessel to the support structure.

The second long, flangeless section of candle had an extremely heavy coating of dust along its fractured surface, implying that the break had occurred earlier during the test. The ash in the bottom plenum of Cluster B may have supported the candle section which had fractured and slightly shifted. We believe that this is the segment of candle that was seen to "hang" below the level of the other candles in the bottom plenum of Cluster B during post-test characterization.

From the 49 broken candle filter pieces that were removed from the ash hopper (Figure 3.6), we were able to reconstruct two near full length candles as shown in Figures 3.26 and 3.27, and two somewhat shorter candle bodies. Unfortunately the flangeless, near full length sections of candles could not be matched with any of the short sections that remained in the filter mount (Figures 3.11 through 3.13). This implied that perhaps an additional section of candle may have been removed between the flange section and the near full length candle body, or that additional chipping may have occurred along the fractured sections of candle that fell into the ash hopper.

The reassembled candles were noted to have an obvious bow along their length. One was bowed 5 mm (0.2 inches) over its 838 mm (33 inch) segment. Bowing suggested some period of sustained bending load that caused the candle to creep or a steady state thermal gradient across the candle diameter which caused a bending stress that was relaxed by

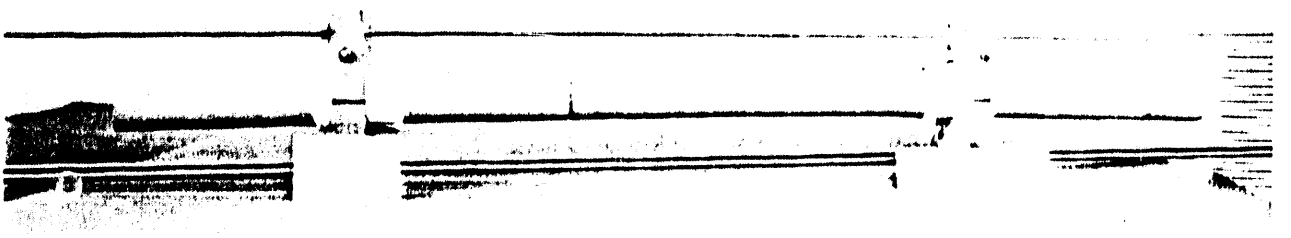

Figure 3.26 - Near Full Length Reconstructed Candle Filter

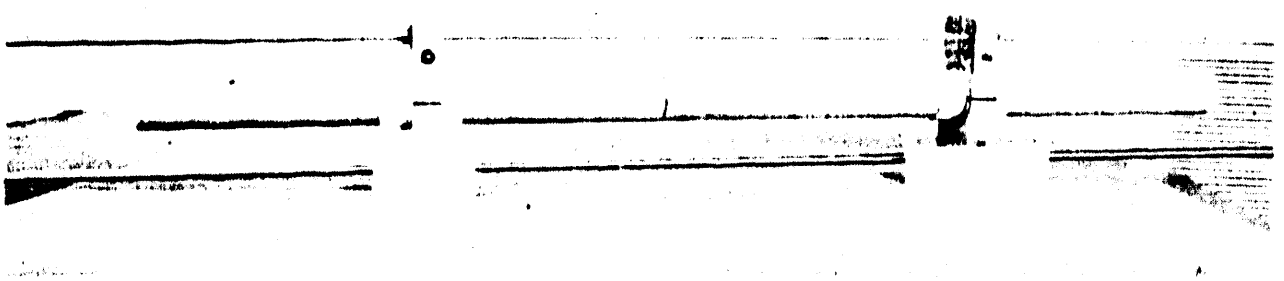

Figure 3.27 - Near Full Length Reconstructed Candle Filter

creeping. Further examination of the extent of bowing along the intact candle filters was also conducted. These results are presented in Section 4.

Fracture analysis of the failed candle filter segment was performed to establish the primary fracture surface and failure mode. Three of the reassembled candle sections had well developed "shear lips", typical of a beam broken in a bending mode. The fourth reassembled candle section did not have a well defined lip, but appeared to have somewhat of an abraded fracture surface. This may have occurred during handling and shipping. There was no evidence of longitudinal cracking along any of the primary fracture surfaces. Similarly the secondary fractures were virtually all transverse breaks.

Since the top and middle candle arrays remained completely intact, failure along the bottom candle arrays was related to ash bridging. The presence of the bow along the failed candle filter sections, as well as the "shear lip" on the primary fracture surface suggested that either there was a catastrophic event (i.e., in addition to a sustained load) such as a cascade of ash which caused a shock wave, or a sustained bending load which caused delayed failure in bending. The bow appeared in general to be in the appropriate direction relative to the "shear lip", suggesting the latter scenario.

4. PHYSICAL PROPERTIES OF THE CLAY BONDED SILICON CARBIDE CANDLE FILTERS AFTER EXPOSURE AT TIDD

After termination of the Westinghouse APF test in December 1992, inspection and characterization of the top, middle, and bottom plenum candles were performed. As shown in Figures 4.1 through 4.9, all candles in the top and middle arrays appeared to remain virtually intact, while failure of 21 candle filter elements occurred in the bottom arrays. Notably the bottom candle arrays were heavily bridged with ash, while ash bridging between adjacent candles along the top and middle arrays was limited. Ash dumpling-like deposits were readily evident along the top and middle candle arrays, as well as a white surface coating which was characteristic of sorbent carryover to each filter element surface.

In an attempt to determine whether there were any major process system differences between the top, middle, and bottom candle locations during the 500 hours of hot gas filtration, inspection and physical property characterization were performed on:

- Twenty-three (23) surveillance candles that were removed from the bottom plenums. Note A/B-1 #150 which was one of the original 24 surveillance candles in the bottom cluster fractured during the 500 hour hot gas filtration test period.

- Two (2) surveillance candles that were removed from the middle plenum arrays.

- Two (2) surveillance candles that were removed from the top plenum arrays.

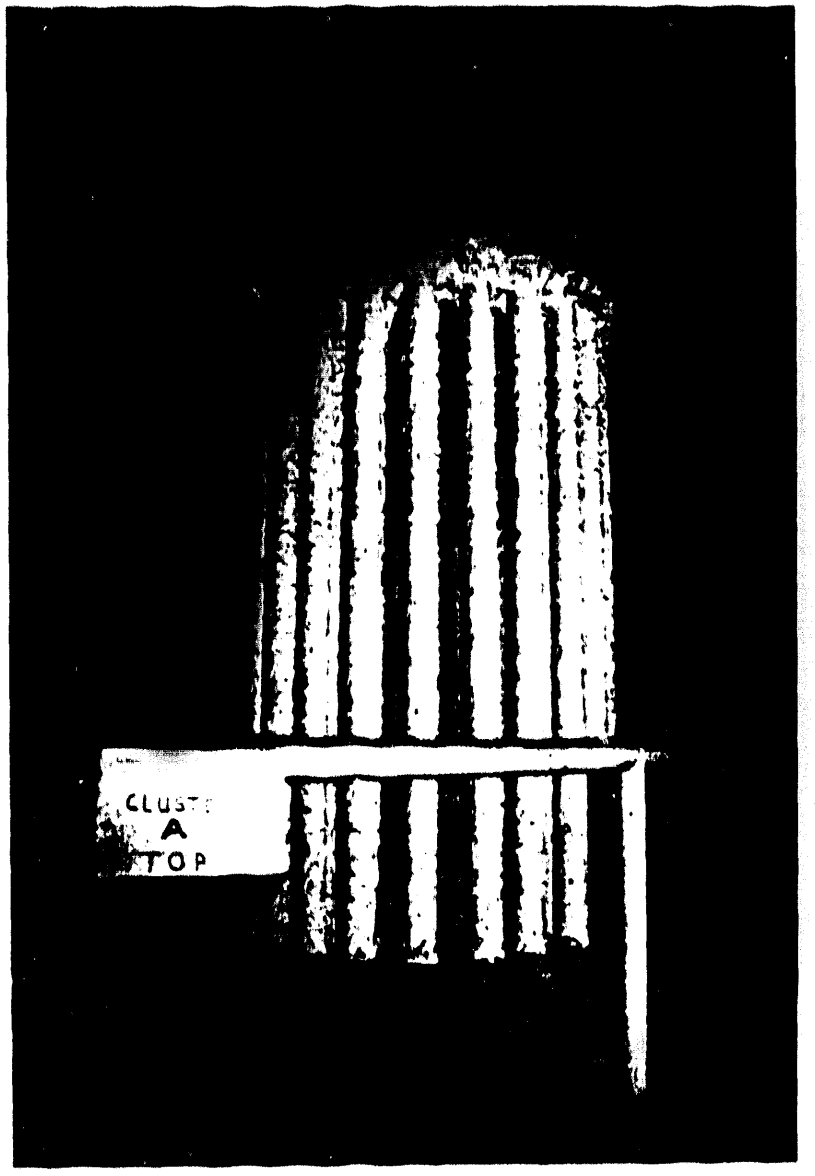

Figure 4.1 - Candle Filter Cluster A/T After 500 Hours Of Hot Gas Filtration

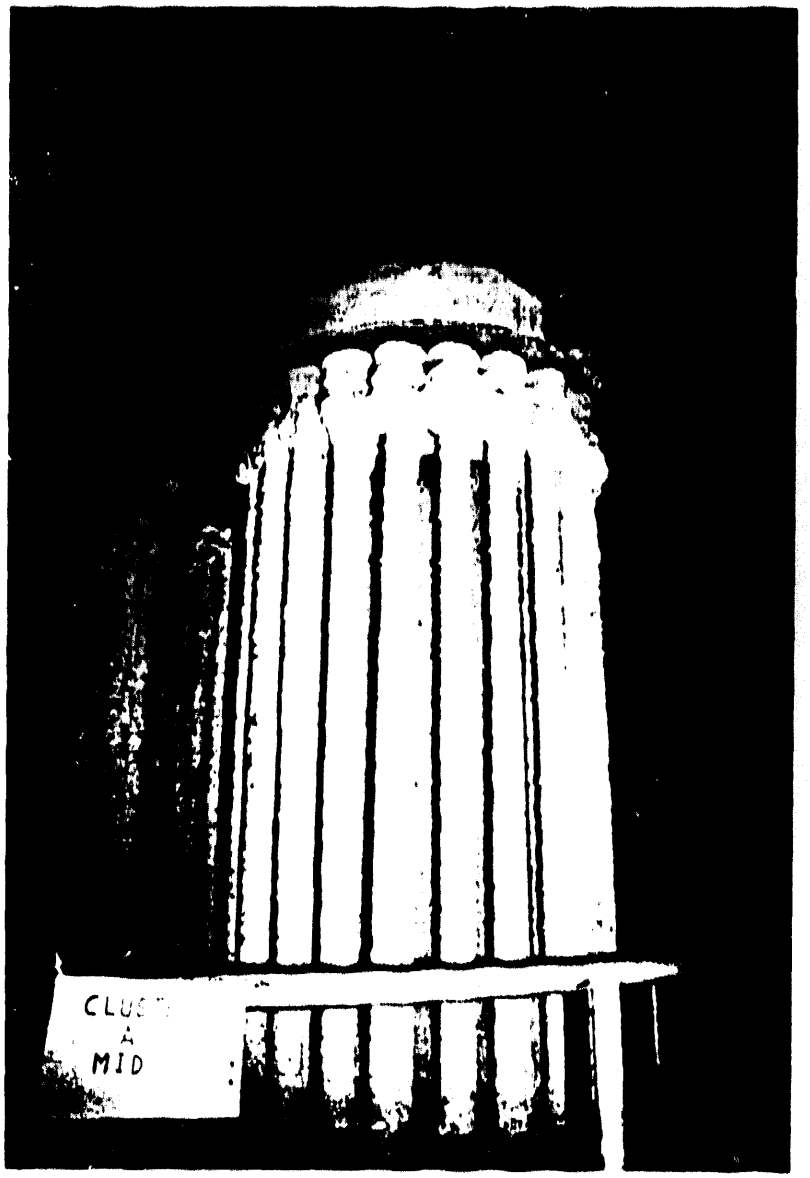

Figure 4.2 - Candle Filter Cluster A/M After 500 Hours Of Hot Gas Filtration

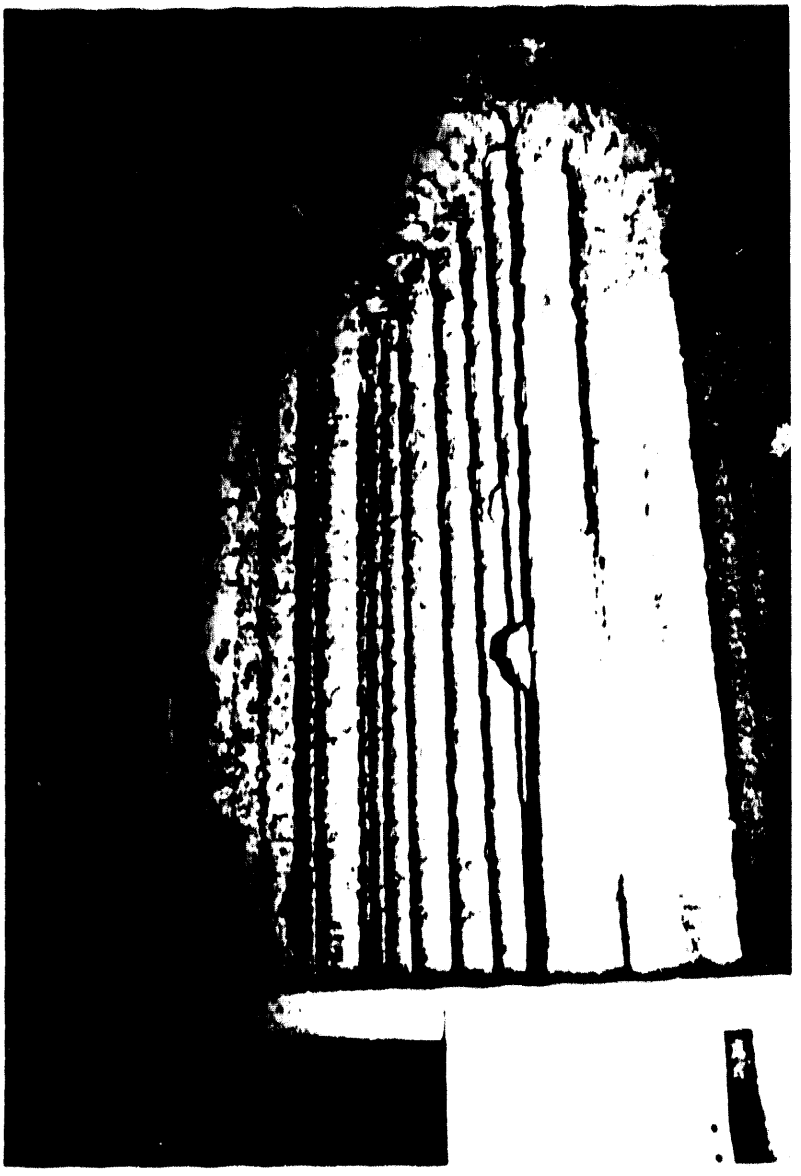

Figure 4.3 - Candle Filter Cluster A/B After 500 Hours Of Hot Gas Filtration

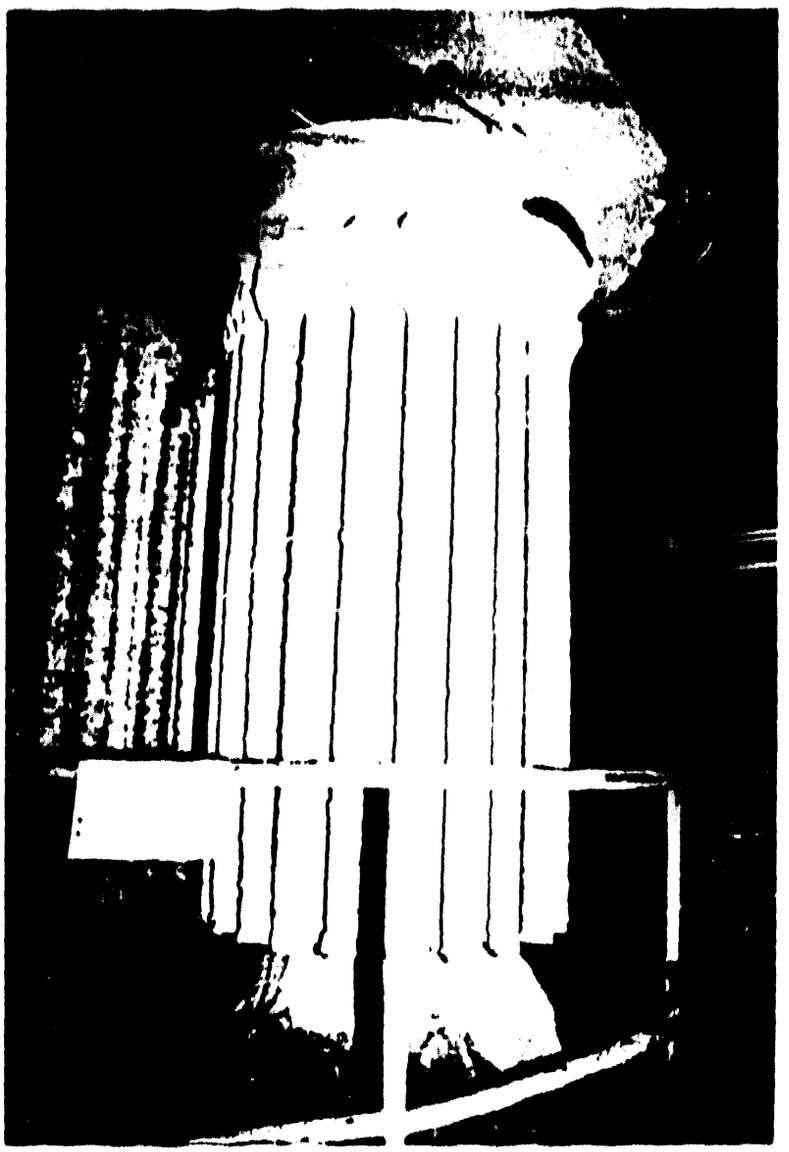

Figure 4.4 - Candle Filter Cluster B/T After 500 Hours Of Hot Gas Filtration

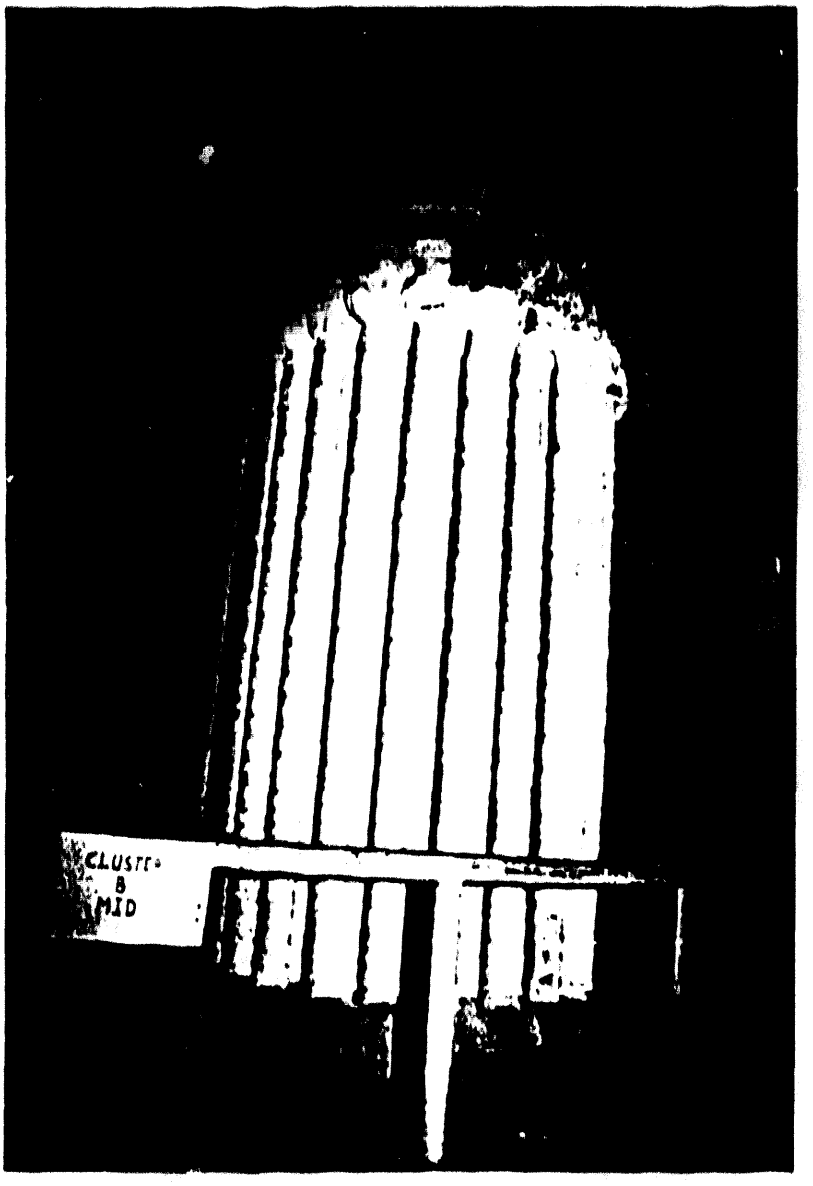

Figure 4.5 - Candle Filter Cluster B/M After 500 Hours Of Hot Gas Filtration

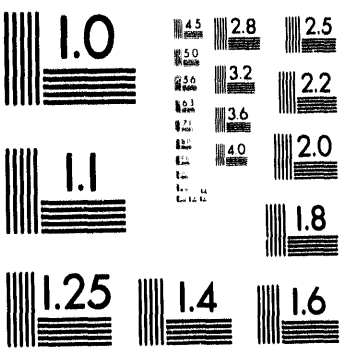
1.0
1.1
1.25
1.4
1.6
1.8
2.0
2.2
2.5
2.8
3.2
3.6
4.0
4.5
5.0
5.6
6.3
7.1
8.0
9.0
10.0

2 of 3

Figure 4.6 - Candle Filter Cluster B/B After 500 Hours Of Hot Gas Filtration

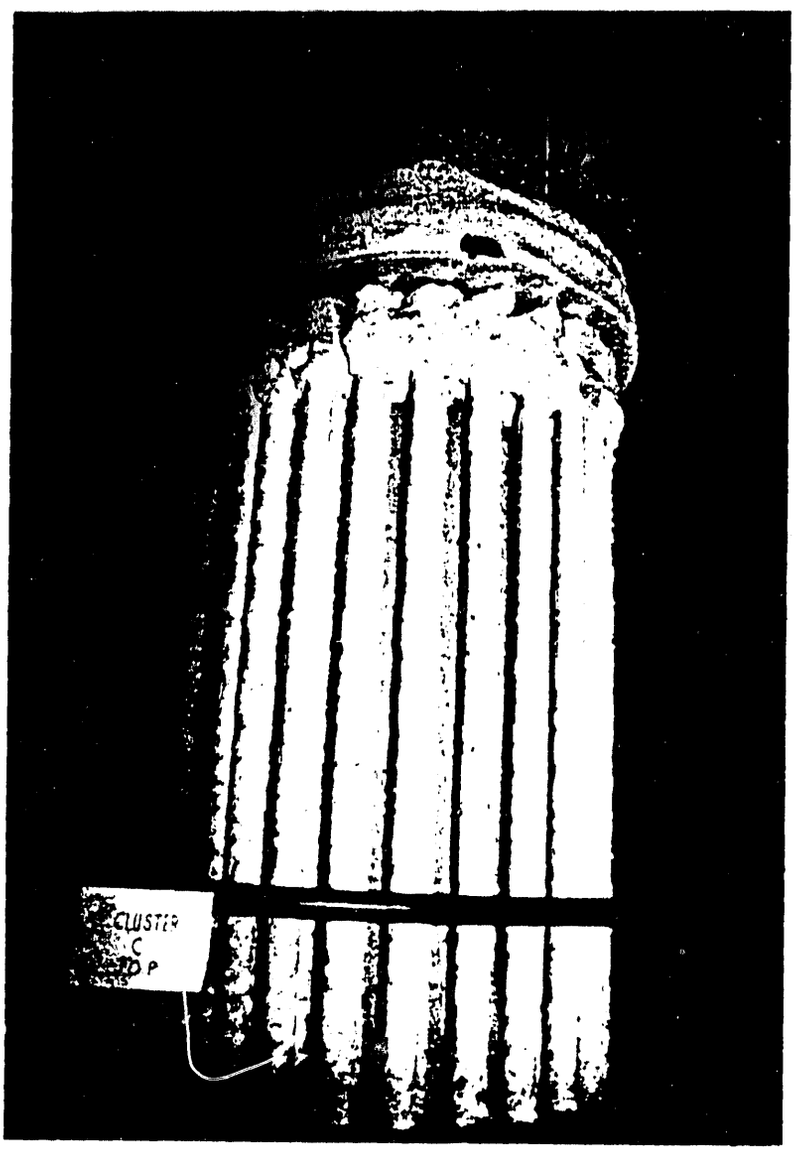

Figure 4.7 - Candle Filter Cluster C/T After 500 Hours Of Hot Gas Filtration

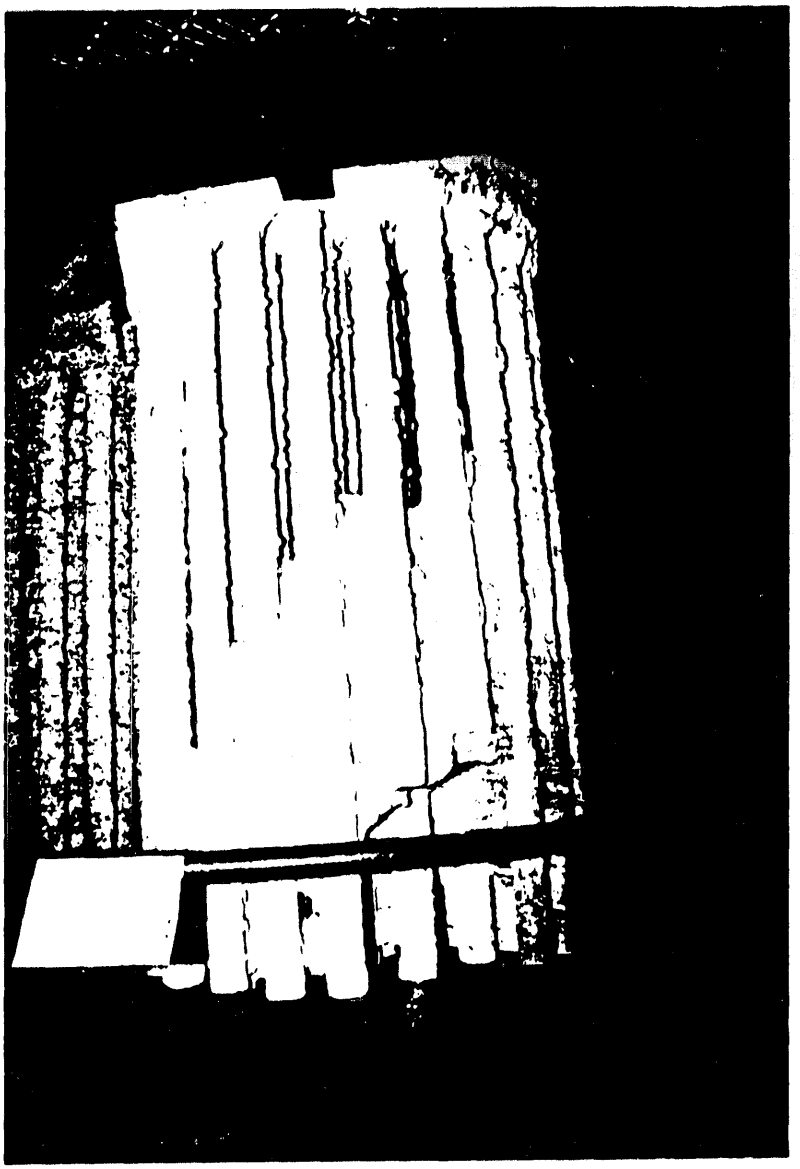

Figure 4.9 - Candle Filter Cluster C/B After 500 Hours Of Hot Gas Filtration

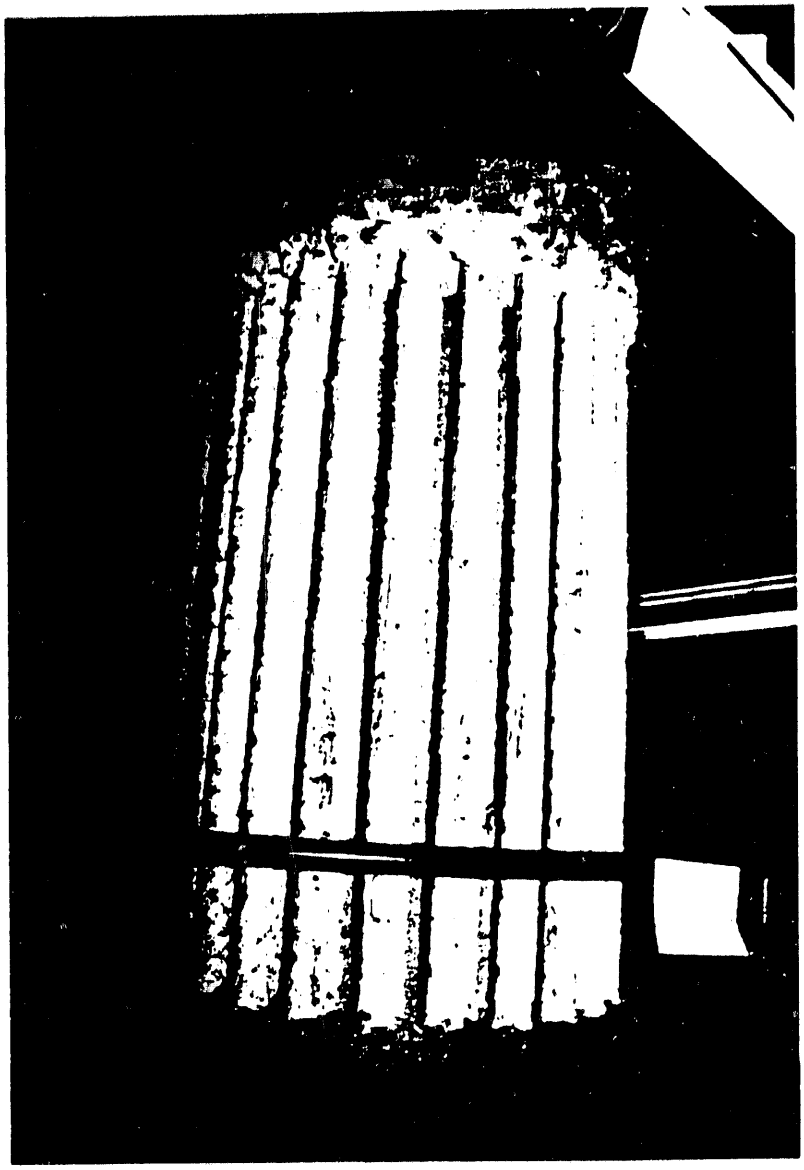

Figure 4.8 - Candle Filter Cluster C/M After 500 Hours Of Hot Gas Filtration

Five (5) additional candles were removed for inspection and physical property characterization. These included:

- One candle from an inner ring along a top array (B/T-23 #459)
- One candle from an inner ring along a middle array (B/M-23 #244)
- One additional candle along the outer ring in the bottom array of Cluster C (C/B-5 #187)
- Two bowed candles along the inner rings in the bottom array of Cluster B (B/B-34 #127; B/B-45 #106).

Figure 4.10 identifies the location of the candle filters that underwent in-depth physical and chemical post-test characterization. Post-test characterization of each filter element included pressure drop, length, and bow, as well as time-of-flight (TOF) measurements. The results of these analyses are presented in this section. A comparison of these results will be made with similar as-manufactured candle measurements. A discussion of the changes that resulted in the morphology and composition of the filter matrix is presented in Section 6. Strength characterization which included both C-ring compression and burst strength testing, as well as Auger analysis and gravimetric analysis to determine the extent of oxidation that may have occurred in the clay bonded silicon carbide matrix are presented in Section 7.

4.1 POST-TEST CANDLE FILTER PRESSURE DROP MEASUREMENTS

All thirty-two (32) field-tested candle filters were tested in terms of pressure drop across each filter at room temperature. The dumpling-like ash deposits along the candle OD were retained initially during the pressure drop measurements. In comparison to the as-

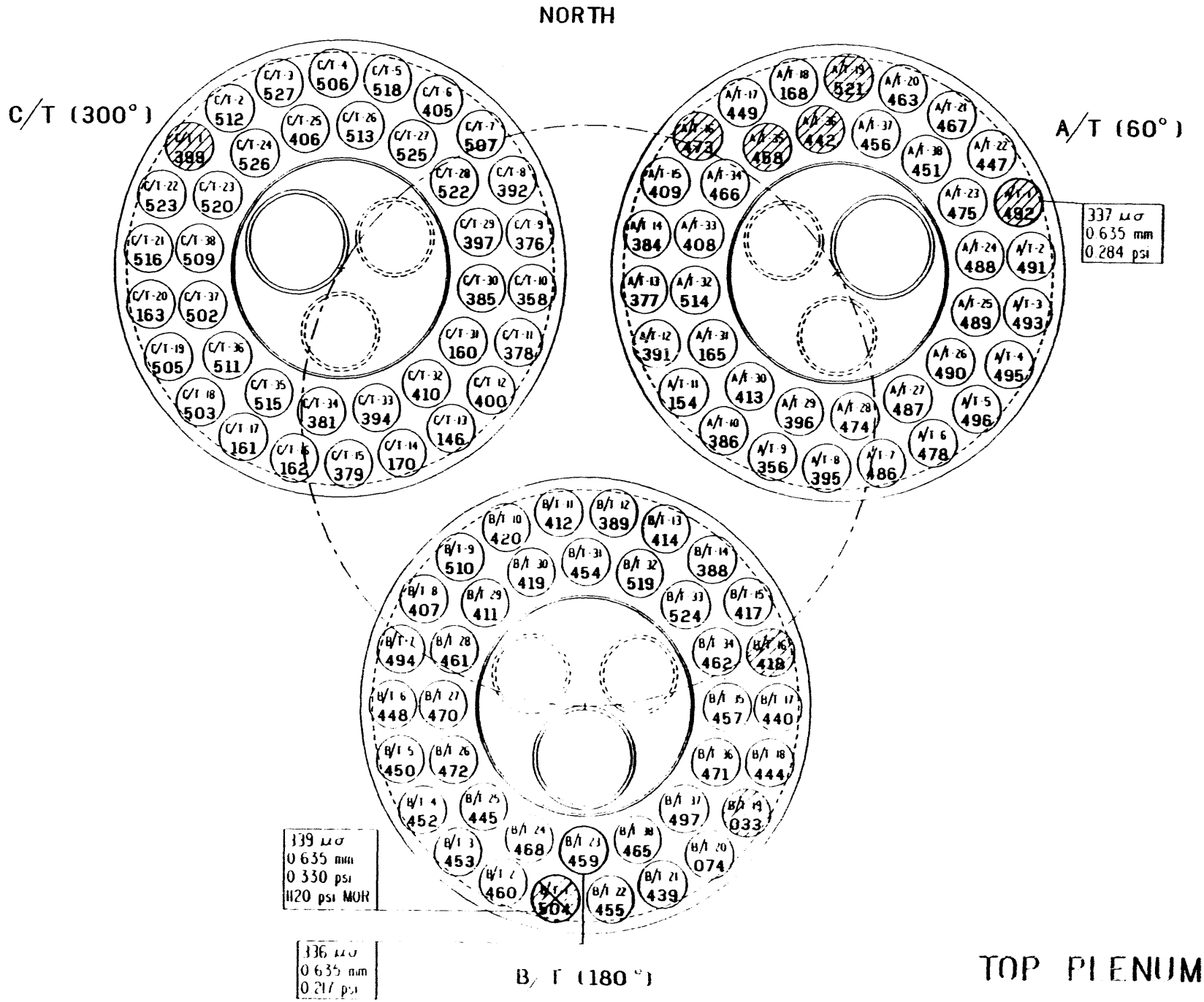

Figure 4.10 - Location of Candle Filters That Underwent In-Depth Physical/Chemical Post-Test Characterizations

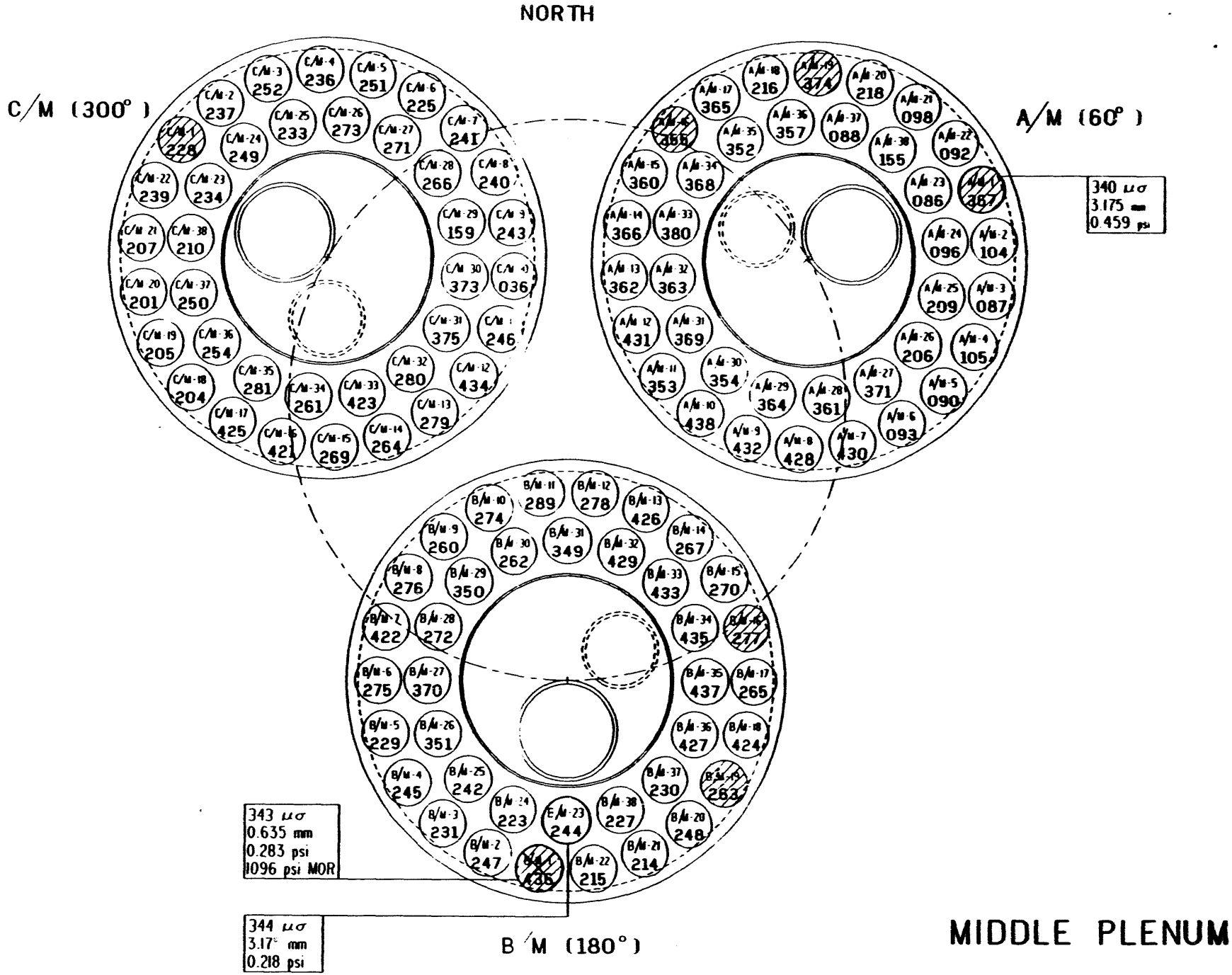

Figure 4.10 (Cont'd) - Location of Candle Filters That Underwent In-Depth Physical/Chemical Post-Test Characterizations

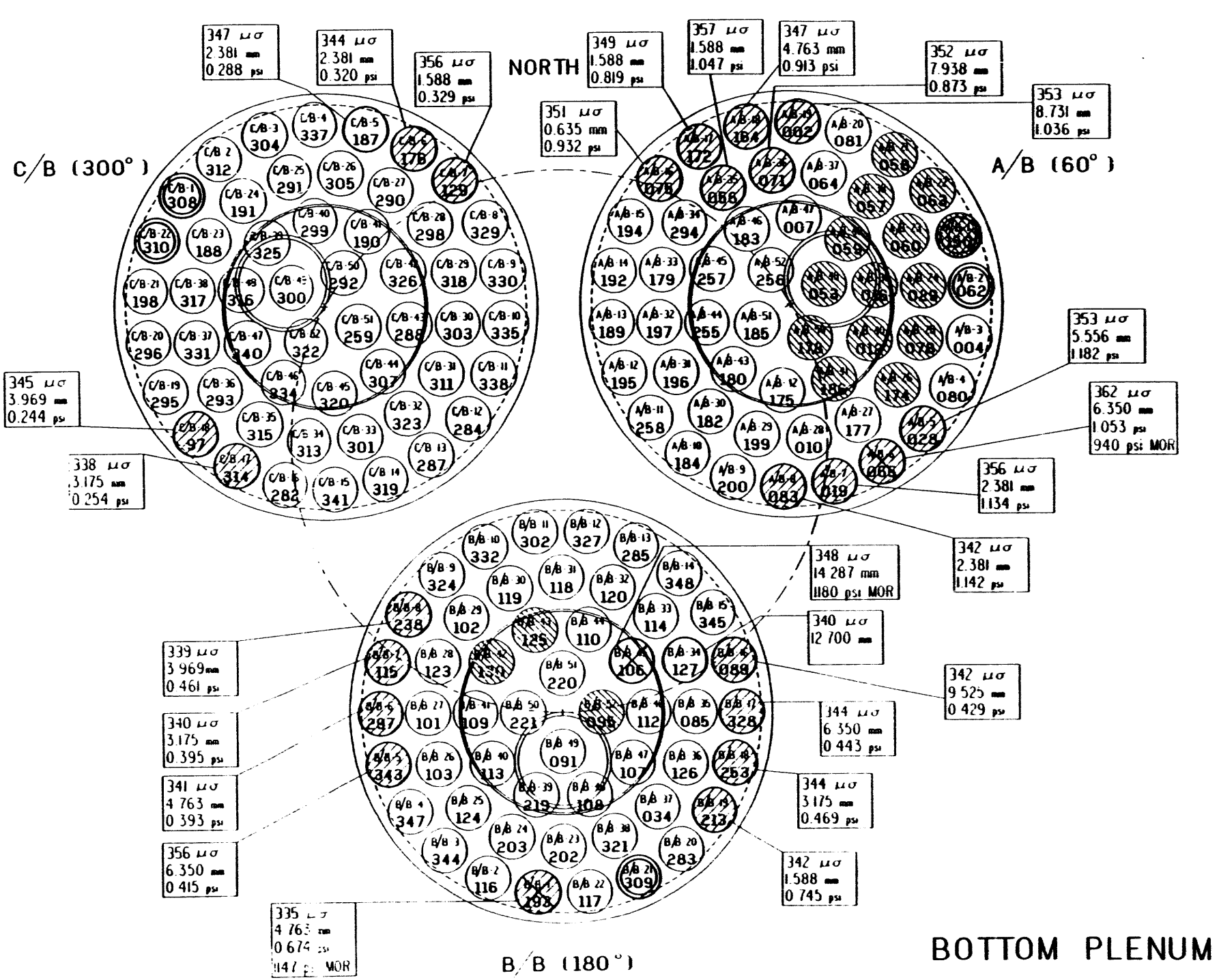

Figure 4.10 (Cont'd) - Location of Candle Filters That Underwent In-Depth Physical/Chemical Post-Test Characterizations

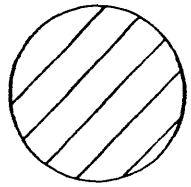

INITIAL SURVEILLANCE CANDLES

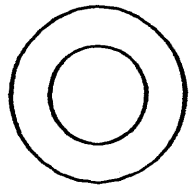

FRACTURE 12/92: CANDLE LENGTH REMAINING IN FLANGE/MOUNT
> 1100 mm

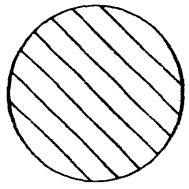

FRACTURE 12/92: CANDLE LENGTH REMAINING IN FLANGE/MOUNT
< 165 mm

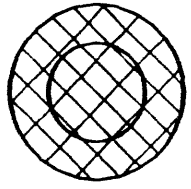

INITIAL SURVEILLANCE CANDLE: DURING INITIAL INSPECTION
LOWER PORTION WAS REMOVED DURING LIFT.
FRACTURE OCCURED NEAR FLANGE/MOUNT.

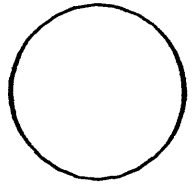

TOF AND/OR PERMEABILITY CHARACTERIZATION 1/93.

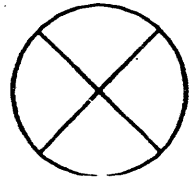

C-RING COMPRESSION TESTING 2/93

Figure 4.10 (Cont'd) - Location of Candle Filters That Underwent In-Depth Physical/Chemical Post-Test Characterizations

manufactured clay bonded silicon carbide candle filters, the dumpling-like ash deposits and thin white sorbent layer restrict air flow through the filter, and consequently a higher pressure drop across the 500 hour PFBC exposed candle filter resulted. In principle when the ash and sorbent fines are removed from the filter OD (i.e., vacuumed brushed), the pressure drop should decrease to an intermediate value (i.e., between the pressure drop for the original, as-manufactured candle filter and the "dirty" candle after field testing). As process temperature increases the projected pressure drop increases across the field tested candle filters (Figures 4.11 through 4.14).

The pressure drop data generated for each of the 32 candles is presented in Table 4.1. These data include the actual room temperature measurements for each candle in its as-received state (i.e., ash dumpling deposits, as well as thin sorbent layer), and projected pressure drop across each candle at nominal hot gas filtration temperatures (843°C; 1550°F). Similar data are provided for each of the 32 candle filters after vacuum brushing.

Based on previous experience using the clay bonded silicon carbide candle filters, a factor of 1.95 was used to calculate the projected pressure drop across the filter at high temperature, in comparison to the room temperature data. In contrast, laboratory data generated at Westinghouse STC indicated that a 2.5 factor resulted between the room temperature and high temperature pressure drop data for the alumina/mullite filter elements.

Table 4.1 indicates that the ash cake dumplings and thin sorbent layer significantly increase the pressure drop across the candle filters. Review of Table 4.1 indicates that vacuum brushing the OD of each candle either removed significant ash and sorbent to lower the pressure drop across the filter element, or enhanced pore plugging along the OD surface to increase the filter pressure drop measurement.

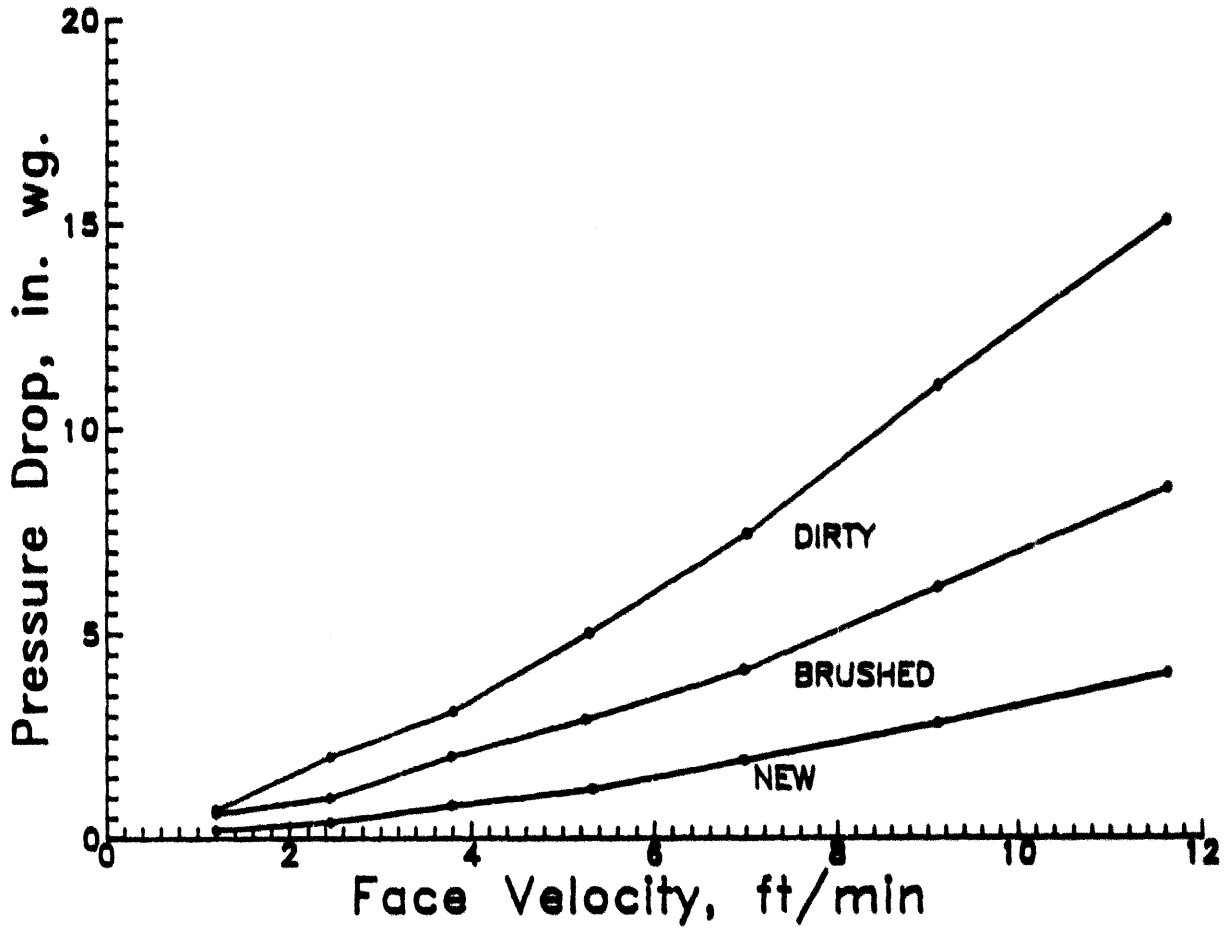

Figure 4.11 - Room Temperature Measurement Of The Pressure Drop Across The Clay Bonded Silicon Carbide Candle Filters

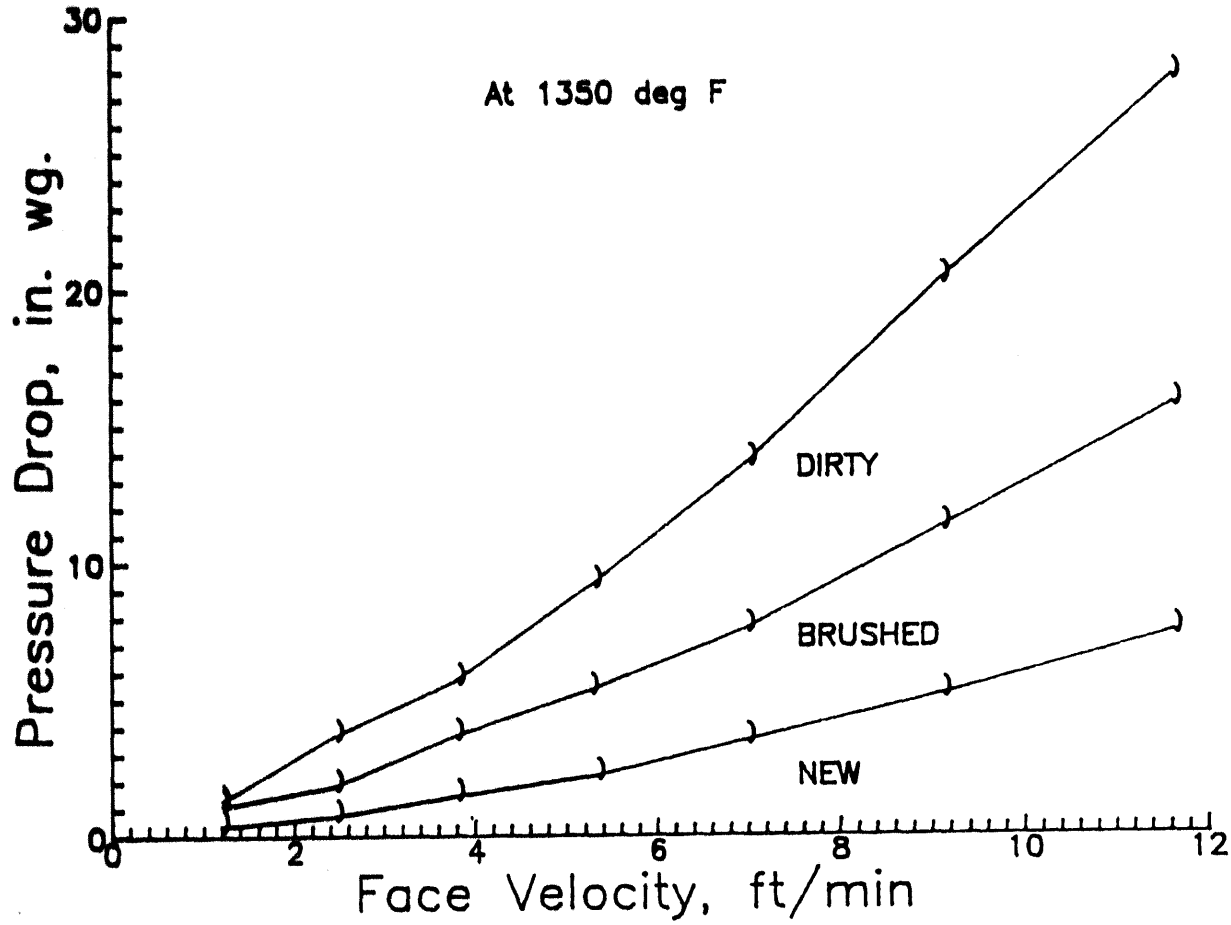

Figure 4.12 - Pressure Drop Across The Clay Bonded Silicon Carbide Candle Filters Projected At 730°C (1350°F) Hot Gas Filtration Temperatures

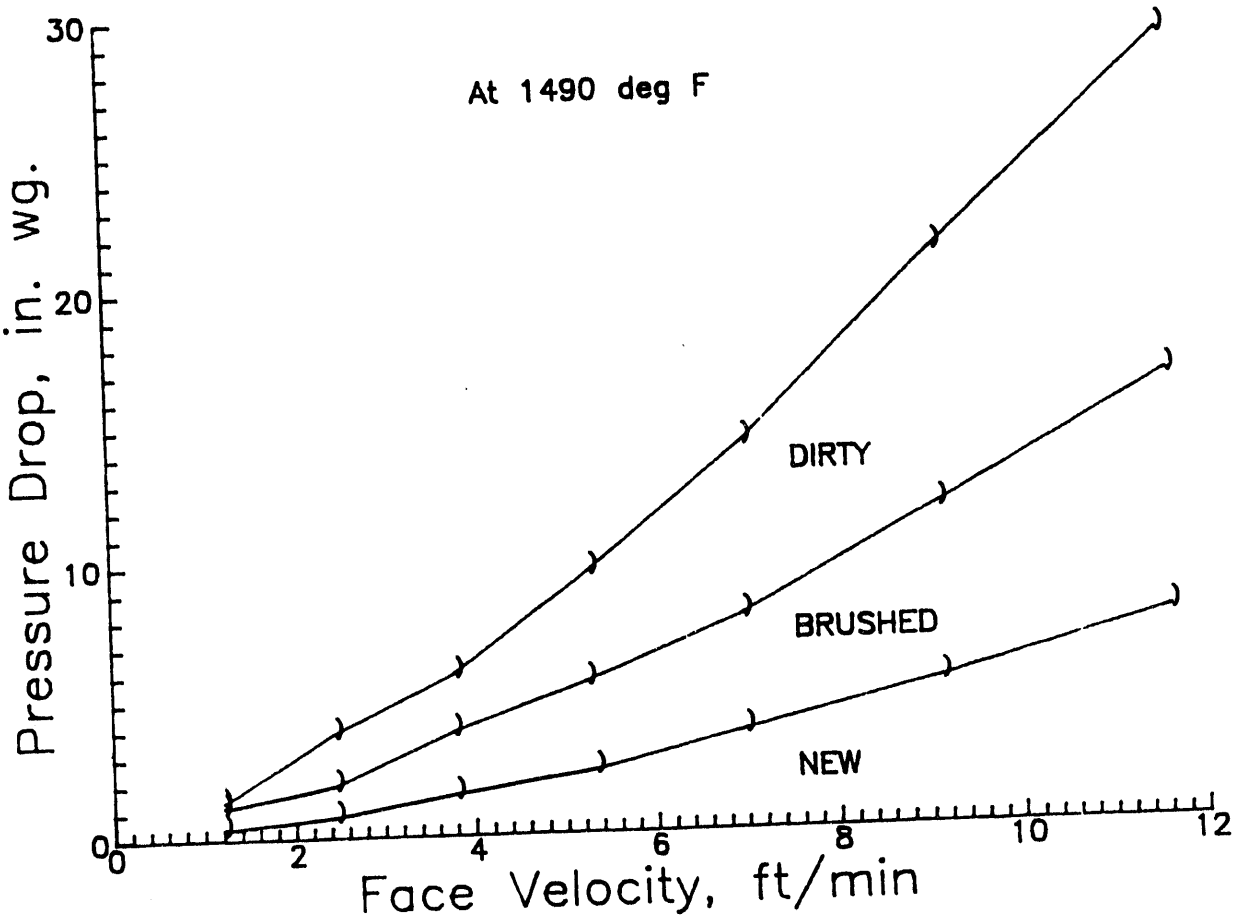

Figure 4.13 - Pressure Drop Across The Clay Bonded Silicon Carbide Candle Filters Projected At 810°C (1490°F) Hot Gas Filtration Temperatures

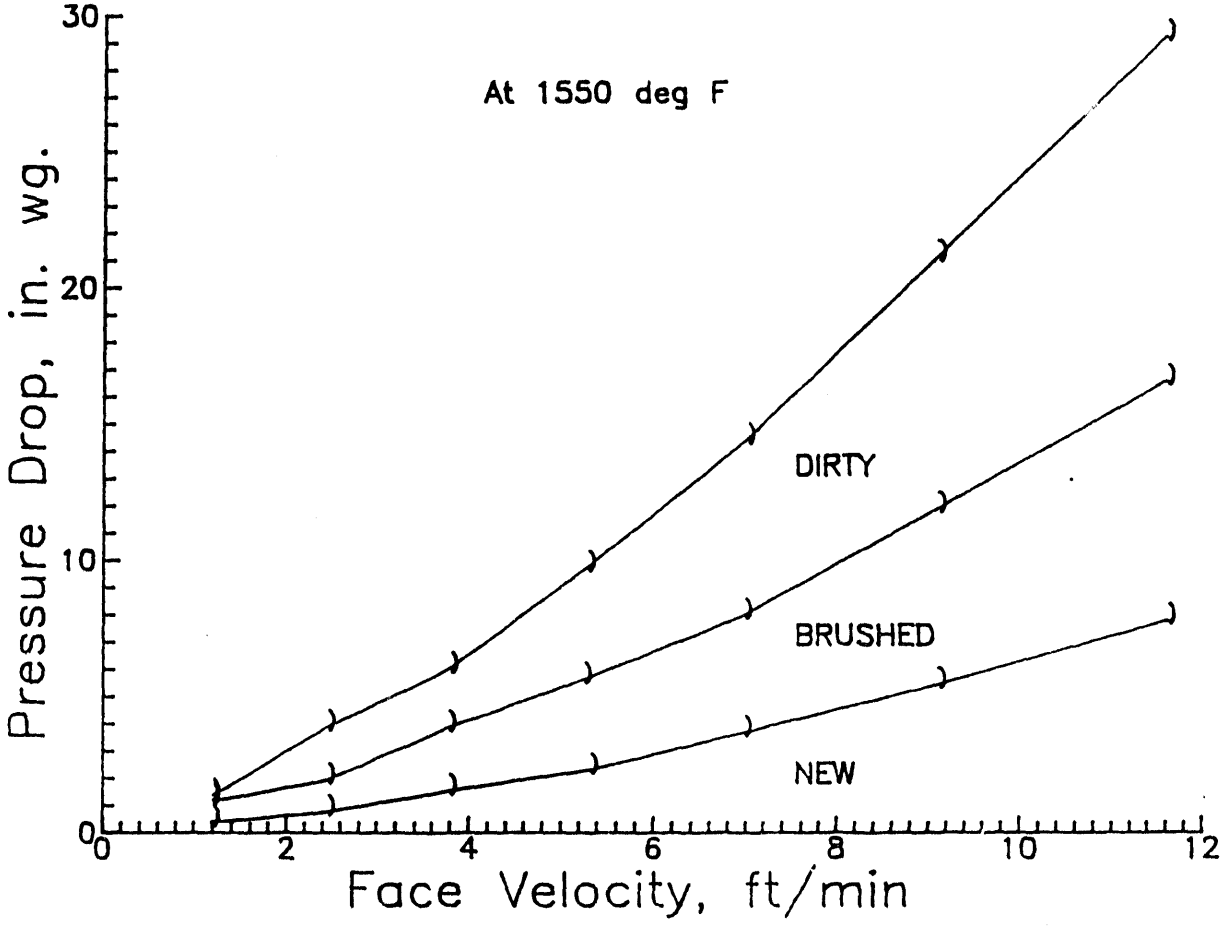

Figure 4.14 - Pressure Drop Across The Clay Bonded Silicon Carbide Candle Filters Projected At 843°C (1550°F) Hot Gas Filtration Temperatures

TABLE 4.1

POST-TEST CANDLE FILTER PRESSURE DROP MEASUREMENTS

Candle	Position	ID No.	Pressure Drop, psi at 10 ft/min				
			Initial	As-Received		Vacuumed	Brushed
			21°C (70°F)	21°C (70°F)	843°C (1550°F)**	21°C (70°F)	843°C (1550°F)
1	A/T-1 *	492		0.284	0.553	0.309	0.602
2	B/T-1 *	504	0.123	0.330	0.642	0.230	0.447
3	B/T-23	459		0.217	0.422	0.214	0.417
4	A/M-1 *	367		0.459	0.894	0.257	0.501
5	B/M-1 *	436		0.283	0.552	0.209	0.408
6	B/M-23	244		0.218	0.424	0.233	0.454
7	A/B-5 *	028		1.182	2.302	1.182	2.302
8	A/B-6 *	065		1.053	2.050	1.029	2.004
9	A/B-7 *	019		1.134	2.209	1.101	2.131
10	A/B-8 *	083		1.142	2.223	1.190	2.318
11	A/B-16 *	075		0.932	1.814	0.913	1.778
12	A/B-17 *	172	0.120	0.819	1.595	0.848	1.651
13	A/B-18 *	164		0.915	1.781	0.914	1.780
14	A/B-19 *	002		1.036	2.018	1.065	2.067
15	A/B-35 *	056		0.873	1.910	0.954	1.858
16	A/B-36 *	071		1.047	2.039	1.026	1.998
17	B/B-1 *	193		0.674	1.313	0.797	1.552
18	B/B-5 *	343		0.415	0.809	0.464	0.904
19	B/B-6 *	297		0.393	0.765	0.377	0.734
20	B/B-7 *	115		0.395	0.768	0.342	0.667
21	B/B-8 *	238		0.461	0.898	0.417	0.814
22	B/B-16 *	089		0.429	0.836	0.397	0.773
23	B/B-17 *	328		0.443	0.863	0.425	0.827
24	B/B-18 *	253	0.126	0.469	0.915	0.586	1.142
25	B/B-19 *	213		0.745	1.451	0.761	1.483
26	B/B-34	127					
27	B/B-45	106					
28	C/B-5	187		0.288	0.561	0.228	0.444
29	C/B-6 *	176	0.131	0.320	0.624	0.224	0.437
30	C/B-7 *	129	0.107	0.329	0.642	0.214	0.417
31	C/B-17 *	314		0.254	0.494	0.204	0.397
32	C/B-18 *	097	0.132	0.244	0.476	0.216	0.421

* Initial Surveillance Candles.

** Previous Data With Alumina/Mullite Candles Established A 2.5 Factor Between Room Temperature and 843°C (1550°F) Permeability Data. Factor Used To Establish The High Temperature Permeability For The Clay Bonded Silicon Carbide Candles Was 1.95.

An attempt was made to water wash several of the surveillance candles (i.e., ID to OD) in order to remove collected ash and sorbent fines. After water washing, filter peremeability increased when ash fines collected only along the candle OD surface. When ash and sorbent fines collected along the ID candle surface, pressure drop across the candle was seen to further increase as a result of forcing the ID fines into the coarse clay bonded silicon carbide wall.

4.2 POST-TEST CANDLE FILTER DIMENSIONS

After vacuum brushing and/or water washing, each of the 32 candle filters was measured in terms of overall length (i.e., flange to end cap) and extent of bowing. These data are presented in Table 4.2. The initial length and bow measurements that were provided by Schumacher at the time of candle shipment are also provided in Table 4.2. The original specification for candle filter length was 1515 * 10 mm. As shown in Table 4.2, the length of the candles after 500 hours of exposure to PFBC conditions was comparable to that of the original candle lengths. Any observable creep of the candles was not evident within the 500 hour exposure time period.

The candles particularly along the bottom plenum arrays did, however, bow after 500 hours of hot gas filtration in the PFBC gas environment. The original candle filter specification for bow was <3 mm, end-to-end. The double asterisks in Table 4.2 indicate those candles (i.e., surveillance and non-surveillance candles that were tested in this effort) which exceeded the 3 mm tolerance for bow. A 1.3- to 29-fold increase in candle bow resulted in these specific candles after 500 hours of exposure to PFBC gas conditions. The greatest bow was experienced by candles located in B/B-34 and B/B-45 (12.7 and 14.28 mm, respectively).

TABLE 4.2

POST-TEST CANDLE FILTER DIMENSIONS

Candle	Position	ID No.	Length, mm Initial (a)	Length, mm Final (b)	Bow, mm Initial (a)	Bow, mm Final (b)	
1	A/T-1 *	492	1515	ND	0.5	0.635	
2	B/T-1 *	504	1515	1515	0.5	0.635	
3	B/T-23	459	1513	1514	0.7	0.635	
4	A/M-1 *	367	1516	1516	0.7	3.175	**
5	B/M-1 *	436	1515	1515	0.4	0.635	
6	B/M-23	244	1515	1515	1.8	3.175	(**)
7	A/B-5 *	028	1515	1514	0.4	5.556	**
8	A/B-6 *	065	1516	1516	0.9	6.350	**
9	A/B-7 *	019	1515	1515	0.4	2.381	
10	A/B-8 *	083	1516	1516	0.4	2.381	
11	A/B-16 *	075	1515	1516	0.4	0.635	
12	A/B-17 *	172	1515	1515	0.6	1.588	
13	A/B-18 *	164	1518	1516	0.9	4.763	**
14	A/B-19 *	002	1513	1513	0.3	8.731	**
15	A/B-35 *	056	1515	1514	0.7	1.588	
16	A/B-36 *	071	1515	1515	0.5	7.938	**
17	B/B-1 *	193	1516	1516	0.9	4.763	**
18	B/B-5 *	343	1515	1515	0.6	6.350	**
19	B/B-6 *	297	1515	1515	0.6	4.763	**
20	B/B-7 *	115	1515	1514	1.0	3.175	**
21	B/B-8 *	238	1515	1516	0.6	3.969	**
22	B/B-16 *	089	1513	1515	0.6	9.525	**
23	B/B-17 *	328	1515	1514	0.7	6.350	**
24	B/B-18 *	253	1518	1517	0.5	3.175	**
25	B/B-19 *	213	1516	1516	0.4	1.588	
26	B/B-34	127	1516	ND	0.5	12.700	(**)
27	B/B-45	106	1513	ND	1.0	14.287	(**)
28	C/B-5	187	1515	1515	0.6	2.381	
29	C/B-6 *	176	1515	1516	1.6	2.381	
30	C/B-7 *	129	1513	1515	1.0	1.588	
31	C/B-17 *	314	1515	1516	0.6	3.175	**
32	C/B-18 *	097	1515	1514	0.9	3.969	**

* Original Surveillance Candles.
ND: Not Determined.
(a) Schumacher Measurements.
(b) Westinghouse Measurements.
** Surveillance Candles That Were Out Of Tolerance (>3mm).
(**) Nonsurveillance Candles That Were Out Of Tolerance (>3 mm).

Bowing was expected to result from ash bridging in the candle array. The ash and sorbent bridge pushed against the middle-to-bottom end of the candles, while the entire candle remained at high temperature and was firmly held at the flange in the filter mount. In addition a temperature and/or pressure difference between the surface of the candle that was embedded within the bridged ash cake, and the surface of the candle that was more directly exposed to the process gas (i.e., along the outside of the array rings) may be contributing to the resulting bow of each of the bottom candle arrays that were bridged with ash.

All of the remaining candle filters that were located in the bottom plenum arrays were initially cleaned prior to removal and return to Westinghouse STC. The cleaned candles were also evaluated in terms of bow in an attempt to further determine the extent of bowing, as well as the orientation of the bow. Table 4.3 indicates that the largest bow was ~24 mm (~1 inch) along candle #123 which was located in B/B-28. Note that B/B-28 was located along an inner ring (i.e., second ring from the outside in the candle array), closest to the failure locations of candle #130 in location B/B-42, and candle #125 in B/B-43.

Since many of the reported bows that are shown in Table 4.3 were less than the original bow, we suspected that these candles may not have been completely cleaned prior to measurement. Any residual ash deposit or "clump" along the candle OD wall would prevent an accurate measurement of candle bow. We do not believe, based on the rigorous cleaning techniques that were used for the original 32 candle filters, that the bottom candle filters relaxed after 500 hours of PFBC hot gas filtration changing the original direction of the minor bow. As a result, we currently have not pursued our initial intentions of attempting to determine the extent and direction of bowing in the candle filters that were located along the bottom plenum arrays.

TABLE 4.3

POST-TEST DETERMINATION OF BOW ALONG THE BOTTOM PLENUM CANDLE FILTERS

Candle No.	Position	ID No.	Bow, mm Initial (a)	Bow, mm Final (b)
1	A/B-1	150	0.8	Broken *
2	A/B-2	062	0.7	Broken *
3	A/B-3	004	0.5	3.175
4	A/B-4	080	0.9	4.726
5	A/B-5	028	0.4	5.556
6	A/B-6	065	0.9	6.350
7	A/B-7	019	0.4	2.381
8	A/B-8	083	0.4	2.381
9	A/B-9	200	1.2	1.588
10	A/B-10	184	1.3	--
11	A/B-11	258	0.8	Broken **
12	A/B-12	195	0.6	Broken **
13	A/B-13	189	1.4	0.79
14	A/B-14	192	1.1	1.59
15	A/B-15	194	1.2	1.59
16	A/B-16	075	0.4	0.635
17	A/B-17	172	0.6	1.588
18	A/B-18	164	0.9	4.763
19	A/B-19	002	0.3	8.731
20	A/B-20	081	0.7	9.53
21	A/B-21	098	0.5	Broken *
22	A/B-22	092	0.6	Broken *
23	A/B-23	475	1.2	Broken *
24	A/B-24	029	1.3	Broken *
25	A/B-25	078	0.7	Broken *
26	A/B-26	174	1.0	Broken *

(a) Schumacher Data.
(b) Westinghouse Data.
* Failed During Testing.
** Broken During Shipment To Westinghouse Or During Evaluation.
NA Not Available.

TABLE 4.3 (Cont'd)

POST-TEST DETERMINATION OF BOW ALONG THE BOTTOM PLENUM CANDLE FILTERS

Candle No.	Position	ID No.	Bow, mm Initial (a)	Final (b)
27	A/B-27	177	1.5	9.525
28	A/B-28	010	0.6	2.381
29	A/B-29	199	0.9	1.588
30	A/B-30	182	0.9	--
31	A/B-31	196	0.7	0.79
32	A/B-32	197	1.8	--
33	A/B-33	179	0.6	--
34	A/B-34	294	0.7	0.397
35	A/B-35	056	0.7	1.588
36	A/B-36	071	0.5	7.938
37	A/B-37	064	0.7	12.7
38	A/B-38	451	0.7	Broken *
39	A/B-39	016	0.7	Broken *
40	A/B-40	012	0.4	Broken *
41	A/B-41	186	0.5	Broken *
42	A/B-42	175	1.0	2.38
43	A/B-43	180	0.9	--
44	A/B-44	255	1.0	--
45	A/B-45	257	0.9	--
46	A/B-46	183	0.7	--
47	A/B-47	007	0.5	13.49
48	A/B-48	059	0.8	Broken *
49	A/B-49	053	0.4	Broken *
50	A/B-50	178	1.0	Broken *
51	A/B-51	185	1.2	1.588
52	A/B-52	256	1.0	1.588

(a) Schumacher Data.
(b) Westinghouse Data.
* Failed During Testing.
** Broken During Shipment To Westinghouse Or During Evaluation.
NA Not Available.

TABLE 4.3 (Cont'd)

POST-TEST DETERMINATION OF BOW ALONG THE BOTTOM PLENUM CANDLE FILTERS

Candle No.	Position	ID No.	Bow, mm Initial (a)	Final (b)
1	B/B-1	193	0.9	4.76
2	B/B-2	116	0.7	--
3	B/B-3	344	0.6	NA
4	B/B-4	347	0.4	3.97
5	B/B-5	343	0.6	6.350
6	B/B-6	297	0.6	4.763
7	B/B-7	115	1.0	3.175
8	B/B-8	238	0.6	3.969
9	B/B-9	324	1.1	2.38
10	B/B-10	332	0.4	--
11	B/B-11	302	0.6	--
12	B/B-12	327	1.0	--
13	B/B-13	285	0.4	--
14	B/B-14	348	1.2	--
15	B/B-15	345	0.6	5.56
16	B/B-16	089	0.6	9.525
17	B/B-17	328	0.7	6.350
18	B/B-18	253	0.5	3.175
19	B/B-19	213	0.4	1.588
20	B/B-20	283	0.7	NA
21	B/B-21	309	0.6	Broken *
22	B/B-22	117	0.8	4.76
23	B/B-23	202	1.0	5.56
24	B/B-24	203	1.0	1.59
25	B/B-25	124	0.4	4.76
26	B/B-26	103	0.4	4.76

(a) Schumacher Data.
(b) Westinghouse Data.
* Failed During Testing.
** Broken During Shipment To Westinghouse Or During Evaluation.
NA Not Available.

TABLE 4.3 (Cont'd)

POST-TEST DETERMINATION OF BOW ALONG THE BOTTOM PLENUM CANDLE FILTERS

Candle No.	Position	ID No.	Bow, mm Initial (a)	Final (b)
27	B/B-27	101	0.5	14.288
28	B/B-28	123	0.6	23.873
29	B/B-29	102	0.4	7.938
30	B/B-30	119	0.5	--
31	B/B-31	118	0.9	--
32	B/B-32	120	0.6	--
33	B/B-33	114	0.4	5.556
34	B/B-34	127	0.5	12.700
35	B/B-35	085	0.5	12.700
36	B/B-36	126	0.7	3.175
37	B/B-37	034	0.9	6.35
38	B/B-38	321	0.5	3.175
39	B/B-39	219	1.0	3.175
40	B/B-40	113	0.6	6.35
41	B/B-41	109	0.5	14.288
42	B/B-42	130	2.0	Broken *
43	B/B-43	125	0.5	Broken *
44	B/B-44	110	0.7	3.969
45	B/B-45	106	1.0	14.287
46	B/B-46	112	0.5	Broken **
47	B/B-47	107	0.5	2.381
48	B/B-48	108	0.6	3.175
49	B/B-49	091	1.7	8.731
50	B/B-50	221	0.4	16.669
51	B/B-51	220	1.0	6.35
52	B/B-52	095	0.7	Broken *

(a) Schumacher Data.
(b) Westinghouse Data.
* Failed During Testing.
** Broken During Shipment To Westinghouse Or During Evaluation.
NA Not Available.

TABLE 4.3 (Cont'd)

POST-TEST DETERMINATION OF BOW ALONG THE BOTTOM PLENUM CANDLE FILTERS

Candle No.	Position	ID No.	Bow, mm Initial (a)	Final (b)
1	C/B-1	308	0.4	Broken *
2	C/B-2	312	0.5	1.588
3	C/B-3	304	0.6	1.588
4	C/B-4	337	0.8	--
5	C/B-5	187	0.6	2.381
6	C/B-6	176	1.6	2.381
7	C/B-7	129	1.0	1.588
8	C/B-8	329	0.9	0.794
9	C/B-9	330	0.4	--
10	C/B-10	335	1.3	--
11	C/B-11	338	0.7	--
12	C/B-12	284	0.5	--
13	C/B-13	287	0.7	--
14	C/B-14	319	1.3	0.794
15	C/B-15	347	0.4	1.588
16	C/B-16	282	0.4	--
17	C/B-17	314	0.6	3.175
18	C/B-18	097	0.9	3.969
19	C/B-19	295	0.9	--
20	C/B-20	296	0.5	2.381
21	C/B-21	198	1.9	NA
22	C/B-22	310	0.7	Broken *
23	C/B-23	188	0.4	3.175
24	C/B-24	191	0.7	2.381
25	C/B-25	291	0.6	--
26	C/B-26	305	0.5	1.588

(a) Schumacher Data.
(b) Westinghouse Data.
* Failed During Testing.
** Broken During Shipment To Westinghouse Or During Evaluation.
NA Not Available.

TABLE 4.3 (Cont'd)

POST-TEST DETERMINATION OF BOW ALONG THE BOTTOM PLENUM CANDLE FILTERS

Candle No.	Position	ID No.	Bow, mm Initial (a)	Final (b)
27	C/B-27	290	0.8	--
28	C/B-28	298	0.4	--
29	C/B-29	318	0.5	1.588
30	C/B-30	303	0.7	--
31	C/B-31	311	0.8	0.794
32	C/B-32	323	0.7	--
33	C/B-33	301	0.7	--
34	C/B-34	313	0.4	0.794
35	C/B-35	315	0.7	3.969
36	C/B-36	293	0.5	6.35
37	C/B-37	331	0.7	5.556
38	C/B-38	317	0.8	5.556
39	C/B-39	325	0.6	6.35
40	C/B-40	299	0.5	0.794
41	C/B-41	190	1.2	0.794
42	C/B-42	326	0.7	0.794
43	C/B-43	288	0.7	--
44	C/B-44	307	0.4	--
45	C/B-45	320	0.7	--
46	C/B-46	334	0.5	2.381
47	C/B-47	340	0.6	4.763
48	C/B-48	316	0.7	5.556
49	C/B-49	300	0.7	0.794
50	C/B-50	292	0.5	--
51	C/B-51	259	1.6	1.588
52	C/B-52	322	1.0	1.588

(a) Schumacher Data.
(b) Westinghouse Data.
* Failed During Testing.
** Broken During Shipment To Westinghouse Or During Evaluation.
NA Not Available.

4.3 POST-TEST CANDLE FILTER TIME-OF-FLIGHT MEASUREMENTS

Time-of-flight (TOF) measurements of the 32 candle filters after exposure to the PFBC gas environment are shown in Table 4.4. With the exception of two candles (B/B-16 #089, and C/B-18 #097), each candle experienced an increase in its TOF measurement after exposure at Tidd. An increase in TOF implied a reduction in candle filter material strength.

Although ash and sorbent fines remained along and through the candle filter body after each filter was vacuum brushed, the presence of particles did not affect the TOF measurement. As shown in Table 4.4, once the candles were washed and dried after vacuum brushing, the TOF measurements of the "cleaned" candles were nearly comparable to the TOF measurements reported after only vacuum brushing.

4.4 SUMMARY OF THE BOW, TOF, AND PRESSURE DROP CHARACTERISTICS OF THE CLAY BONDED SILICON CARBIDE FILTERS AFTER REMOVAL FROM THE WESTINGHOUSE APF SYSTEM IN DECEMBER 1992

Table 4.5 summarizes the bow, TOF, and pressure drop characteristics of the clay bonded silicon carbide candles as a function of plenum and array location within the Westinghouse APF system. There appeared to be negligible bowing in the top plenum candles (i.e., A/T and B/T). A slight increase in bow resulted along the middle plenum candles (i.e., A/M and B/M), while the largest extent of bowing resulted along the bottom plenum candles (i.e., A/B, B/B, and C/B). The largest extent of candle bowing occurred in the bottom array of Cluster B which had the greatest extent of ash bridging between the remaining candles at test termination in December 1992.

The TOF measurements for the 500 hour PFBC exposed candles ranged from 336 to 362 μsec. Adherence and/or inclusion of dust fines did not appreciably affect the resulting TOF measurements. All of the

TABLE 4.4

POST-TEST CANDLE FILTER TIME-OF-FLIGHT MEASUREMENTS

Candle	Position	ID No.	TOF, μsec Initial	Vacuumed Brushed	ΔTOF	Vacuumed Brushed Washed/Dried	ΔTOF
1	A/T-1 *	492	330	337	7	337	7
2	B/T-1 *	504	332	339	7	331	-1
3	B/T-23	459		336		333	
4	A/M-1 *	367	332	340	8	339	7
5	B/M-1 *	436	336	343	7	343	7
6	B/M-23	244		344		334	
7	A/B-5 *	028	343	353	10		
8	A/B-6 *	065	348	362	14		
9	A/B-7 *	019	340	356	16		
10	A/B-8 *	083	339	342	3		
11	A/B-16 *	075	343	351	8		
12	A/B-17 *	172	342	349	7		
13	A/B-18 *	164	338	347	9	346	8
14	A/B-19 *	002	339	353	14		
15	A/B-35 *	056	346	357	11		
16	A/B-36 *	071		352		351	
17	B/B-1 *	193	323	335	12	334	11
18	B/B-5 *	343	345	356	11		
19	B/B-6 *	297	334	341	7		
20	B/B-7 *	115	335	340	5		
21	B/B-8 *	238	331	339	8		
22	B/B-16 *	089	350	342	-8		
23	B/B-17 *	328	339	344	5		
24	B/B-18 *	253	335	344	9	346	11
25	B/B-19 *	213	323	342	19		
26	B/B-34	127		340			
27	B/B-45	106		348			
28	C/B-5	187		347			
29	C/B-6 *	176	333	344	11		
30	C/B-7 *	129	347	356	9		
31	C/B-17 *	314	332	338	6		
32	C/B-18 *	097	351	345	-6	347	-4

* Initial Surveillance Candles.

TABLE 4.5

SUMMARY OF BOW, TOF AND PRESSURE DROP
CHARACTERISTICS OF THE SCHUMACHER DIA SCHUMALITH F40 CANDLES
REMOVED FROM THE W-APF SYSTEM ON 12/92

Location	Bow, mm	TOF, μs	Δp, psi at 10 fpm (RT)*
A/T (1) **	0.635	337	0.284
B/T (2)	0.635	337.5 ± 2.121	0.274 ± 0.080
A/M (1)	3.175	340	0.459
B/M (2)	1.905 ± 1.796(a)	343.5 ± 0.707	0.251 ± 0.046
A/B (10)	4.191 ± 2.872	352.2 ± 5.554	1.013 ± 0.123
B/B (9)	6.422 ± 4.085(b)	342.8 ± 5.474(b)	0.492 ± 0.128
C/B (5)	2.699 ± 0.905	346 ± 6.519	0.287 ± 0.038

* Pressure Drop Across As-Fabricated, Untested Candle Filters Is 0.123 ± 0.009 psi.

** Number In Parentheses Indicate The Number Of Candles Characterized At Each Location.

(a) 1σ Variation.

(b) Two Very Bowed Candles Were Included In The Bow And TOF Characterizations.

32 candle filters that were characterized in this effort had higher TOF measurements after exposure in the PFBC environment in comparison to their as-fabricated TOF measurement. This implied that the candles lost strength during hot gas filtration operation.

Although we had only a limited number of TOF measurements, and a more extensive effort would be required to generate a statistically meaningful database, the following general observations were evident:

- The top plenum candles had the lowest TOF measurements which implied highest strength.
- The middle plenum candles had intermediate TOF measurements
- The bottom plenum candles had the highest TOF measurements which implied the lowest strength.

A review of the pressure drop data for the 32 candles indicates that the room temperature pressure drop at 10 ftm increases from the top to the bottom candle filter arrays. This was particularly evident along Cluster A. The increase in pressure drop was attributed to residual ash cake and sorbent remaining along the candle OD, as well as along the candle ID surface (i.e., pore plugging of fines along the ID surface of the bottom plenum filters after the initial candle failure occurred). Note that candles in the bottom array of Cluster A had the highest pressure drop of all candles characterized. This array had the greatest number of fractured candles at termination of the hot gas filtration test in December 1992.

5. ASH CHARACTERIZATION

A discussion of the composition and morphology of the ash that was carried into the Westinghouse APF system is presented in Section 5. Ash dumpling-like deposits, as well as a thin, white layer of sorbent material which coated the intact ceramic candle filters were subjected to scanning electron microscopy/energy dispersive x-ray analysis (SEM/EDAX). Ash and sorbent materials that remained along the candle filter sections that fell into the ash hopper during hot gas filtration testing were also analysed. A characteristically different ash-sorbent deposit was identified along the ID of the fractured candle filter sections that remained rigidly held in the filter holder mounts. In addition, a cement-like ash-sorbent deposit was identified along the ID of several candles that had fallen into the ash hopper. The cement-like characteristics of the ID ash deposit were similar to the ash-sorbent material that was extracted from the bottom of the ash hopper. A discussion of the SEM/EDAX analyses of each of these materials follows.

5.1 ASH DEPOSITS FORMED ALONG THE OUTER SURFACE OF INTACT CANDLE FILTERS

A dust heavy cake surrounded each of the 384 filter mount holders in all nine Westinghouse APF candle arrays. The color of the ash was pinkish-orange with white areas of fines detected within the ash. The entire length of each intact candle appeared to have a white layer of fines deposited along the grey candle filter membrane (Figure 5.1 and 5.2). Dumpling ash deposits, as well as scale-like ash layers were formed intermittently along the outer surface of each candle filter element (Figure 5.3 and 5.4).

Dumpling-like ash deposits were easily removed from the candle surface, exposing the original grey candle filter membrane. Typically the outer color of the thick dumpling and scale-like deposits was a

Figure 5.1 - Heavy Dust Cake Deposit Formed Around The Filter Holders

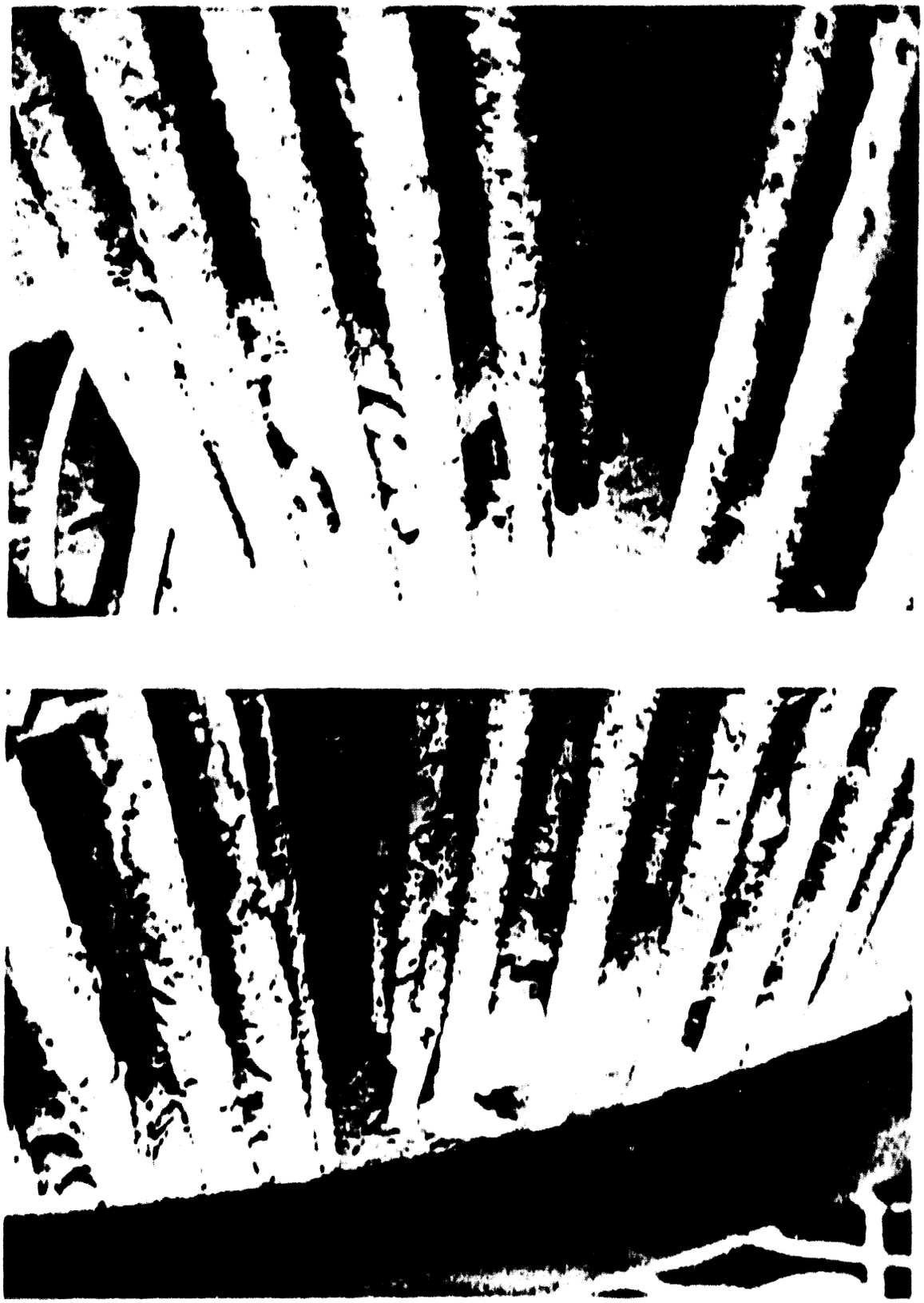

Figure 5.2 - Dumpling Ash Deposits That Formed Along The OD Candle Surface. Ash Cake Bridging Is Evident Between Adjacent Candles In The Cluster Array.

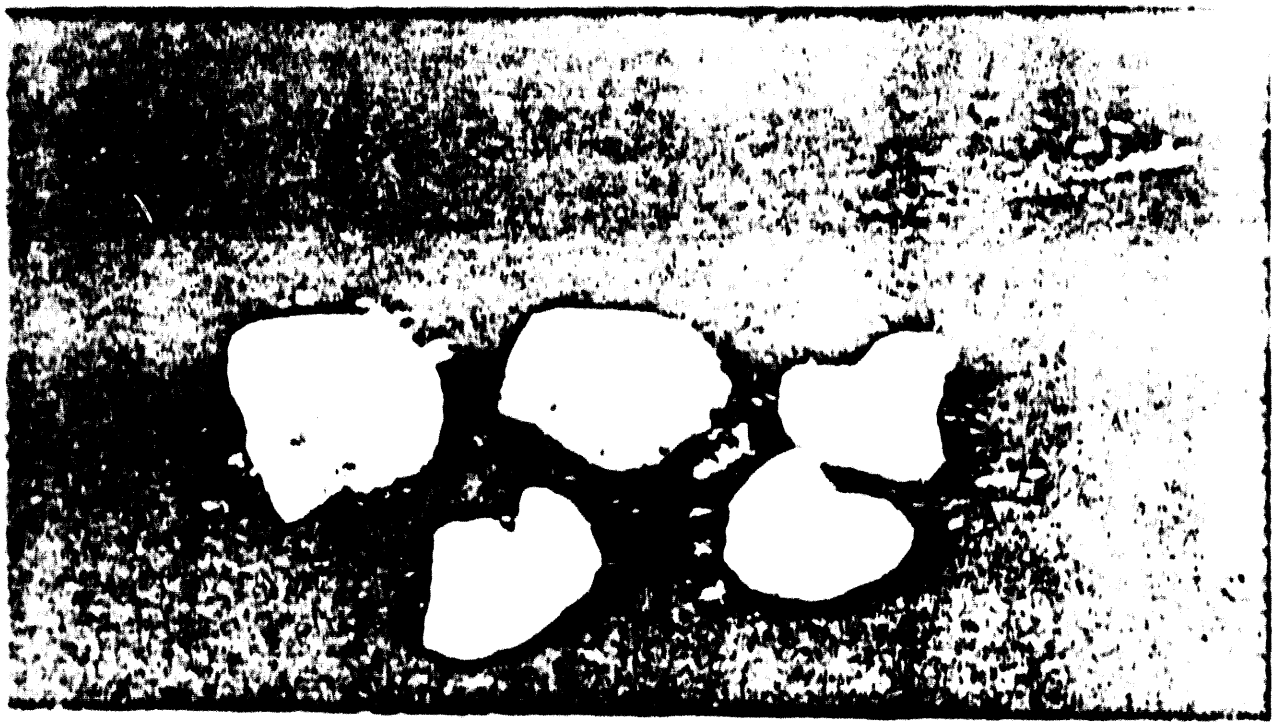

0 1 2 3 4

Figure 5.3 Ash Dumplings Remaining Along The OD Surface Of Intact Candle Filters

Figure 5.4 - Scale-Like Ash Deposits That Form Along The OD Surface Of Intact Candle Filters

pinkish-orange. When the dumpling deposits were removed from the candle OD, the surface of the deposit that contacted the candle filter retained the contour of the candle wall, and appeared pinkish-orange in color (Figure 5.5). Note that a thin white layer of dust coated the surface of the candle wall that was adjacent to the dumpling deposits. Since the pinkish-orange ash was observed along the surface of the dumpling that was in direct contact with the candle wall, we are not certain at this time whether the white candle coating layer was actually included within the ash dumpling deposit, and that it had been "peeled away" during removal of the ash dumplings from the candle filter wall. It was impossible to easily brush away the pink-orange ash layer and not disturb any underlying white ash-sorbent layer which may have been actually present in the ash dumpling deposit. It will become apparent in the following discussion that characterising the actual thickness of the white layer of fines along the candle OD surface was also extremely difficult. Note that the thickness of the dumpling-like ash deposits extended between 5 and 15 mm above the surface of the candle filter wall.

An intact ash ~5 mm thick dumpling was removed from candle filter #193 which was located in position B/B-1. SEM/EDAX characterisation was performed on the dumpling in an attempt to discern whether there were any changes in the morphology and/or composition through the ~5 mm thick dumpling deposit. Analyses were performed initially along the surface of the dumpling that was in contact with the candle OD wall. Additional SEM/EDAX analyses were then performed at 0.25 to 0.5 mm depth through the thickness of the dumpling. Figures 5.6 through 5.12 indicate the relatively open porous structure of the fines that were contained within the ~5 mm thick dumpling deposit.

Typically 3-5 μm cenosphere-like structures were present in the ash-sorbent deposit, as well as micron and submicron finer agglomerates which were interconnected, forming the porous network of fines. From a morphology viewpoint, the dumplings appeared to be relatively

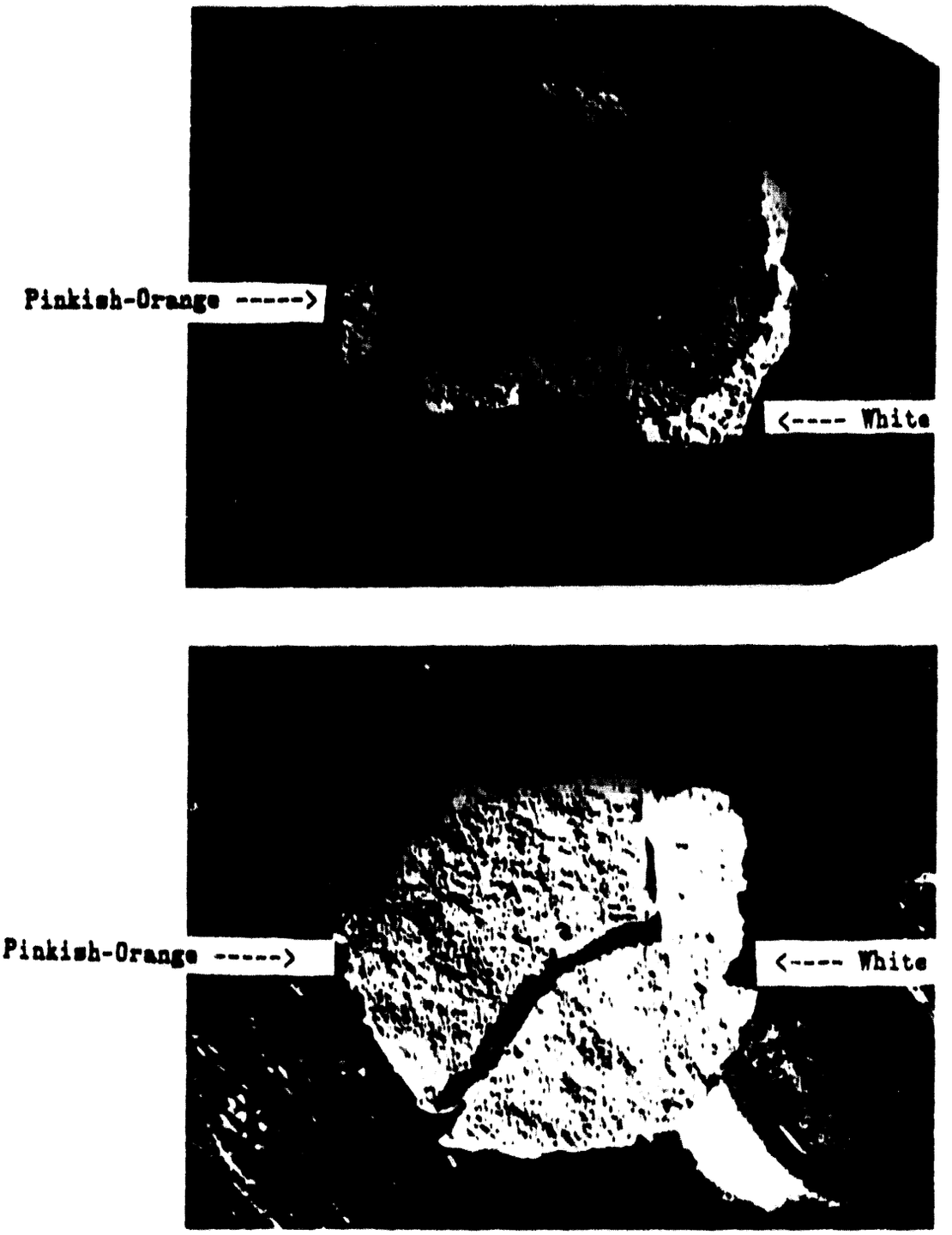

Figure 5.5 - ID Surface Of Dumpling Deposit Removed From An Intact Candle. Both Pinkish-Orange Ash As Well As White Sorbent Areas Are Evident.

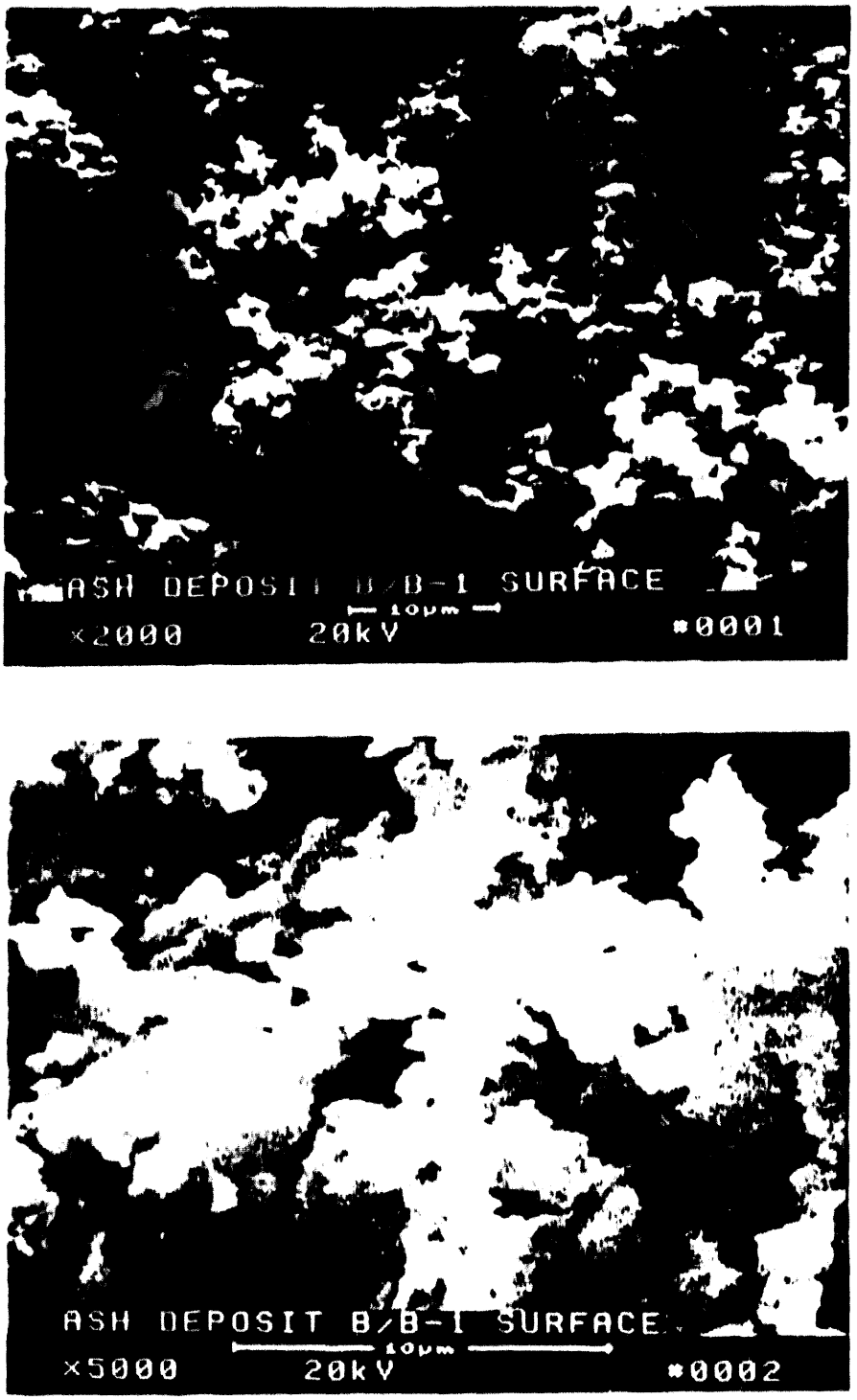

Figure 5.6 - Morphology Of The Fines Along The ID Surface Of An Ash Dumpling That Was Removed From Candle #193. This Candle Was Located In Position B/B-1.

0.25 mm

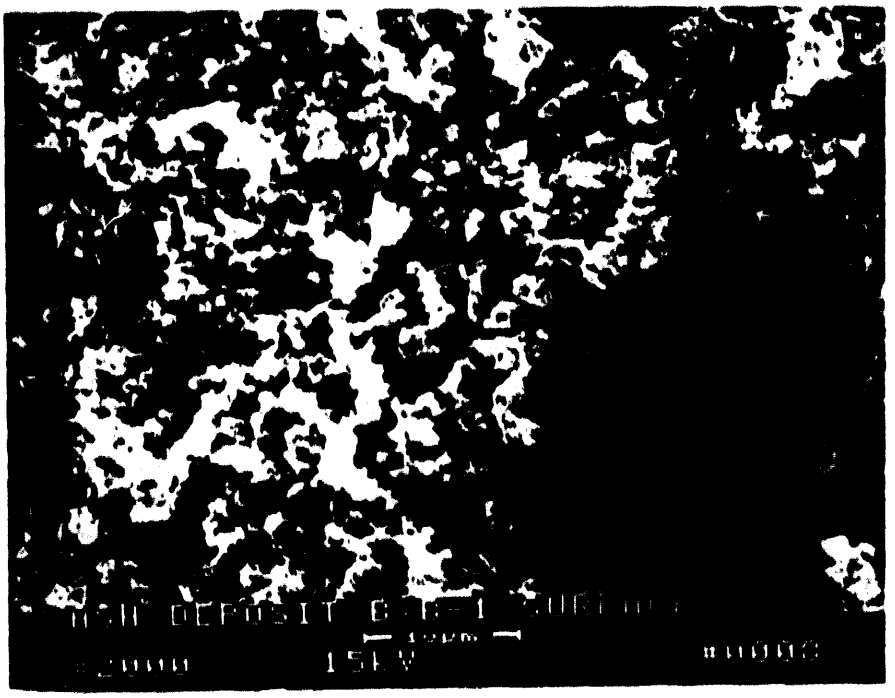

0.75 mm

Figure 5.7 - Morphology Of The Ash Dumpling At 0.25 And 0.75 mm From The ID Surface Of The Deposit

1.25 mm

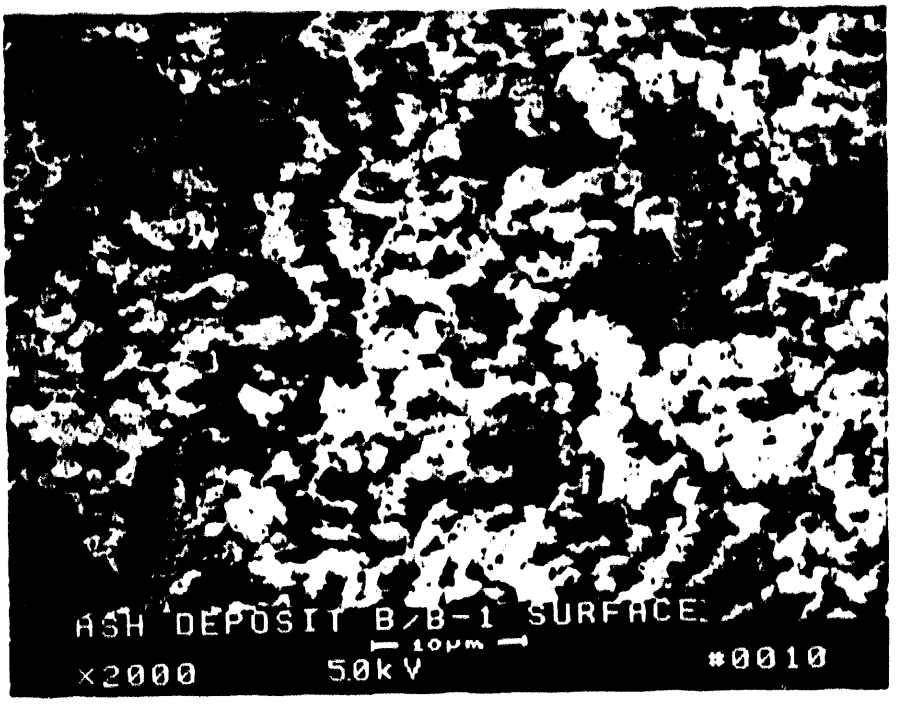

1.75 mm

Figure 5.8 - Morphology Of The Ash Dumpling At 1.25 And 1.75 mm From The ID Surface Of The Deposit

2.25 mm

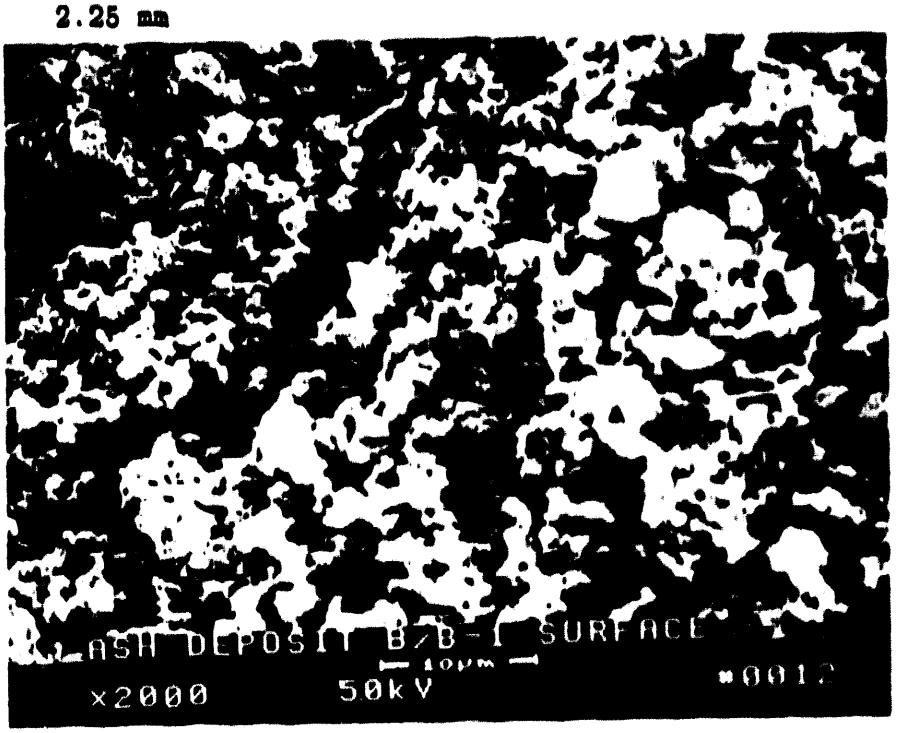

2.75 mm

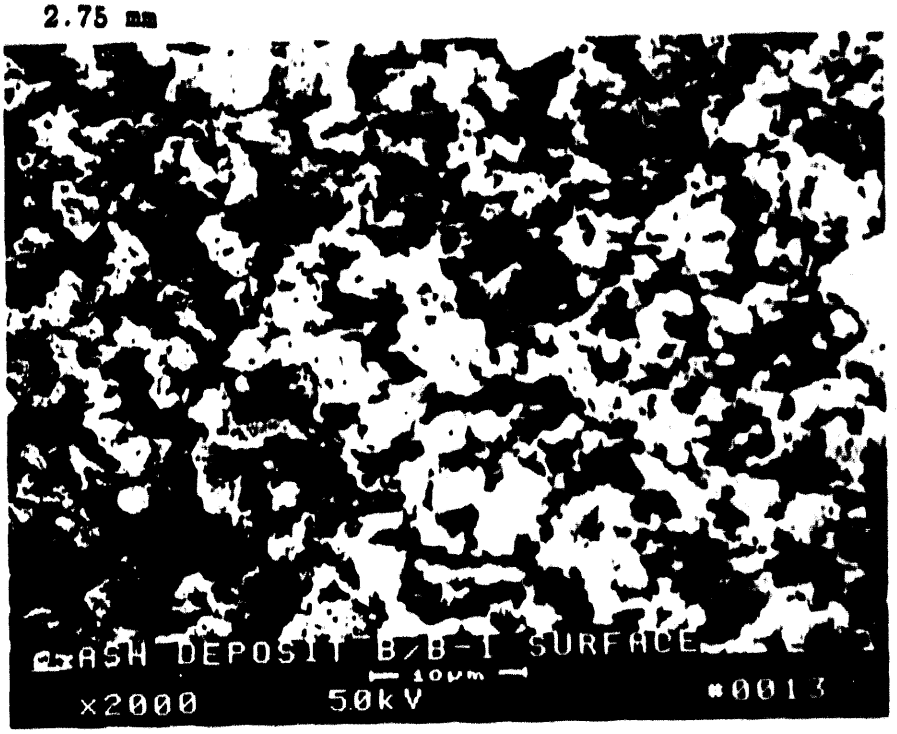

Figure 5.9 - Morphology Of The Ash Dumpling At 2.25 And 2.75 mm From The ID Surface Of The Deposit

3.25 mm

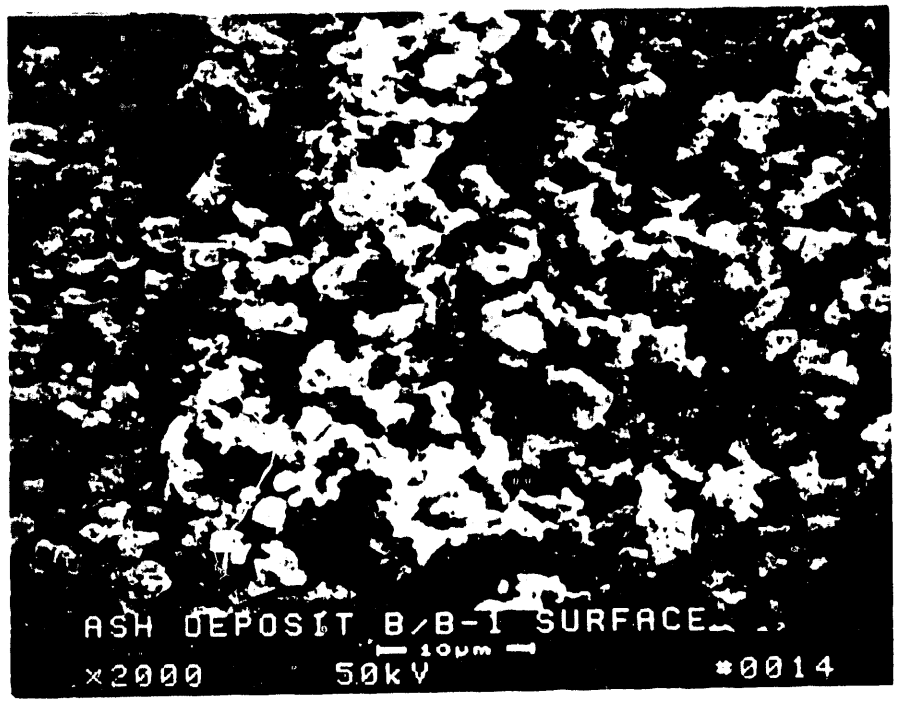

3.75 mm

Figure 5.10 - Morphology Of The Ash Dumpling At 3.25 And 3.75 mm From The ID Surface Of The Deposit

4.25 mm

4.75 mm

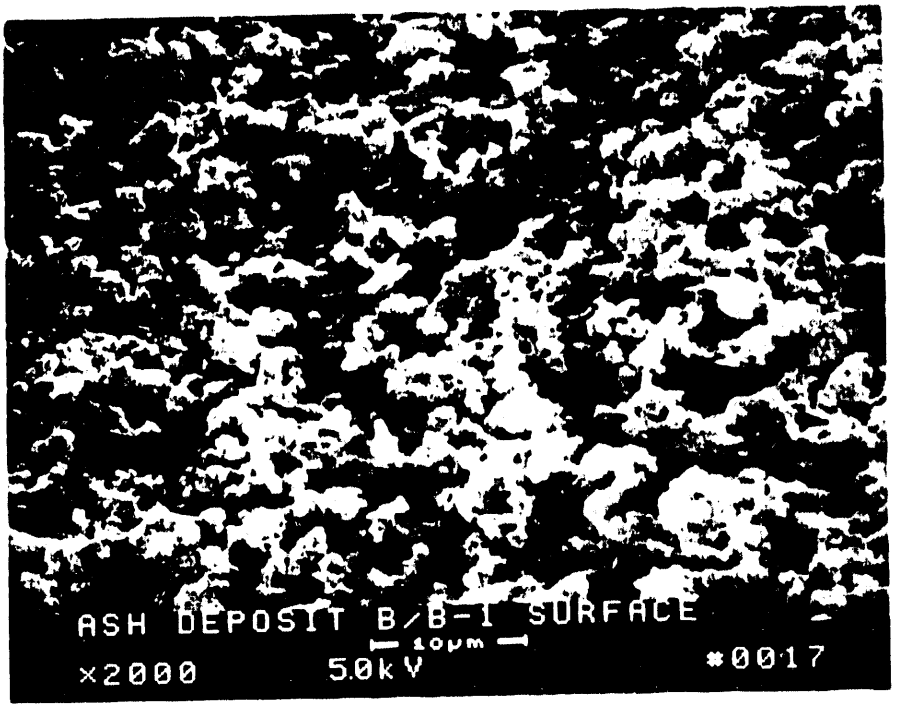

Figure 5.11 - Morphology Of The Ash Dumpling At 4.25 And 4.75 mm From The ID Surface Of The Deposit

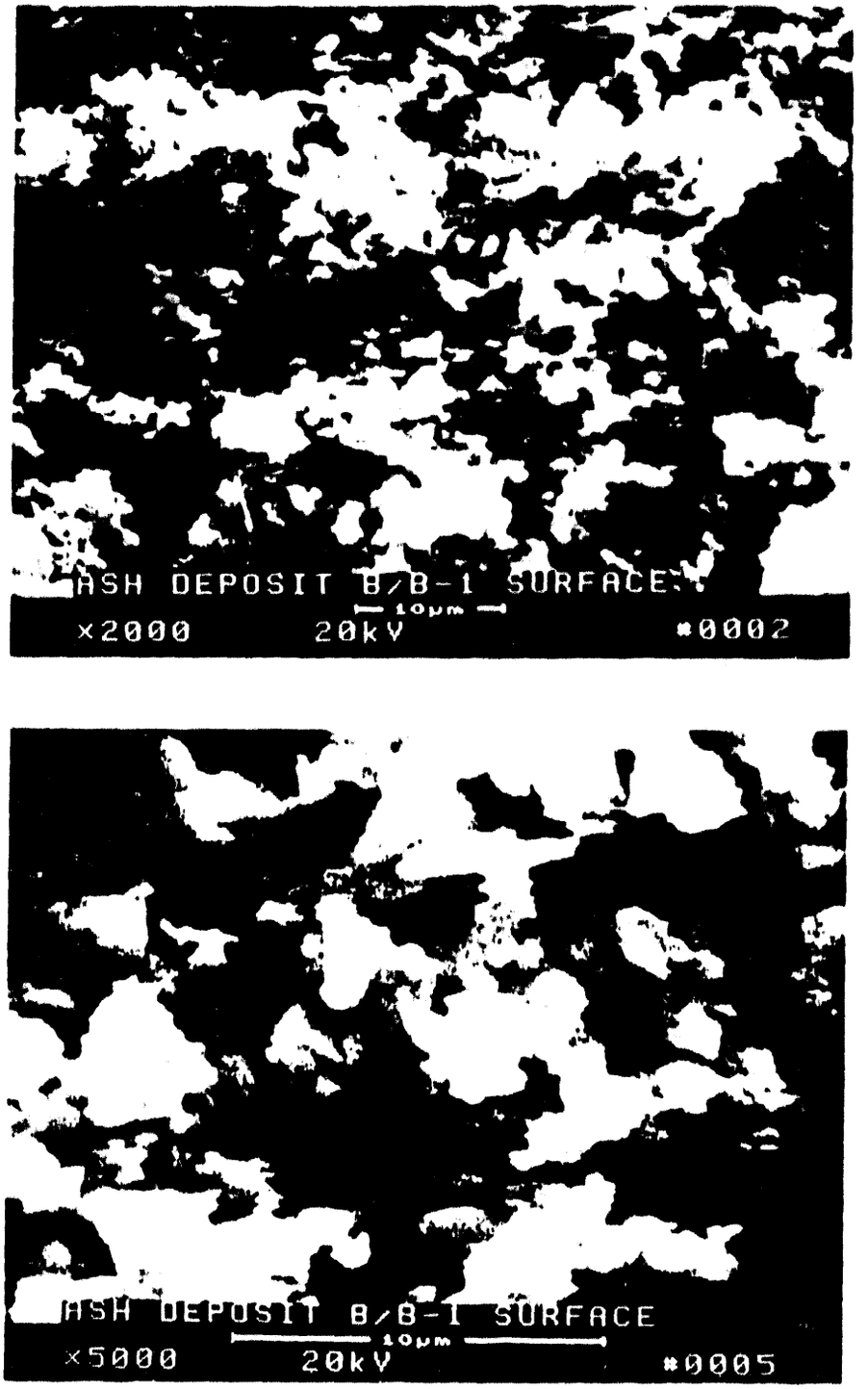

Figure 5.12 - Morphology Of The OD Surface Of The Ash Dumpling That Was Removed From Candle #193 (B/B-1) Prior To Cleaning

homogeneous throughout the 5 mm thick deposit. In contrast what was readily evident in the EDAX analysis (Table 5.1) was that at both the ID and OD surfaces of the dumplings, a higher magnesium and slightly enriched calcium layer had been formed. Titanium which was also present at relatively low concentrations within the dumpling deposits, was absent along the ID and OD dumpling surfaces. Notably the concentration of iron was also lower along the ID and OD dumpling surfaces, while a somewhat reduced potassium concentration was also detected. Sulfur appeared to be present at relatively high concentrations throughout the entire thickness of the ash-sorbent dumpling. These preliminary analyses implied that the OD and ID surfaces were somewhat enriched with the dolomitic sorbent material (i.e., Plum Run dolomite) that was used for gas phase sulfur removal.

In an attempt to resolve whether there was a compositional difference in the pinkish-orange versus white deposit layers, the pinkish-orange ash (Figure 5.5) was further characterised. Figure 5.13 details the morphology of the fines that were contained in this layer. Round agglomerates that consisted of micron and submicron fines were evident. Compositionally the fines consisted of:

Atomic Percent

Element	Area 1	Area 2
Mg	10.39	8.74
Al	11.30	8.51
Si	21.90	18.84
S	36.06	37.87
K	2.25	2.48
Ca	15.50	19.26
Fe	2.61	3.78
Ti	--	0.51
Normalisation Factor	0.639	0.667

TABLE 5.1

EDAX CHARACTERIZATION OF THE 5 mm ASH DEPOSIT THAT WAS REMOVED FROM THE CANDLE FILTER WALL (B/B-1, #193), Atomic %

Element	Location OD		0.25 mm	0.75 mm	1.25 mm	1.75 mm	2.25 mm
Mg	12.12,	9.98	8.55	7.79	6.74	6.34	8.05
Al	11.95,	12.76	12.96	13.17	14.65	14.27	12.89
Si	21.14,	22.02	21.53	23.77	25.65	25.29	22.70
S	34.51,	34.91	33.51	32.57	29.58	30.50	33.19
K	2.41,	2.45	2.60	3.09	2.92	2.82	2.81
Ca	15.73,	15.52	16.25	15.04	14.43	15.24	16.06
Ti	---	---	0.42	0.51	0.59	0.55	0.42
Fe	2.14,	2.35	4.07	3.89	5.13	4.97	3.89
NF*	0.63,	0.64	0.64	0.64	0.63	0.64	0.64

Element	Location 2.75 mm	3.25 mm	3.75 mm	4.25 mm	4.75 mm	ID	
Mg	8.15	8.96	6.87	8.28	9.77	14.02,	19.54
Al	12.72	12.76	12.41	10.95	11.43	10.71,	9.36
Si	22.73	21.68	22.10	19.33	20.24	18.09,	15.70
S	33.10	33.99	33.12	33.67	34.02	33.78,	31.00
K	2.81	2.68	2.95	2.67	2.72	2.25,	1.83
Ca	15.86	15.86	17.36	20.57	17.81	18.57,	20.35
Ti	0.50	0.44	0.54	0.62	0.39	---	---
Fe	4.10	3.62	4.64	5.83	3.60	2.58,	2.22
NF	0.64	0.64	0.65	0.67	0.65	0.64,	0.64

* NF: Normalisation Factor.

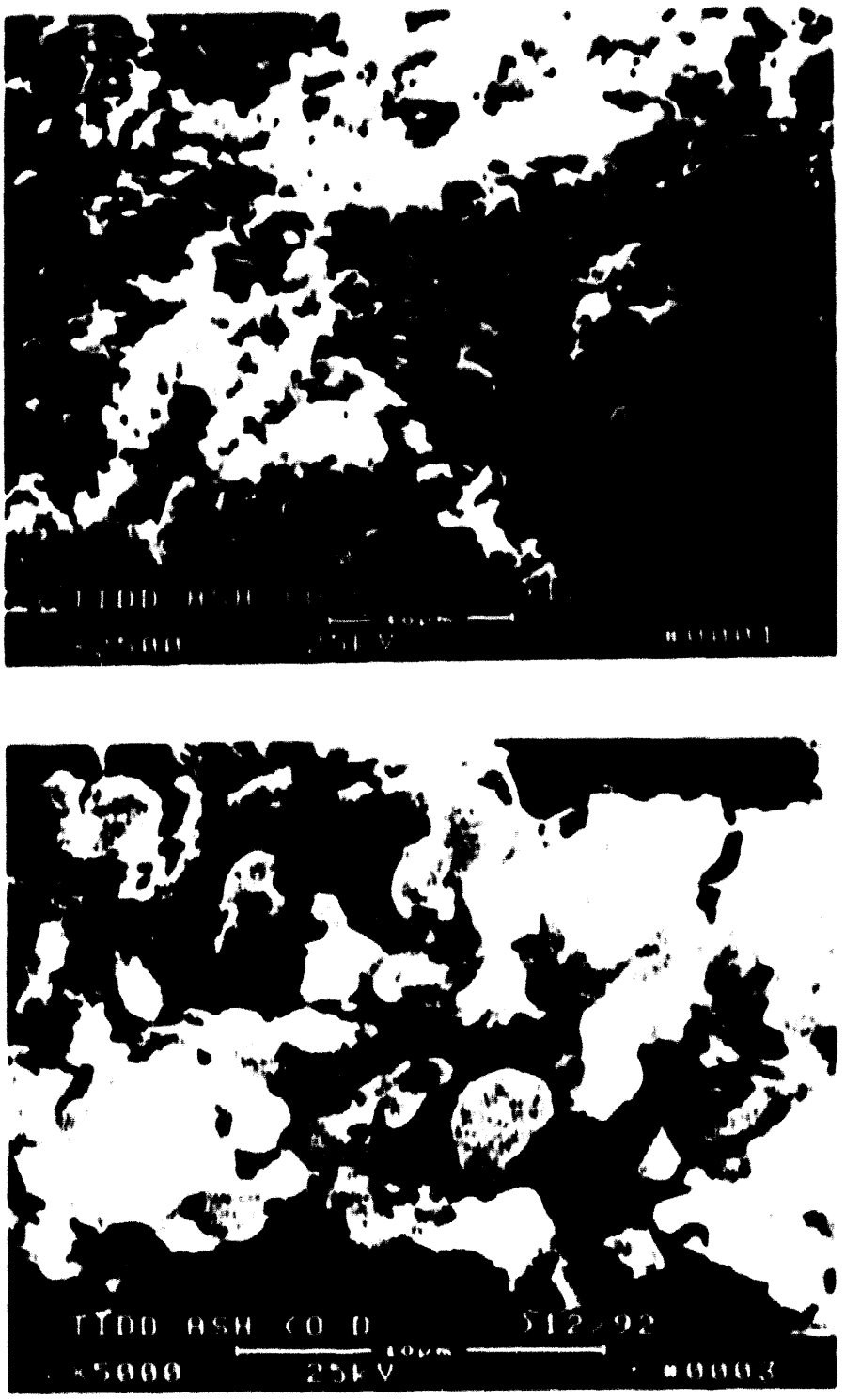

Figure 5.13 - Morphology Of The Ash Fines Formed Along The Dumpling Surface That Was Adjacent To The Candle OD Wall

In contrast, the morphology along the white area of the dumpling deposit is shown in Figure 5.14 and 5.15. The particle size of fines in the white deposit area appeared to be somewhat smaller (i.e., < 1 μm) than the fines in the pinkish-orange ash deposit (Figure 5.13, Photo 3; Figure 5.15; Photo 6). Compositionally the white area consisted of:

	Atomic Percent
Mg	34.50
Si	7.03
S	23.19
Ca	32.72
Fe	2.56
Normalisation Factor	0.682

Based on these analyses, we concluded that the white areas were enriched with the dolomitic sorbent material, while both ash and sorbent were present in the pinkish-orange dust cake layer. The sorbent layer was typically a thin "egg-shell-like" layer in comparison to the 5-15 mm thick dumpling which was predominantly a mixture of ash and sorbent fines.

Figures 5.16 and 5.17 illustrate the variation in the ash/sorbent layer formed along the dumpling coated candle surface, as well as a section of the candle that had fallen into the ash hopper of the Westinghouse APF vessel. Notably the section of candle that was removed from the ash hopper did not have the dumpling-like deposits along its OD surface, but did contain the thin white sorbent layer of fines, as well as the thicker ash-sorbent outer layer of fines. Large "descaled" deposit areas were evident along the ash hopper candle sections which revealed the membrane surface of the candle filter wall.

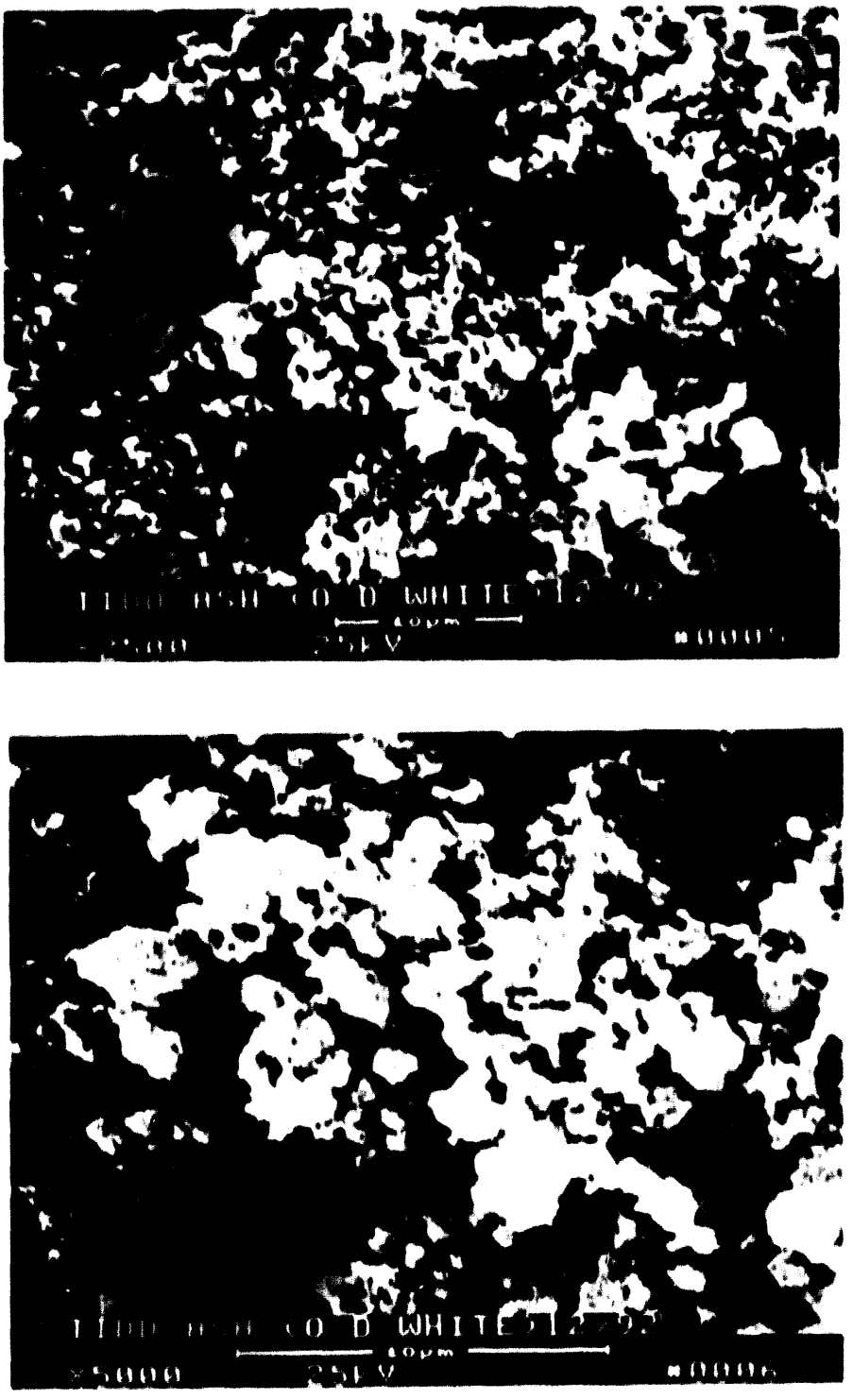

Figure 5.14 - Morphology Of The White Sorbent Material Formed Along The Dumpling Surface That Was Adjacent To The Candle OD Wall

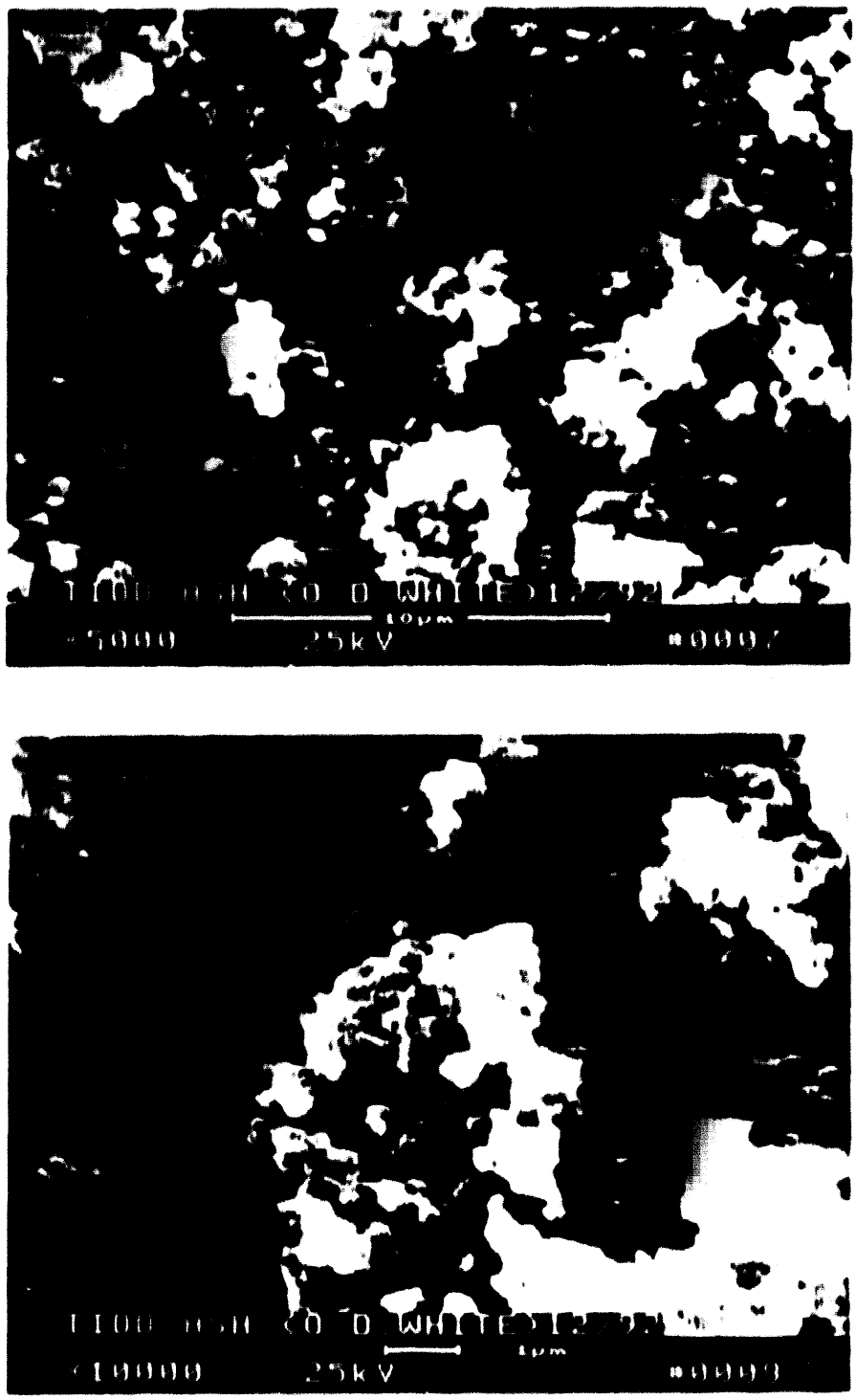

Figure 5.15 - Higher Magnification Micrographs Illustrating The Morphology Of The White Sorbent Material Formed Along The Dumpling Surface That Was Adjacent To The Candle OD Wall

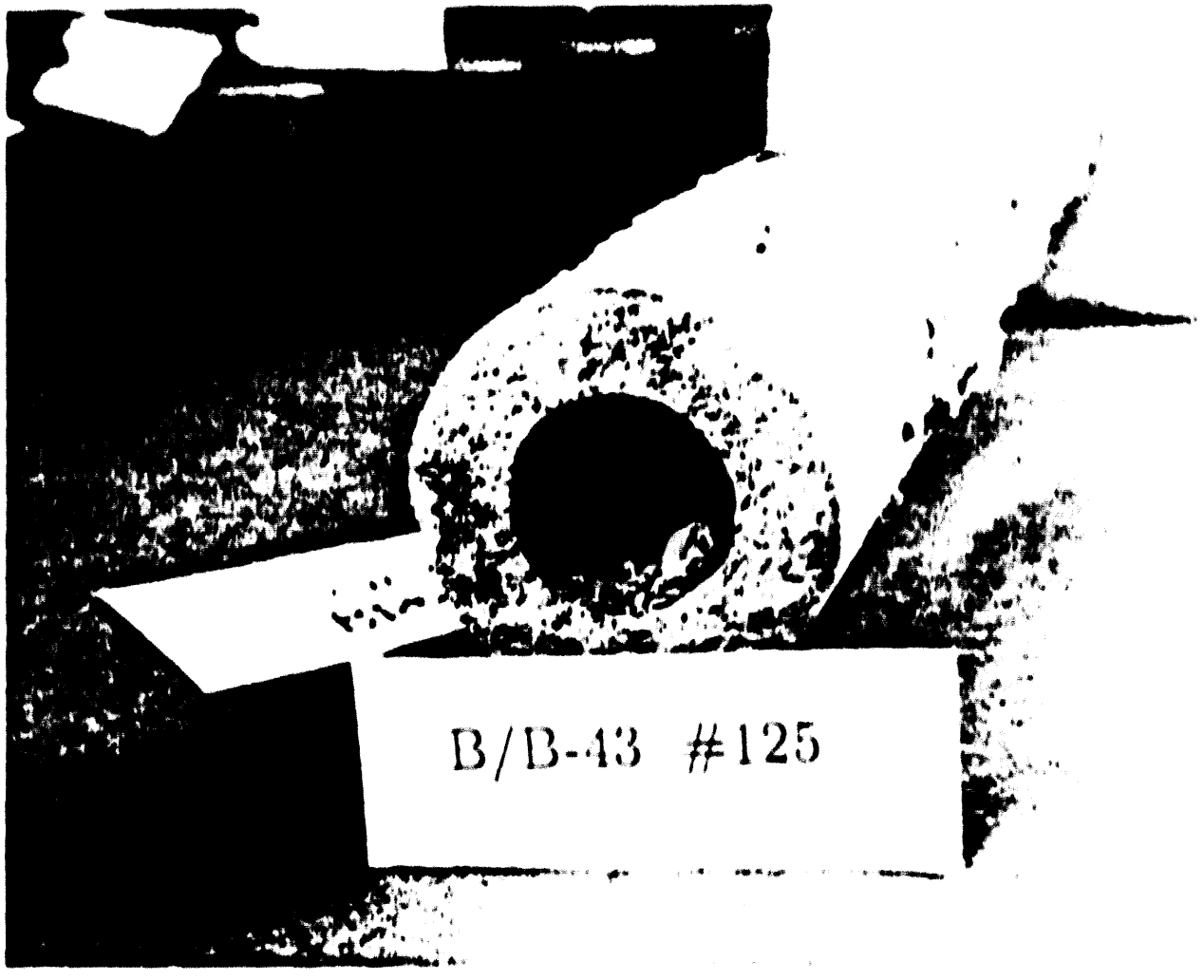

Figure 5 16 Candle With Attached Ash Dumplings

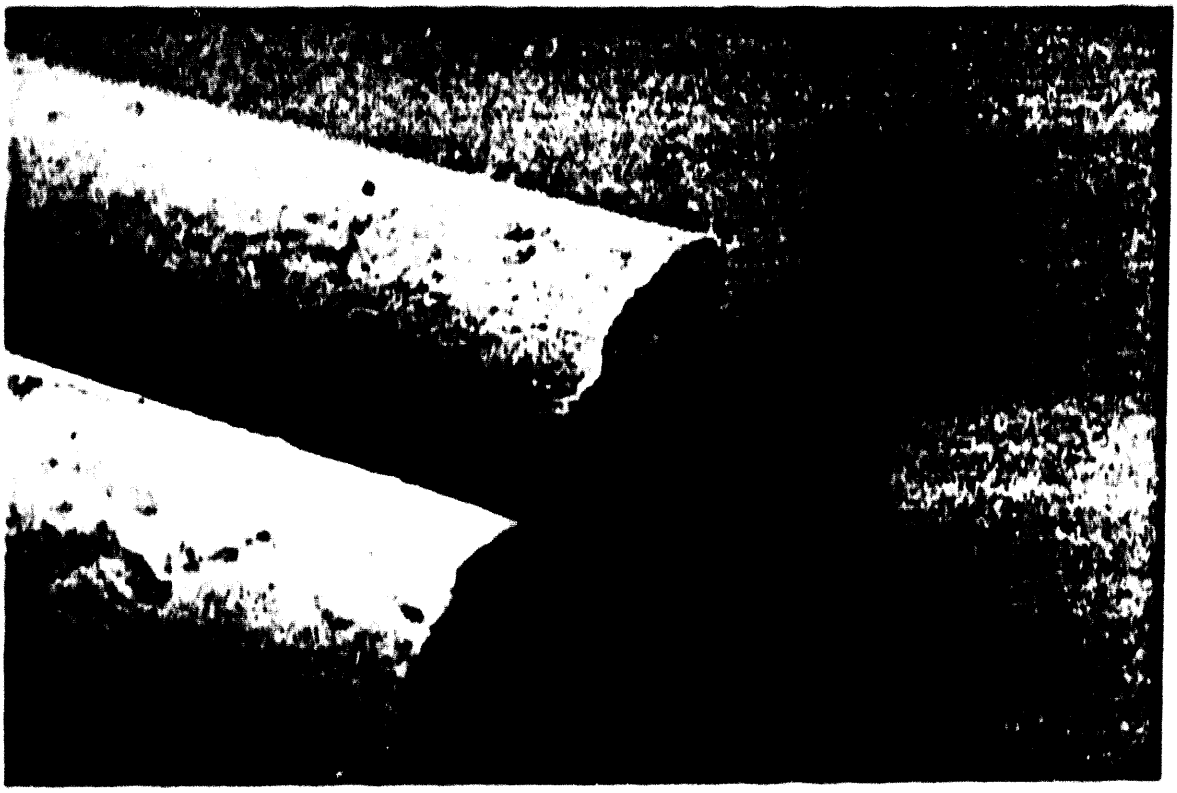

Again in these areas the white sorbent layer was not present. Dumpling or scale-like ash deposits were most likely present along the candle wall, which upon impact with either the ash in the hopper or contact with the filter vessel wall, were stripped from the candle surface, exposing the candle membrane.

Westinghouse conducted a preliminary analysis of the hopper ash material using emission spectroscopy techniques. These data which are presented in Table 5.2 indicated the presence of both ash and sorbent fines. High calcium and magnesium concentrations in the ash were confirmed by these analyses. Similarly a high sulfur concentration was determined, and an ash pH of 4-5 was estimated. Note that the ash had an alkali concentration of 0.03 wt% sodium (Na) and 2% potassium (K). The concentration of soluble alkali will be determined by quantitative atomic absorption (AA) analyses to reflect the concentration of sodium and/or potassium that was released during coal combustion, and which had the potential to recondense along entrained ash particle surfaces.

For comparison, Table 5.2 provides the ash analyses that were determined at AEP. Minor variation in the Westinghouse and AEP elemental concentrations reflect both the analytical procedures that were used in the two independent laboratories, as well as expected inhomogeneity in the sampled ash materials.

5.2 CHARACTERIZATION OF FINES DEPOSITED ALONG THE FRACTURED CANDLE ID SURFACE

After removal of the fractured candle filter segments that remained firmly held in the Westinghouse APF filter holder mounts, it was apparent that the white sorbent layer coated many of the broken candle ID surfaces (Figure 5.18). EDAX analyses indicated the presence of the sulfated dolomitic material which was carried through the Westinghouse AFP vessel during system shutdown (Figures 5.19 and 5.20). High magnification micrographs of the candle filter ID sulfated sorbent deposit are shown in Figure 5.20.

TABLE 5.2

ANALYSIS OF THE PFBC DUST COLLECTED IN THE W-APF VESSEL

(12/92)

Element	Westinghouse Emission* Spectroscopy Data, Wt%	AEP X-Ray Mass** Concentration Data, %
Al	> 5	5.55
Ag	< 0.001	
B	0.02	
Ba	0.03	
Be	0.001	
Bi	< 0.005	
Ca	> 5	9.67
Cd	< 0.02	
Co	0.003	
Cr	0.04	157.572 ppm
Cu	0.01	21.823 ppm
Fe	> 1	3.56
Ga	---	13.133 ppm
Ge	0.008	
K	2	1.25
Li	0.03	
Mg	> 5	5.64
Mn	0.02	140.078 ppm
Mo	0.004	
Na	0.03	NR
Nb	< 0.02	
Ni	0.02	45.707 ppm
Pb	0.04	140.894 ppm
Sb	< 0.02	
Si	> 5	8.11
Sn	< 0.01	
Sr	0.04	158.934 ppm
Ti	1	0.36
V	0.02	45.316 ppm
Zn	0.02	104.254 ppm
Zr	0.06	72.233 ppm
As	< 0.01	119.897 ppm
Rb	0.03	
P	< 0.1	
O		52.17
S		13.59

NR: Not Reported.

* Ash Removed From The Surface Of A Candle That Was Retrieved From The Ash Hopper.

** Characterisation of the W-APF Hopper Ash.

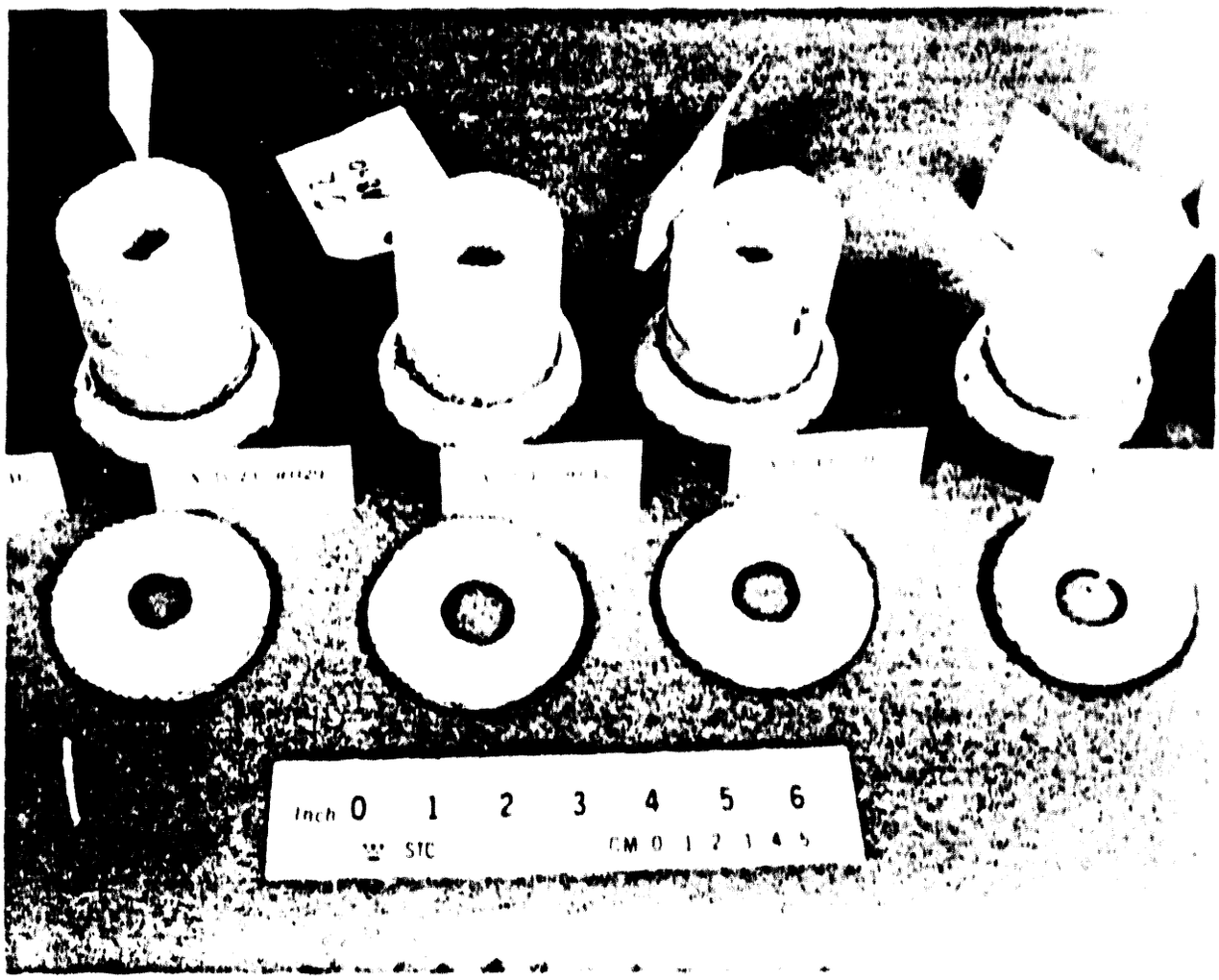

Figure 5.18 - Sorbent Deposit Along The ID Surface Of The Fractured Candle Filters

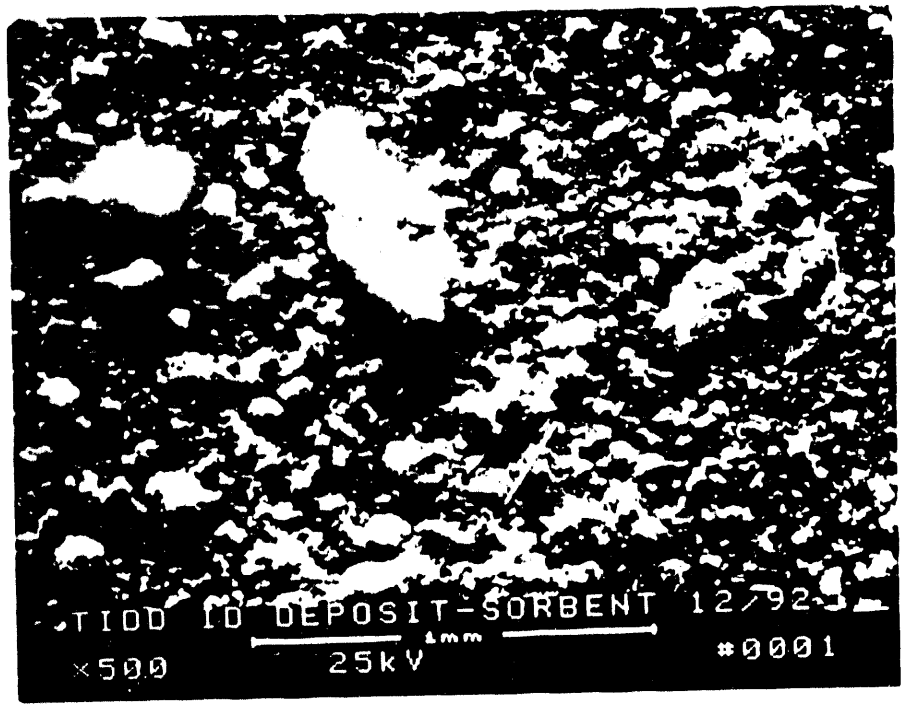

Atomic Percent	
Mg	28.07
Si	7.79
S	26.42
Ca	34.85
Fe	2.87

Normalization Factor=0.719

Figure 5.19 - Morphology Of The Fine Layer Of Sulfated Sorbent Material That Was Removed From The ID Wall Of The Fractured Candle Filters

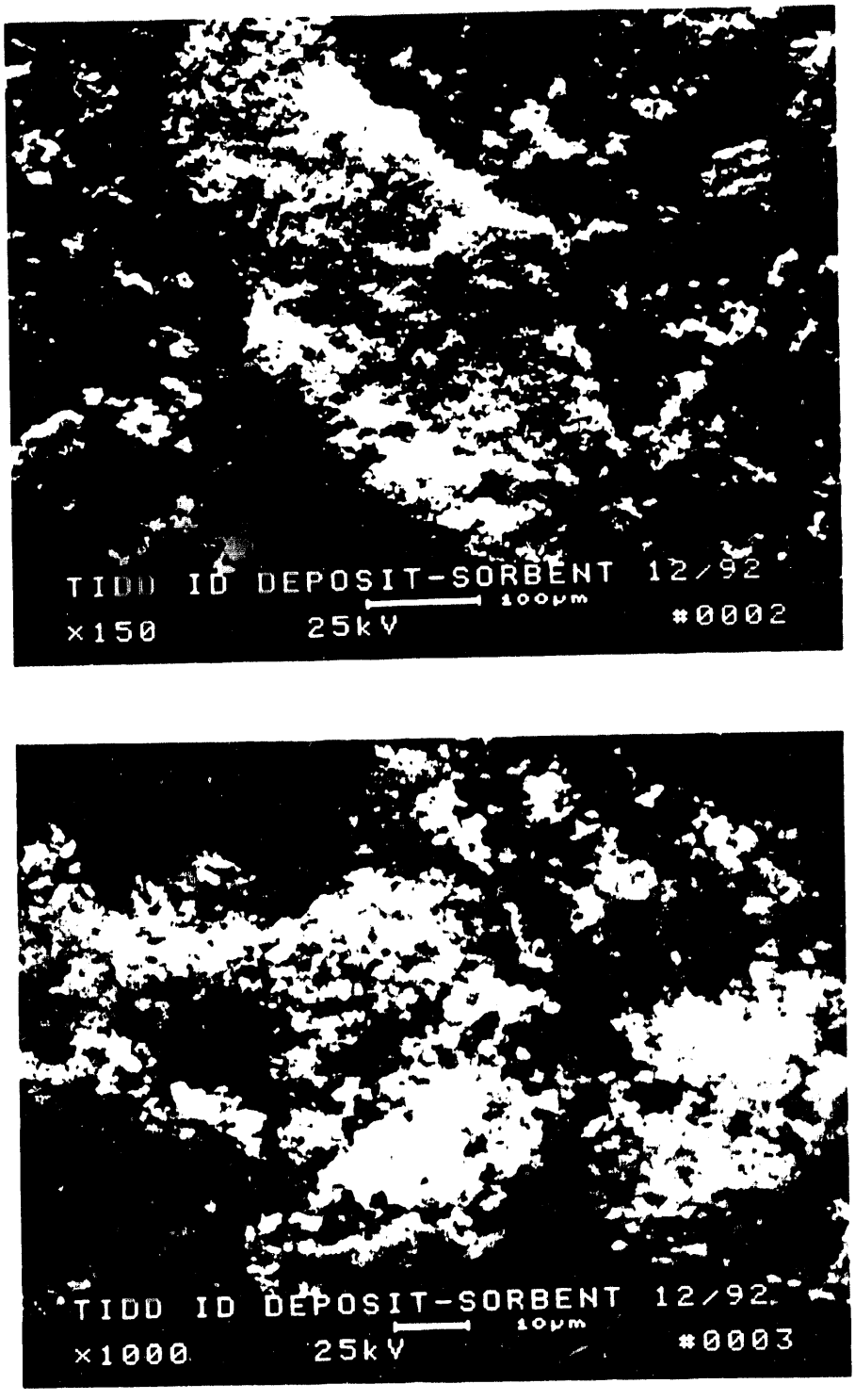

Figure 5.20 - Higher Magnification Micrographs Illustrating The Morphology Of The Sulfated Sorbent Fines Deposited Along The Fractured Candle Filter ID Surfaces

Based on this information, it appeared that sorbent carryover occurred at least twice during the 500 hours of hot gas filtration testing — once when the candles were intact and the sorbent coated the candle OD surface (Figure 5.17), and at a later point in time when sections of the candles failed, resulting in the sorbent coating the candle ID surfaces (i.e., either prior to or at test termination).

5.3 CHARACTERIZATION OF THE WESTINGHOUSE APF HOPPER ASH

In contrast to the relatively "fluffy" or "talc-like" consistency of the ash and/or sorbent material deposited along the ID or OD surfaces of the candles, a very hard, cement-like ash was removed from the bottom of the Westinghouse APF vessel, as well as from the ID of candles that had plummeted to the bottom of the ash hopper (Figure 5.21). A section of the cement-like deposit was removed from one of the candle IDs, and is shown in Figure 5.22. Notably the deposit was very dense, and had characteristic white striations in the pinkish-orange ash/sorbent deposit (Figure 5.23).

SEM/EDAX analyses were performed on both the pinkish-orange and white striated areas of the nonporous deposit. The pinkish-orange matrix consisted of 45.22% S, 21.55% Mg, 11.70% Si, 10.82% Ca, 6.01% Al, 2.99% K, and 1.71% Fe (Normalization Factor (NF) = 0.666). Rather uniform particle sized, spherical micron fines were evident in this material (Photo 4, Figure 5.24). In contrast, the white striated areas contained an extremely high sulfur and magnesium concentration, with limited concentrations of silicon and calcium (Figure 5.25 and 5.26).

X-ray diffraction (XRD) analyses were also performed on select areas that were removed from the cement-like deposit. XRD powder patterns shown in Figures 5.27 through 5.30 indicated that the white areas consisted of hydrated magnesium sulfate or kieserite. In a second

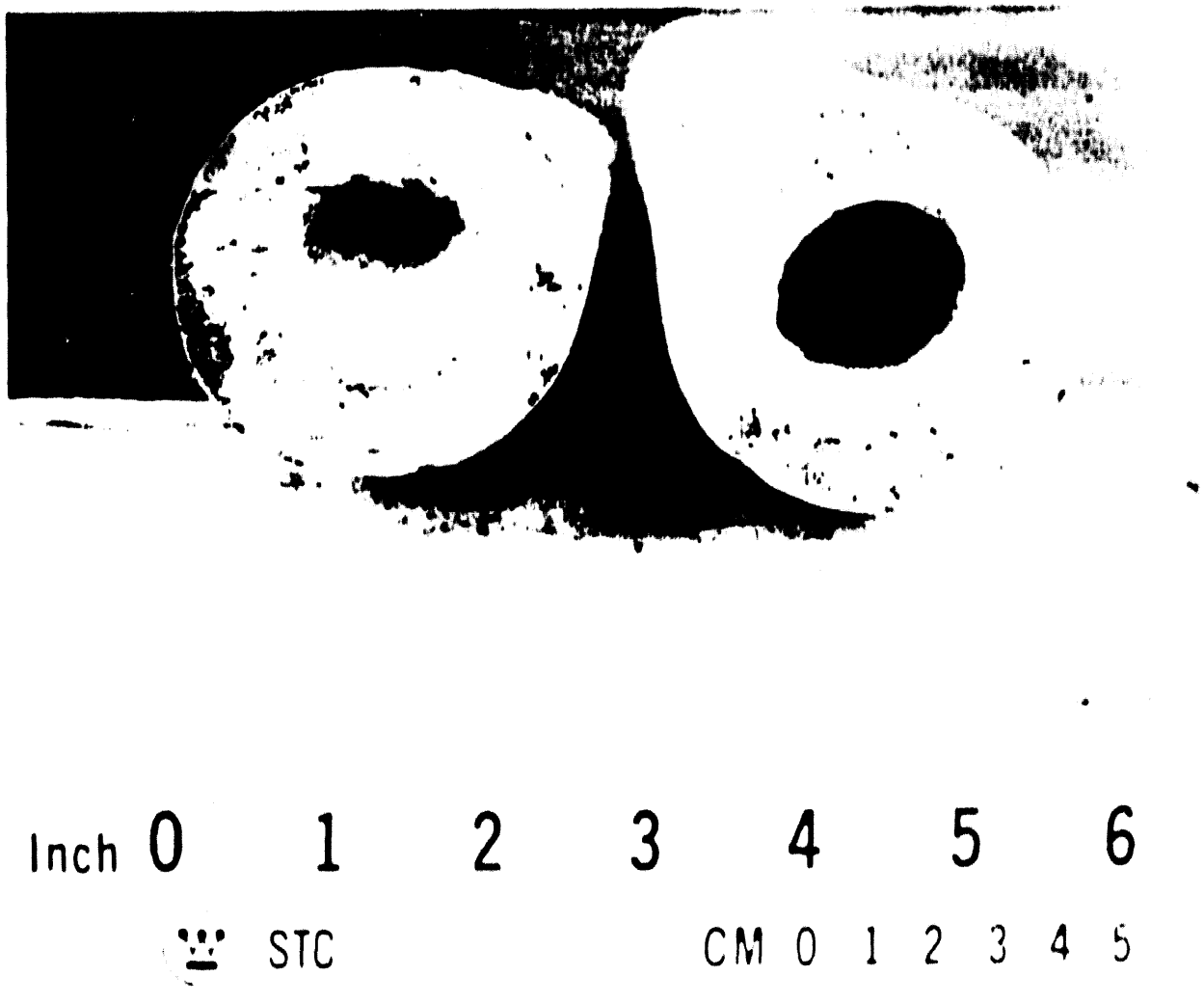

Figure 5.21 - Cement-Like Ash Deposit Formation In The ID Of Candles That Had Fallen Into The Bottom Of The Ash Hopper

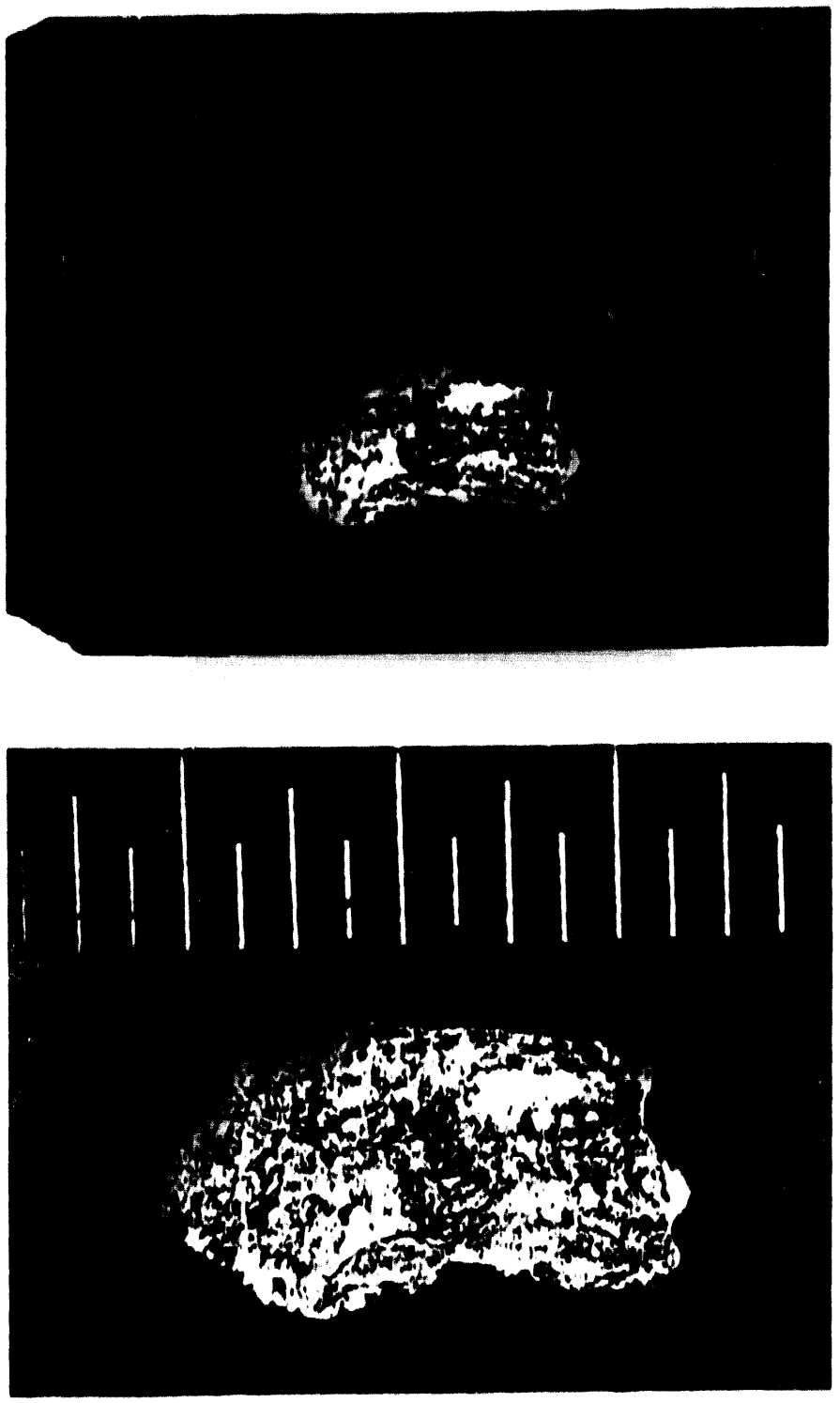

Figure 5.22 - Cement-Like Ash Deposit Formed In The ID Of Candles That Had Fallen Into The Bottom Of The Ash Hopper

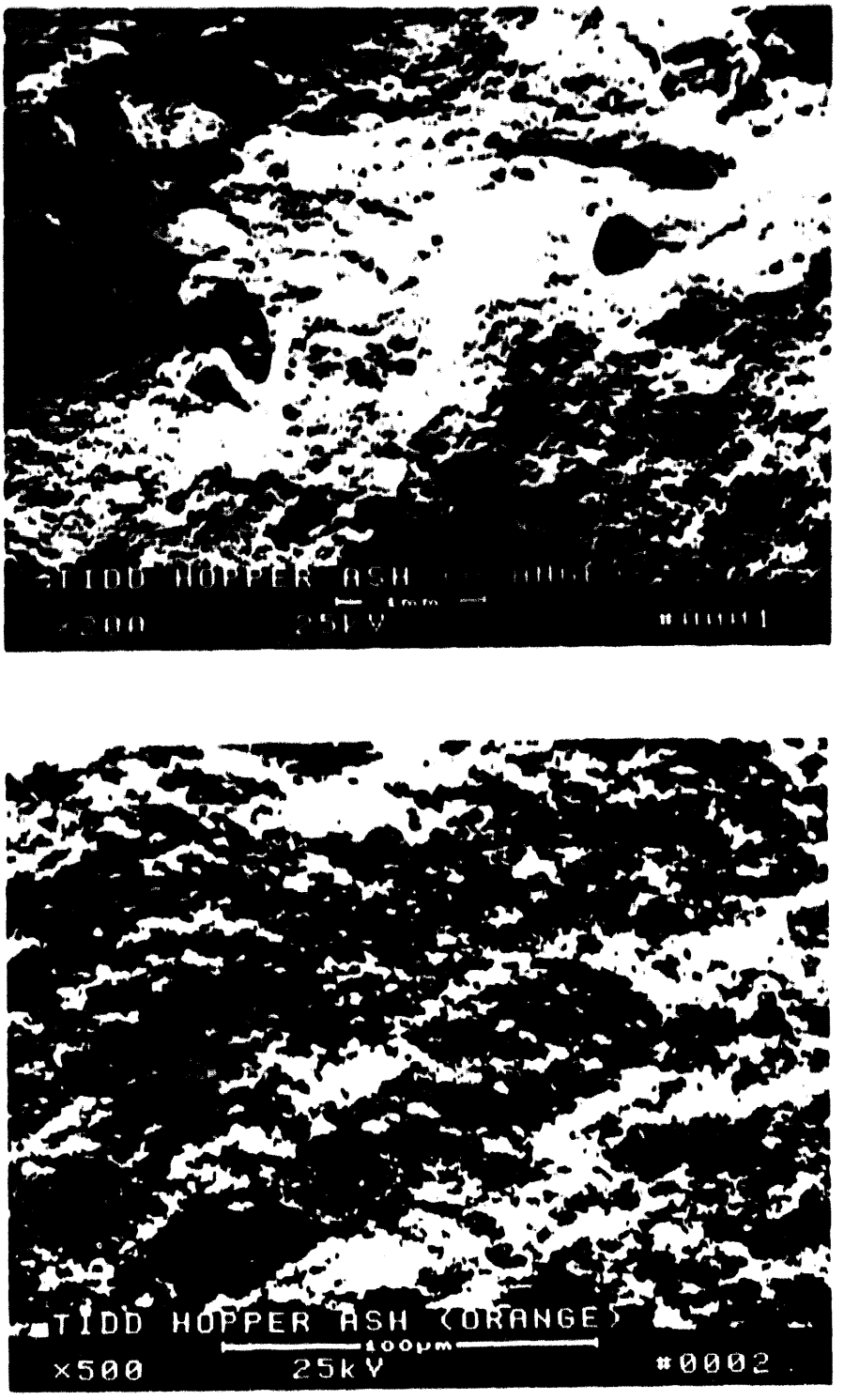

Figure 5.23 - Morphology Of Ash And Sorbent Fines Collected In The Cement-Like Deposit That Formed In The ID Of Candle Filter That Had Fallen Into The Bottom Of The Ash Hopper

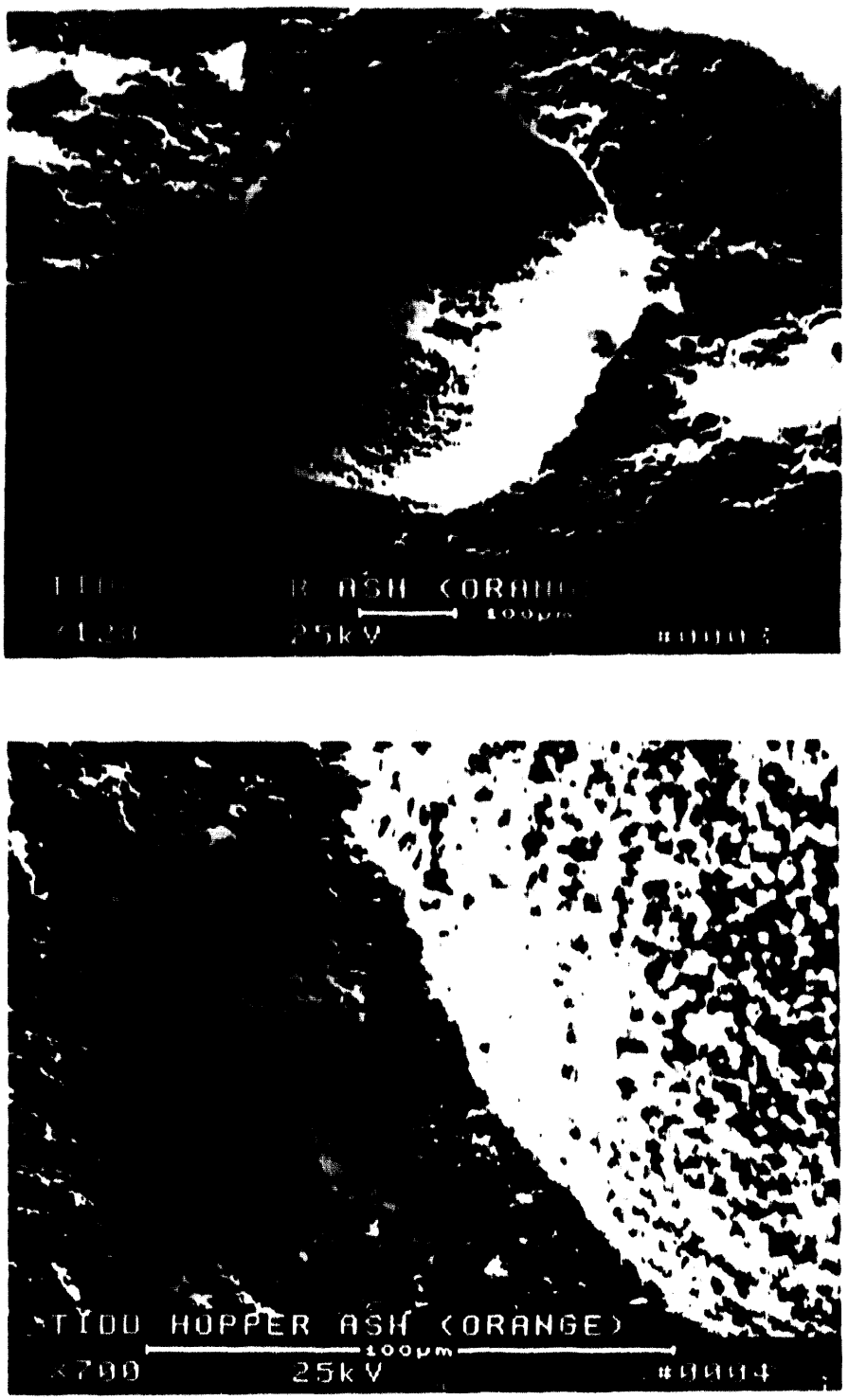

Figure 5.24 - Higher Magnification Micrographs Illustrating The Morphology Of The Ash And Sorbent Fines Collected In The Cement-Like Deposit Formed In The ID Of Candles That Had Fallen Into The Bottom Of The Ash Hopper

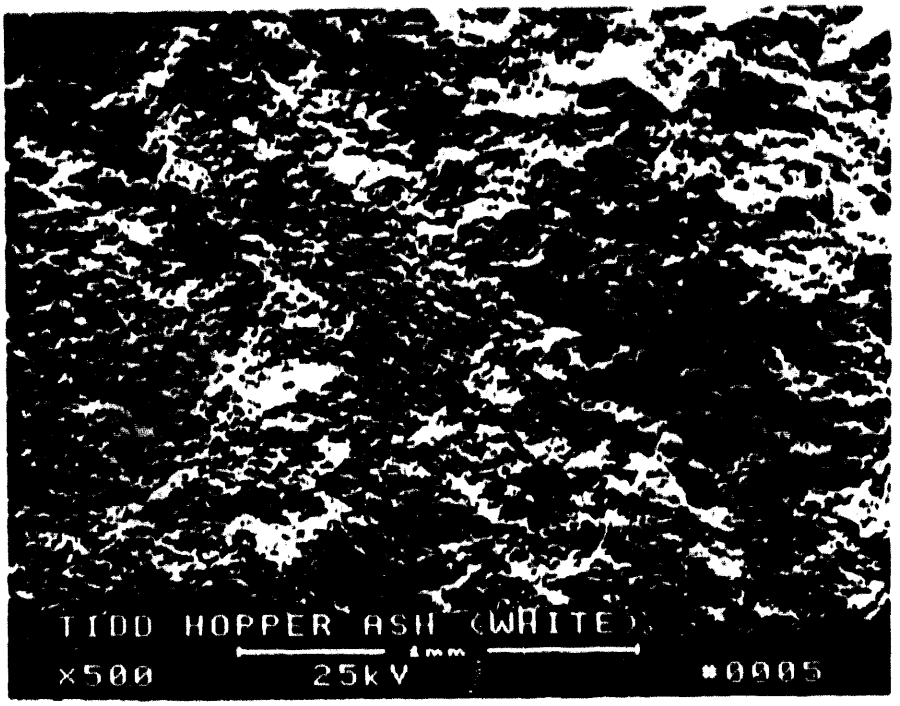

Figure 5.25 - Morphology Of The White Inclusions That Are Present In The Cement-Like Ash Hopper Deposit. Matrix Is Principally Hydrated Magnesium Sulfate

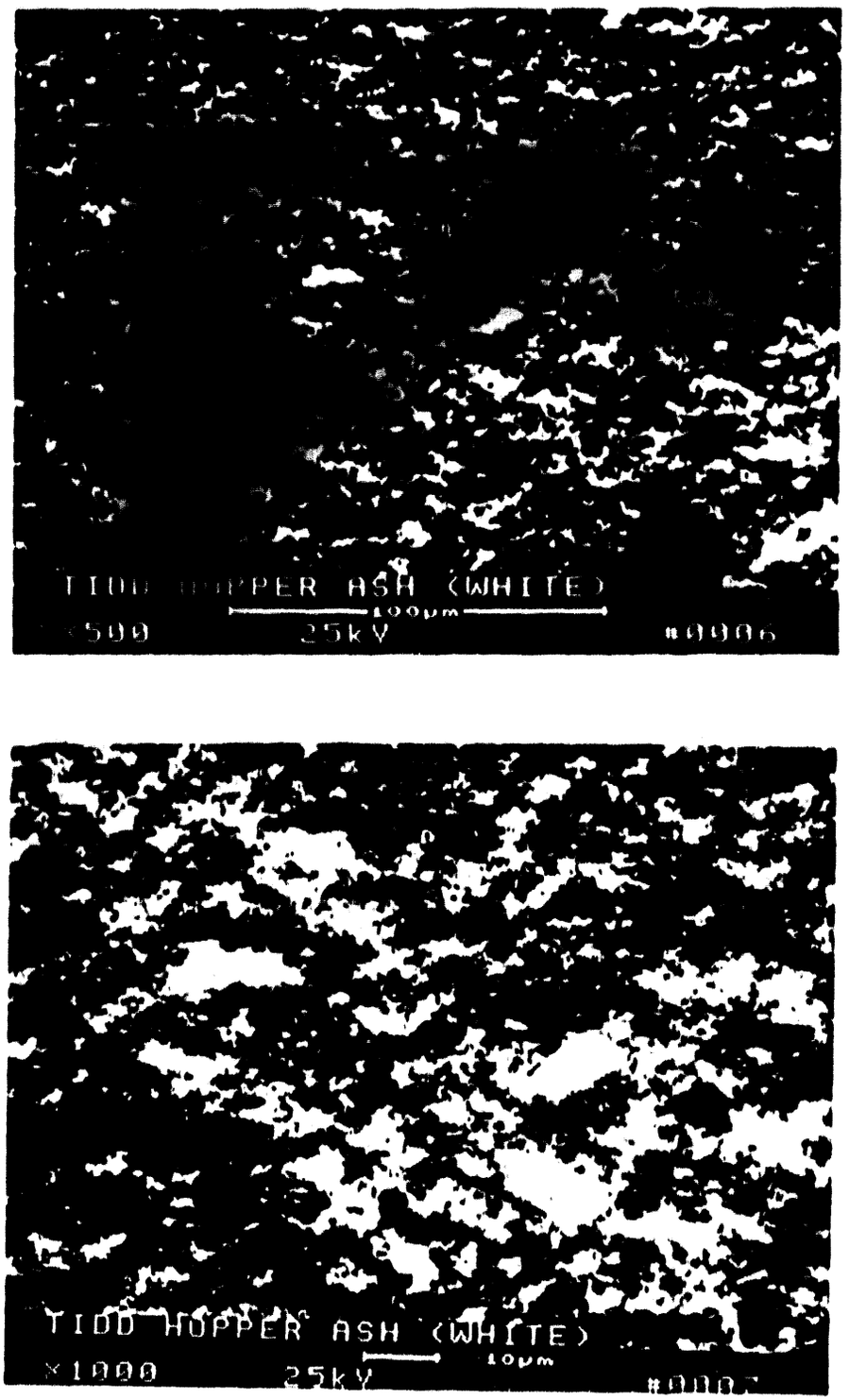

Figure 5.26 - Higher Magnification Micrographs Illustrating The Morphology Of The Densely Packed Hydrated Magnesium Sulfate-Enriched Fines In The White Isolated Inclusions In The Bottom Hopper Ash Of The Westinghouse APF Vessel

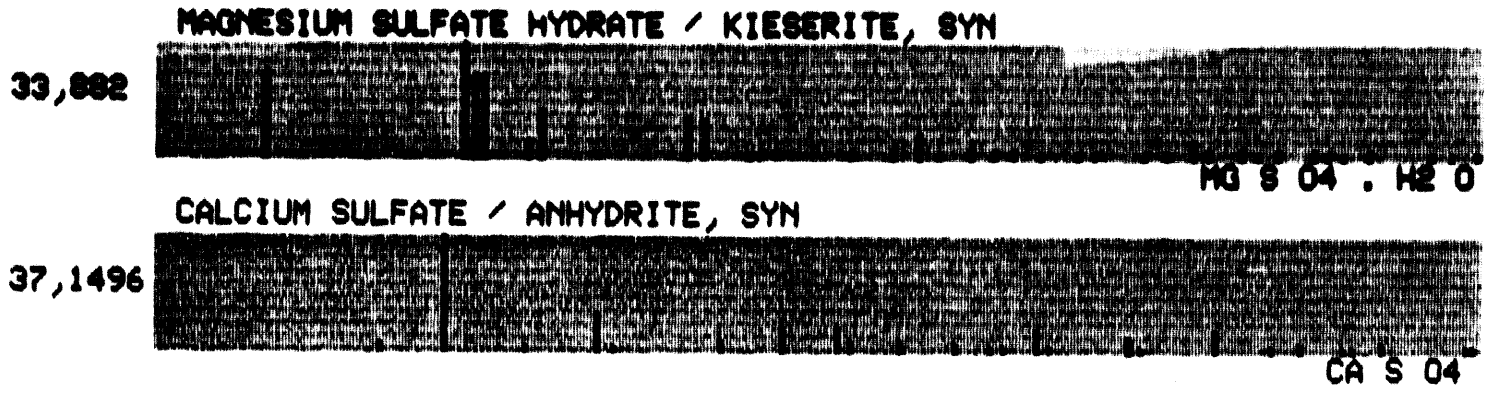

Figure 5.27 - X-Ray Diffraction Analysis Of The White Cement-Like Striated Material Found In The Hopper Ash

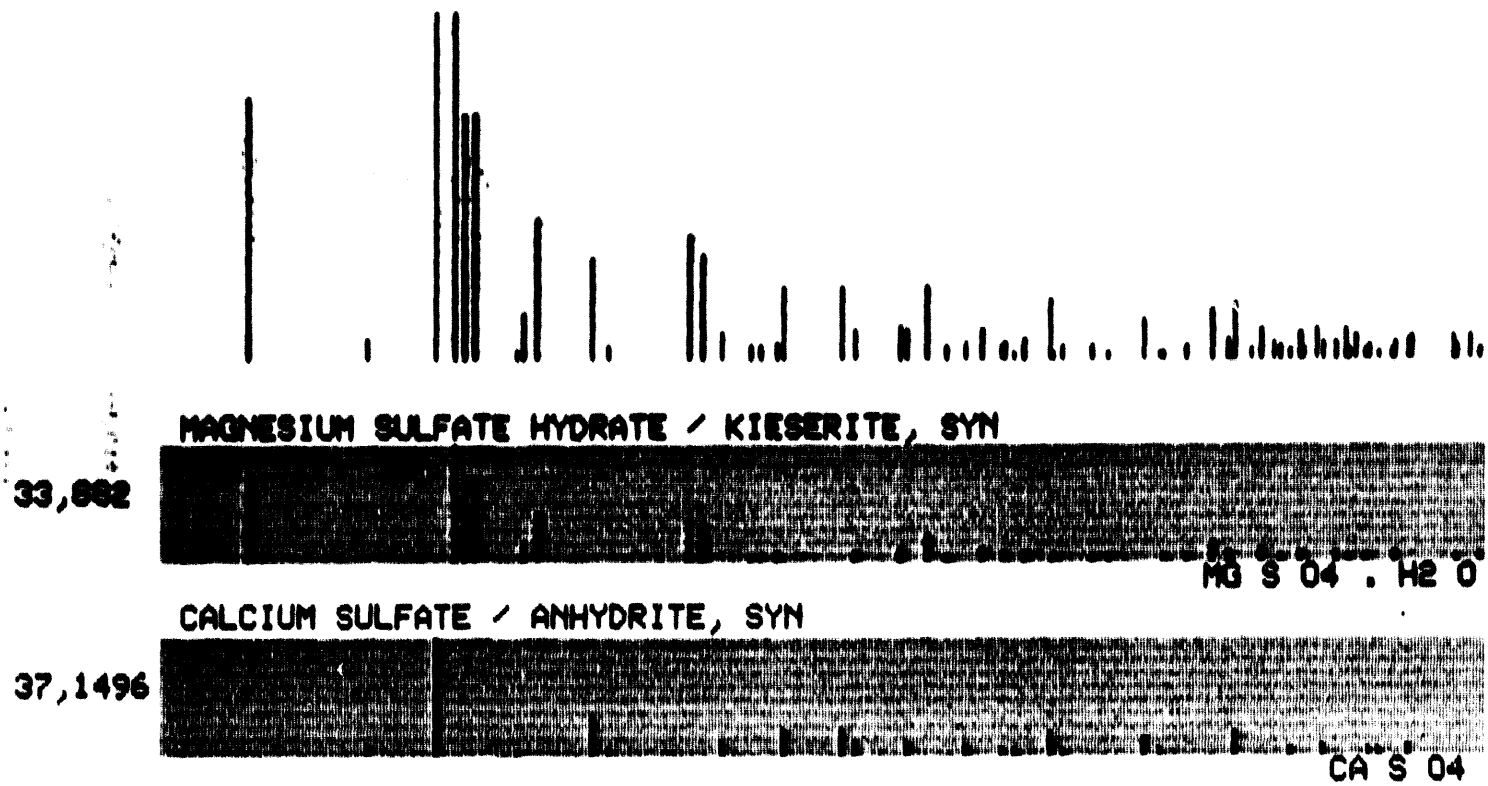

Figure 5.28 - X-Ray Diffraction Analysis Of The Cement-Like Hopper Ash Deposit

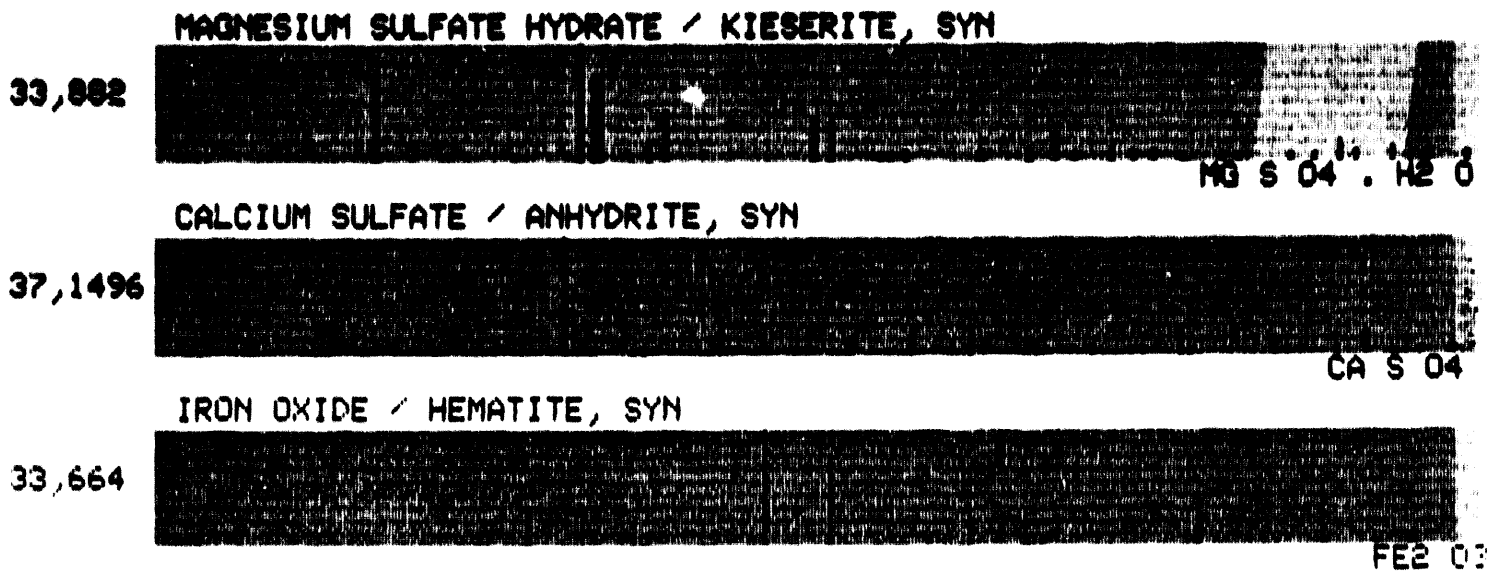

Figure 5.29 - JCPDS Patterns For Best Fit Compounds In Relationship To The Cement-Like Hopper Ash Deposit

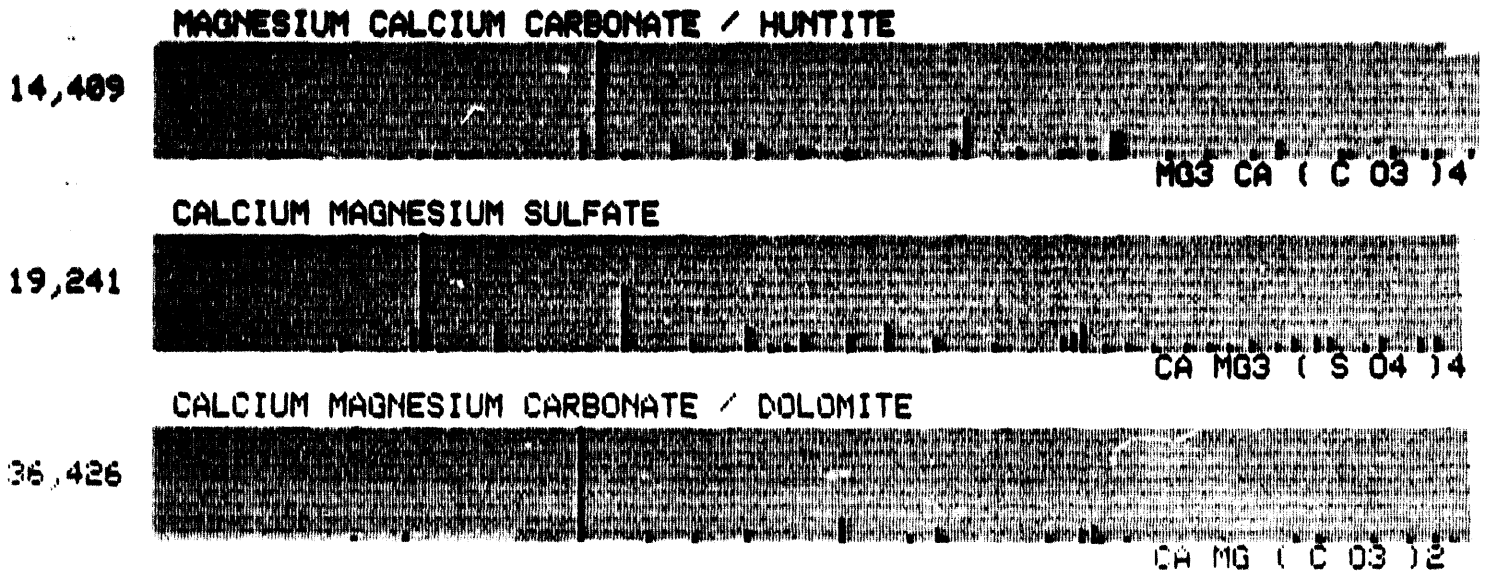

Figure 5.30 - JCPDS Patterns For Best Fit Compounds In Relationship To The Cement-Like Hopper Ash Deposit

analyses of what appeared to be a white area, we detected not only kiersite, but also calcium sulfate (anhydrite), as well as iron oxide (hematite). The presence of iron oxide indicated that the white striated areas which were used in these analyses also contained the pinkish-orange ash material. An additional sample indicated that the white striated region contained both kieserite and anhydrite, while the dark pinkish-orange material contained kiersite, anhydrite, and hematite.

What was peculiar was that the hardened ash deposit contained a higher concentration of magnesium than would be expected for the typical calcium-magnesium sulfur sorbent matrix. Note, however, that the principal constituents of the ash — calcium and magnesium — were sulfated. At this point in time we are not able to explain why the sorbent would selectively split into a discrete calcium and magnesium phase, and in particular why the hydrated magnesium sulfate phase was selectively enriched in comparison to what should have been an equivalent calcium-magnesium (i.e., dolomitic) complex.

5.4 PROXIMATE, ULTIMATE, AND ASH FUSION CHARACTERIZATION

Table 5.3 presents the proximate and ultimate analysis of the typical dust cake layer that formed along the outer surface of the intact candle filters. As-received, the ash content of the ash/sorbent layer was ~82%, with only 3.62% total carbon being detected (i.e., carbon from both coal and sorbent materials). The dust cake layer had a relatively high sulfur content (i.e., 11%).

Fusion temperature data presented in Table 5.4 indicated that there were some definite differences between the various ash materials that were removed from the Westinghouse APF vessel. For example, the ash that formed along the fractured candle ID walls was characteristically white in appearance. The contribution of sorbent in the ID deposit had a tendency to increase the fusion temperatures

TABLE 5.3

PROXIMATE AND ULTIMATE ANALYSIS OF THE DUST CAKE LAYER FORMED ALONG THE OUTER SURFACE OF AN INTACT CANDLE FILTER

	As-Received	Dry
Proximate Analysis		
Moisture	8.07	
Ash	81.65	88.82
Volatile Matter	19.19	20.87
Ultimate Analysis		
Hydrogen	1.47	0.62
Carbon	3.62	3.94
Nitrogen	0.04	0.04
Sulfur	11.00	11.97
Ash	81.65	88.82
Heating Value (BTU/lb)	54	59

TABLE 5.4

ASH FUSION TEMPERATURES, °C (°F)*

Ash Material Location	Initial Deformation	Softening	Hemispherical	Fluid
Outside Intact Candle	1132 (2070)	1171 (2140)	1177 (2150)	1182 (2160)
Outside Broken Candle	1271 (2320)	1282 (2340)	1293 (2360)	1304 (2380)
White Deposit Inside Candle	1171 (2140)	1182 (2160)	1193 (2180)	1216 (2220)
Ash Hopper ID Ash **	1216 (2220)	1271 (2320)	1293 (2360)	1304 (2380)

* Reducing Atmosphere.
** $MgSO_4$-Hydrate (Major), $CaSO_4$, Fe_2O_3.

Tammann Temperature: 1/2 Absolute Melting Point Where Bulk Diffusion Begins.

Huttig Temperature: 1/3 Absolute Melting Point Where Surface Diffusion Begins.

slightly above those reported for the ash that deposited along the OD surface of the intact candle filters. The intact candle ash cake layer was predominantly ash which had a smaller contribution of sorbent in the deposit in comparison to the ash fines.

The cement-like ash deposit along the ID of the broken candle sections that had fallen into the ash hopper had an even higher ash fusion temperature profile, while the "fluffy" ash deposit along the broken candle segments that had fallen into the ash hopper had a somewhat higher initial deformation and softening temperature. Although all of these temperatures are well above the operating temperature of the Westinghouse APF system, surface and bulk diffusion in the ash begins to occur at 1/3 and 1/2 of the material's melting temperature. Surface and bulk diffusion should therefore be expected to occur in the ash materials at APF process operating temperatures. Whether the ash had a sticky surface when it contacts the filter remains to be determined.

5.5 FILTER MOUNT ASH

Ash that was removed from the filter mount area (i.e., area between the gasket and metal holder) had a characteristic reddish brown appearance. The color of this ash was a much deeper red than the pinkish-orange ash found elsewhere within the Westinghouse APF vessel. Figures 5.31 through 5.36 illustrate the morphology of the filter mount ash. Large agglomerates of micron- and submicron-sized fines were evident. The "fluffy", "billowy" agglomerates contained the sulfated sorbent matrix (i.e., sulfur atomic percent was nearly equivalent to the combined calcium and magnesium atomic percent, implying that both the calcium and magnesium constituents of the dolomitic sorbent were nearly completely sulfated). Aluminum and silicon (i.e., ash constituents) were also detected in the filter mount ash. What was unique in this

	Atomic Percent	
Element	Area 1	Area 2
Mg	6.98	4.19
Al	11.86	11.20
Si	21.17	21.63
S	20.14	25.02
Cl	15.21	0.45
K	2.36	3.09
Ca	13.62	19.61
Ti	0.60	0.78
Cr	0.91	2.01
Fe	7.14	12.01
Normalization Factor	0.620	0.662

Figure 5.31 - Large Ash Agglomerate Formed In The Flange Mount/ Gasket Area Of The Candle Filter

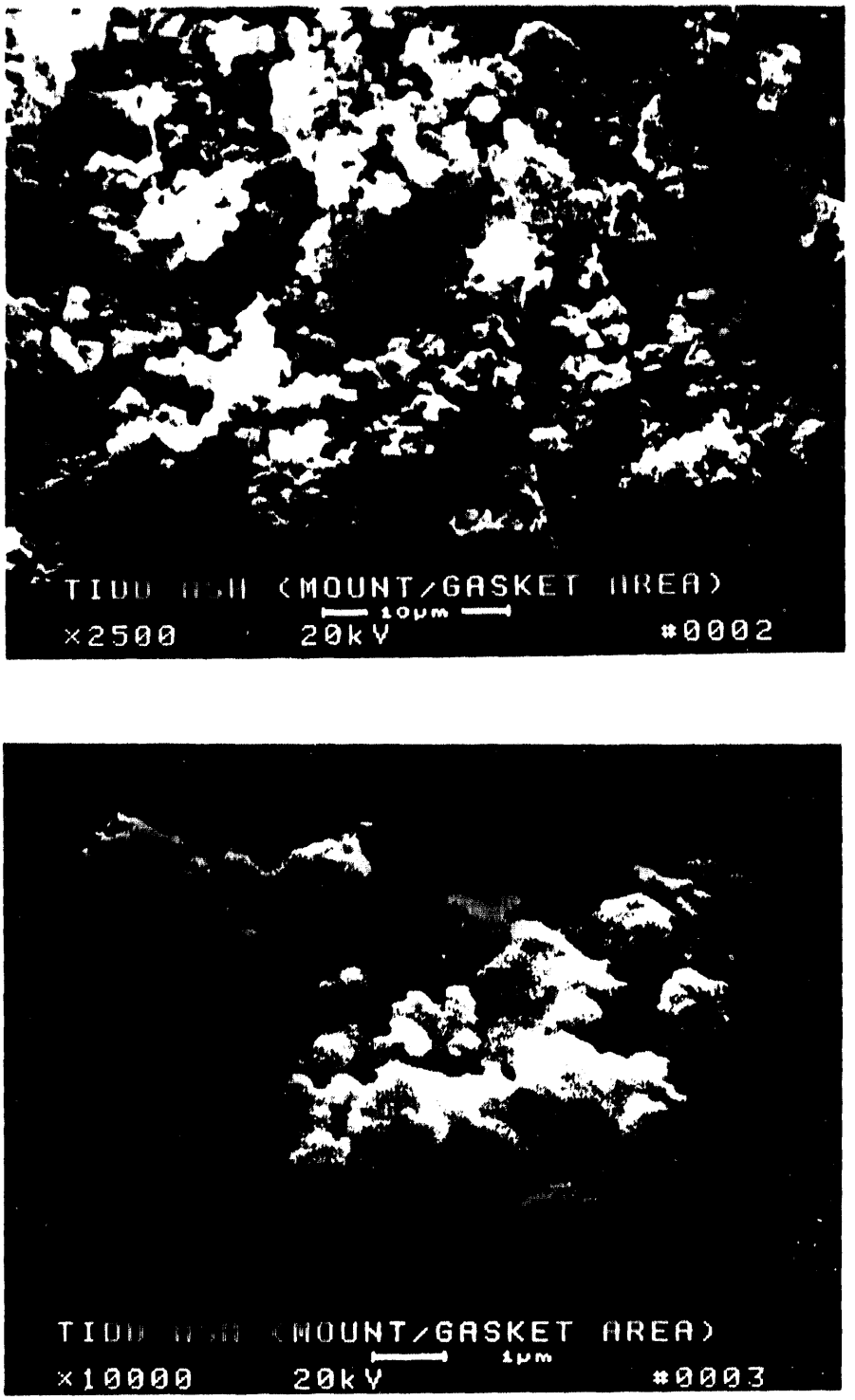

Figure 5.32 - Higher Magnification Of The Ash Agglomerates Formed In The Flange Mount/Gasket Area Of The Candle Filter Holder

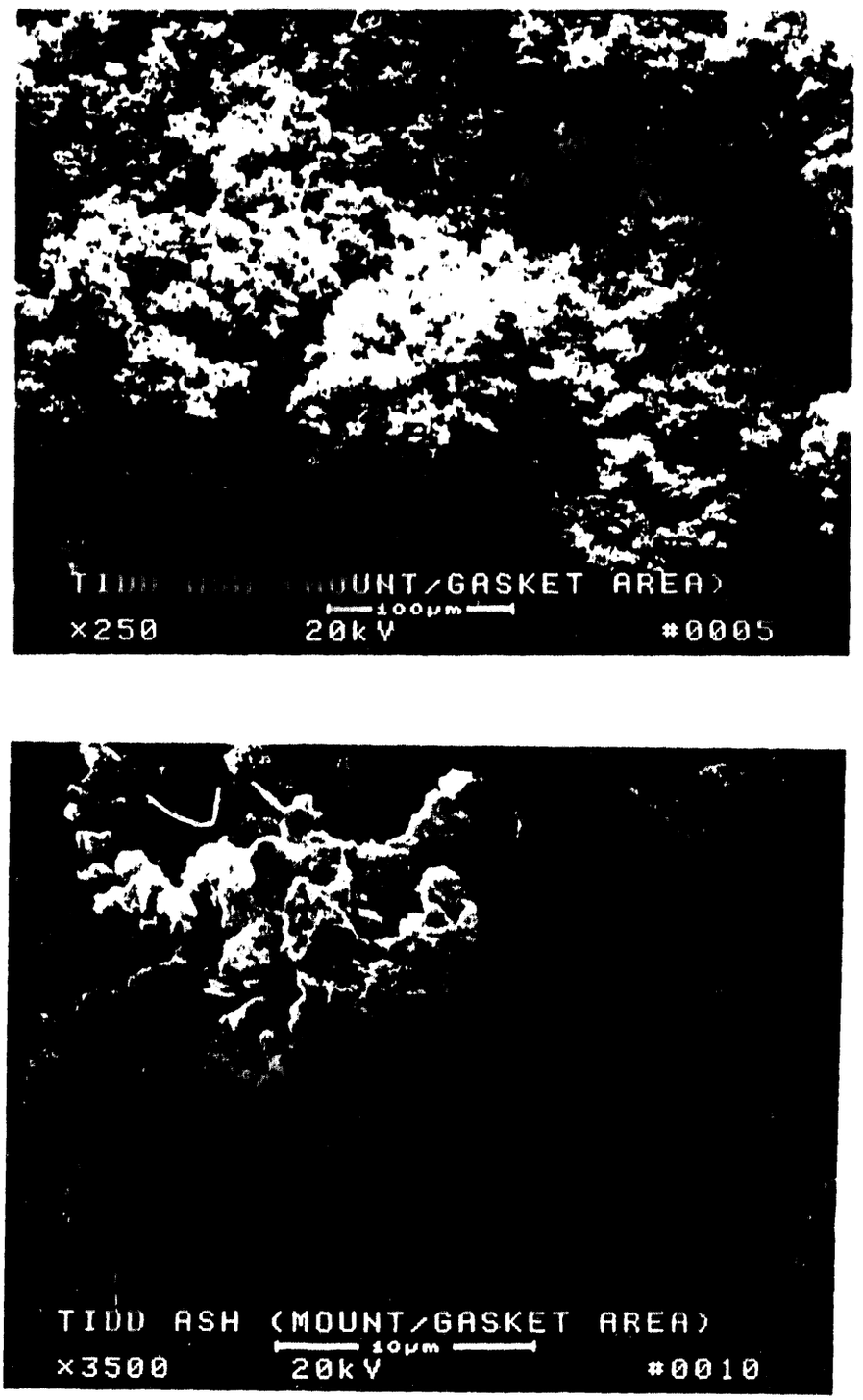

Figure 5.33 - Ash Agglomerates Formed In The Flange Mount/Gasket Holder Area Of The Candle Filter

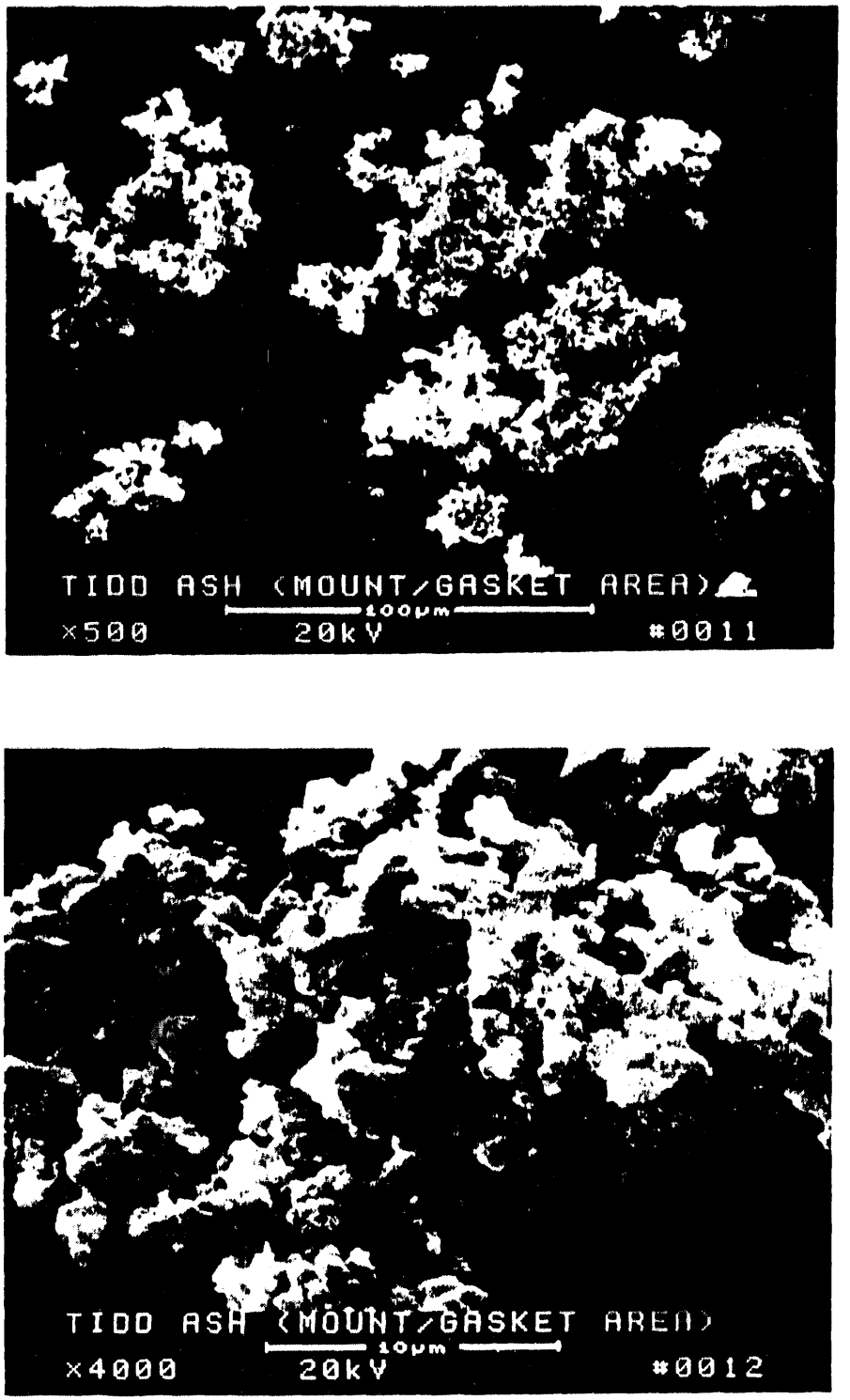

Figure 5.34 - Ash Agglomerates Formed In The Flange Mount/Gasket Area Of The Candle Filter Holder

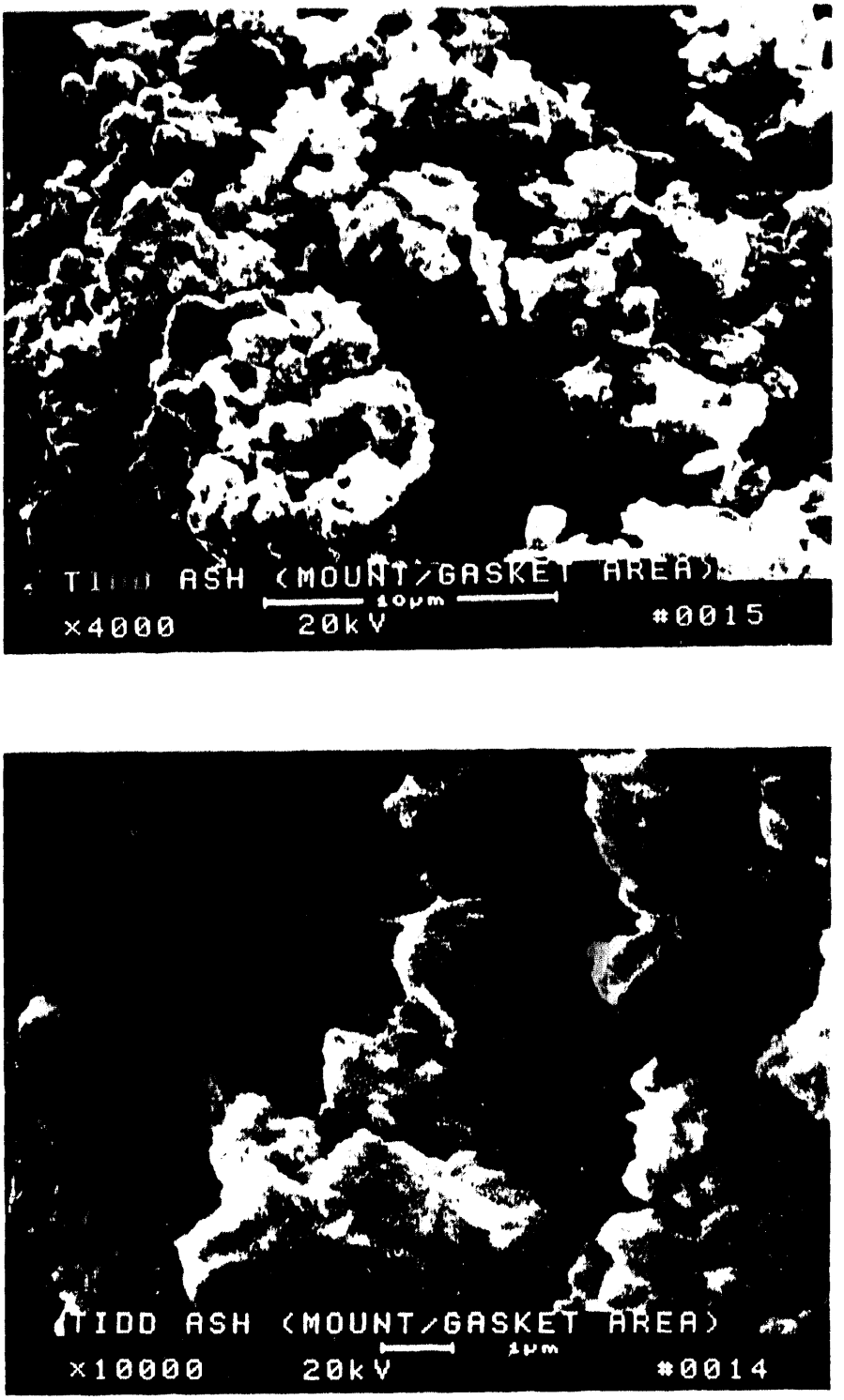

Figure 5.35 - Ash Agglomerates Formed In The Flange Mount/Gasket Area Of The Candle Filter Holder

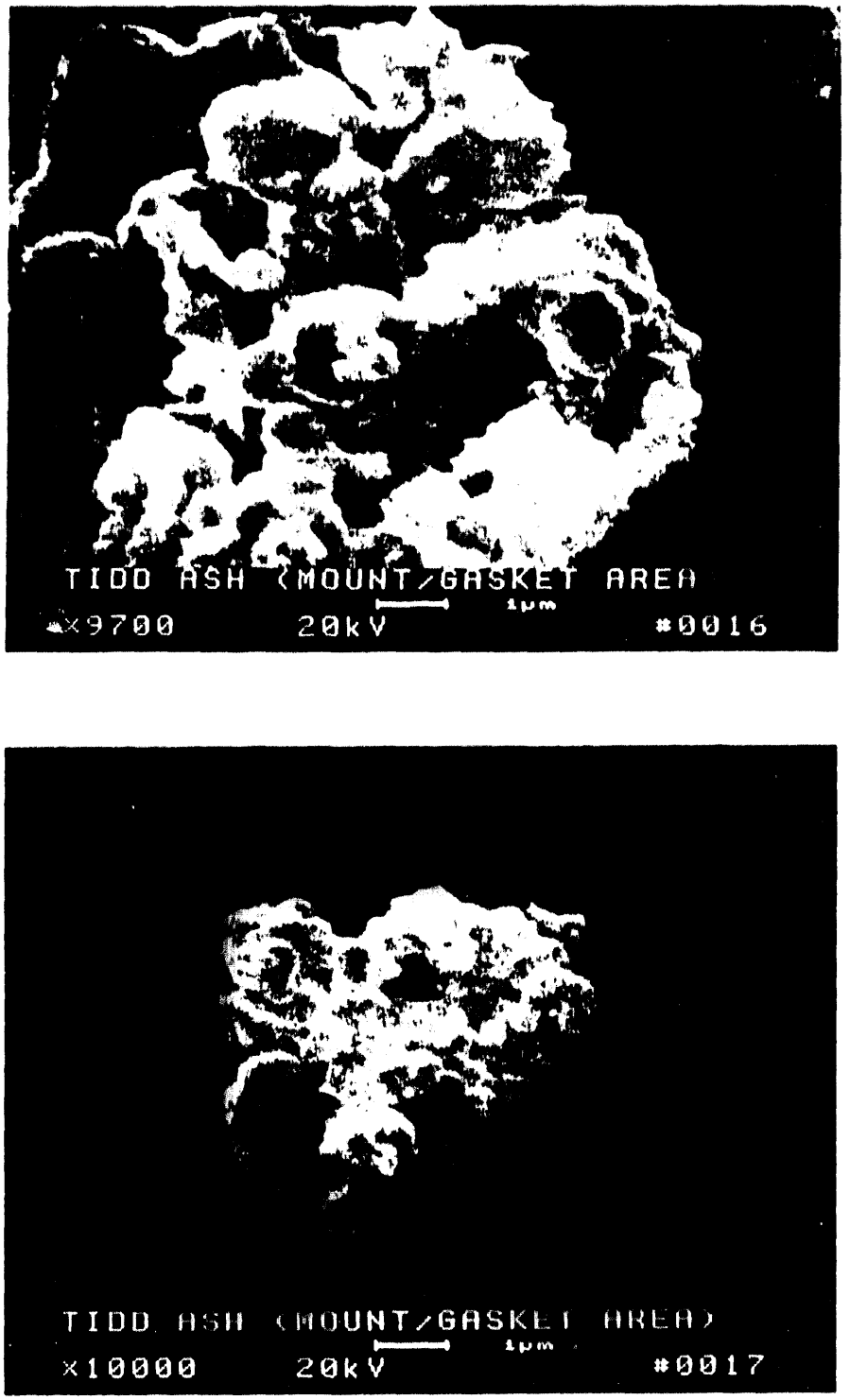

Figure 5.36 - Ash Agglomerates Formed In The Flange Mount/Gasket Area Of The Candle Filter Holder

material was the relatively high concentration of iron (i.e., 7 to 12 atomic percent), as well as chlorine concentration (i.e., 0.5 to 15 atomic percent). Chromium was also detected in the filter holder ash. The high concentration of iron, as well as chromium implied residual metallic debris (i.e., oxidation and/or erosion of the filter holders may have occurred). We do not suspect at this time, that any metal oxidation and/or erosion warrants concern for excessive filter holder metal wastage.

What was rather unique in this ash material were several interconnecting areas between adjacent ash particles. As shown in Photo 14 of Figure 5.35 there appears to be a "bond-like" channel connecting two adjacent cenosphere ash particles. Further effort would be required to verify the extent of bonding in this material, as well as to qualitatively identify the composition of the interconnecting "bond-like" channel material.

5.6 ELEMENTAL MICROPROBE ANALYSES OF THE ASH DEPOSIT FORMED ALONG THE CLAY BONDED SILICON CARBIDE CANDLE FILTER

Figure 5.37 illustrates the morphology and composition of the ash deposit along the OD and ID surfaces of the cross-sectioned wall of the clay bonded silicon carbide matrix after 500 hours of exposure to the PFBC oxidizing environment at Tidd. Calcium (Ca), magnesium (Mg), and sulfur (S) were readily detected in the PFBC deposited fines using elemental microprobe analysis (EMA) techniques. Homogeneous background concentrations of oxygen (O), silicon (Si), aluminum (Al), and iron (Fe) were identified in the fines. EMA did not detect sodium (Na) and/or chlorine (Cl) within the deposited ash-sorbent layer.

EMA was also performed along an ash dumpling surface in an attempt to further support the SEM/EDAX and XRD analyses with respect to the compositional variation that existed between the white versus the pinkish-orange ash layers in the 5 to 10 mm dumplings that formed along

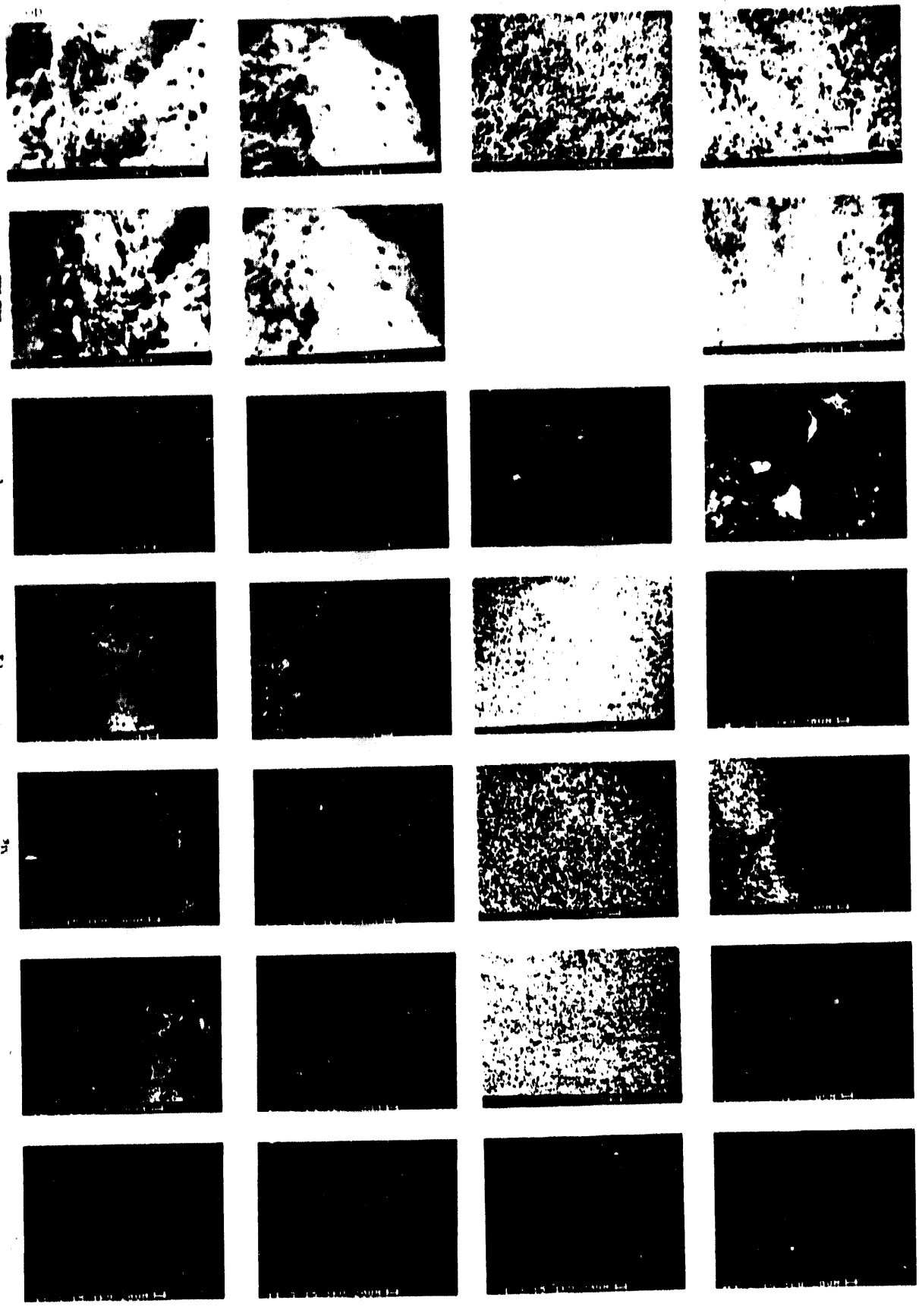

Figure 5.37 - Elemental Microprobe Analysis Of The Ash Deposit Formed Along The Cross-Sectioned Clay Bonded Silicon Carbide Candle Filter

the candle filter wall. The pinkish-orange ash area contained higher concentrations of aluminum and silicon in comparison to the calcium- and magnesium-enriched white sorbent layer in the dumpling deposit (Figure 5.38).

5.7 QUANTITATIVE ANALYSES

Quantitative analyses are currently being performed on the hopper ash, ash dumplings, and sorbent-ash material removed from the ID of fractured candle surfaces. These analyses will determine the concentration of aluminum (Al), silicon (Si), calcium (Ca), magnesium (Mg), iron (Fe), sulfur (S), and potassium (K) that is present in each ash material. In addition a water and acid leach will be conducted to determine the concentration of soluble sodium (Na) that is present in each material, as well as insoluble and total sodium content. The results of these analyses will be presented at a later date.

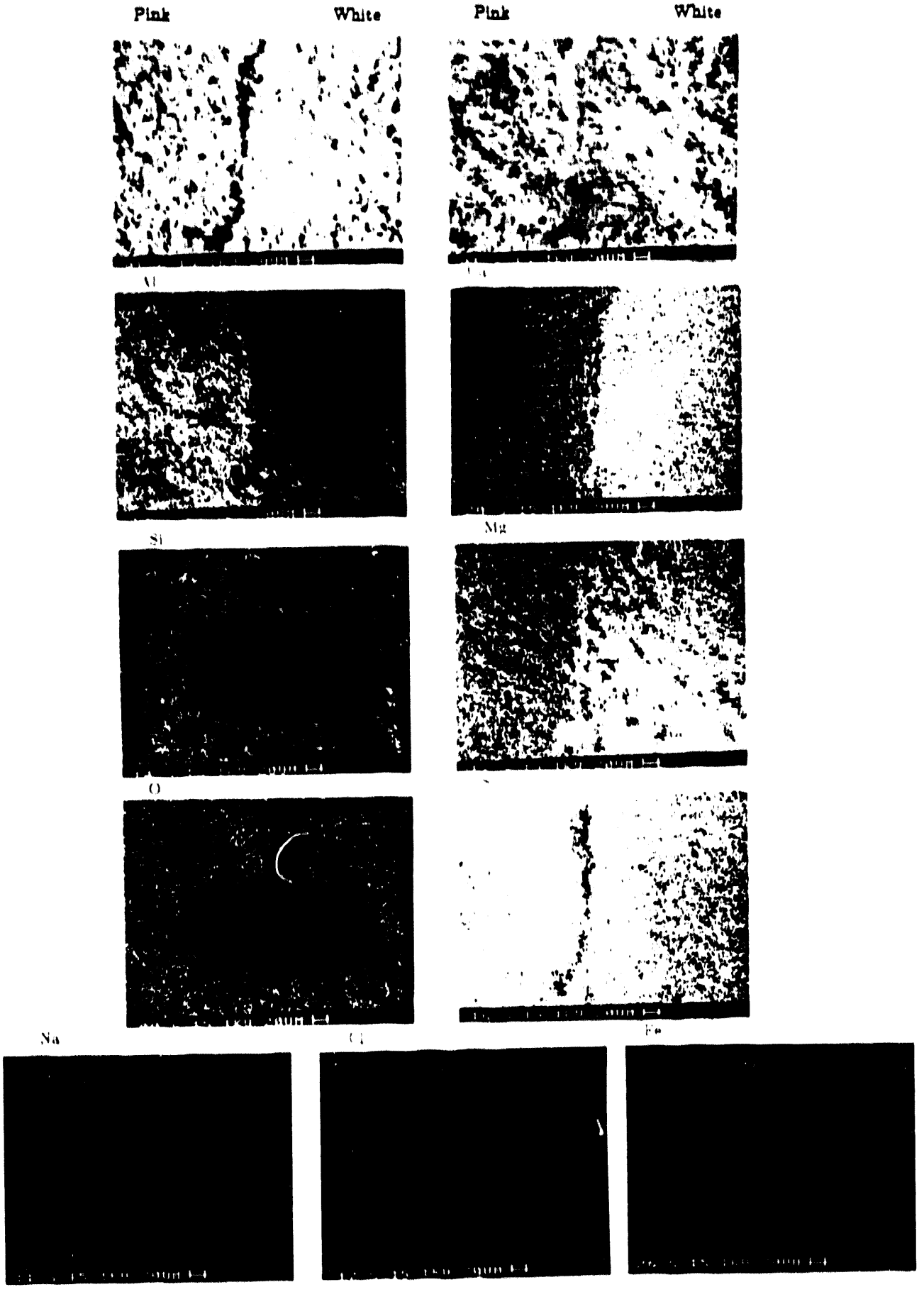

Figure 5.38 - Elemental Microprobe Analyses Detailing The Compositional Variation Within The Ash Dumpling Deposits That Were Formed Along The Candle OD Surface After 500 Hours Of Hot Gas Filtration At Tidd

RM-29895

6. MORPHOLOGY OF THE CLAY BONDED SILICON CARBIDE MATRIX

This section details the results of the scanning electron microscopy/energy dispersive x-ray analyses (SEM/EDAX) and elemental microprobe analyses (EMA) that were performed on the as-manufactured clay bonded silicon carbide Schumacher Dia Schumalith F40 material, as well as on the 500 hour PFBC exposed candle filters.

6.1 AS-MANUFACTURED CLAY BONDED SILICON CARBIDE CANDLE FILTER MATRIX

Figure 6.1 illustrates the morphology of the clay bonded silicon carbide matrix along a cross-sectioned area of the as-manufactured candle filter wall. A membrane layer is formed along the OD surface of the candle filter. The membrane consists of aluminosilicate fibers, a binder phase, as well as small grains of silicon carbide. Below the OD membrane layer are 0.5 to 0.75 mm silicon carbide grains which form the structural support for the filter wall. The coarse silicon carbide grains are held together via the same binder phase that is used to bond the fibers together in the membrane layer. Large pores and pore channels result in the coarse silicon carbide structural wall.

High magnification micrographs shown in Figure 6.2 illustrate the smooth texture of the binder phase which is present along the silicon carbide grains. Small pinholes are frequently evident along the binder coated silicon carbide grains (Photo 2, Figure 6.2). Areas 1 and 2 in Photo 2 (Figure 6.2) were further examined at higher magnification to reveal the texture of the as-manufactured binder coated silicon carbide grains. Area 1 of Photo 2 (Figure 6.2) is shown at 1500x and 7000x in Figure 6.3, Photos 3 and 4, respectively. The morphology of the binder coated grains is rather featureless. Area scan analysis of the binder phase indicated the presence of 70.093% oxygen (O), 19.064% silicon (Si), 4.903% sodium (Na), 4.877% aluminum (Al), 0.699% potassium (K), and 0.364% iron (Fe) (atomic percent basis).

Fibrous Membrane Surface

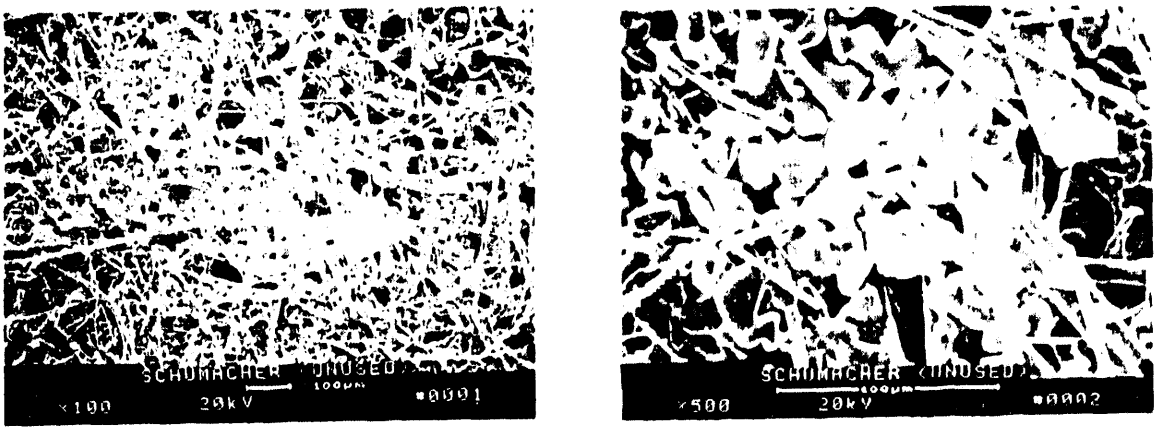

Membrane-Grain Interface

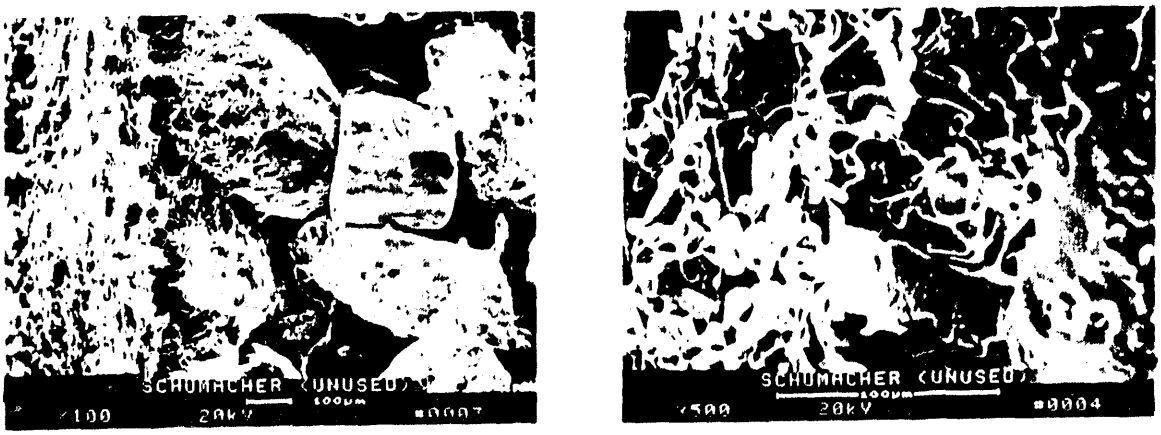

Silcon Carbide Grain Substrate

Figure 6.1 - Scanning Electron Micrographs Illustrating The Morphology Of The Schumacher Dia Schumalith F-40 Clay Bonded Silicon Carbide Candle Filter Matrix

Figure 6.2 - High Magnification Micrographs Illustrating The Morphology Of The Binder Coated Silicon Carbide Grains In The As-Manufactured Candle Filter Matrix

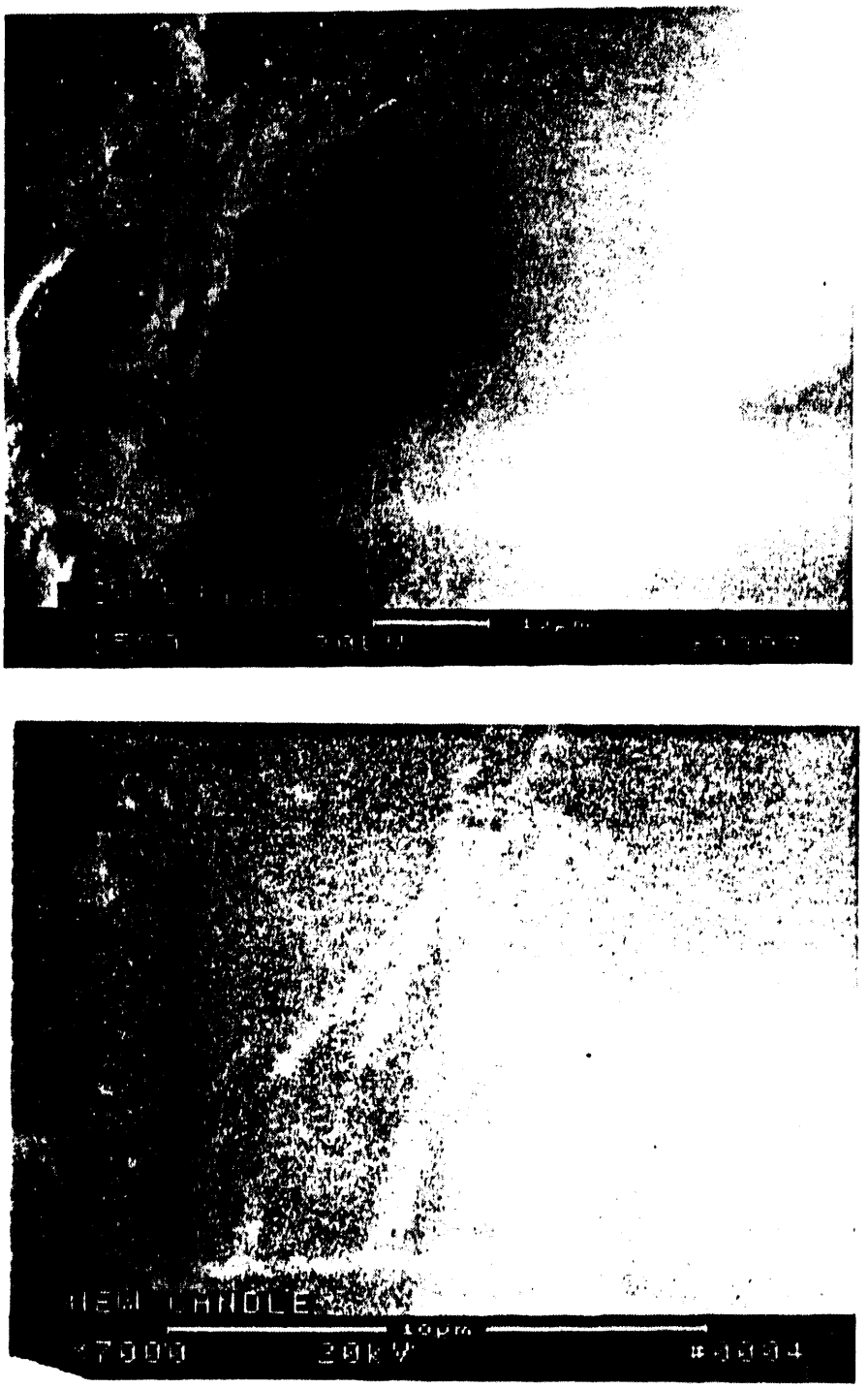

Figure 6.3 - High Magnification Micrographs Illustrating The Featureless Morphology Of The Binder Phase Which Coats The As-Manufactured Clay Bonded Silicon Carbide Candle Filter Matrix

High magnification micrographs of Area 2 (Photo 2, Figure 6.2) are shown in Photos 5 and 6 of Figure 6.4. Once again the morphology of the binder coated grain is featureless, and the matrix was identified to contain 64.737% O, 24.745% Si, 5.005% Al, 4.073% Na, 1.096% K, and 0.345% Fe.

Figure 6.5 illustrates a cross-sectioned area along the matrix where the 10-15 thick μm binder coating was evident along a silicon carbide grain. EDAX analysis through the binder phase indicated the presence of an enriched aluminosilicate phase at the surface of the binder phase. Moving through the binder towards the silicon carbide grain, the concentration of aluminum appeared to decrease, while the concentration of silicon and sodium appeared to increase. The concentration of potassium appeared to remain relatively constant through the binder wall. Area 4 in Photo 8 of Figure 6.5 contained silicon, with only minor concentrations of carbon. Note that the Link XL EDAX system which was used in these analyses had the capabilities to detect both carbon and oxygen. When low concentrations of carbon are present in a sample, quantitative results for carbon are somewhat in question.

6.2 SILICON CARBIDE MATRIX AFTER 500 HOURS OF EXPOSURE AT TIDD

One 305 mm (12 inch) section of the fractured Schumacher candle filter that had fallen into the Westinghouse ash hopper was selected for SEM/EDAX characterization. A whitish layer of fines was evident below the dust cake layer along the OD surface of this candle segment. Both ends of the candle were fractured and heavily caked with dust. Fines were visually evident along the ID surface of this candle segment. One area of the candle appeared to contain a gouge along its membrane surface. The gouged area was heavily covered with packed dust. This implied that this section of candle had been chipped from impact of an adjacent candle section during filter operation.

A section of the broken candle was initially removed, and the exposed fresh fractured surface was carbon coated in preparation for

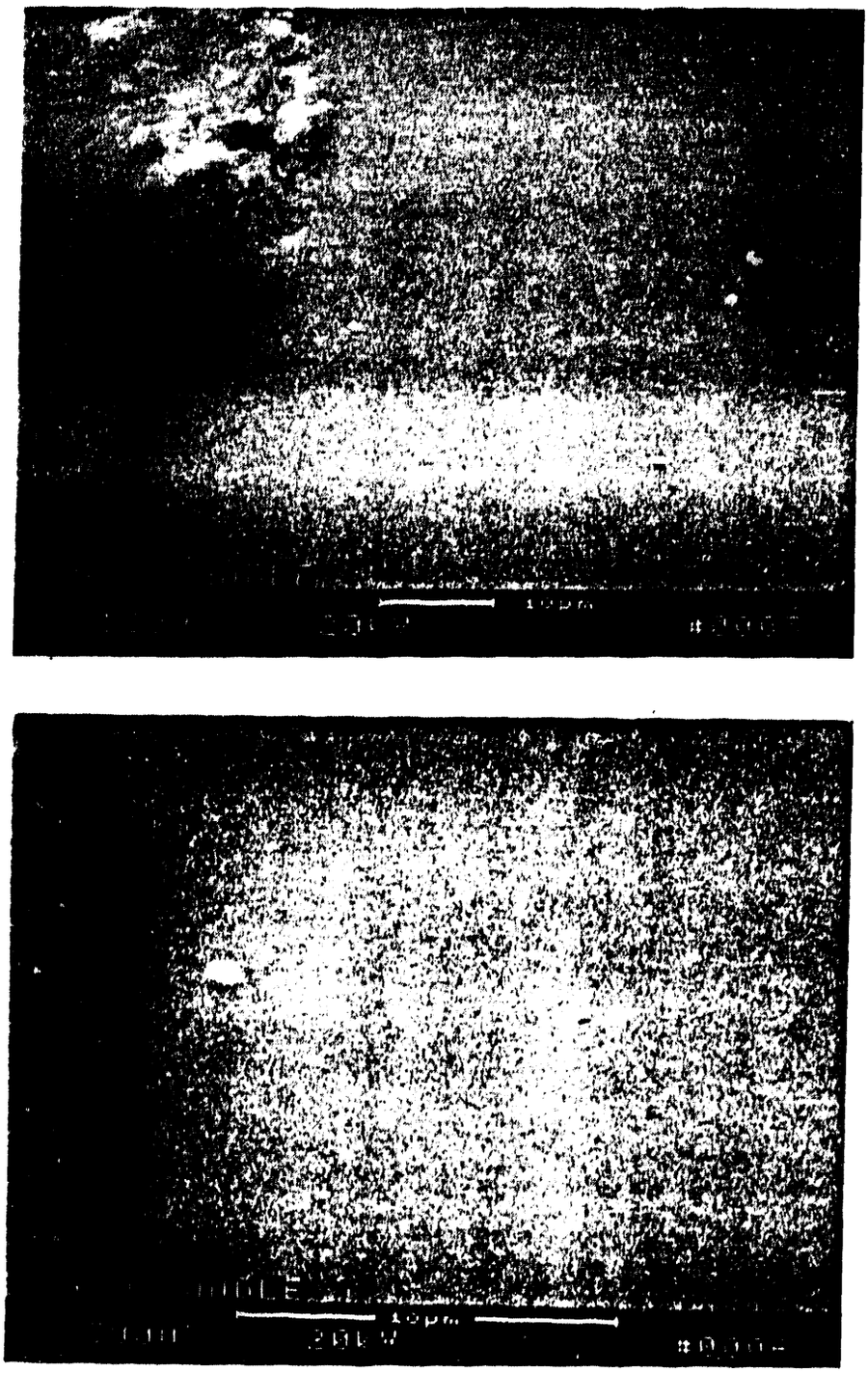

Figure 6.4 - High Magnification Micrographs Illustrating The Featureless Morphology Of The Binder Phase Which Coats The As-Manufactured Clay Bonded Silicon Carbide Candle Filter Matrix

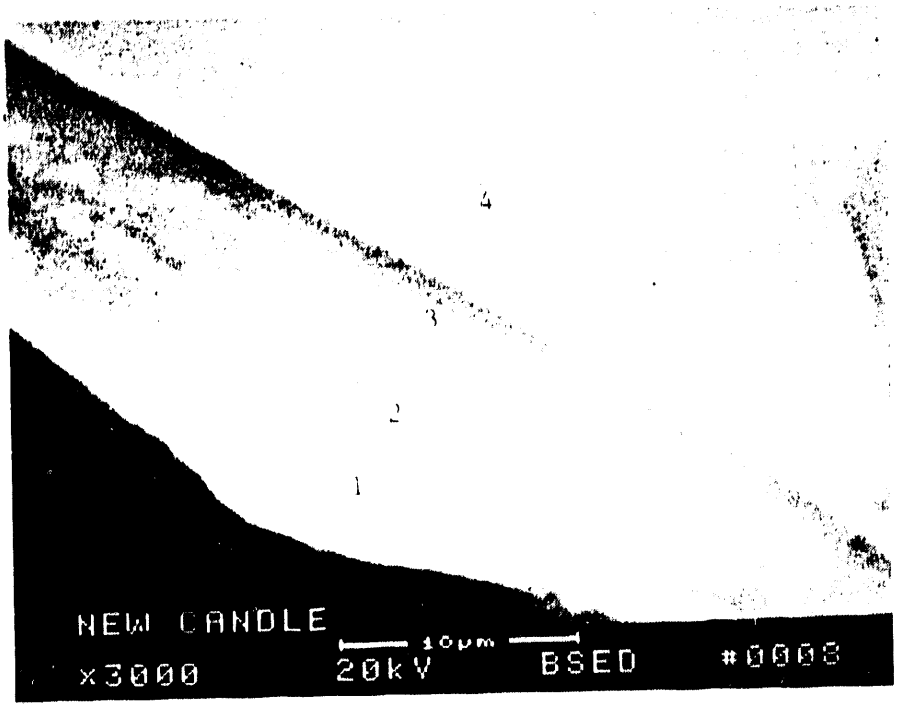

Atomic Percent

	Area 1	Area 2	Area 3	Area 4
Oxygen	67.530	66.694	64.729	---
Sodium	---	2.425	3.351	---
Potassium	0.749	0.848	0.785	---
Titanium	0.146	---	---	---
Aluminum	10.596	7.700	3.370	---
Silicon	19.259	22.332	27.765	100.000
Iron	0.359	---	---	---

Figure 6.5 - Micrograph And EDAX Analysis Through The Binder Phase That Coats A Silicon Carbide Grain

SEM/EDAX analysis. Figure 6.6 indicates that fines had penetrated into the silicon carbide matrix along the candle ID wall. The depth of fines penetration into the ID matrix was ~3-4 mm, representing ~20% of the 15 mm candle filter wall thickness. Accumulation of fines along the ID is expected to have resulted from an initial failure of a candle(s) during hot gas filtration, which permitted dust to be carried into the various plenum areas. Dust was then returned to the ID of candle filters that remained in the various plenums during each successive pulse cleaning event.

Figure 6.7 illustrates the morphology of the cross-sectioned silicon carbide matrix at higher magnifications. Photo 2 in Figure 6.7 illustrates the "bonding" of aluminosilicate membrane to the underlying silicon carbide grains. The OD membrane layer remained virtually intact after 500 hours of exposure in the PFBC gas environment. No apparent penetration of fines was evident through the OD membrane. All pores along the OD membrane appeared to be completely open. In the area that was characterized it was difficult to determine whether the extent of binder phase had been retained between adjacent grains. Several "patchy or blotchy" areas were evident along the binder coated SiC grains which may be attributed to binder "pull-away" during sample preparation, or perhaps to isolated phase enrichment.

A higher magnification micrograph illustrating the attachment of the membrane layer to the subsurface silicon carbide grains is shown in Photo 3 of Figure 6.8. Even at 300x, a somewhat mottled surface feature was evident along the binder phase surface that coated each silicon carbide grain. At the membrane/grain interface, EDAX analysis indicated the presence of 77.61% Si, 16.63% Al, 3.72% K, 1.69% S, and 0.35% Fe (Normalization Factor (NF) = 0.766).

The mottling of the binder phase surface was evident in the micrograph shown in Photo 4 of Figure 6.8. Note that the particle-laden, bumpy texture of the binder phase existed along the first grain layer, immediately below the fibrous OD membrane. The rounded nature, extensive quantity, as well as the micron- and submicron-size of the

Figure 6.6 - Photograph Illustrating The Section Of The Filter Material That Was Removed From A Candle Filter That Had Fallen Into The W-APF Ash Hopper. Penetration Of Fines Along The ID Surface Is Evident.

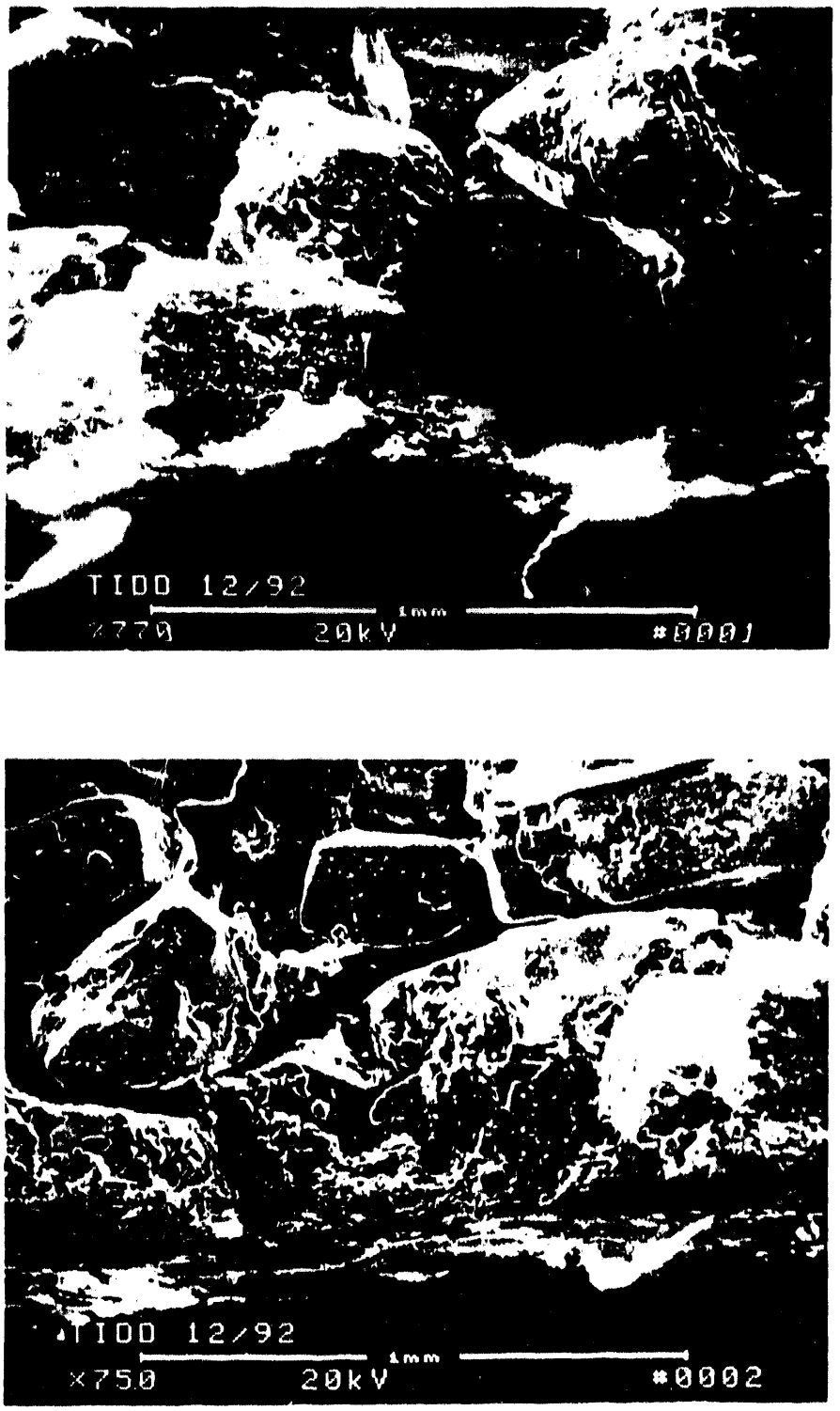

Figure 6.7 - Micrographs Illustrating The Morphology Of The 500 Hour PFBC Exposed Clay Bonded Silicon Carbide Matrix Near The OD Wall

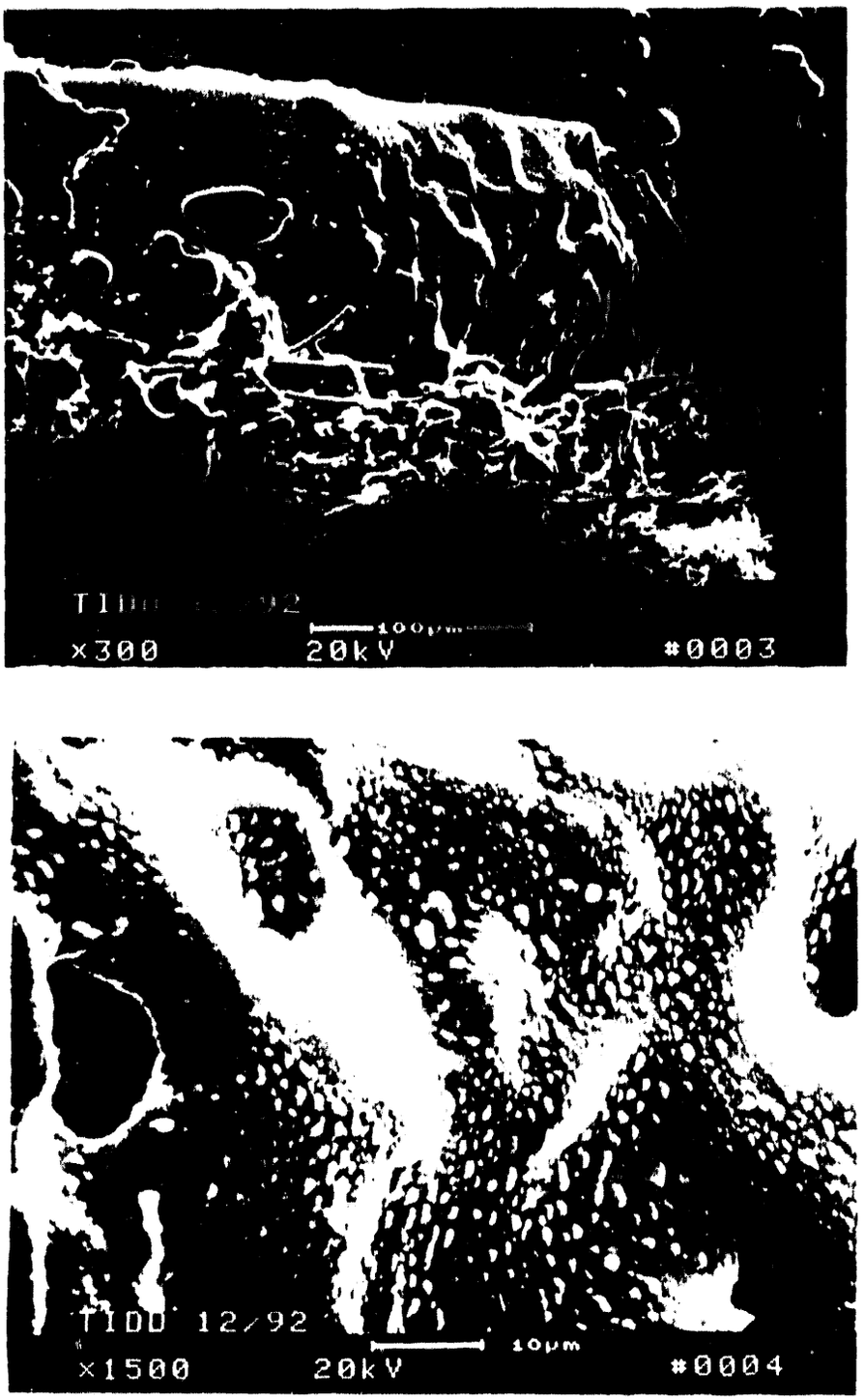

Figure 6.8 - Morphology Of The Membrane/Grain Interface Along The Cross-Sectioned Clay Bonded Silicon Carbide Wall. Extensive Aerosol Droplet Particle-Like Features Are Evident In This Area

"particles" implied deposition and adherence of "aerosol" droplet formations in this area of the filter wall.

A higher magnification micrograph of the "aerosol" droplet-enriched area along the first silicon carbide grain layer in the Schumacher Dia Schumalith candle filters after exposure at Tidd is presented in Figure 6.9. The composition of Area 1 in Photo 5 of Figure 6.9 indicated the presence of 49.68% Si, 21.02% S, 12.70% Al, 10.19% Ca, 4.64% K, 1.00% Ti, and 0.78% Fe (NF = 0.678). The underlying substrate (Area 2, Photo 5, Figure 6.9) below the micron- and submicron-size particles consisted of 68.42% Si, 18.60% Al, 6.12% K, 5.47% S, 0.78% Ti, and 0.62% Fe (NF = 0.688). The relative sulfur to calcium atomic percent ratio implied that in addition to a "sorbent-enriched phase" (i.e., $CaSO_4$) which was attached to the binder coated silicon carbide grain surface, sulfur was also sorbed into the binder phase coating. Note that the binder phase also appeared to be mottled, no longer having the smooth, featureless texture shown in Figures 6.3 and 6.4.

The high magnification micrographs shown in Figure 6.10 illustrate the morphology of a grain in the upper right section of Photo 2, Figure 6.7. Area 1 in Photo 7, Figure 6.10, is silicon-enriched (i.e., SiC or SiO_2). In this effort we utilized an SEM which did not have the capabilities for detecting oxygen or carbon. At the second grain layer from the OD surface, extensive changes along the binder surface of the silicon carbide grains were evident.

Figures 6.11 through 6.13 detail the morphology of the binder coating along the second grain layer in the clay bonded silicon carbide matrix. Crystalline-like particles were evident. Based on the characteristic morphology of these particles, bonding or an attachment of these particles to the underlying binder phase was implied. In several locations below the attached particles, deterioration of the binder was evident, as well as the formation of rod-like features. The formation of the rod-like phase was considered to result from mullitization of the binder phase.

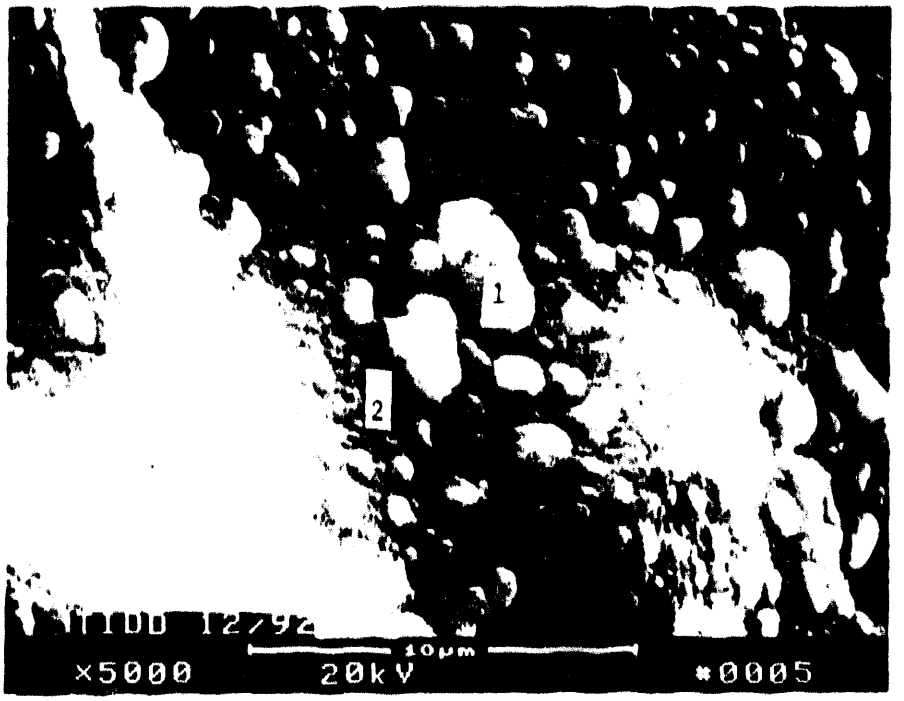

Figure 6.9 - Micrograph Illustrating The Morphology Of The Sulfur- And Calcium-Enriched Micron And Submicron Fines Along The Sulfur-Containing Binder Coating

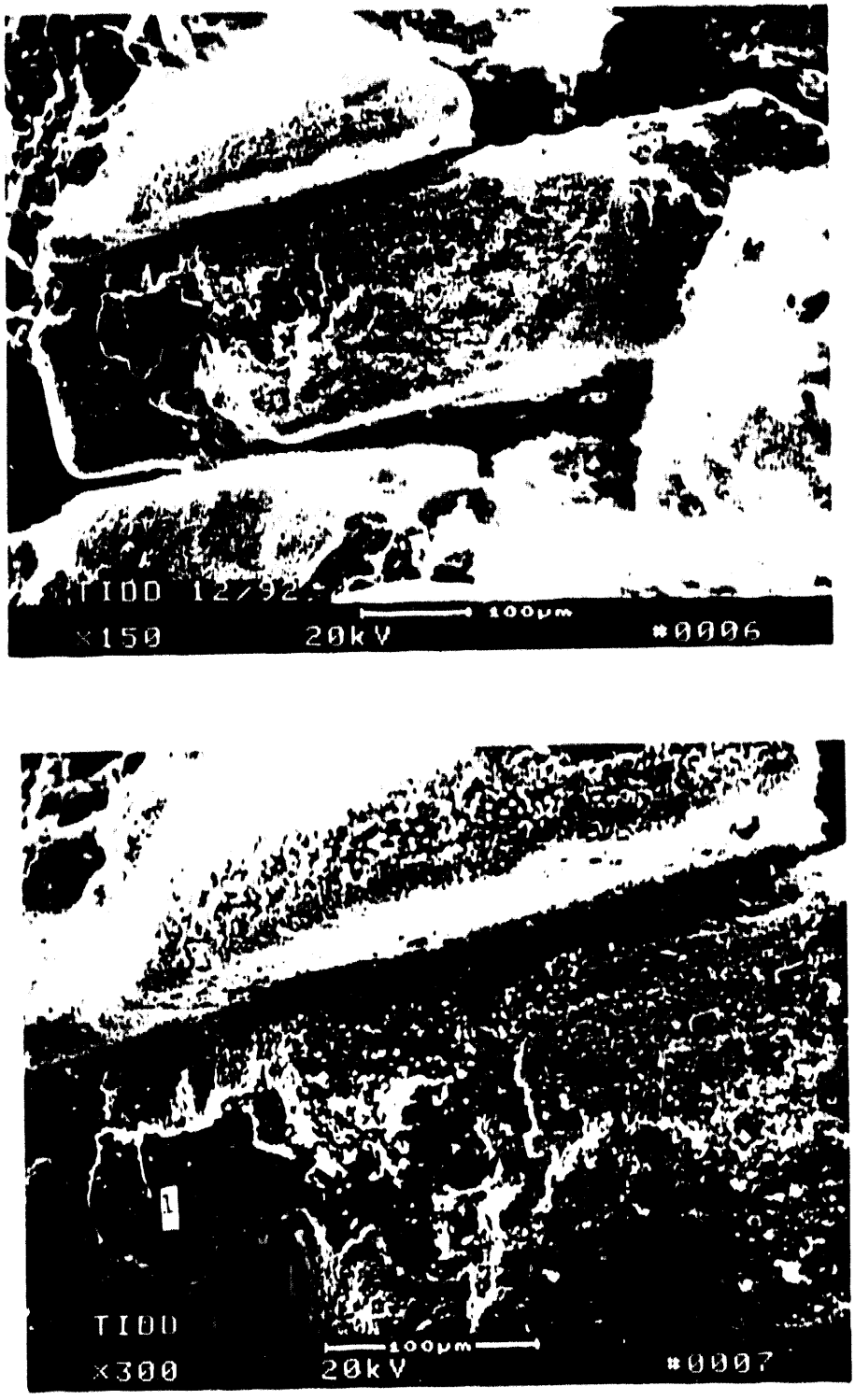

Figure 6.10 - Morphology Of The Binder Coated Silicon Carbide Grains At The Second Grain Layer From The OD Wall Of The PFBC Exposed Schumacher Dia Schumalith Candle Filters

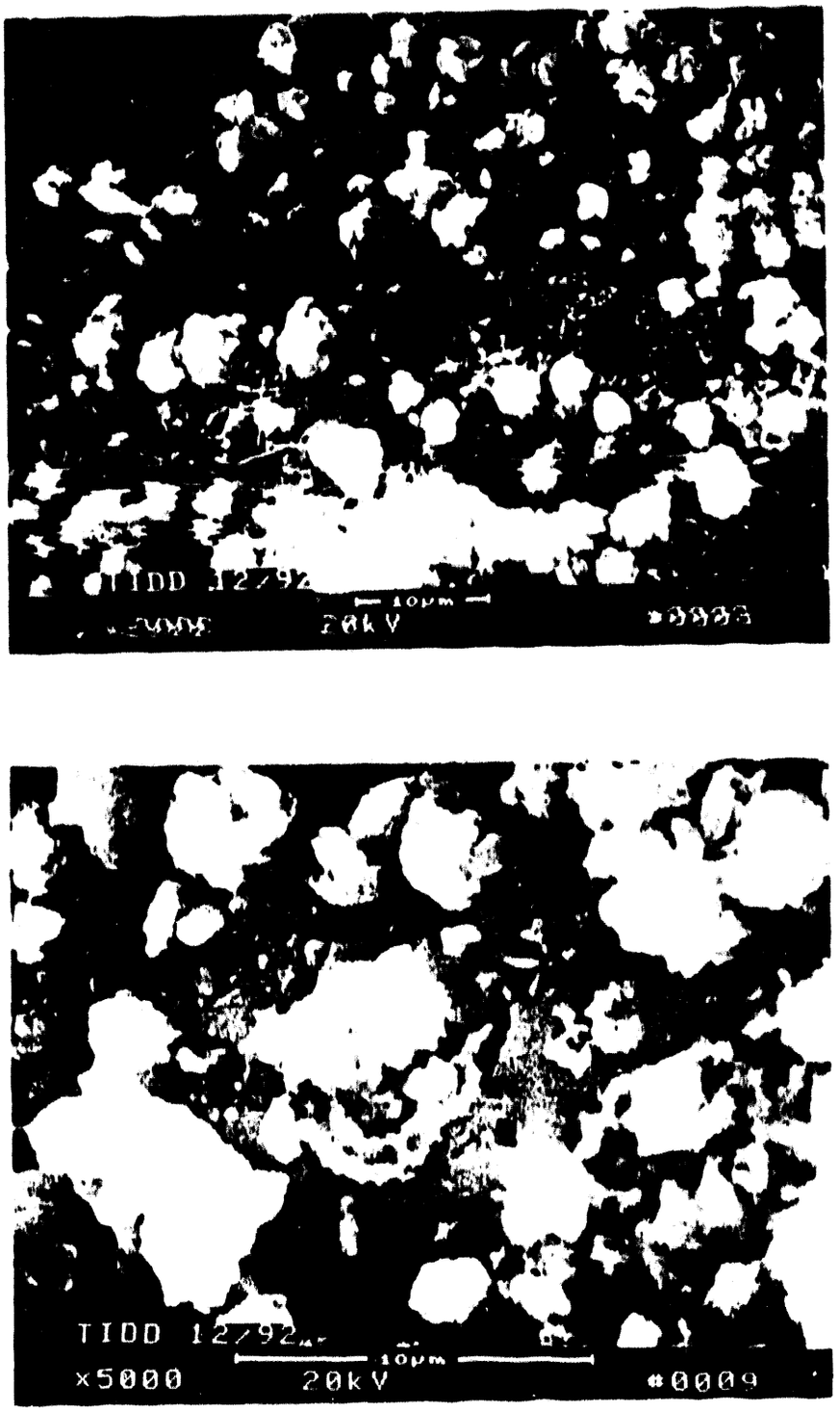

Figure 6.11 - Adherence Of A Crystalline-Like Phase Along The Binder Coating Of The Second Silicon Carbide Grain Layer. Deterioration Of The Binder Coating Beneath The Adhering, Deposited Phase Is Evident.

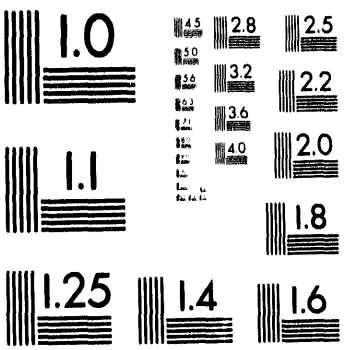
1.0
1.1
1.25
1.4
1.6
1.8
2.0
2.2
2.5
2.8
3.2
3.6
4.0
4.5
5.0
5.6

3 of 3

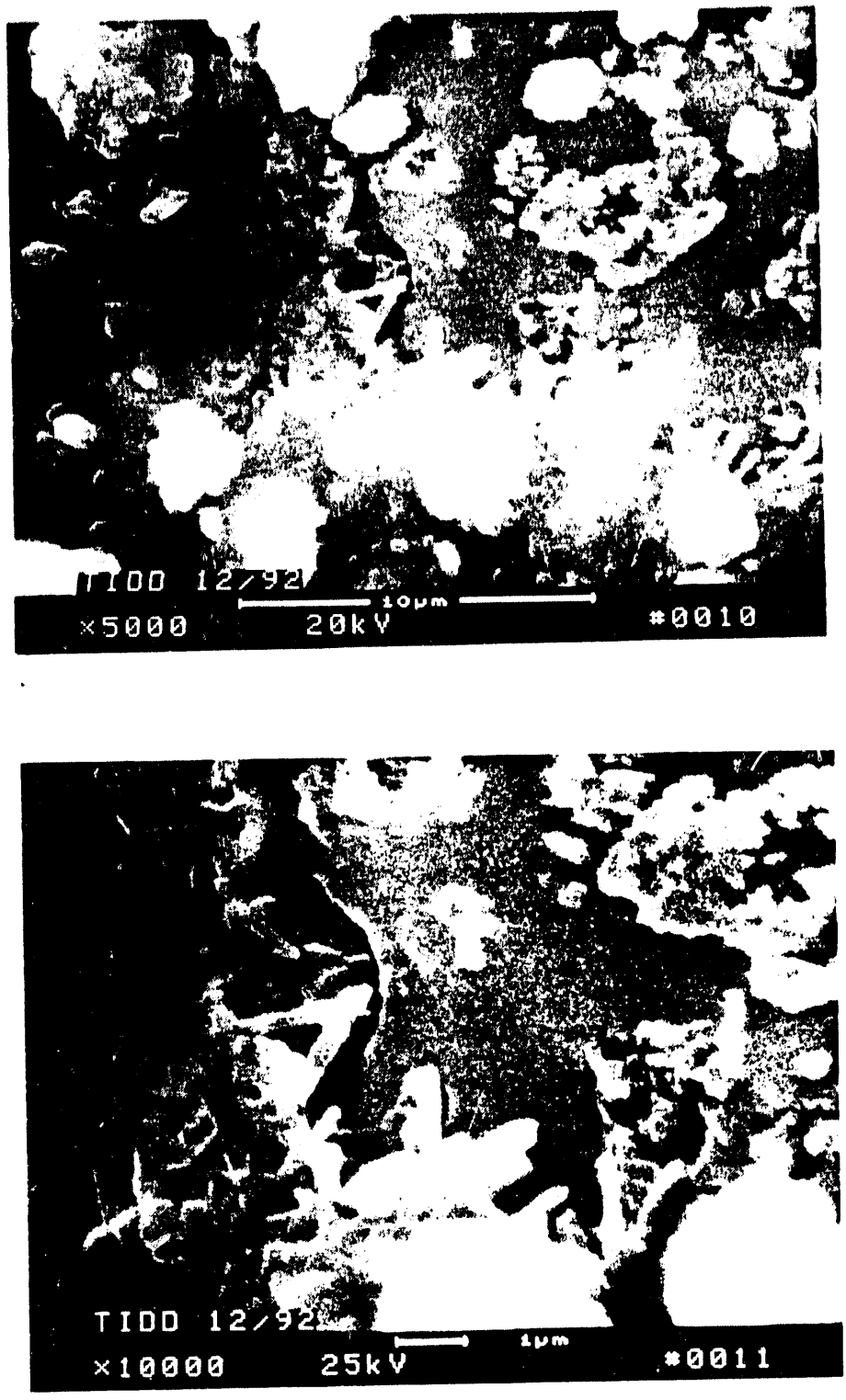

Figure 6.12 - Mullitization Of The Binder Phase Beneath The Surface Deposited Phase

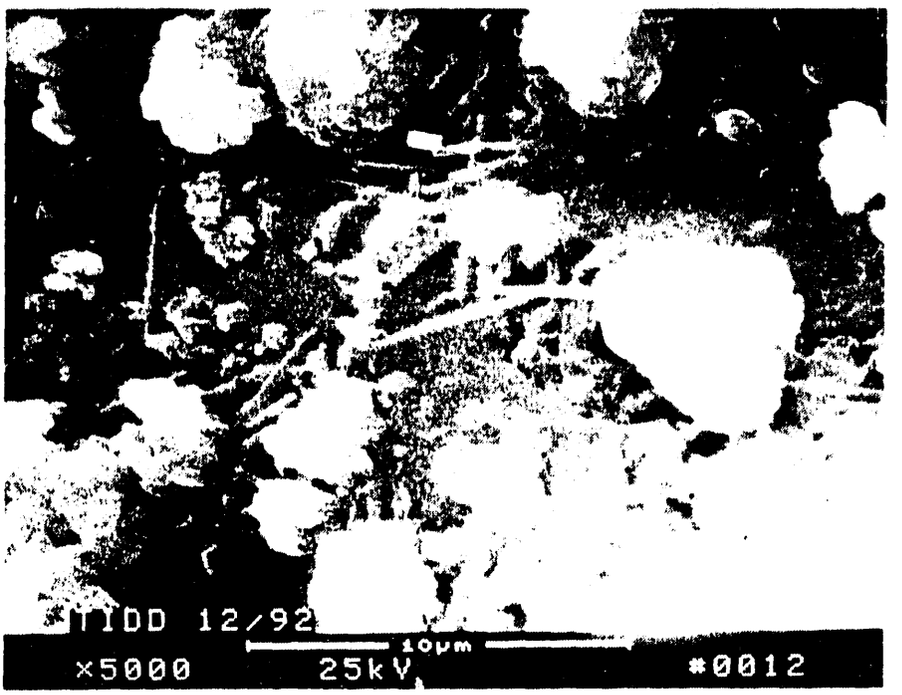

Figure 6.13 - Mullitization Of The Binder Phase Beneath The Surface Deposited Phase

Another series of micrographs (Figures 6.14 through 6.18) detail the morphology of the third and fourth grain layers in the silicon carbide matrix (upper left side of Photo 2, Figure 6.7). The "aerosol" droplet phase formation was evident along the surface of the binder interconnecting channels which bonded adjacent silicon carbide grains together. The flattened surface where the particles were attached to the binder phase implied either bonding of the particles, or the result of a gas phase reaction (i.e., sulfur oxides) with the binder substrate which then led to the production of the mottled surface.

Photo 15 in Figure 6.15 illustrates an area which was initially considered to have a crack at the base of the binder interconnect channel, near an adjacent silicon carbide grain. This area did not contain a detectable opening between the interconnecting channel and the silicon carbide grain. Therefore, if this were indeed a crack at one point in time, dislocation, followed by "healing" would most likely have occurred.

Figure 6.16 (Photo 16) attempts to detail the morphology of the binder phase along two adjacent silicon carbide grains (approximately at the center of Photo 13, Figure 6.14). Once again surface mottling was apparent along the binder phase. The somewhat smoother areas of the grain surface were apparently areas where the binder interconnect channel had been fractured during sample preparation.

Figure 6.17 presents higher magnification micrographs of the "patchy", fractured, binder interconnect areas along the silicon carbide grain shown in Photo 13 and 14, Figure 6.14. The surface mottling effect of the binder phase is evident in these micrographs. Area 1 in Photo 19 of Figure 6.18 was determined to contain aluminum, silicon, potassium, and titanium, indicative of the binder phase which had fractured between two adjoining grains.

Figure 6.19 illustrates the morphology of the binder coated silicon carbide grains at another location near the OD surface of the clay bonded silicon carbide candle filter wall.

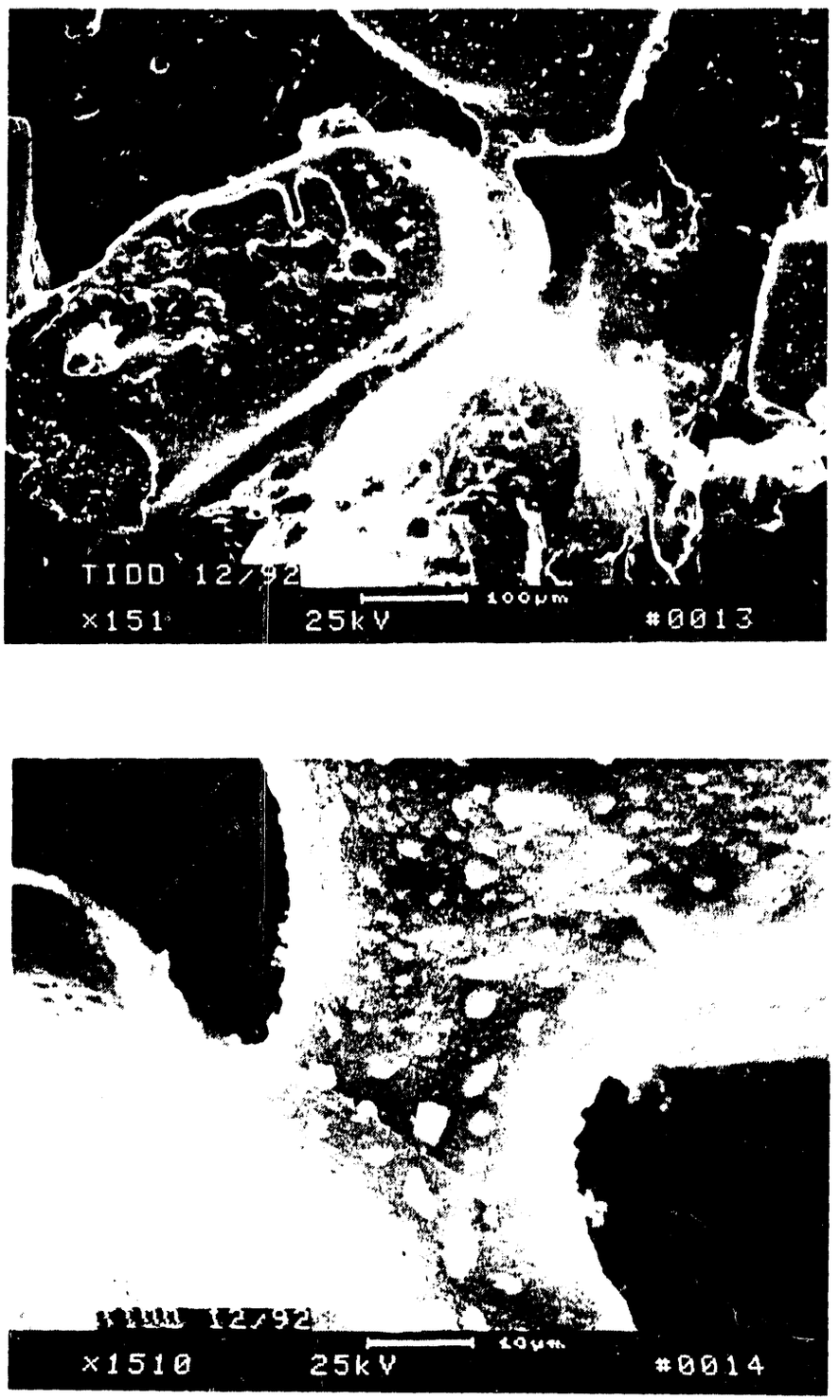

Figure 6.14 - Morphology Of The Third And Fourth Grain Layers In The Silicon Carbide Matrix. Surface Binder Phase Changes Are Evident.

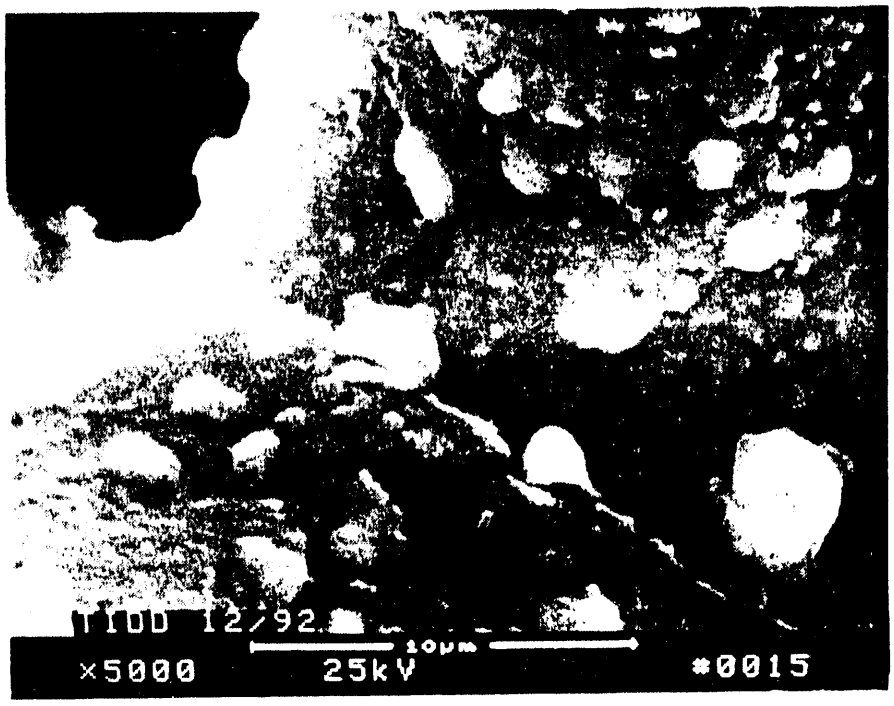

Figure 6.15 - High Magnification Micrograph Illustrating A Crack-Like Feature, As Well As Surface Adhering Or Binder Phase Change Along The Binder Interconnect Areas Between Two Adjoining Silicon Carbide Grains

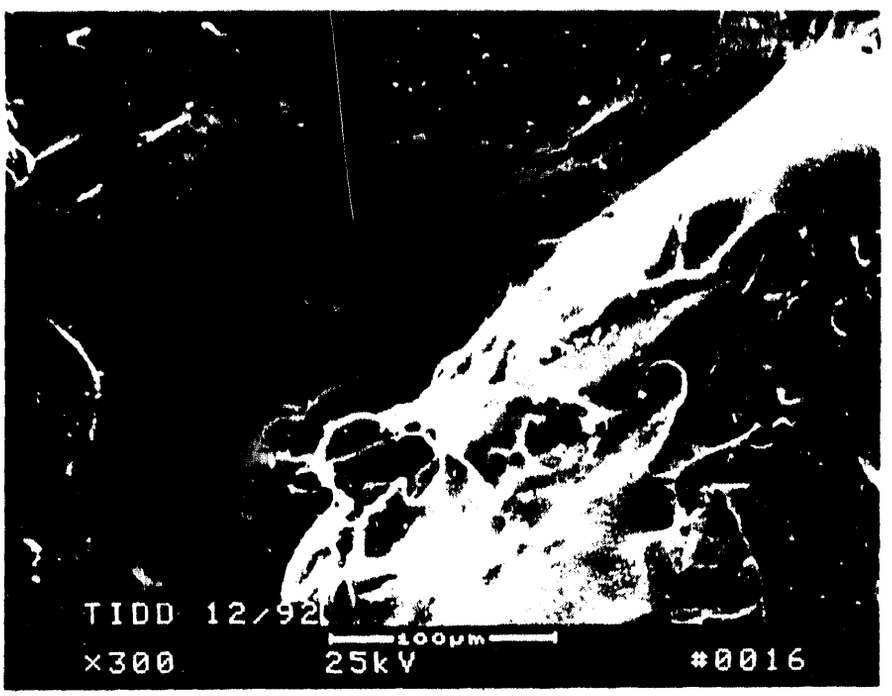

Figure 6.16 - Morphology Of The Interconnecting Binder Phase Between Adjoining Silicon Carbide Grains

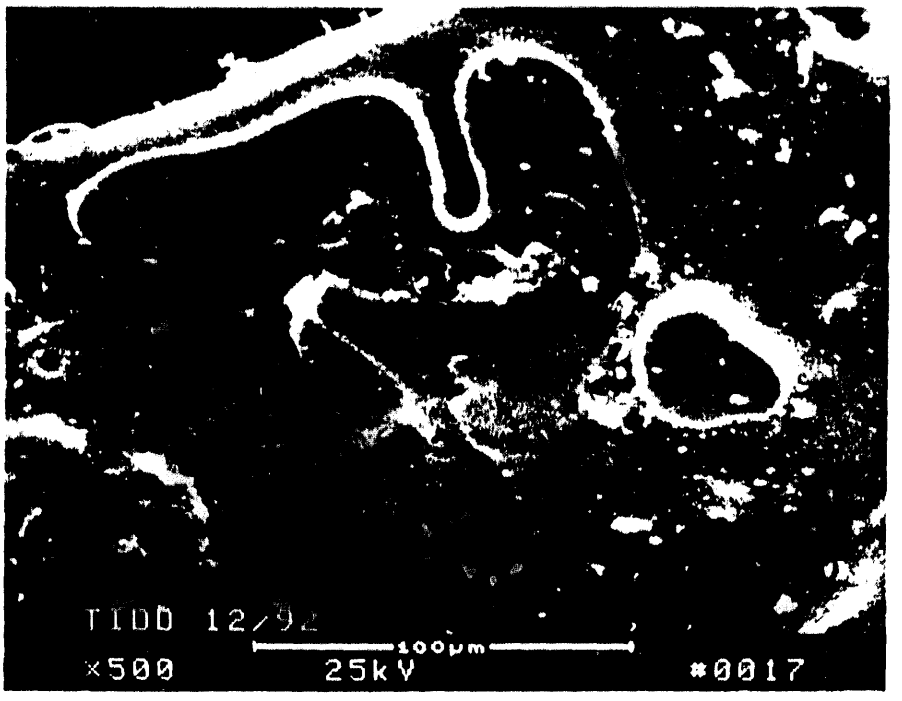

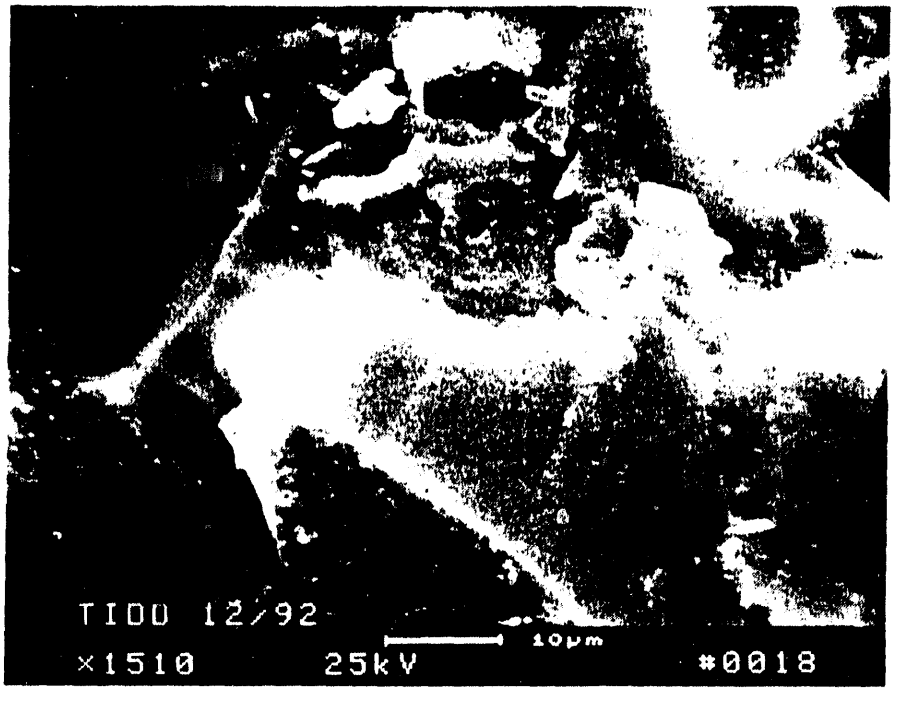

Figure 6.17 - Micrographs Illustrating That The Binder Phase Change That Results In The Clay Bonded Silicon Carbide Candle Filters Is Limited To The Surface Of The Binder Coating And Interconnect Areas

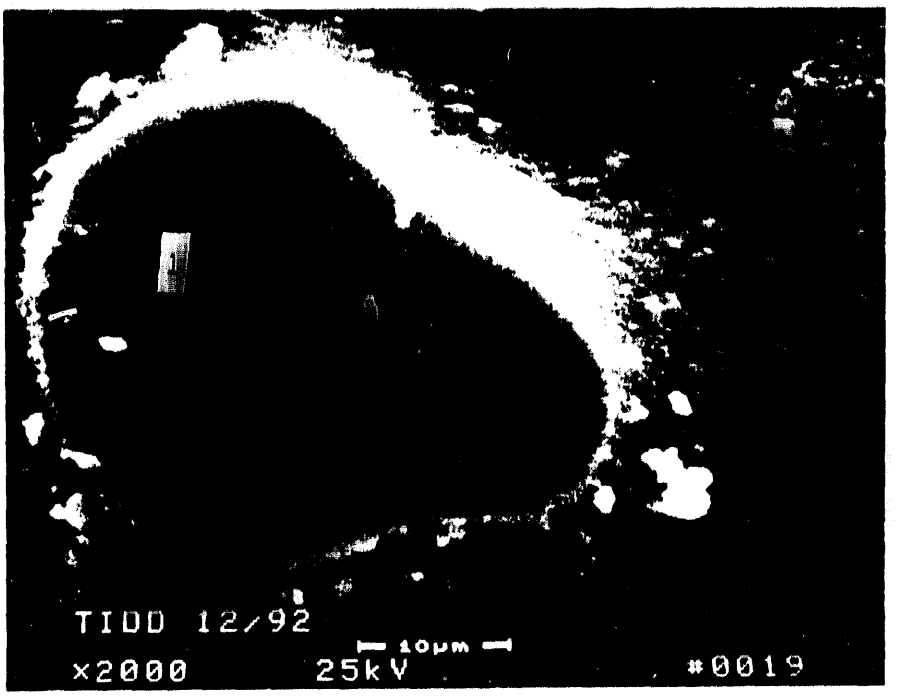

Figure 6.18 - Micrograph Illustrates The Morphology Of A Cross-Sectioned Binder Interconnect Channel

Figure 6.19 - Micrograph Illustrating The Morphology Of The Binder Coated Silicon Carbide Grains At An Alternate Location Near The OD Candle Filter Surface

Moving inward from the OD, extensive mottling of the binder surface was evident as shown in Figures 6.20 through 6.22. Photo 23 in Figure 6.21 illustrates that mottling was a surface feature of the binder phase. Along the binder interconnect areas, the mottled area was ~5 μm thick. Area 1 of Photo 23 in Figure 6.21 was identified to consist solely of silicon (i.e., SiC), while Area 2 was identified to be enriched with sulfur in the binder coating surface (71.04% Si, 13.47% S, 9.43% Al, 3.73% K, 2.33% Na; NF = 0.727). Calcium was not detected in these analyses.

Figure 6.22 shows another area along the silicon carbide matrix where the mottled sulfur-enriched aluminosilicate binder phase existed extensively along the binder coated grain surface, as well as along the surface of the binder interconnect channel areas. Note the fracture along the binder interconnect area at the base of an adjoining silicon carbide grain. Once again the phase change that had occurred within the binder was a surface effect, which was supported by negligible change in the binder interconnect channels.

Figures 6.23 through 6.28 illustrate the morphology of the silicon carbide matrix at approximately 5 grain layers from the candle filter OD surface. Once again the binder coating along the silicon carbide grains contained extensive mottled surface features. The rather rounded, crystalline-like phase appeared as discrete agglomerates, which had grown into an extensive mat that completely covered the binder surface layer (Figure 6.24).

EDAX analyses of Area 1 in Photo 5 of Figure 6.25 indicated the presence of 83.86% Si, 8.80% Al, 5.18% K, 1.66% S, and 0.50% Na (NF = 0.824). Area 1 was considered to represent the binder surface phase that coated the silicon carbide grain, and which also served as the substrate layer for the formation of the sulfur-enriched crystalline phase. The extensive phase that formed along the binder surface (Area 2 in Photo 5 of Figure 6.25) was identified to contain 83.77% Si, 9.38% S, 4.67% Al, 1.65% K, and 0.54% Na (NF = 0.825). The smaller particles that formed on the binder substrate (Area 3, Photo 5, Figure 6.25)

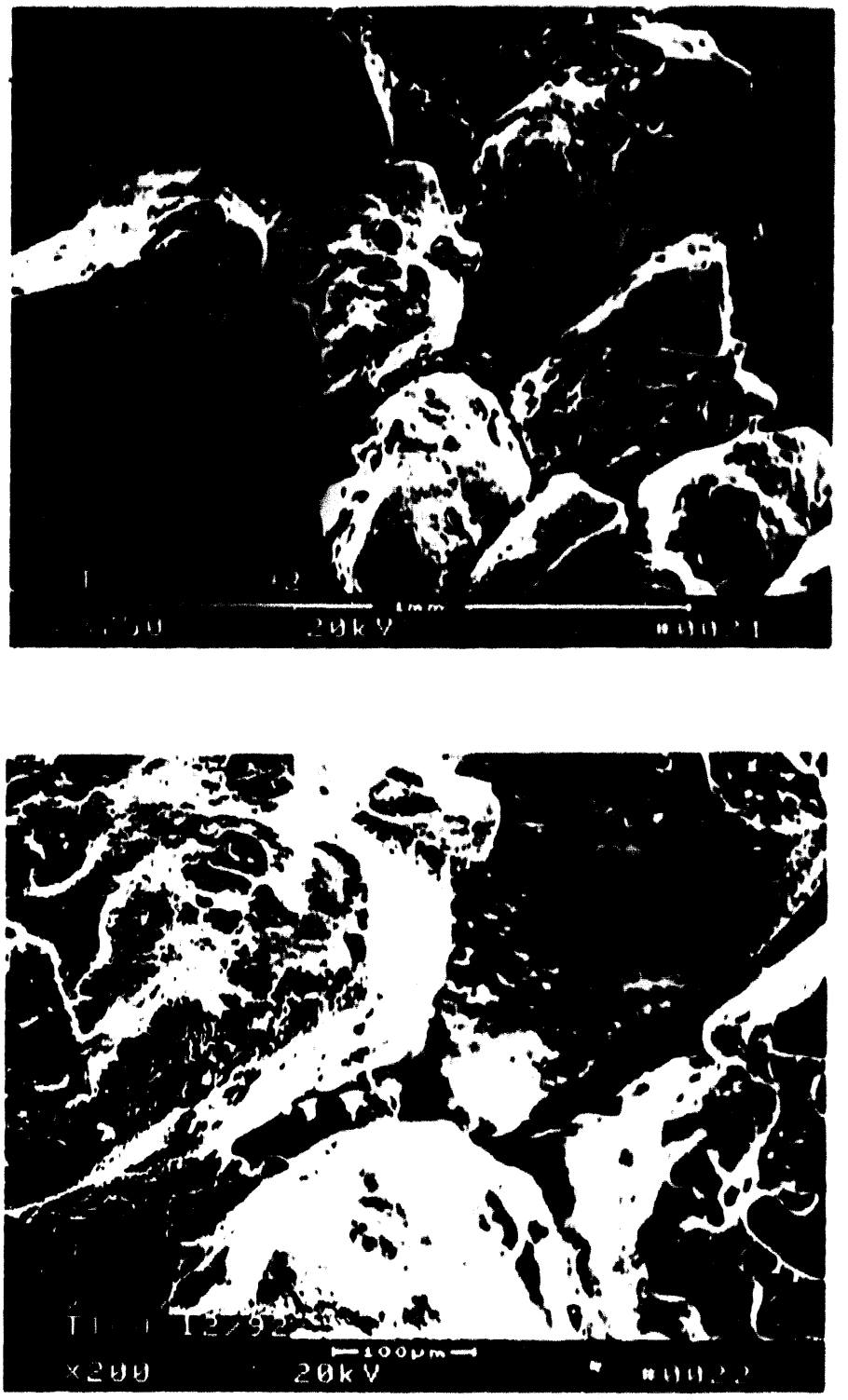

Figure 6.20 - Micrographs Illustrating The Morphology Of The Binder Phase Along The Clay Bonded Silicon Carbide Grains Near The OD Surface

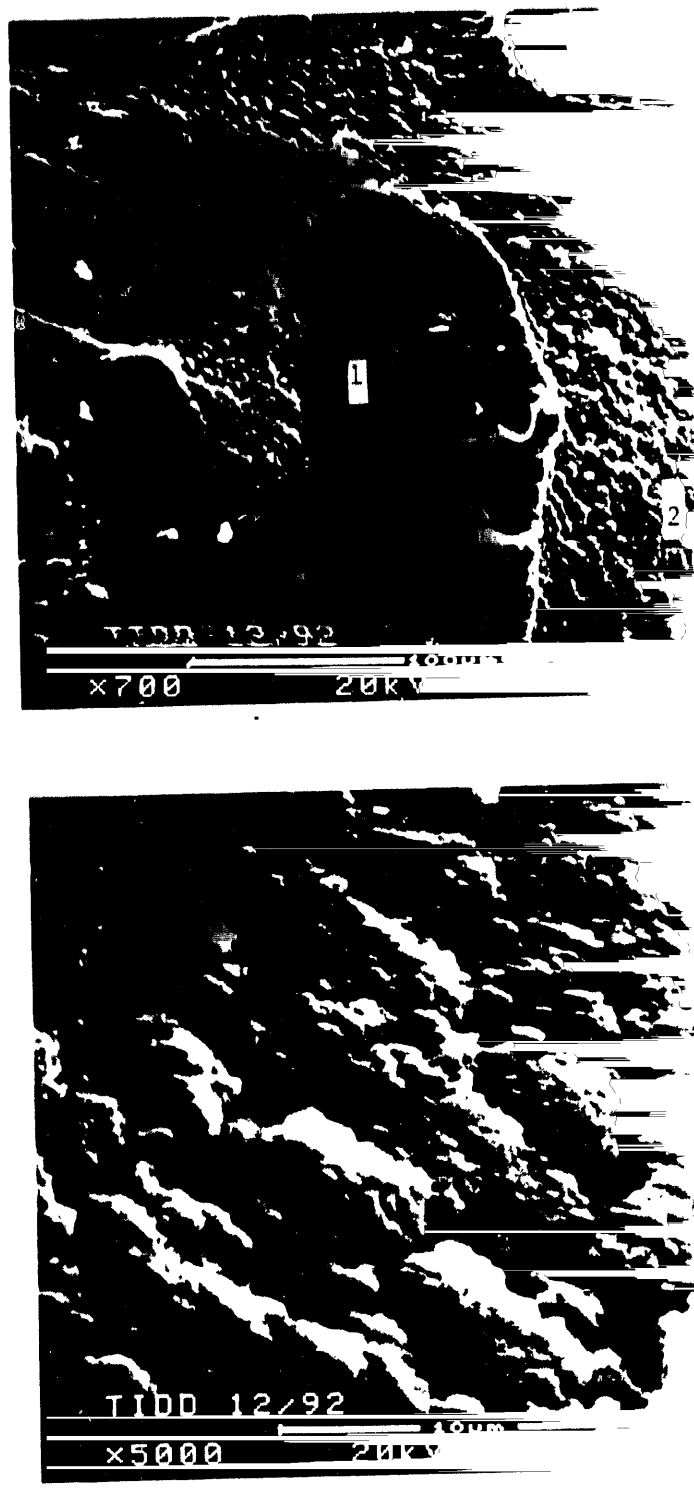

Figure 6.21 - High Magnification Micrographs Illu
Morphology Of The Sulfur-Enriched B
The Sulfur-Enriched Phase Is ~5 μm

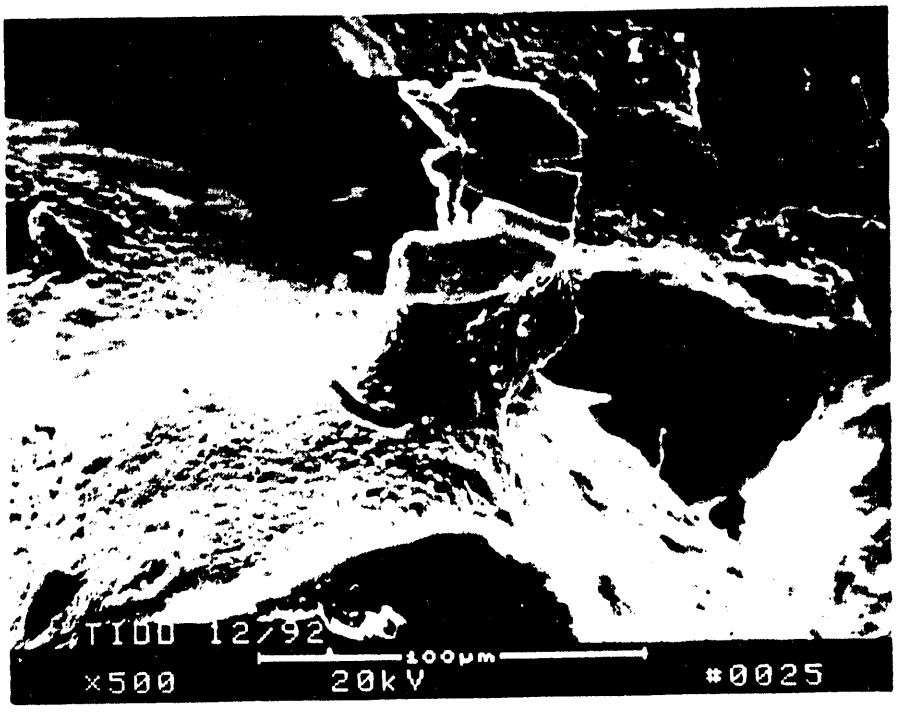

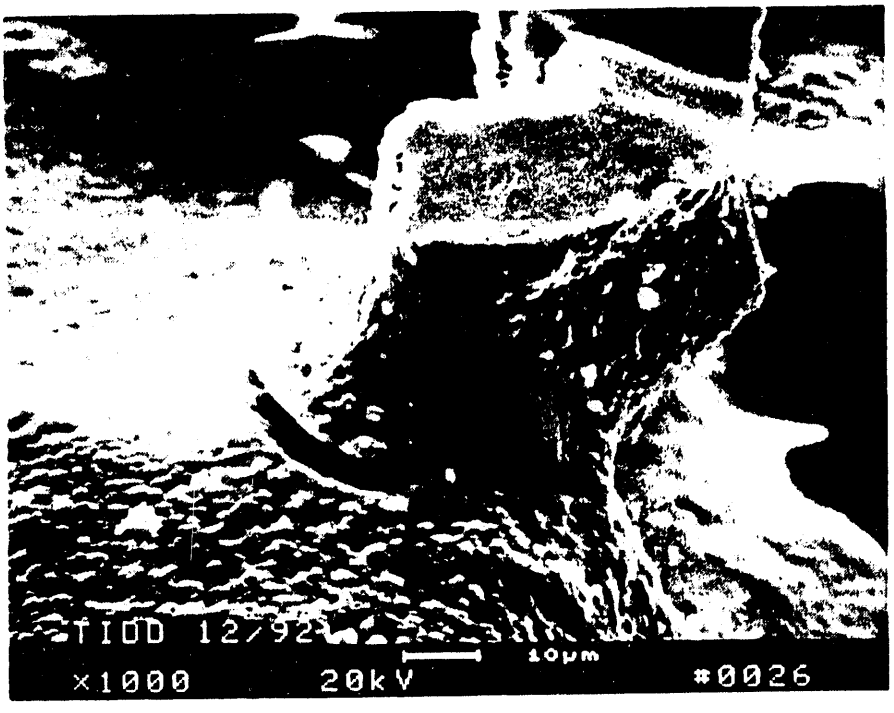

Figure 6.22 - Micrographs Illustrate That The Sulfur-Enriched Phas
Is A Surface Effect Which Extends ~5 µm Into The
Binder Interconnect Area

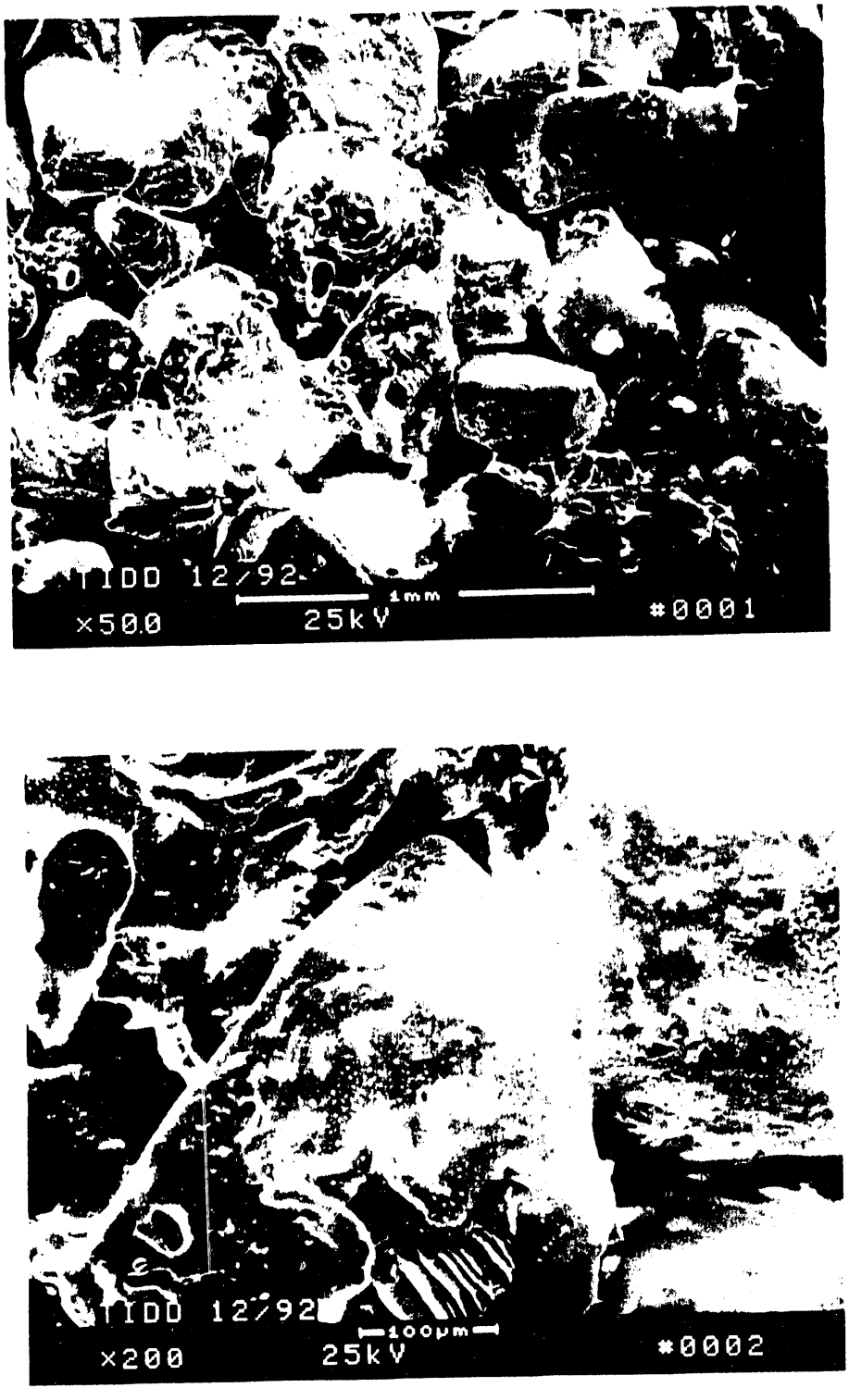

Figure 6.23 - Micrographs Illustrating The Morphology Of The Binder Coated Silicon Carbide Grains At ~5 Grain Layers From OD Surface Of The Candle Filter

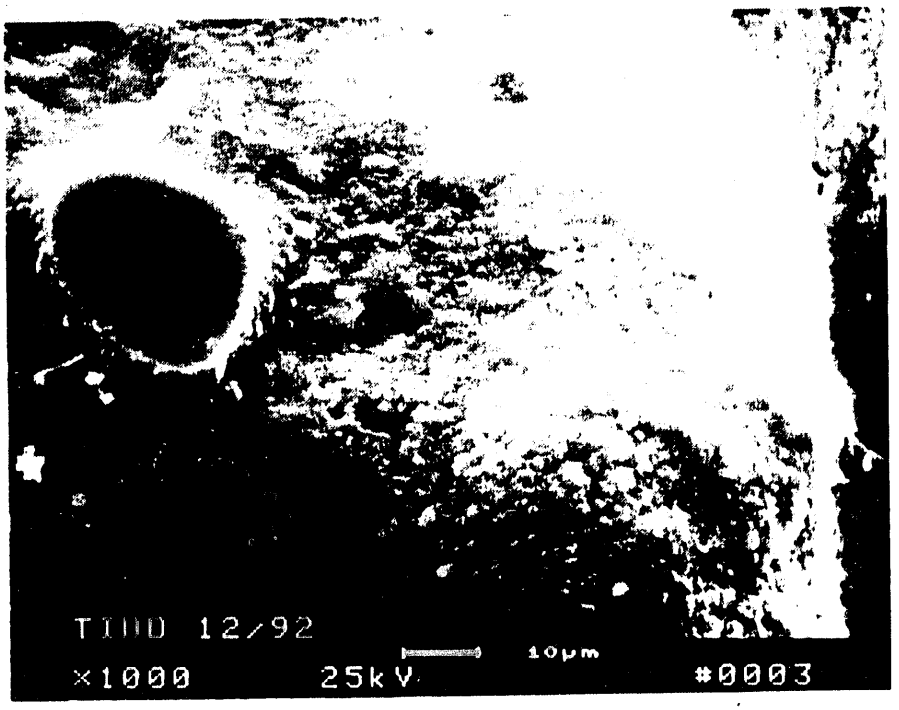

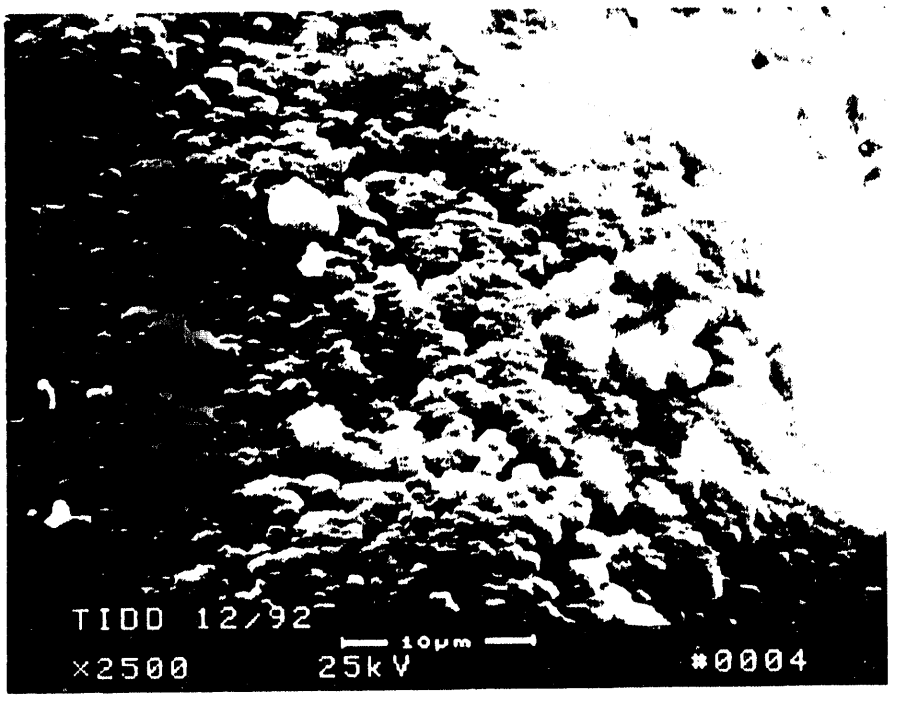

Figure 6.24 - High Magnification Micrographs Illustrating The Extensive Binder Surface Phase Formation Along The Silicon Carbide Grains That Are ~5 Grain Layers Below The OD Membrane Surface

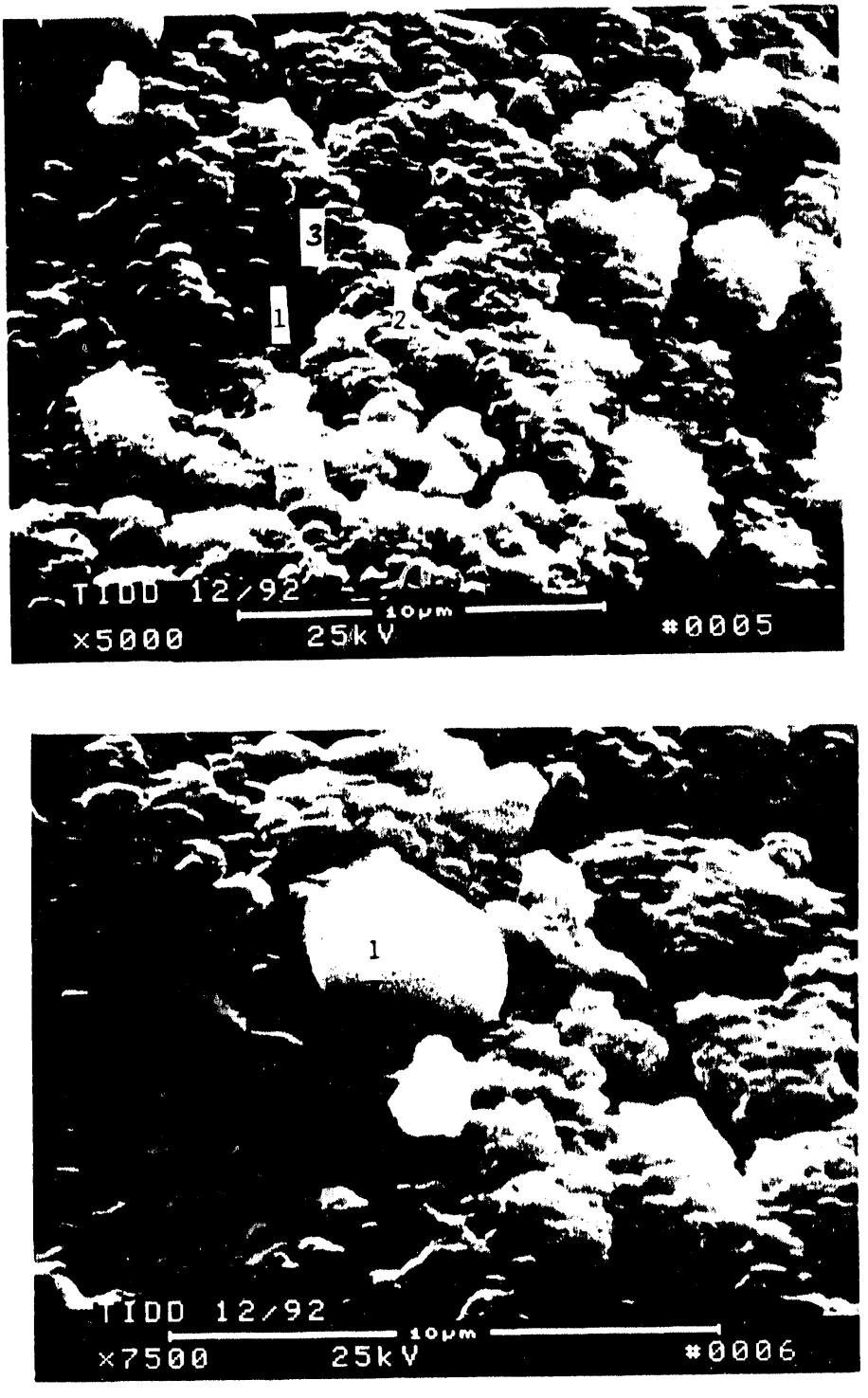

Figure 6.25 - High Magnification Micrographs Detailing The Morphology Of The Binder Phase Along The Silicon Carbide Grains That Are ~5 Grain Layers Below The OD Membrane Surface

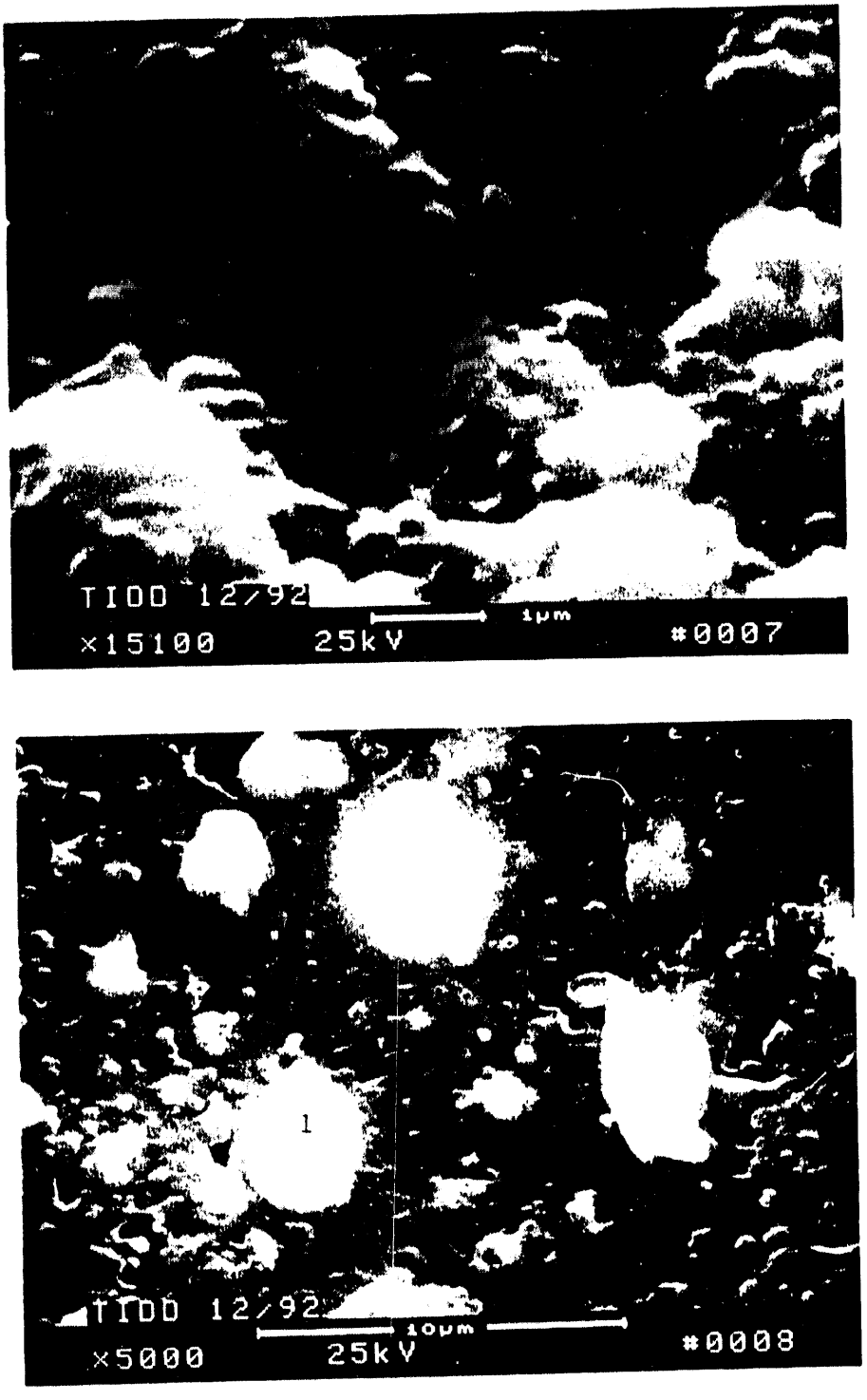

Figure 6.26 - Micrographs Illustrating The Morphology Of The Sulfur-Enriched Binder Phase And Deposited Fly Ash Particles

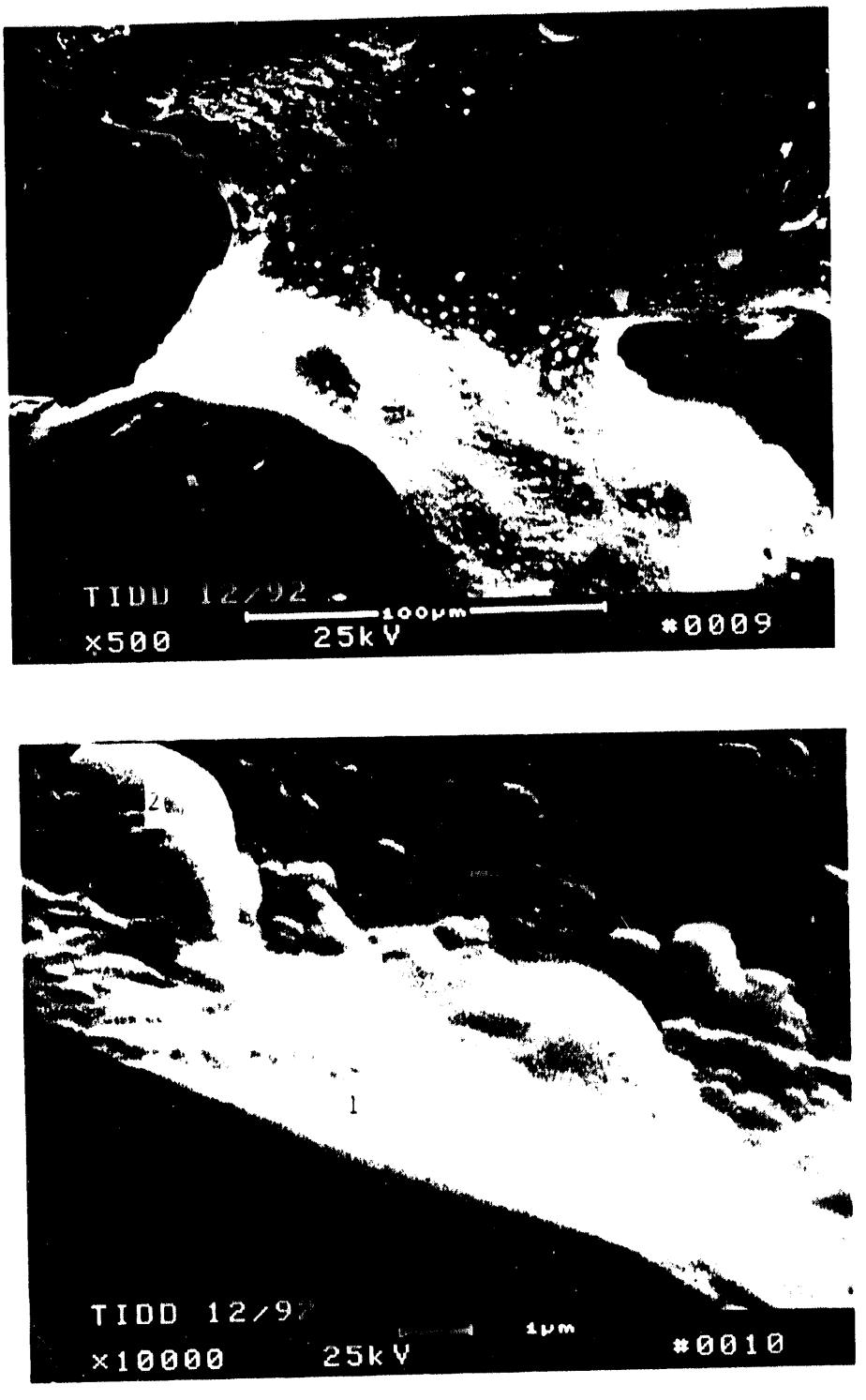

Figure 6.27 - High Magnification Micrographs Illustrating The Morphology Of The Binder Interconnect Channels Which Bond The Silicon Carbide Grains Together At ~5 Grain Layers Below The Membrane Coated OD Surface

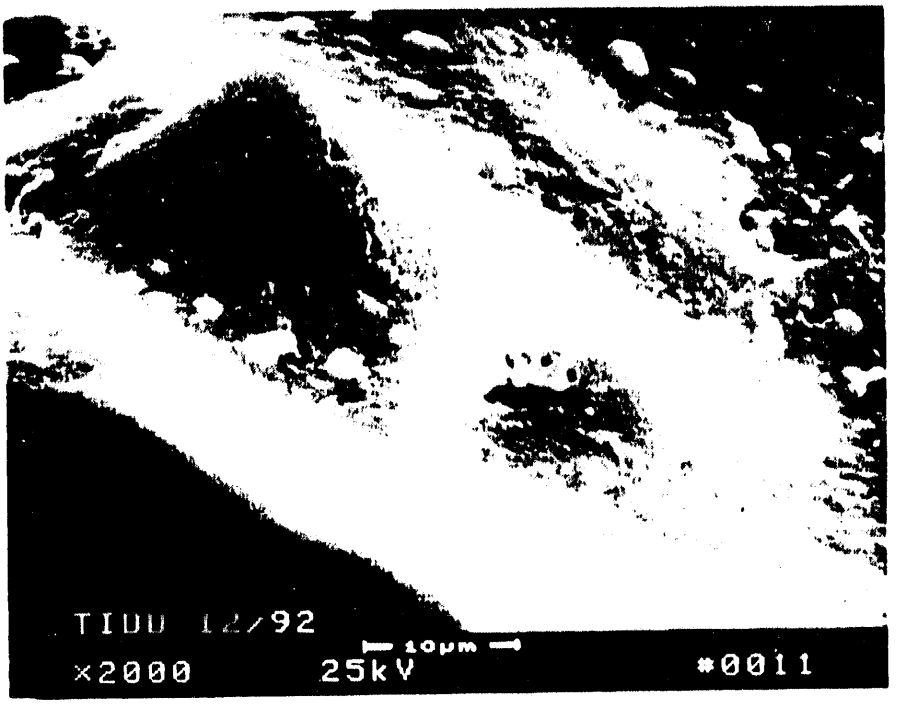

Figure 6.28 - Additional Micrograph Illustrating The Complex Morphology Of The Binder Phase That Coats The Silicon Carbide Grains At ~5 Grain Layers Below The Membrane Coated OD Surface

contained 82.83% Si, 10.31% Al, 3.44% K, and 3.42% S (NF = 0.817). Note the relatively low concentration of sodium detected in the binder phase, as well as the absence of calcium in this area.

The rather globular, 2-3 μm particle shown in Photo 6, Figure 6.25, was a randomly occurring feature which contained 34.13% S, 31.97% Si, 23.59% Ca, 9.98% Al, and 0.33% Fe (NF = 0.684). The composition of this particle was representative of a fly ash fine that had been carried over and deposited within the silicon carbide matrix.

Figure 6.26 (Photo 7) is a high magnification micrograph which details the morphology of the surface phase which had formed along the binder coated grains. Note the rather crystalline-like appearance of the agglomerates which appeared to contain submicron, rounded surface features.

At another location along the silicon carbide grain (Photo 2 of Figure 6.23), we encountered surface features which indicated the attachment of 2-5 μm fines along the binder phase. Area 1 in Photo 8, Figure 6.26, was identified to consist of 38.06% Si, 28.86% S, 16.96% Ca, 12.18% Al, 2.60% K, 0.90% Fe, and 0.44% Ti (NF = 0.661). The underlying binder phase beneath the ash fines was seen to coalesce, deteriorating the binder layer in many areas, as well as tending to enhance the formation of the mullite rod-like features.

High magnification micrographs were taken and EDAX analyses were performed on several grains along the lower, central section of the matrix shown in Photo 1 of Figure 6.23. The interconnect binder phase between two adjoining grains is shown in Figure 6.27. Area 1 in Photo 10 of Figure 6.27 was near the binder substrate layer, and was identified by EDAX to contain 66.45% Si, 14.48% Al, 11.62% S, 3.60% K, 3.29% Ca, and 0.57% Fe (NF = 0.675). The 3 μm cenosphere particle shown in Area 2 of Photo 10, Figure 6.27, appeared to be attached to the binder substrate (as seen by the flatness of the bottom of the particle, as well as its "tailing" features), and consisted of 41.78% Si, 25.19% S, 13.22% Al, 10.07% Ca, 6.59% Mg, 2.41% K, and 0.75% Fe (NF = 0.620). Figure 6.28 illustrates the morphology of the binder coated grain at an

alternate location along the same grain. Note the adherence of micron and submicron "aerosol" or fly ash particles, the mottling of the binder surface, as well as the "mountains, valleys, and holes" that had formed at this location.

Figures 6.29 through 6.32 illustrate the morphology of the silicon carbide grains at approximately 5 mm from the membrane coated candle filter OD surface. Fine particle agglomerates were seen to accumulate along the crevices between two adjacent grains (Photo 13, Figure 6.29). EDAX analysis of the fines indicated the presence of 38.72% Si, 31.13% S, 10.54% Ca, 10.01% Mg, 6.79% Al, 1.67% K, and 1.14% Fe (NF = 0.632), representing ash and sorbent constituents. The composition of Area 2 in Photo 14 of Figure 6.30 was principally a silicon-containing phase. Surface mottling was also apparent in this area.

Figures 6.31 and 6.32 illustrate the morphology of additional grains that were ~5 mm from the candle filter OD wall. EDAX analysis of the mottled phase shown in Area 1 of Photo 18 in Figure 6.32 indicated the presence of 79.65% Si, 10.79% S, 5.45% Al, 2.35% K, and 1.76% Na (NF = 0.785). Once again calcium was absent in this area.

At 10 mm from the membrane coated OD wall, we saw evidence of even more extensive binder phase surface changes. Figures 6.33 and 6.34 show that the sulfur-enriched phase formed a continuous layer along the binder coated silicon carbide grain. Note the disconnected (i.e., deteriorated) areas of the binder substrate areas below the sulfur-enriched phase (Photo 21, Figure 6.34). Area scan analyses of the binder substrate indicated the presence of 95.45% Al and 4.55% Al (NF = 0.956), while the agglomerated phase consisted of 87.06% Si, 4.73% S, 4.66% Al, and 3.01% K (NF = 0.862).

Figures 6.35 through 6.39 illustrate the morphology of the clay bonded silicon carbide grains at ~10 mm from the membrane coated OD surface (i.e., 5 mm from the ID). Isolated areas of fines were detected along the binder, not only in crevices that formed between two adjoining grains, but were also deposited along the surface of the silicon carbide

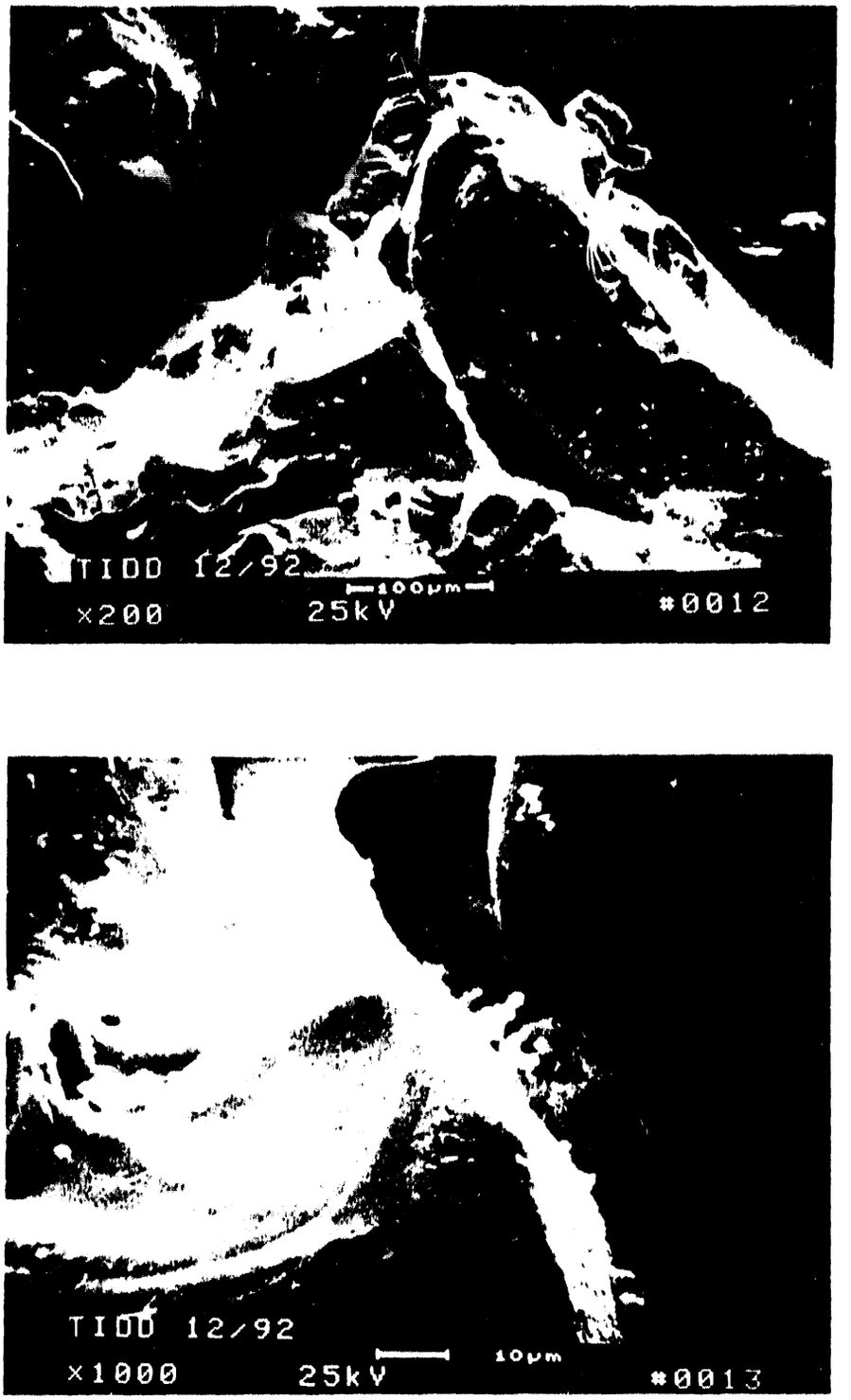

Figure 6.29 - Micrographs Illustrating The Morphology Of The Silicon Carbide Grains At ~5 mm Below The Membrane Coated OD Surface

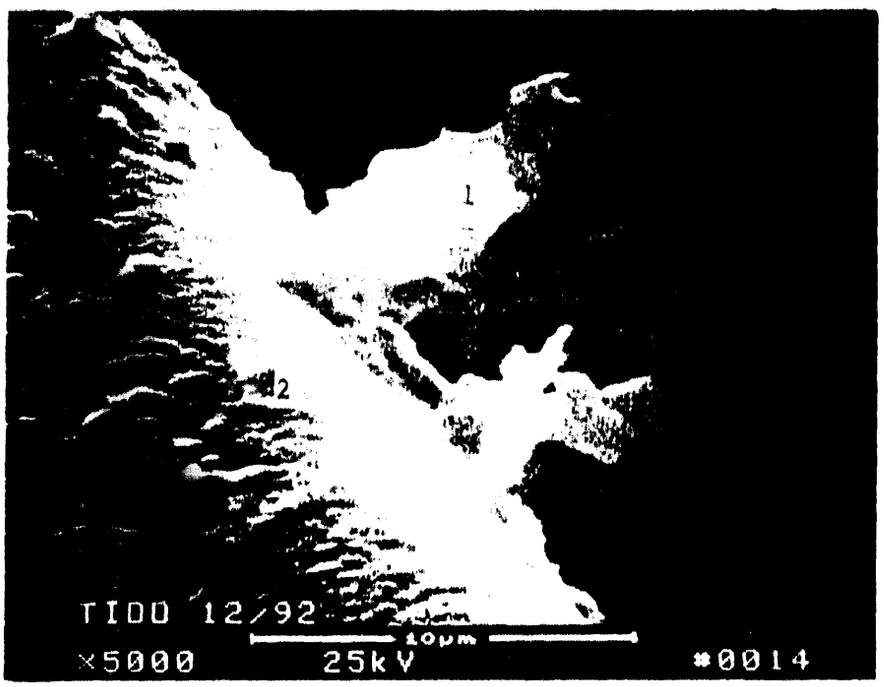

Figure 6.30 - High Magnification Micrograph Illustrating The Retention Of Fines Between Two Adjacent Silicon Carbide Grains At ~5 mm Below The OD Membrane Coated Surface

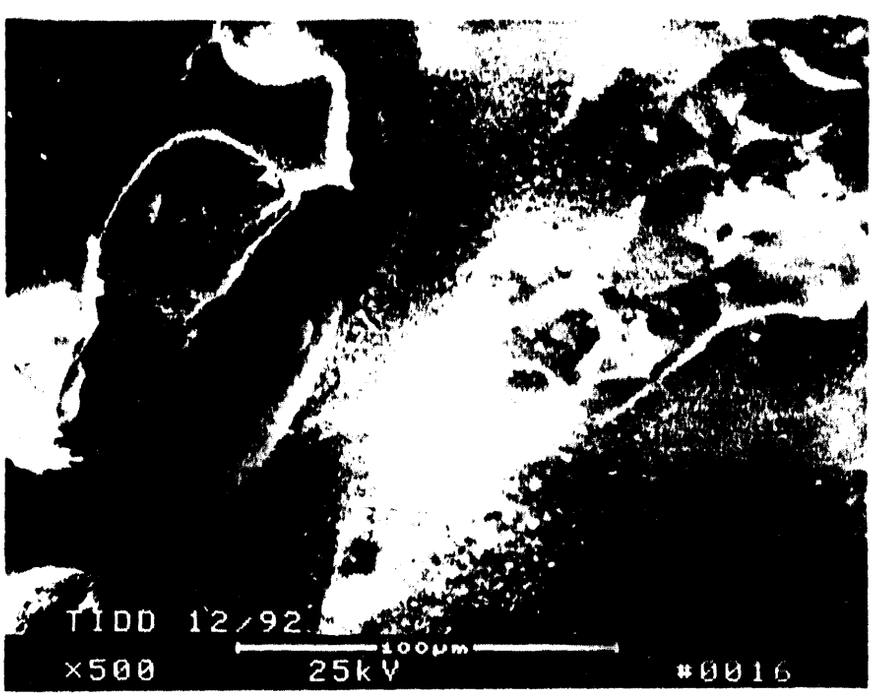

Figure 6.31 - Micrographs Illustrating The Morphology Of The Silicon Carbide Grains At ~5 mm Below The Membrane Coated OD Surface

Figure 6.32 - Micrographs Illustrating The Morphology Of The Silicon Carbide Grains At ~5 mm Below The Membrane Coated OD Surface

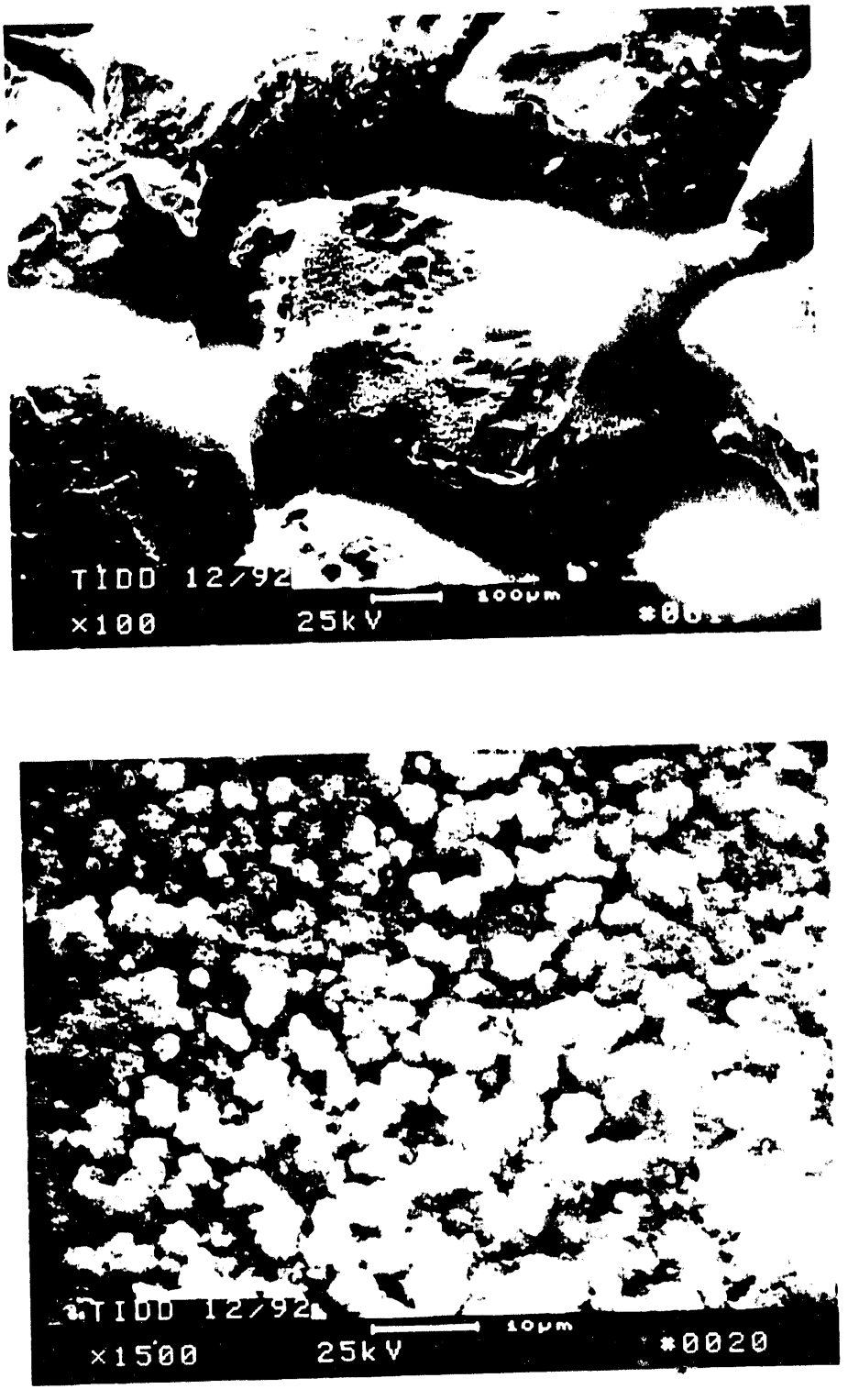

Figure 6.33 - Micrographs Illustrating The Morphology Of The Silicon Carbide Grains At ~10 mm From The Membrane Coated OD Surface

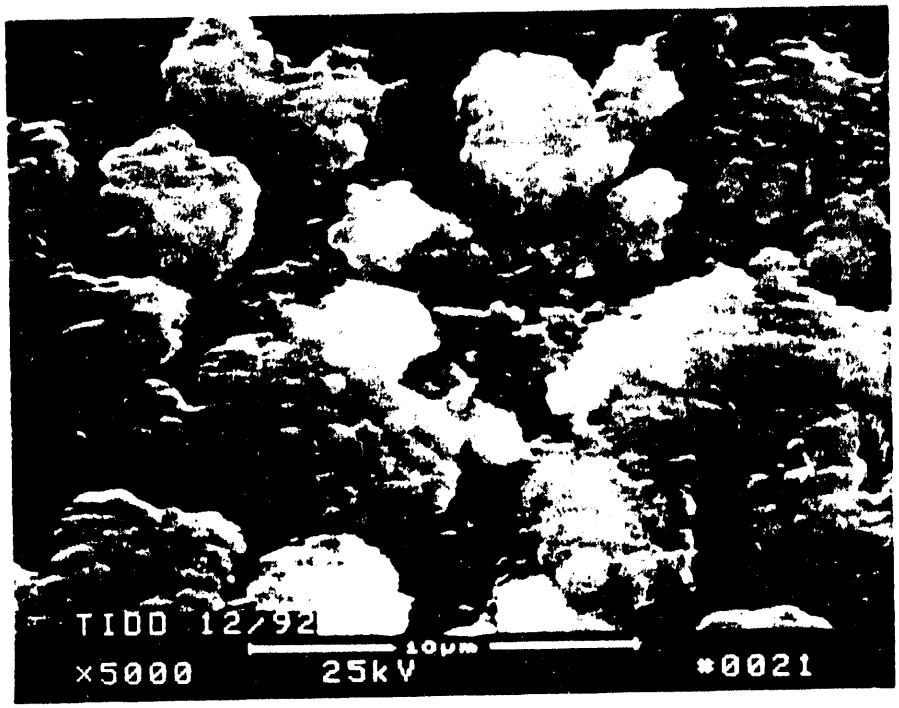

Figure 6.34 - High Magnification Micrograph Illustrating The Extensive Formation Of The Sulfur-Enriched Silicon-Containing Binder Phase Along Grains That Are ~10 mm From The Membrane Coated OD Wall

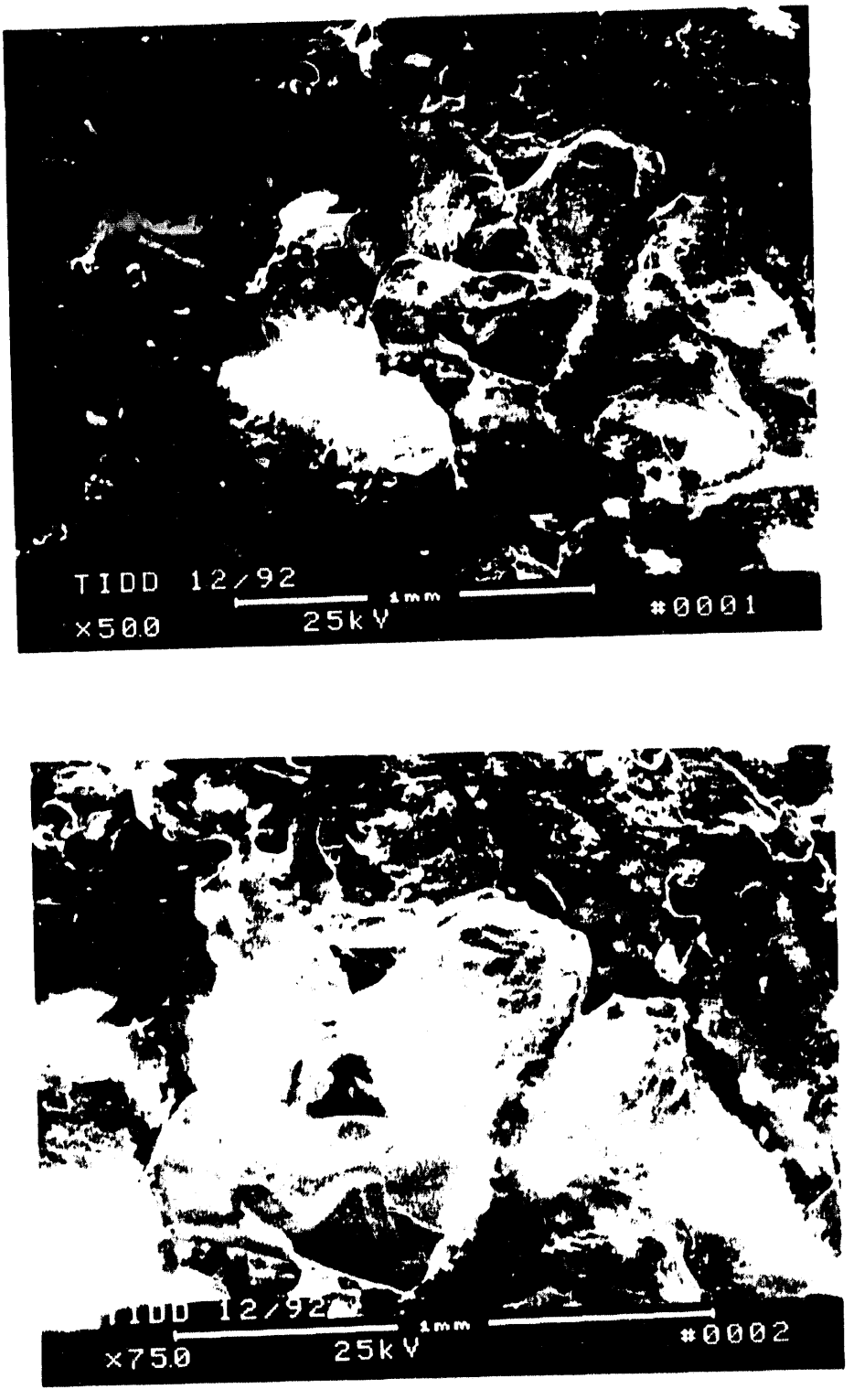

Figure 6.35 - Micrographs Illustrating The Morphology Of The Clay Bonded Silicon Carbide Grains At ~10 mm From The Membrane Coated OD Surface

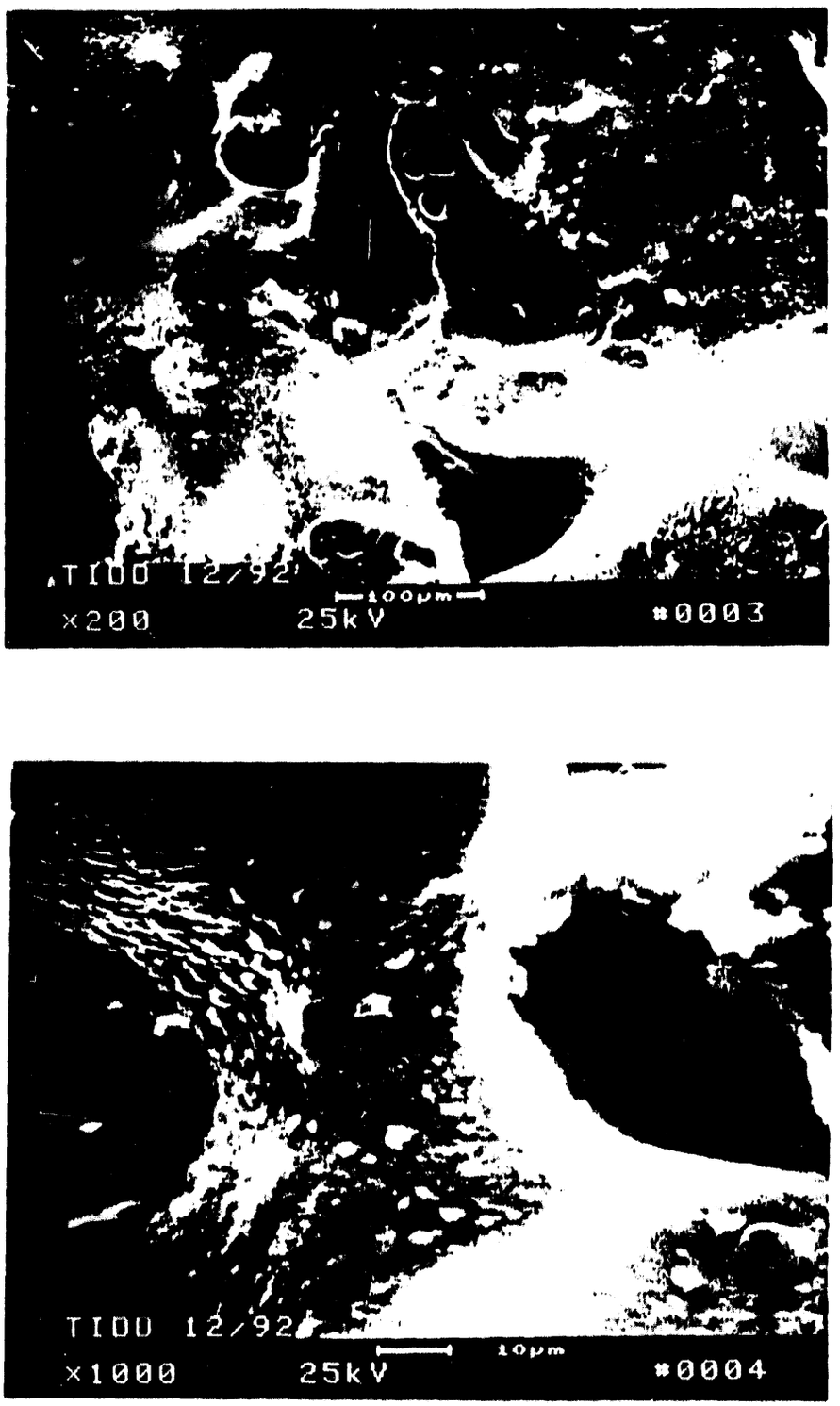

Figure 6.38 - Higher Magnification Micrographs Illustrating The Morphology Of The Binder Coating Along The Silicon Carbide Grains And Binder Interconnect Channels At ~10 mm From The Membrane OD Covered Wall

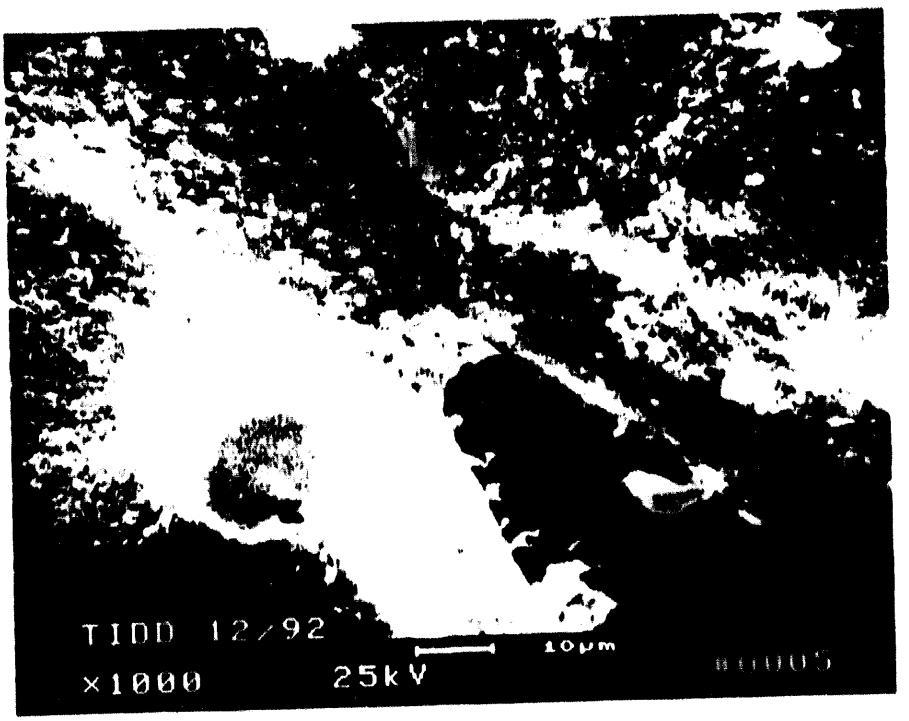

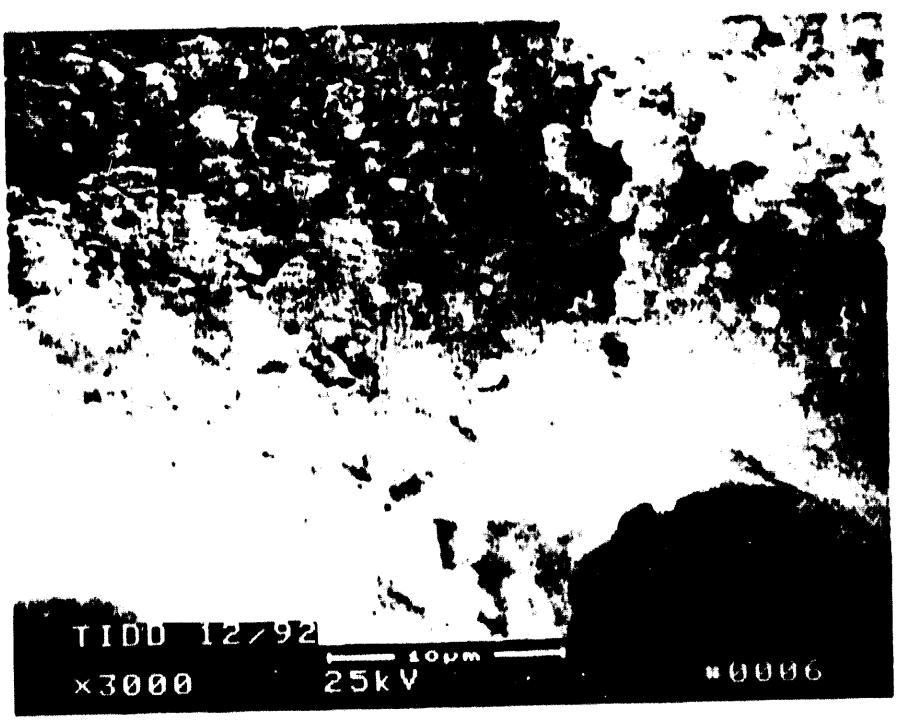

Figure 6.37 - High Magnification Micrographs Illustrating The Extensive Binder Surface Phase Changes That Occurred Along The Silicon Carbide Grains That Are Located At ~10 mm From The Membrane Coated OD Candle Surface

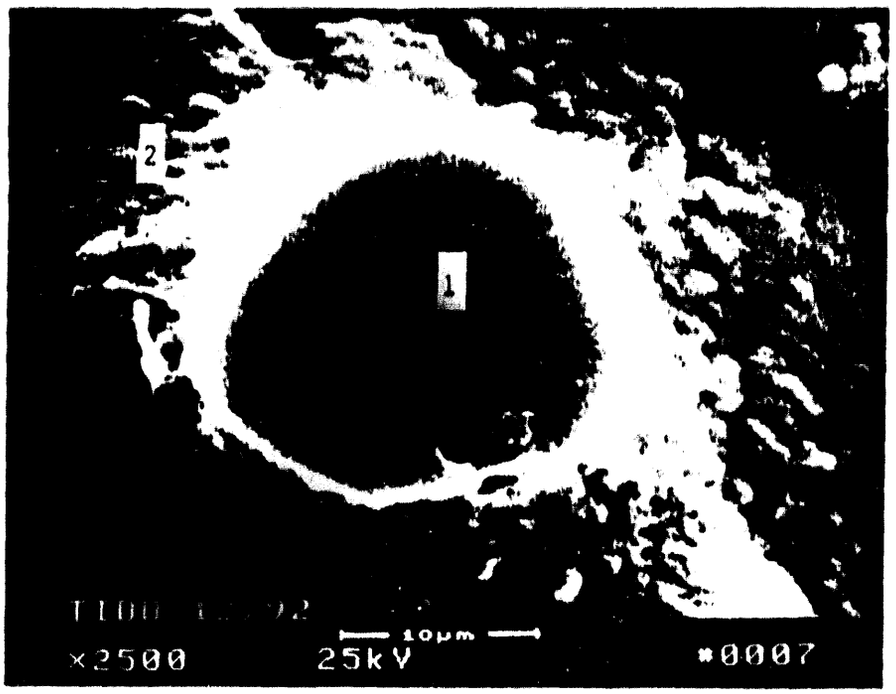

Figure 6.38 - Micrograph Illustrating The Change In The Morphology Of The Binder Phase That Coats The Silicon Carbide Grains Of The Schumacher Dia Schumalith F-40 Matrix After 500 Hours Of Exposure To PFBC Gas Conditions.

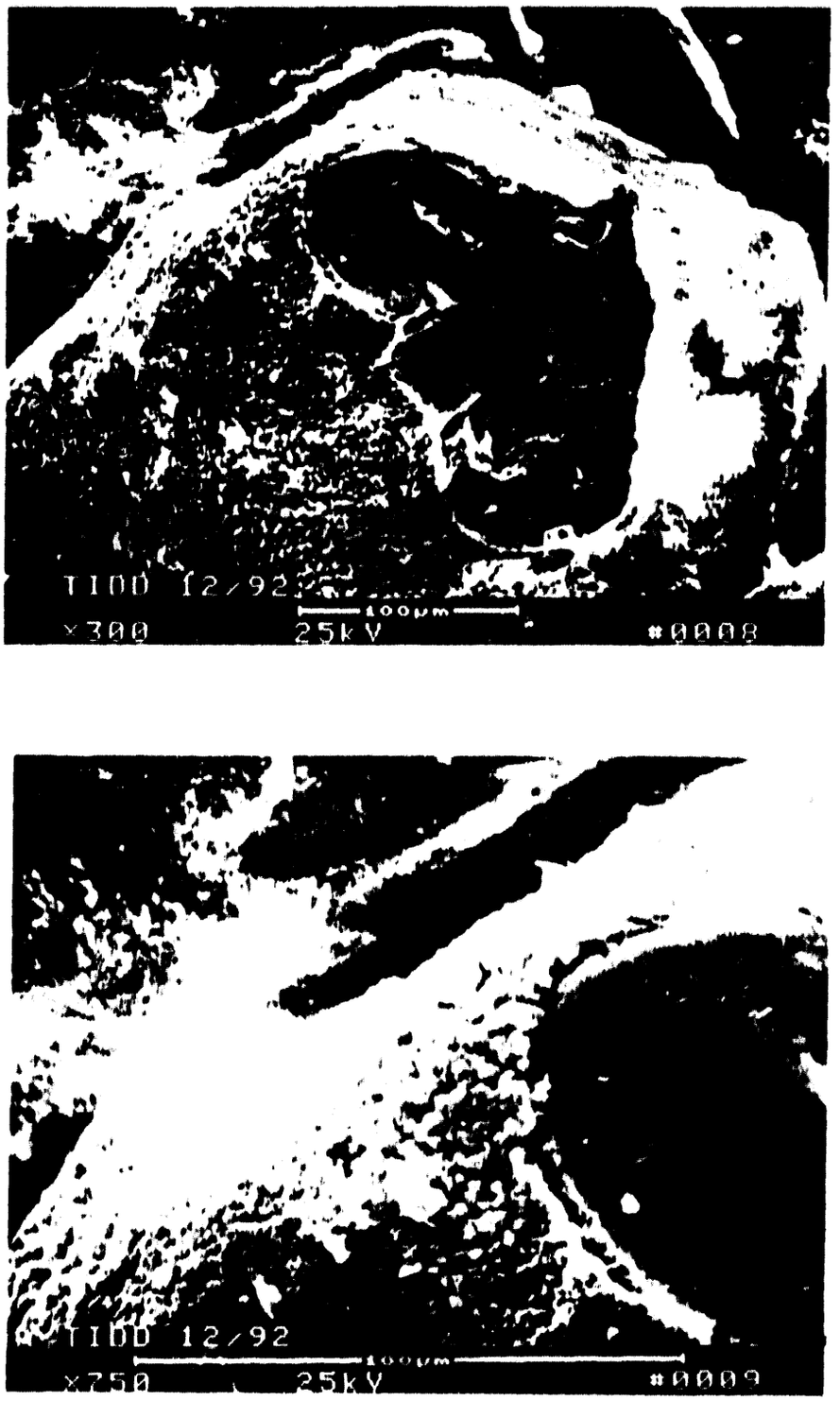

Figure 6.39 - High Magnification Micrographs At An Alternate Location Illustrating The Morphology Of The Silicon Carbide Grains At ~10 mm From THe Membrane Covered OD Surface

grains. Again extensive mottling was evident in the binder phase surface that coated the silicon carbide grains, as well as along the interconnect binder channels (Photos 3 and 4 in Figure 6.36).

High magnification micrographs shown in Photos 5 and 6 of Figure 6.37 indicated that the surface phase effect no longer supported individual agglomerated crystalline-like particles. The binder surface phase had grown and appeared to have formed a more or less continuous mat. In several areas, the subsurface binder phase coalesced, forming the mullite rod-like structure. Figure 6.38 illustrates a section of the binder interconnecting channel which fractured during sample preparation. Area 1 in Photo 7 of Figure 6.38 consisted of 69.02% Si, 26.32% Al, 2.88% K, 1.34% Fe, and 0.44% Ti (NF = 0.679) which was typical of the binder phase. In contrast the mottled surface features of the binder shown in Area 2 of Photo 7 in Figure 6.38 consisted of 72.97% Si, 17.93% Al, 3.52% K, 3.22% S, 1.78% Fe, and 0.59% Ti (NF = 0.707). Figure 6.39 provides additional micrographs of the silicon carbide grains that were ~10 mm from the membrane coated, candle filter OD surface. Again extensive phase change had occurred along the binder surface.

Figures 6.40 and 6.41 present the micrographs that were taken at ~12 mm from the OD membrane covered wall (i.e., 3 mm from ID). Deposition and collection of fines were evident in this region as a result of particulates being blown back into the matrix during pulse cleaning. Extensive mottling of the binder surface phase was evident at this location, as well as development of the rod-like mullite phase along the binder coating surface.

Figure 6.42 illustrates the extensive deposition of ash fines within the pores near the candle filter ID wall. Figure 6.43 illustrates that pores along the ID wall were nearly completely plugged. Extensive mottling of the binder phase was evident along the binder coated grains. Area 1 in Photo 18 of Figure 6.44 consisted of 76.65% Si, 14.22% Al, 6.86% K, 1.48% Na, and 0.79% Ti (NF = 0.749). This area was expected to be within the binder interconnect area that bonded two

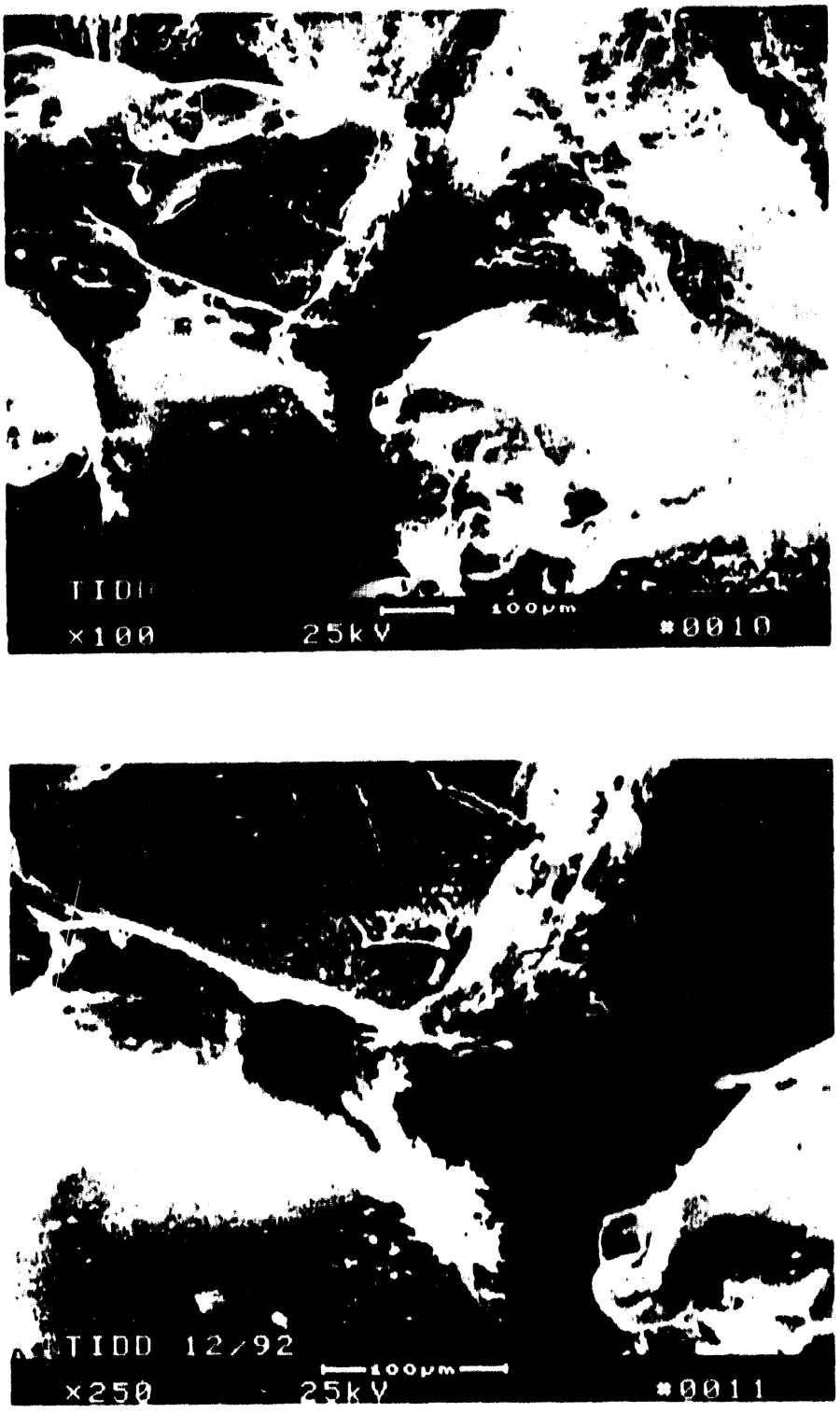

Figure 6.40 - Micrographs Illustrating The Collection Of Dust Fines Within The Silicon Carbide Matrix That Is ~12 mm From The Membrane Covered OD Wall (~3 mm From The ID Wall). Deposition And Collection Of Fines At This Location Resulted During Pulse Cleaning Of The Candles, Prior To Filter Failure.

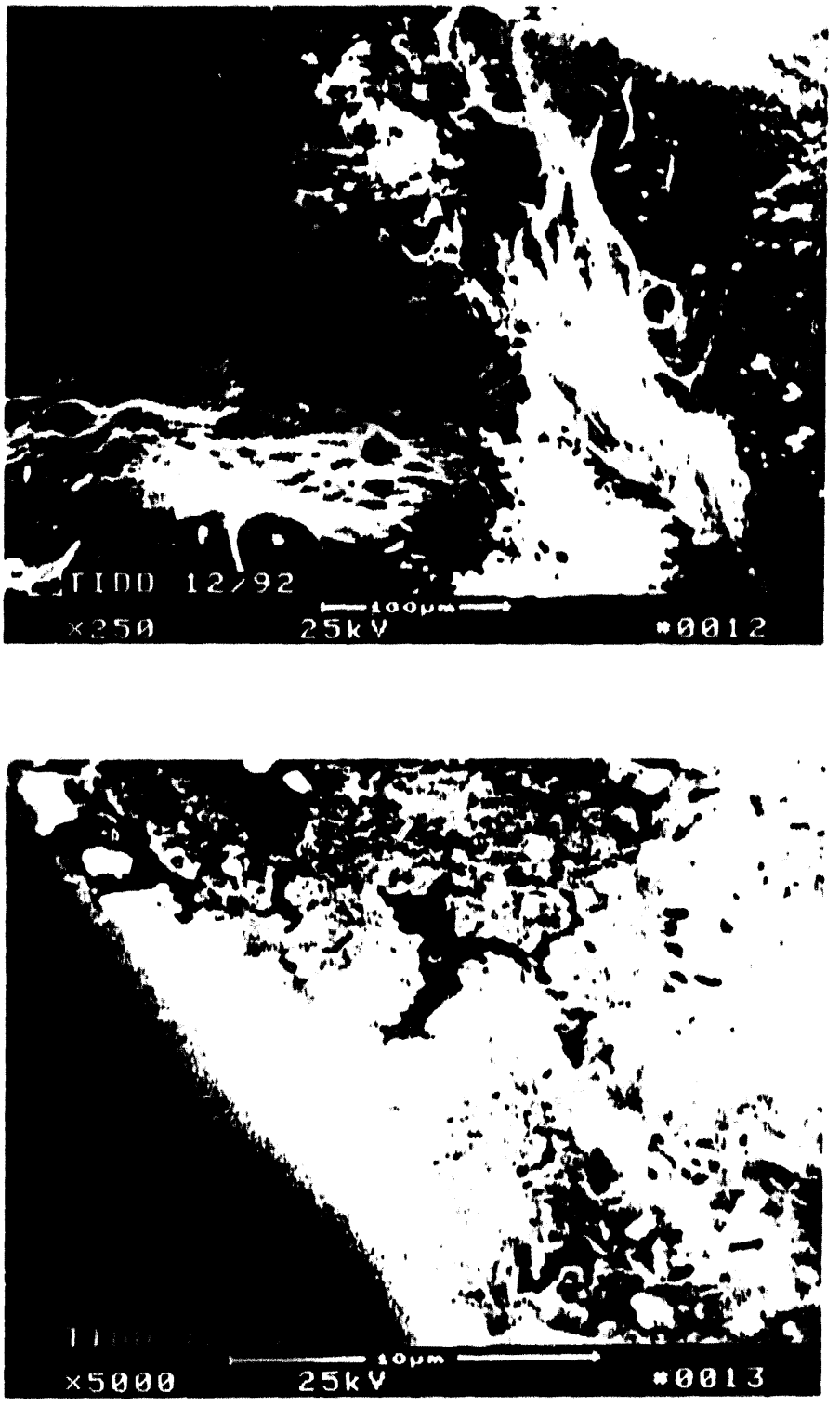

Figure 6.41 - Extensive Phase Change Along The Binder Surface Of The Silicon Carbide Grains That Are Located At ~12 mm From The Membrane Coated OD Wall (~3 mm From The ID Surface)

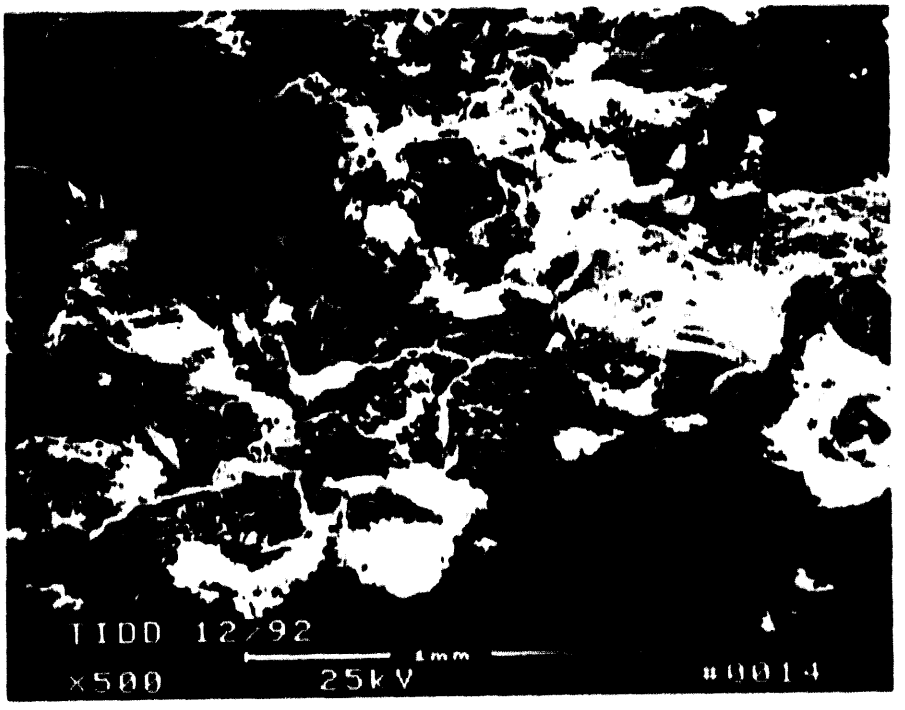

Figure 6.42 - Micrograph Illustrating The Accumulation Of Fines Within ID Pores Of The Clay Bonded Silicon Carbide Candle Filter

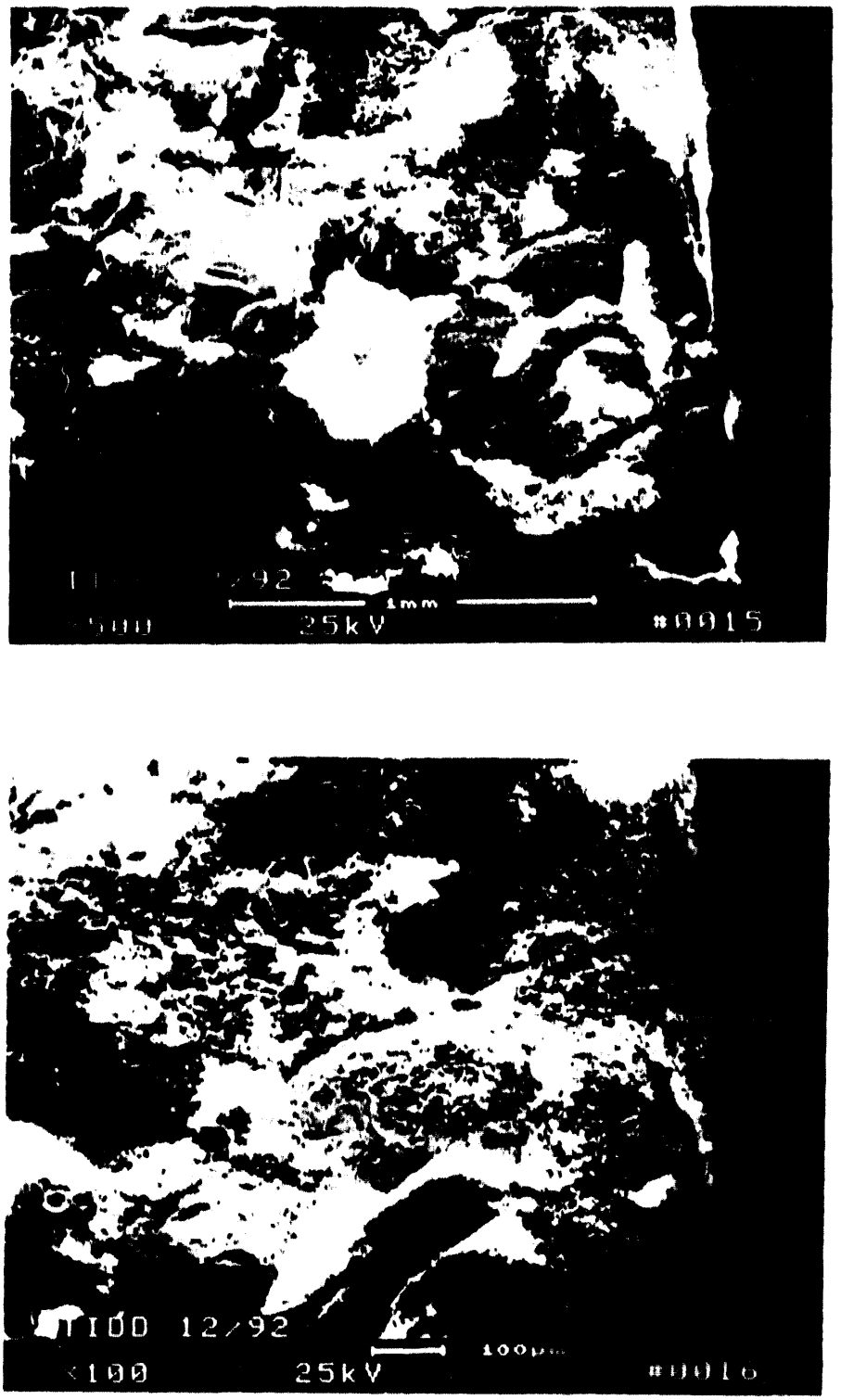

Figure 6.43 - Micrographs Indicate That Nearly Complete Plugging Has Resulted In The Pores That Are Present Along The ID Section Of The Clay Bonded Silicon Carbide Candle Filters

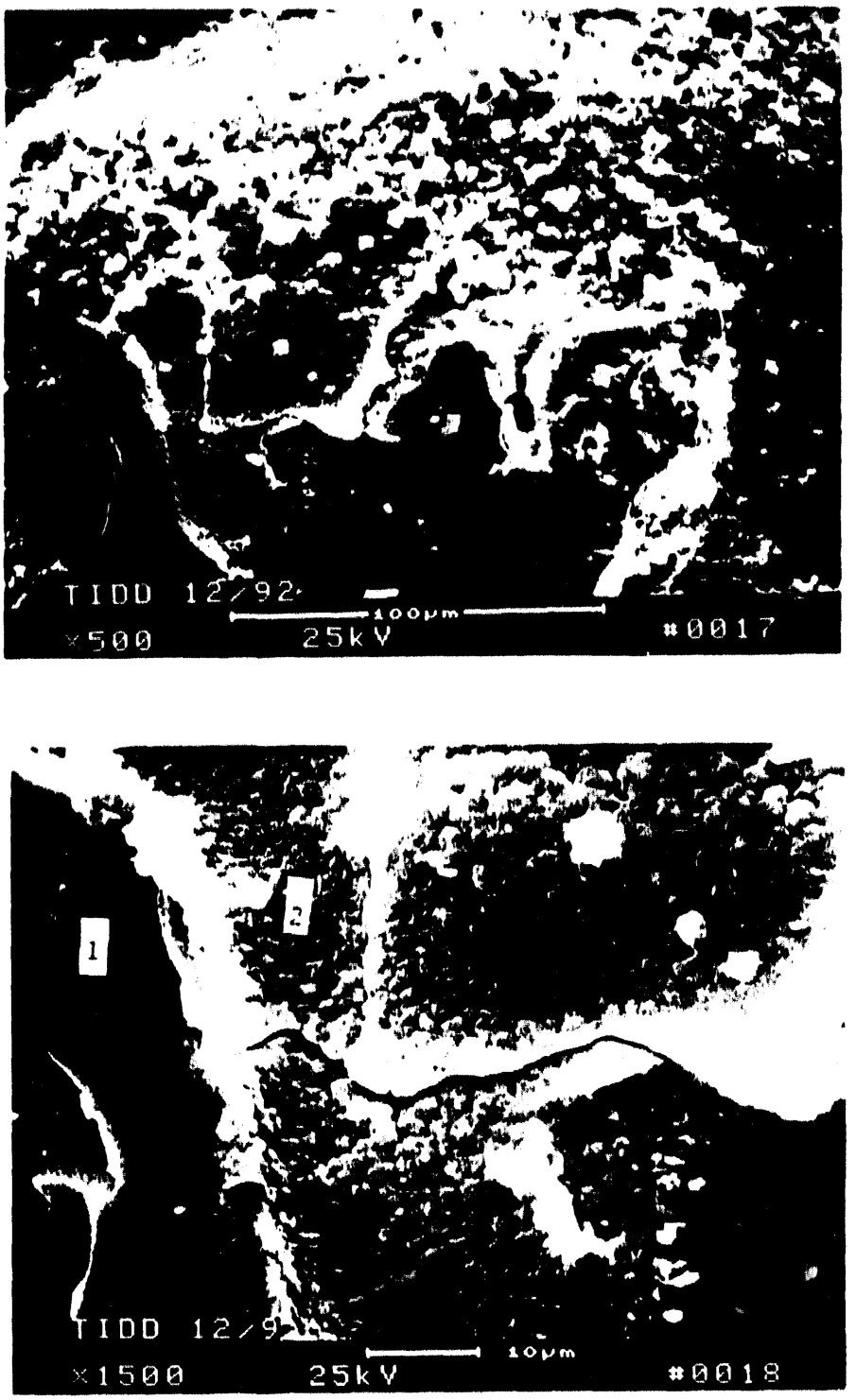

Figure 6.44 - High Magnification Micrographs Illustrate The Enhanced Surface Mottling Along The Sulfur-Enriched Silicon-Containing Binder Phase Near The ID Candle Wall

adjoining silicon carbide grains together. Area 2 in Photo 18 of Figure 6.44 illustrates an area where extensive mottling had occurred along the binder phase. EDAX analysis of Area 2 indicated the presence of 87.19% Si, 9.22% S, 1.91% K, and 1.67% Ca (NF = 0.890). Extensive crack formations were evident along the surface enriched silicon-containing binder phase. Note the relatively high concentration of sulfur that was retained in the silicon-rich binder phase along the ID surface of the candle filter.

Figure 6.45 (Photos 27 and 28) illustrates the accumulation of fines at another location along the ID surface of the silicon carbide matrix. EDAX analysis of the fines indicated the presence of 34.35% S, 24.96% Si, 16.11% Ca, 13.25% Al, 7.20% Mg, 2.17% Fe, and 1.95% K (NF = 0.662). High magnification micrographs of the fines that were entrapped in the ID pores are shown in Figures 6.46 and 6.47. EDAX analyses of the fines shown in Figure 6.47 indicated the presence of 30.07% Si, 26.95% S, 16.06% Al, 14.64% Ca, 8.13% Mg, 2.19% Fe, and 1.97% K (NF = 0.641).

Although fines that were deposited in the pores along the ID surface of the candle filter during pulse cleaning frequently filled the pore cavities and channels, the collected fines typically formed a porous unit. Two questions arise as a result of detecting fines along the ID surface. These include:

- To what extent does the accumulation of fines increase gas flow resistance through the ceramic filter matrix?
- Will the accumulated fines be released back into the clean gas stream during the course of normal hot gas filtration?

Based on the above concerns, removal of the candles from plenums that contain failed candles, and therefore plugged ID pores, was recommended. Similarly the incorporation of a membrane along the ID surface of the candle filter would limit fines penetration into the porous clay bonded silicon carbide matrix in the event of filter failure.

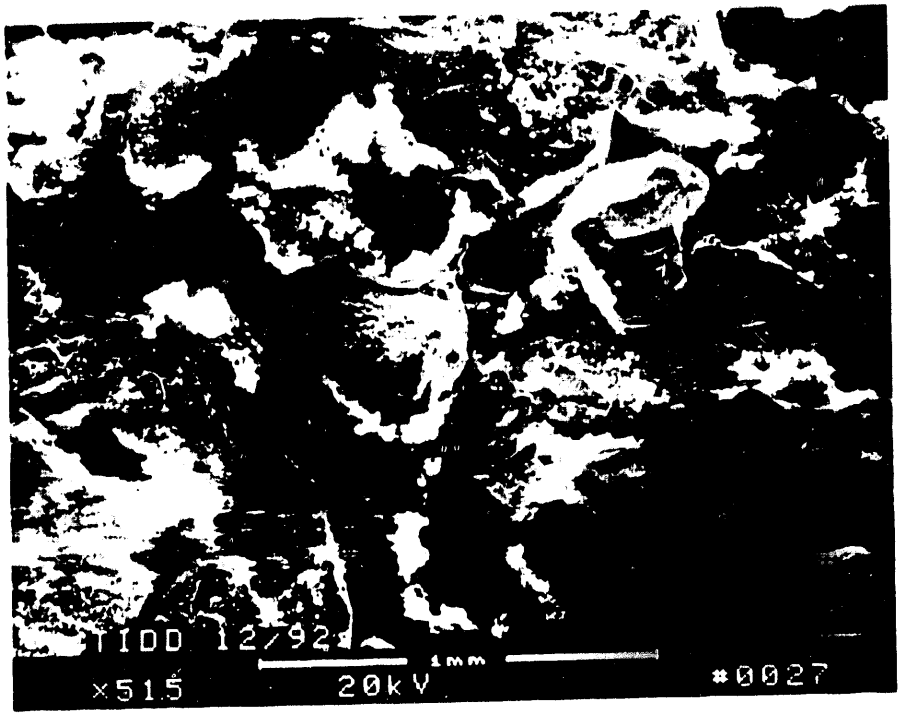

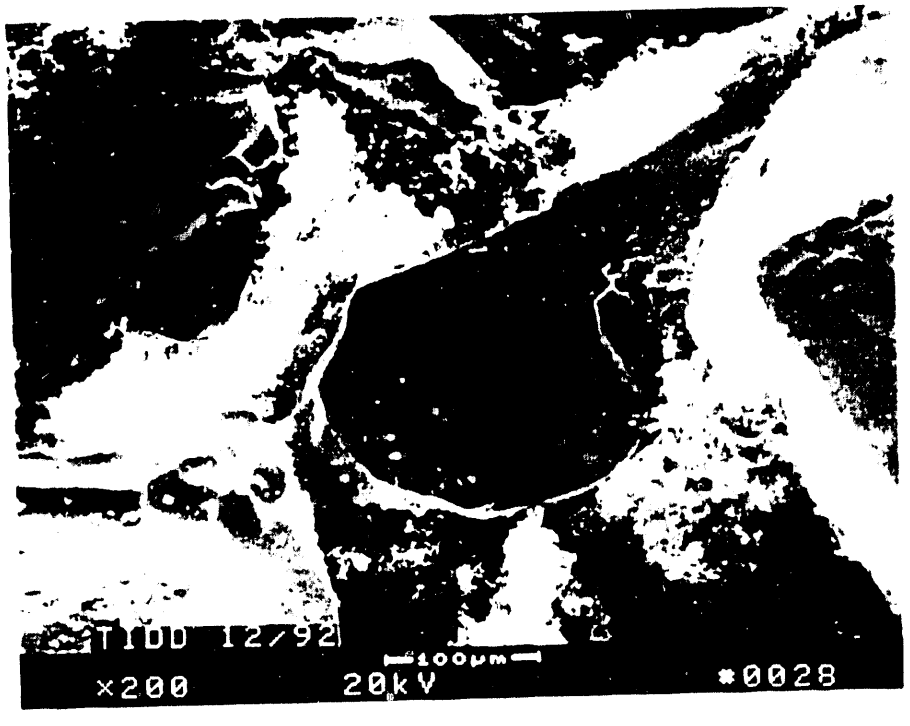

Figure 6.45 - Micrographs Illustrating The Accumulation Of Fines In The Pores Of The Clay Bonded Silicon Carbide Matrix Along The Candle ID Surface. Fines Penetration In This Area Resulted During Pulse Cleaning.

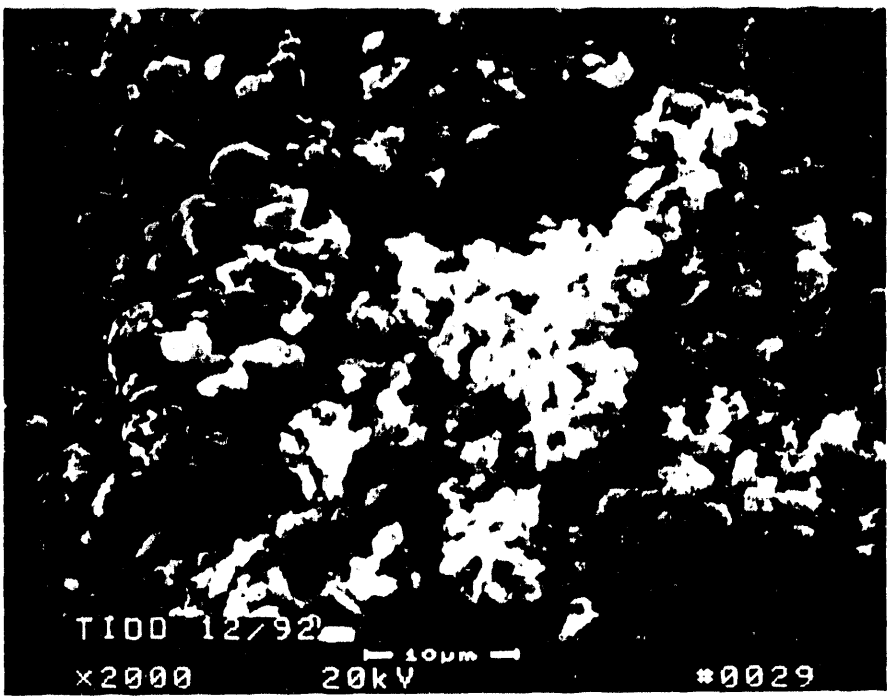

Figure 6.46 - High Magnification Micrograph Of The Fines Collected In The Candle ID Pores

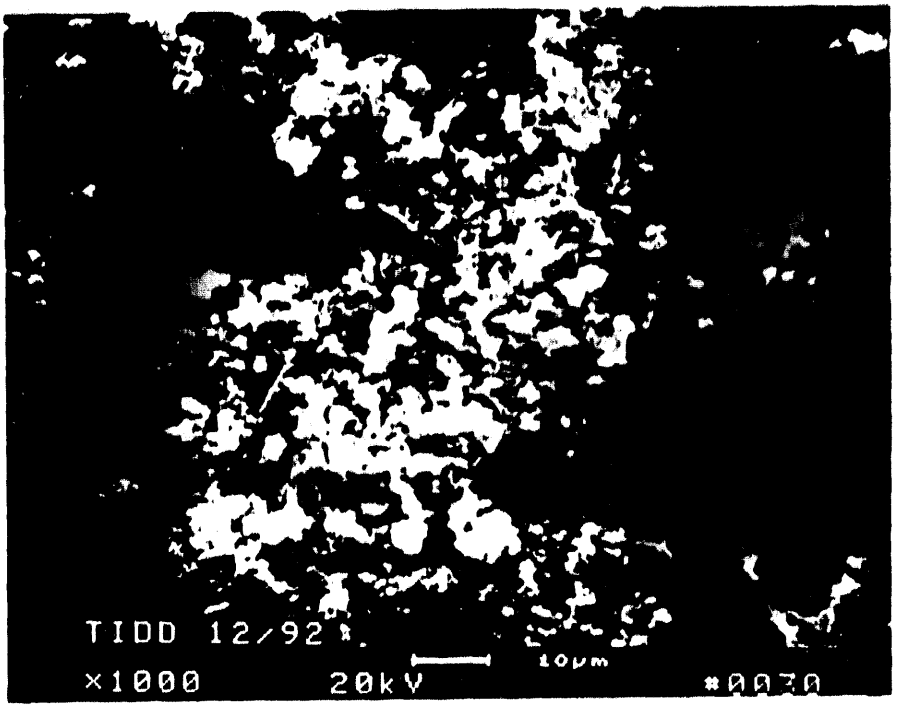

Figure 6.47 - Micrograph Illustrating The Morphology Of The Fines That Collected Along The Silicon Carbide Grains And Pores Along The ID Surface Of The Clay Bonded Silicon Carbide Candle Filters

6.3 OXYGEN ANALYSIS OF THE CLAY BONDED SILICON CARBIDE SEGMENT REMOVED FROM THE WESTINGHOUSE APF ASH HOPPER

The Link XL EDAX system was once again utilised to detail the concentration of oxygen within the binder phase that coated the silicon carbide grains in the Schumacher Dia Schumalith candle filters that experienced 500 hours of exposure in the AEP PFBC gas environment. A section was again removed from the silicon carbide candle filter segment that had fallen into the ash hopper. Note that this section of the candle had a heavy deposit of fines along its ID, as well as on its OD surface. Penetration of fines into the ID wall was evident.

Figure 6.48 indicates the extensive surface mottling that resulted along the binder coated silicon carbide grains. EDAX analysis of the area shown in Photo 2 of Figure 6.48 indicated the presence of 69.021% O, 25.757% Si, 2.612% Na, 2.067% Al, 0.426% S, and 0.117% K. A higher magnification micrograph of this area is shown in Figure 6.49 (Photo 3). Characterisation of the ~5 μm crystalline-like phases that formed along the binder surface indicated the presence of 69.348% O, 27.857% Si, 1.319% Na, 1.292% Al, and 0.185% S (Area 1, Photo 3, Figure 6.49). Area 2 of Photo 3 in Figure 6.49 represents the binder surface which consisted of 72.147% O, 20.615% Si, 3.727% Na, 2.377% Al, 0.657% S, 0.218% Fe, 0.132% K, and 0.127% Ca. Note that the sulfur-enriched agglomerates extend above the binder surface as shown along the fractured interconnecting channel (i.e., left side of Photo 3).

In an attempt to discern whether there was a silica layer (i.e., SiO_2) formed along the binder/grain interface, EDAX analyses were attempted along the cross-sectioned surface shown in Figure 6.50 (Photo 4). The dashed line marks the binder/grain interface as determined by the EDAX analyses that were performed in this area. In this location we were not able to identify the formation of an oxygen-enriched silicon phase at the binder/grain interface.

In an attempt to further demonstrate whether there was an additional oxide phase formed at the binder/grain interface, the clay bonded silicon carbide matrix was cross-sectioned and polished, prior to

Figure 6.48 - Micrographs Illustrating The Sulfur-Enriched Silicon-Containing Phase The Forms Along The Silicon Carbide Grains After Exposure In The PFBC Gas Environment

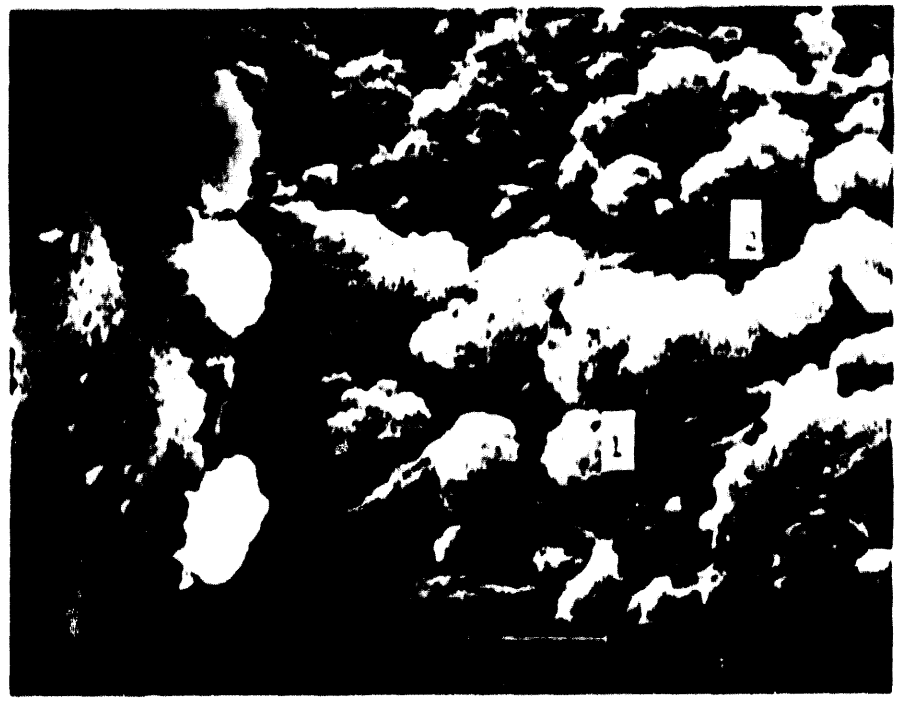

Figure 6.49 - High Magnification Micrograph Illustrating The Sulfur-Enriched Silicon-Containing Binder Phase In The Clay Bonded Silicon Carbide Candle Filter Matrix

Figure 6.50 - Micrograph Delineates The Binder/Grain Interface

SEM and oxygen analysis. Figure 6.51 illustrates the gold coated polished section with the dashed lines marking the location between the binder/grain interface. Since the sample was gold coated, we have eliminated any capability for detecting sulfur using EDAX techniques. As shown in the schematic below Photo 1 in Figure 6.51, silicon and aluminum were identified at the interface. Carbon and oxygen were not present in this area. A silicon-aluminum-potassium-enriched layer (sulfur may be present) formed as the next layer, prior to contacting the binder phase which consisted of oxygen, silicon, aluminum, sodium, and potassium. Further analyses are required to verify these results at alternate locations along the silicon carbide matrix.

6.4 SEM/EDAX CHARACTERIZATION OF AN INTACT CLAY BONDED SILICON CARBIDE CANDLE FILTER

The candle which was designated as #198 was positioned in location C/B-21 during the 500 hour exposure to AEP PFBC gas environment. This candle was sectioned for analysis in order to provide a comparison between an intact candle matrix which experienced long-term exposure, and material from a candle section that had fallen into the ash hopper which presumably experienced fewer hours of actual hot gas filtration operation. Figure 6.52 illustrates the morphology of the intact candle filter clay bonded silicon carbide matrix near the OD membrane coated surface. Extensive surface mottling resulted along the binder coated silicon carbide grains. In addition, regions within the mottled areas appeared to be raised above the binder coated surface (Photos 3 and 4, Figure 6.53). Analysis of the mottled surface indicated the presence of 73.26% O, 18.857% Si, 4.017% Na, 2.923% Al, 0.725% S, and 0.217% K (Area 1, Photo 3, Figure 6.53). The thickness of the surface enriched phase was ~5 μm.

Area 2 in Photo 3 of Figure 6.53 illustrates the smooth features of the fractured binder interconnect channel. EDAX analysis of this area indicated the presence of 49.778% O, 38.699% Si, 5.753% Al, 4.295% K, and 1.475% Na. From these analyses it appeared that either:

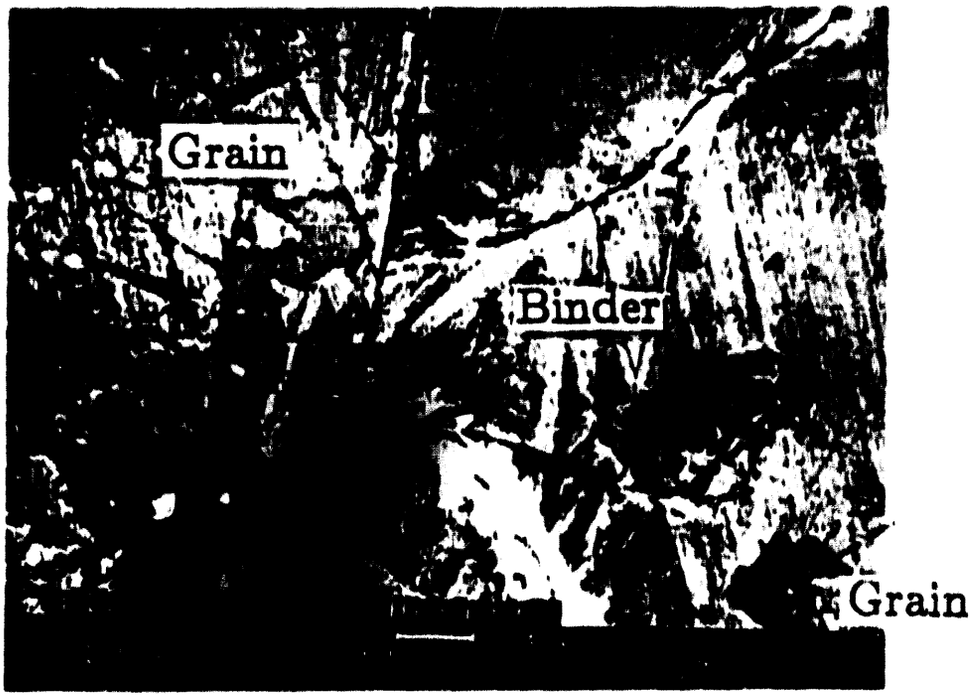

-- Grain -->	:<-- Interface --->	:	:<--- Binder --
SiC	Si - Al	Si	Si
		Al	Al
		K	O
			Na
			K

Figure 6.51 - Micrograph Of The Polished Cross-Sectioned Clay Bonded Silicon Carbide Matrix After 500 Hours Of Exposure In The PFBC Gas Environment. Dashed Lines Delineate The Binder/Grain Interface

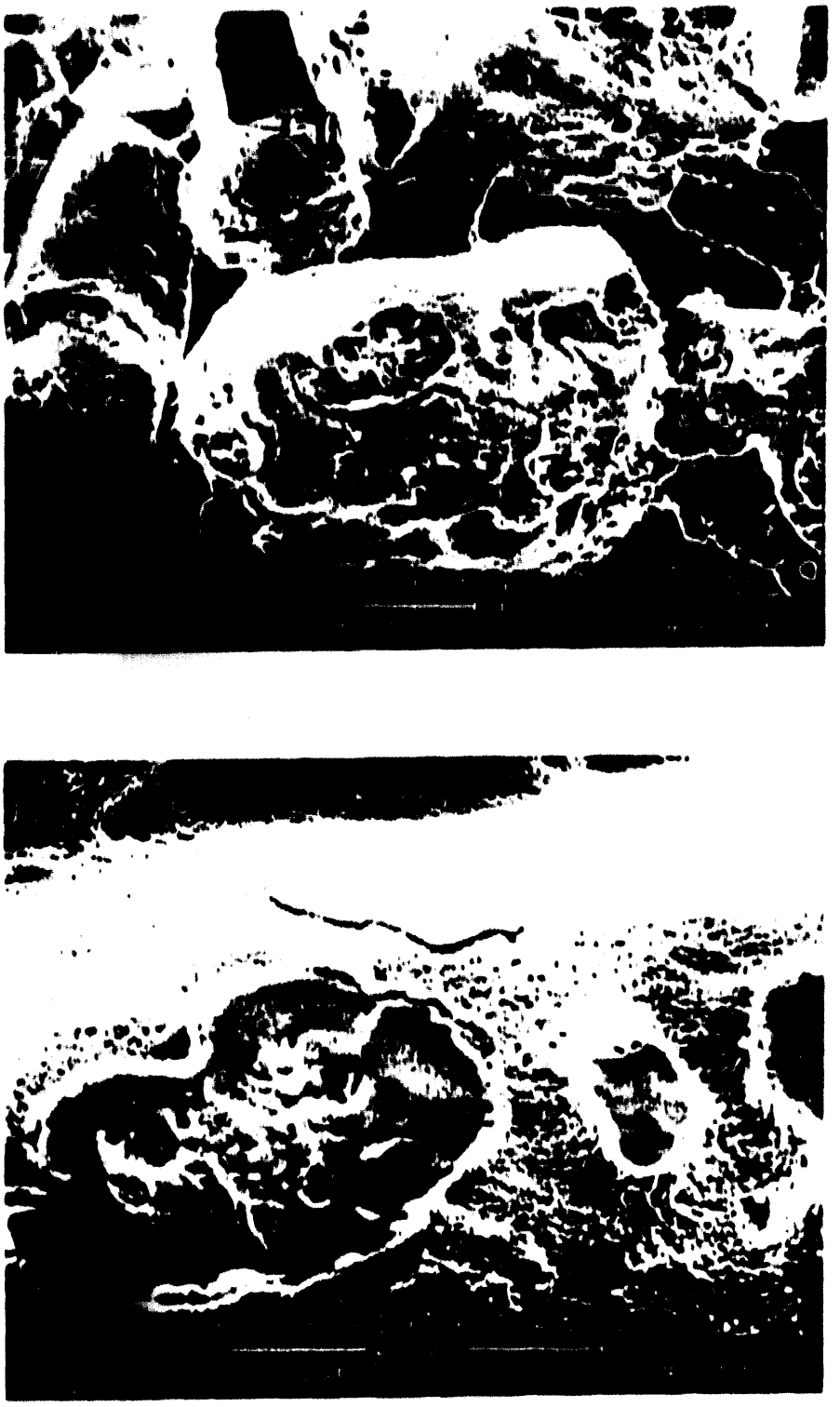

Figure 6.52 - Micrographs Illustrating The Morphology Of The Silicon Carbide Grains Near The OD Surface Of The Clay Bonded Silicon Carbide Candle Filter Which Had Remained Intact During The Entire 500 Hours Of Operation In The PFBC Gas Environment

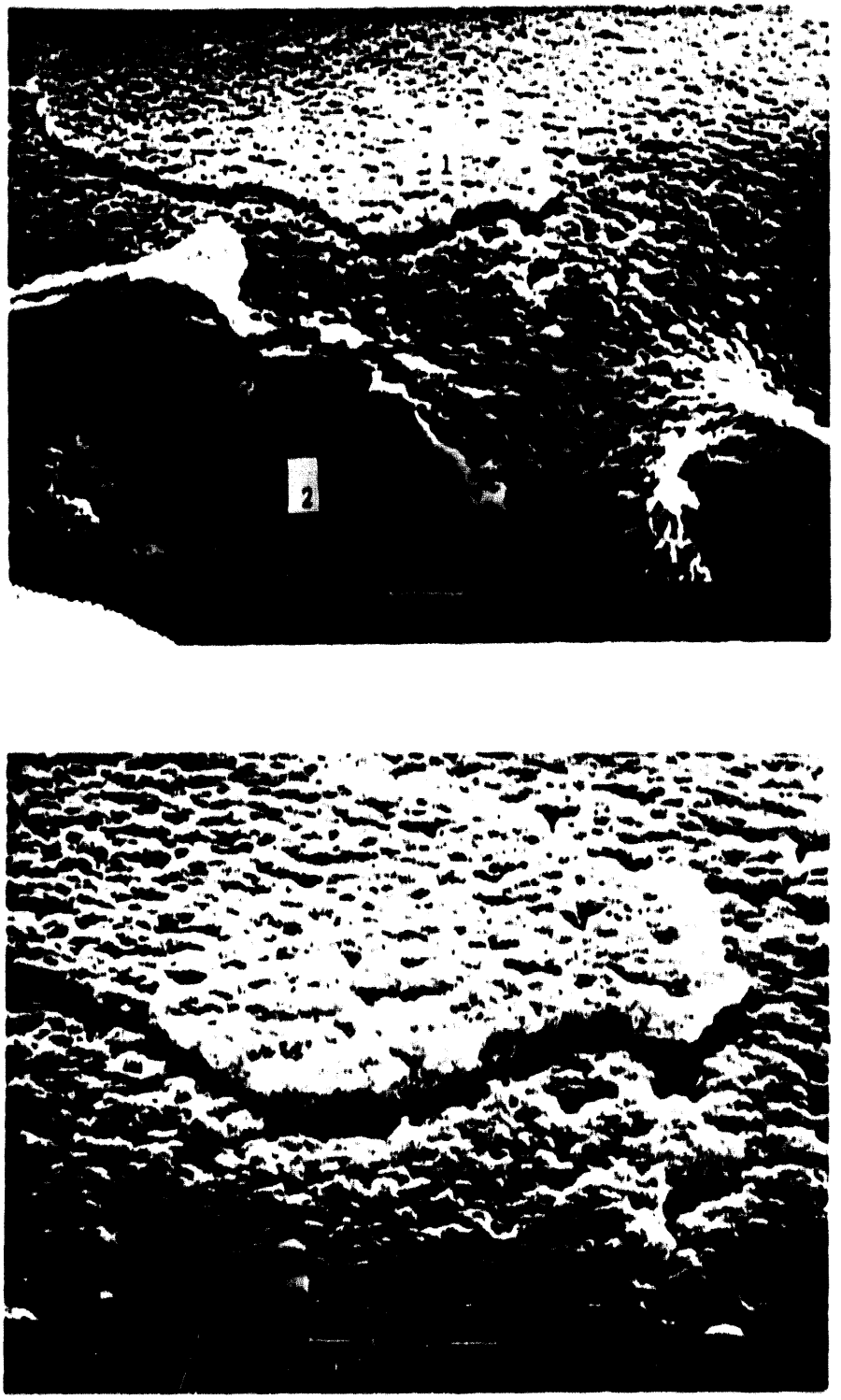

Figure 6.53 - High Magnification Micrographs Illustrating The Surface Morphology Of The Binder Coating Along Silicon Carbide Grains Near The OD Wall Of The Candle Filter That Remained Intact During The Entire 500 Hours Of Hot Gas Filtration In The PFBC Gas Environment

- Sodium had migrated to the surface of the binder phase which was somewhat sulfur-enriched, while potassium appeared to be retained within the matrix,

or

- That sodium and sulfur from the gas phase had been sorbed into the binder surface which then accelerated production of the crystalline phase along the binder surface.

At this point in time we are not able to differentiate between these two scenarios.

Figure 6.54 (Photo 54) illustrates the extensive mottling that resulted along the binder surface that coated the silicon carbide grains, and the binder phase along the interconnecting channels. Higher magnification micrographs of this area are shown in Photos 6 and 7 of Figure 6.55. The rather irregularly shaped particle in Area 1 of Photo 6, Figure 4.55, consisted of 71.709% O, 10.236% S, 8.612% Ca, 4.768% Si, 1.647% Na, 1.639% Al, 1.230% Mg, and 0.160% K, indicative of a fly ash-sorbent particle. Alternately, the globular deposit shown in Area 1 of Photo 7 (Figure 6.55) consisted of 79.737% O, 7.941% Ca, 6.423% S, 4.533% Si, 1.212% Al, and 0.154% K -- again a fly ash-sorbent particle.

Along the silicon carbide grain, the binder phase appeared to coalesce, particularly in the areas where the fly ash-sorbent particles were attached to the grain (Photos 8 and 9 in Figure 6.56). EDAX analysis of the particle shown in Area 1 of Photo 8 (Figure 6.56) indicated the presence of 73.261% O, 7.704% Si, 6.306% S, 4.984% Al, 3.907% Ca, 2.058% Na, 1.222% Mg, 0.305% K, and 0.252% Fe. Note that the rod-like mullite formations were detected in the areas where fines adhered to the binder surface.

6.5 SEM/EDAX (OXYGEN) CHARACTERIZATION OF THE CLAY BONDED SILICON CARBIDE MATRIX AFTER EXPOSURE AT TIDD AND ROOM TEMPERATURE C-RING STRENGTH TESTING

Initially the clay bonded silicon carbide candle that was exposed to the PFBC gas environment was sectioned for C-ring strength

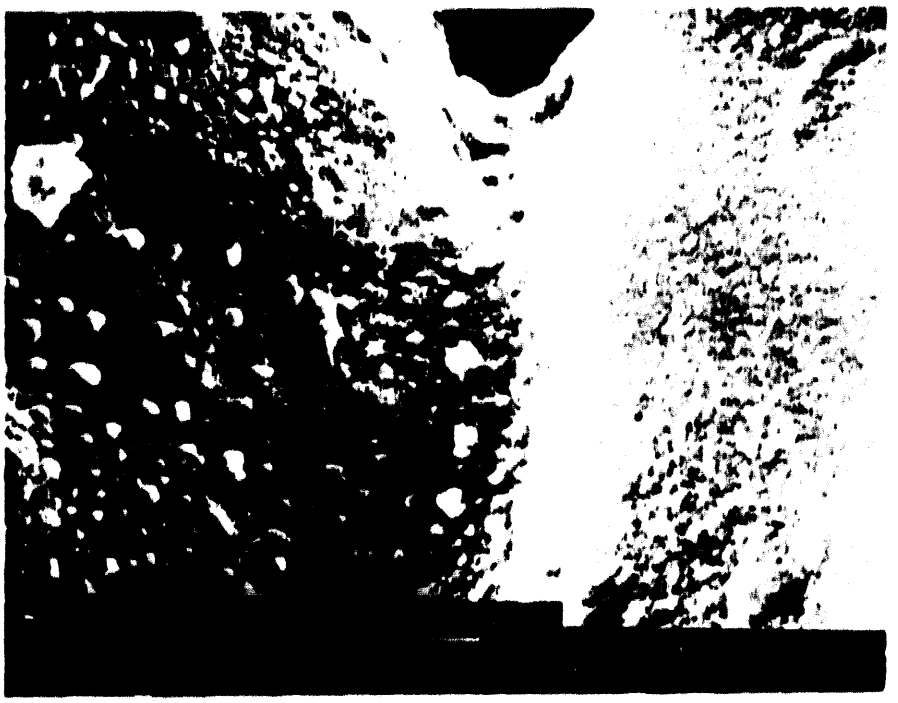

Figure 6.54 - Micrograph Illustrates The Extensive Binder Surface Phase Changes That Resulted Along The Silicon Carbide Grains In The Schumacher Dia Schumalith Candle Filter Matrix After Exposure In The PFBC Gas Environment

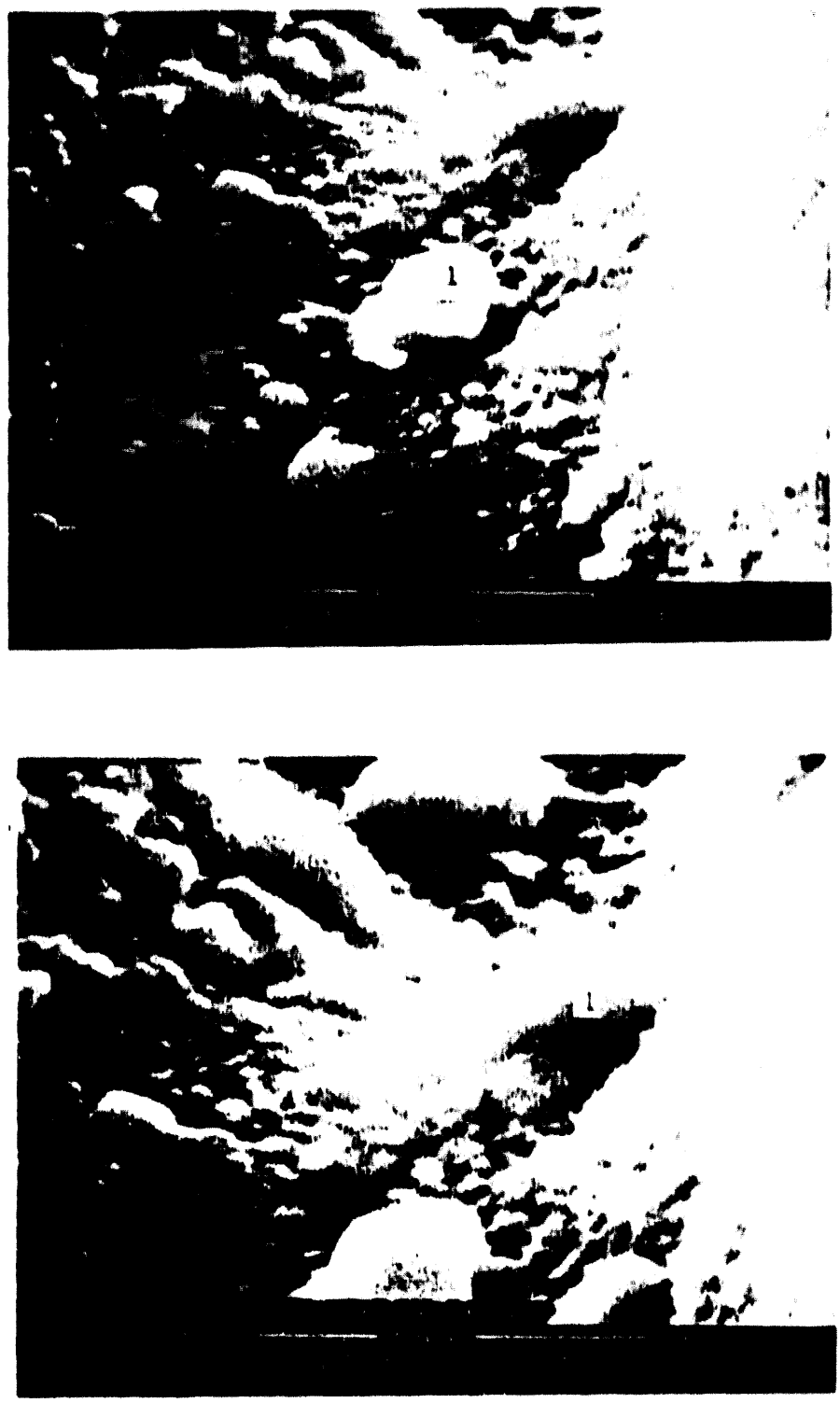

Figure 6.55 - High Magnification Micrographs Illustrating The Adherence And Possible Bonding Of The Ash-Sorbent Fines Along The Silicon Carbide Binder Phase Surface

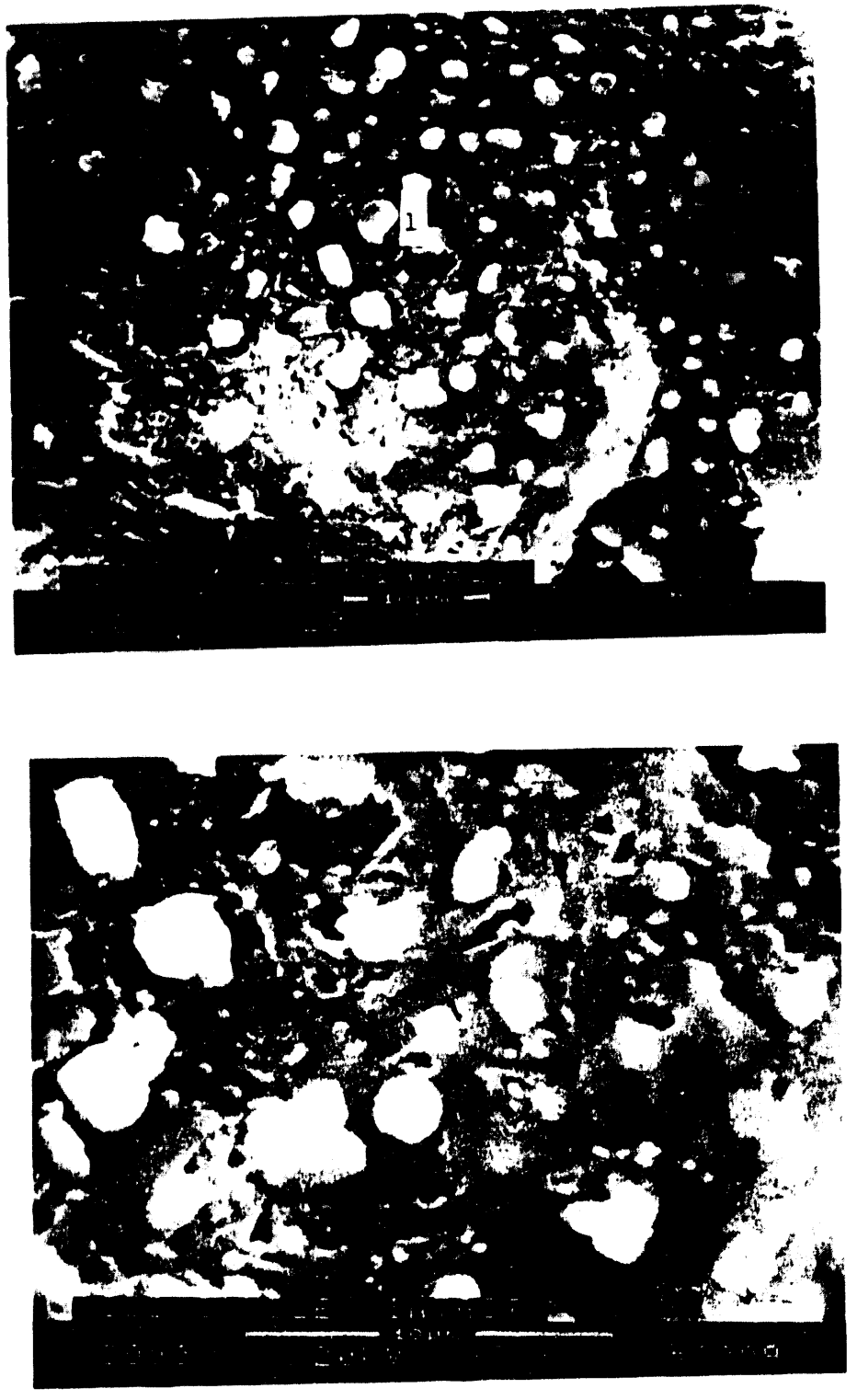

Figure 6.56 - Mullitization Of The Binder Phase Beneath Adhering Ash-Sorbent Fines

determination. During sample preparation the C-rings were cut wet. A C-ring section that was strength tested at room temperature was subjected to SEM/EDAX characterization using the Link XL EDAX system. The morphology of the silicon carbide matrix adjacent to the aluminosilicate fibrous membrane is shown in Figure 6.57. At high magnification the morphology of the binder phase appeared to be mottled (Figure 6.58). EDAX analysis of Area 1 in Photo 3 of Figure 6.58 indicated the presence of 73.049% O, 20.401% Si, 3.081% Al, 2.781% Na, and 0.687% K, indicative of a thin binder phase coating along the debindered silicon carbide grain. Area 1 shown in Photo 4 of Figure 4.58 contained 71.966% O, 19.820% Si, 4.030% Al, 2.977% Na, and 1.207% K, also representative of the binder phase that coated the underlying silicon carbide grain. Area 2 in Photo 4 of Figure 6.58 appeared to consist of the raised agglomerate phase which was previously described. In this sample, the agglomerate consisted of 73.434% O, 18.036% Si, 3.701% Na, 3.257% Al, 0.902% K, and 0.669% Mg. Note the absence of both sulfur and calcium in this area.

Figure 6.59 indicates that the thickness of the binder phase which coated the silicon carbide grains was ~10-20 μm. Note the mottled surface features along the binder coating surface and the ragged edge of the binder at the binder/grain interface. The thick binder coating contained 76.243% O, 18.100% Si, 2.897% Na, 2.249% Al, and 0.511% K (Area 1, Photo 5, Figure 4.59).

At another location along the clay bonded silicon carbide matrix, we attempted to discern whether there was an oxide-silicon-containing phase (i.e., SiO_2) at the binder/grain interface. As shown in Figure 6.60, the grain was oriented in such a manner to clearly analyze the composition in the binder, binder/grain interface, and grain. Area 1 in Photo 6, Figure 6.60, contained both silicon and carbon (i.e., SiC grain). Area 1 in Photo 7, Figure 6.60 attempted to locate the interface. EDAX analysis of Area 1 indicated the presence of 63.718% O, 25.890% Si, 6.240% Al, 2.190% K, 1.597% Na, and 0.366% Ti.

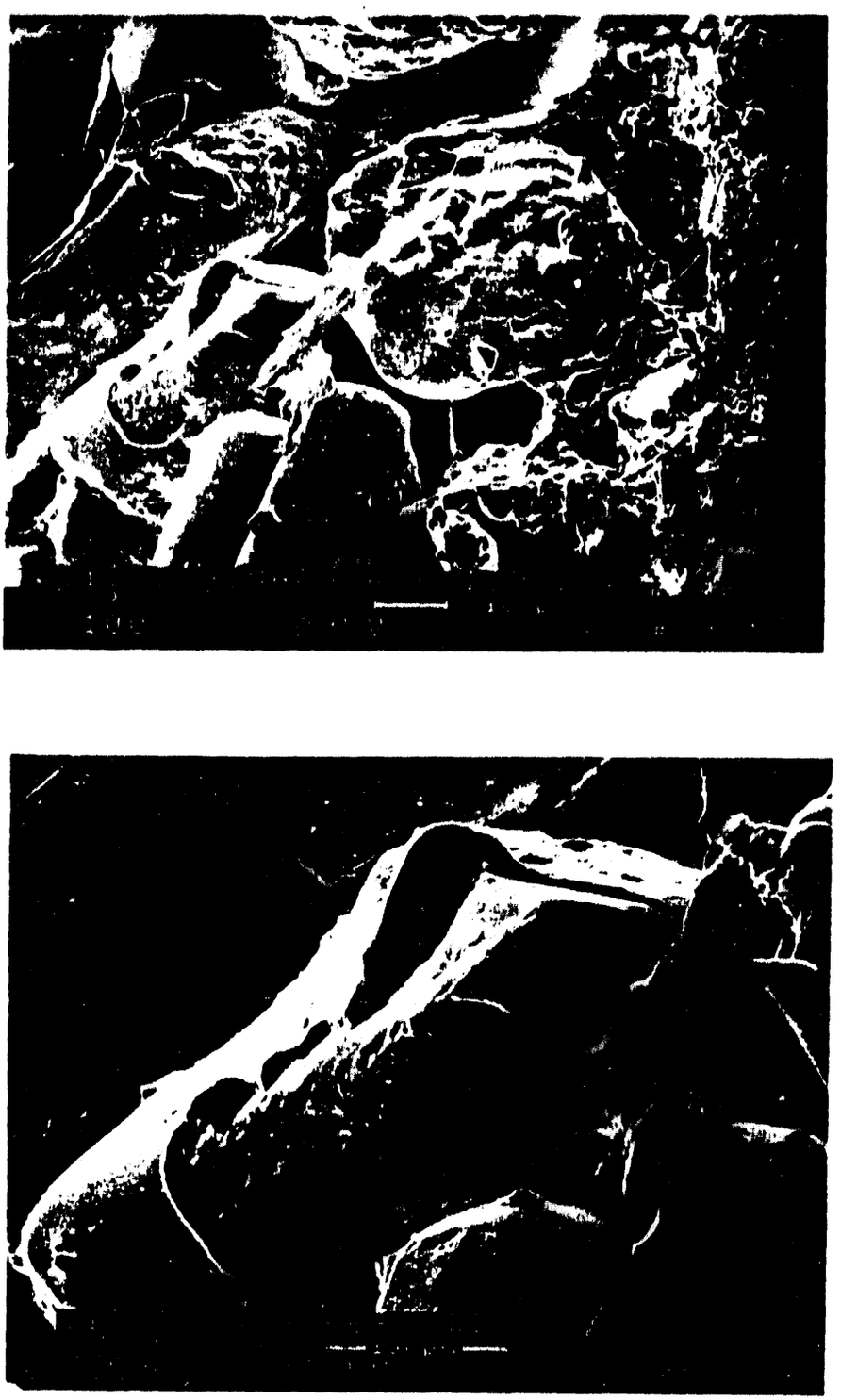

Figure 6.57 - Micrographs Illustrating The Morphology Of The Silicon Carbide Grains Within The Filter Material That Had Been C-Ring Sectioned For Strength Analysis. This Section Was Cut Wet During Sample Preparation.

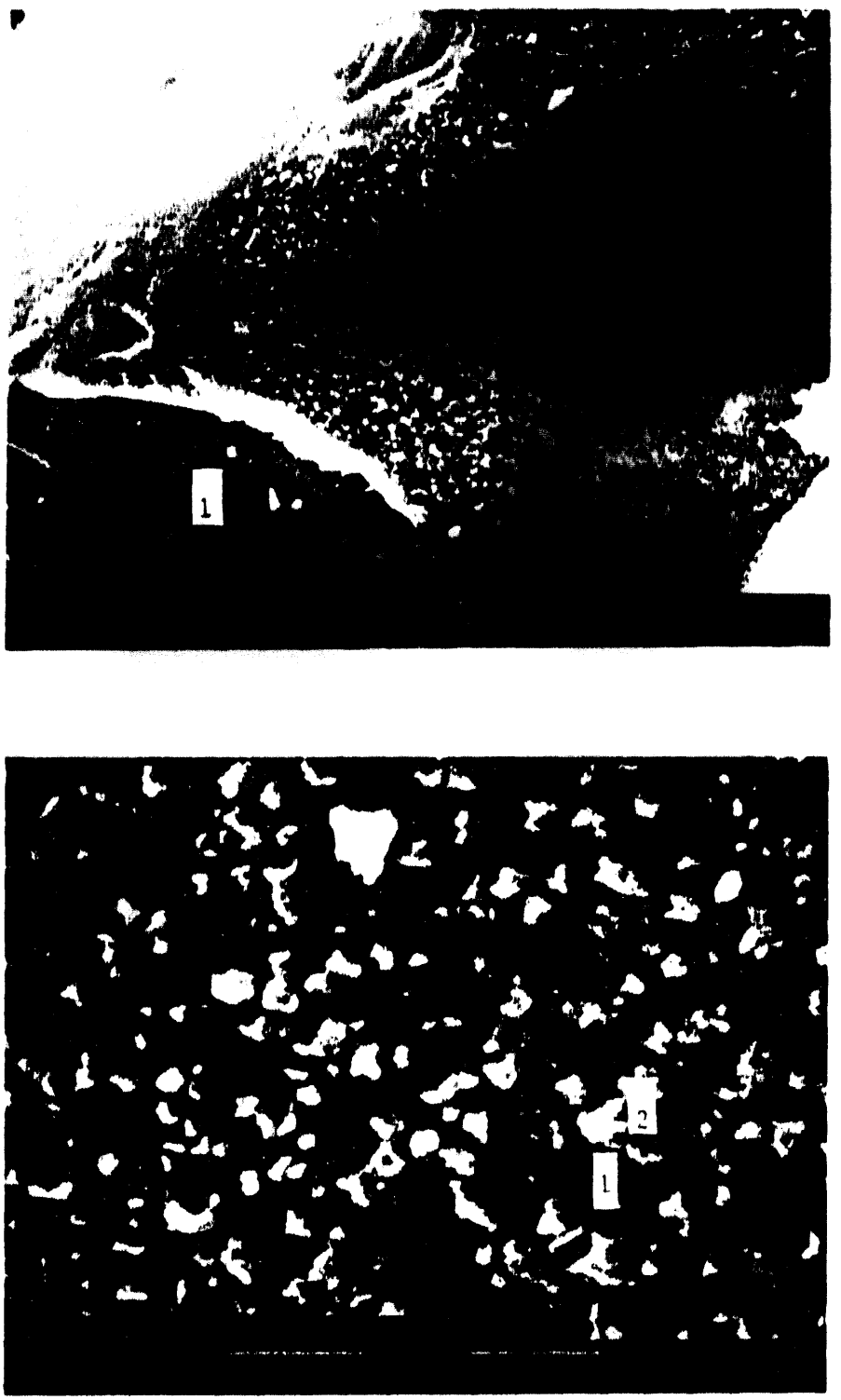

Figure 6.58 - Micrographs Illustrating The Mottling Surface Effect That Results Along The Binder Coating Near The OD Wall Of The Filter Matrix

Figure 6.59 - Micrograph Illustrated The Thickness Of The Binder Phase Along The Silicon Carbide Grain, As Well As The Mottled Surface Features Of The Binder Coating

Figure 6.60 - High Magnification Micrographs Illustrating The Binder Coating Thickness Along A Silicon Carbide Grain

Carbon was also detected in this area. Area 1 therefore contained both the binder and SiC matrix.

Area 2 in Photo 7 of Figure 6.60 consisted solely of silicon and carbon, and represented the SiC matrix. Area 3 in Photo 7 of Figure 6.60 contained the binder phase (70.341% O, 21.018% Si, 3.707% Al, 3.288% Na, 1.135% K, 0.219% Ti, 0.152% Fe, and 0.140% S). Once again calcium was not detected in the area analyzed. A dashed line was added to Photo 7 (Figure 6.60) to designate the binder/grain interface as determined by EDAX analysis.

Moving toward the center of the cross-sectioned silicon carbide wall, we noted that the binder phase which coated the grains was not only mottled, but also contained "pitted" areas (Figures 6.61 and 6.62). Area 1 in Figure 6.62 contained the raised agglomerated surface features of the binder phase which consisted of 70.350% O, 21.407% Si, 3.760% Al, 3.318% Na, and 1.164% K. The "pitted" regions shown in Area 2 of Photo 11 in Figure 6.62 were identified to consist of 74.457% O, 16.832% Si, 4.126% Na, 3.571% Al, 0.783% K, 0.134% Fe, 0.070% S, and 0.048% Ti. What was striking to note was the relatively high sodium concentration, but conversely low sulfur content in the pitted areas, as well as the absence of calcium. Perhaps deposition of high sulfur, calcium-containing "aerosol" droplets formed along the binder coated grain surface, but while the samples were being prepared for C-ring strength determinations, this phase was leached from the clay bonded silicon carbide matrix.

Figure 6.63 illustrates the silicon carbide matrix at another location along the cross-sectioned candle filter wall. Note the extensive formation of the mottled binder surface features. A high magnification micrograph of the binder coating is shown in Photo 14 of Figure 6.64. The agglomerates consisted of 71.539% O, 18.988% Si, 5.293% Na, 3.268% Al, 0.478% K, 0.272% S, and 0.162% Fe. Again note the high sodium concentration, low sulfur content, and absence of calcium.

Figures 6.65 and 6.66 again illustrate the extensive formation of the binder coating agglomerates along a silicon carbide grain, as well

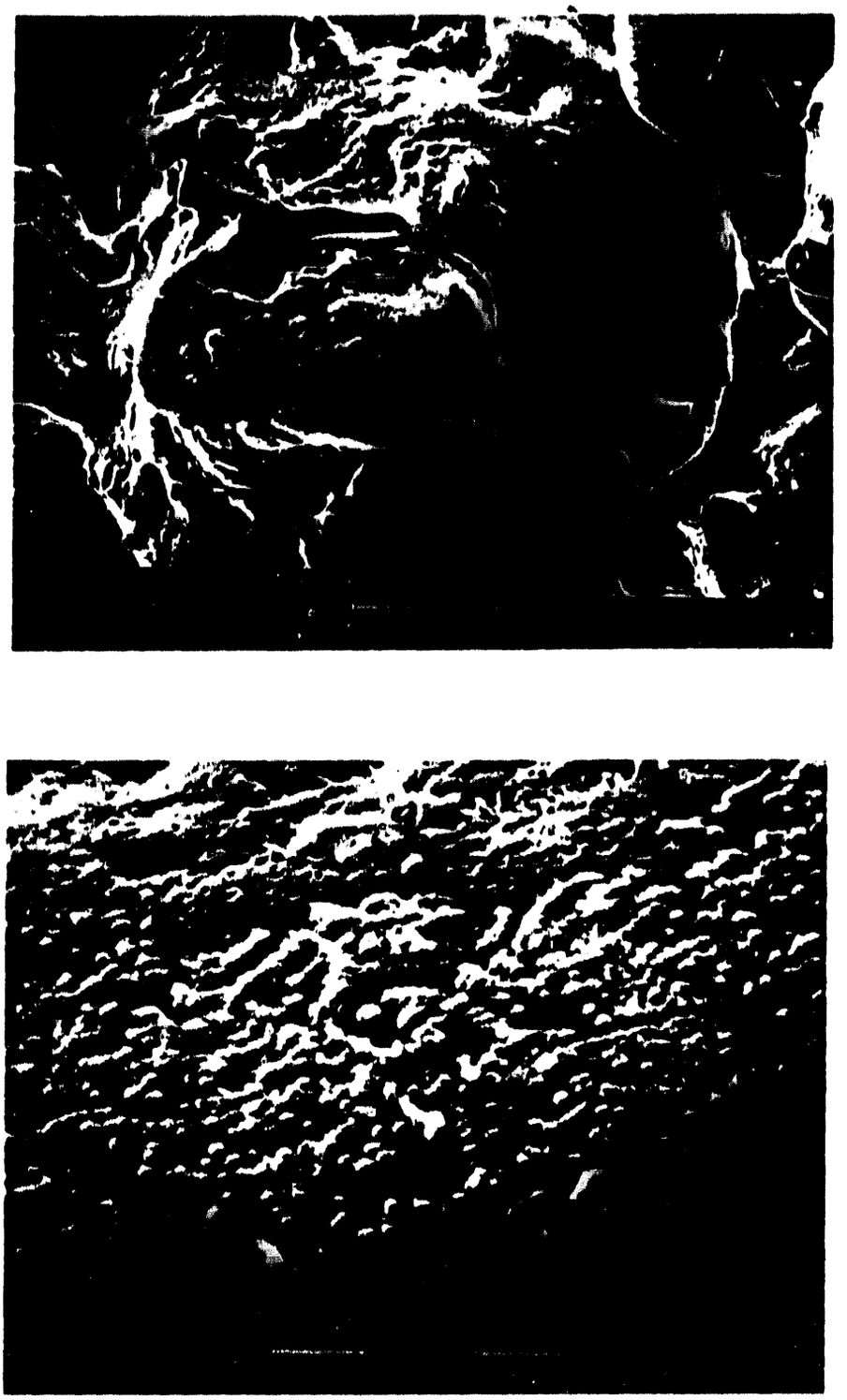

Figure 6.61 - Micrographs Illustrating The Raised Agglomerates Along The Silicon Carbide Binder Phase. Pitted Areas Are Also Evident.

Figure 6.62 - Higher Magnification Micrograph Illustrating The Raised Agglomerates And Pitted Areas Along The Silicon Carbide Binder Coating

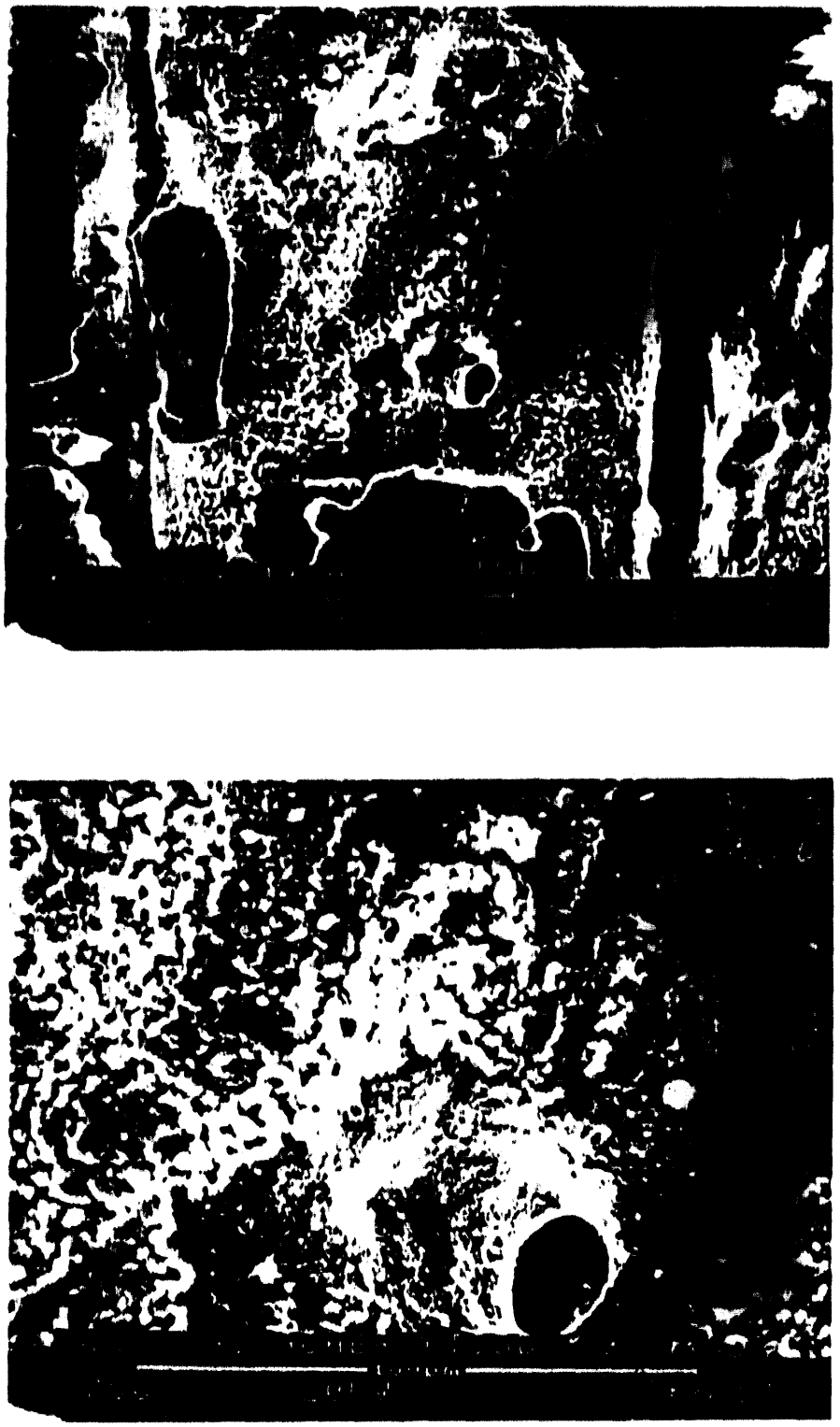

Figure 6.63 - Extensive Formation Of The Surface Agglomerates Along The Silicon Carbide Grain Binder Coating

Figure 6.64 - High Magnification Micrograph Illustrating The Morphology Of The Raised Agglomerates In The Binder Phase That Coats The Silicon Carbide Grains

Figure 6.65 - Micrographs Detailing The Mottled Agglomerate Formations In The Binder Coating And Fractured Binder Interconnect Area

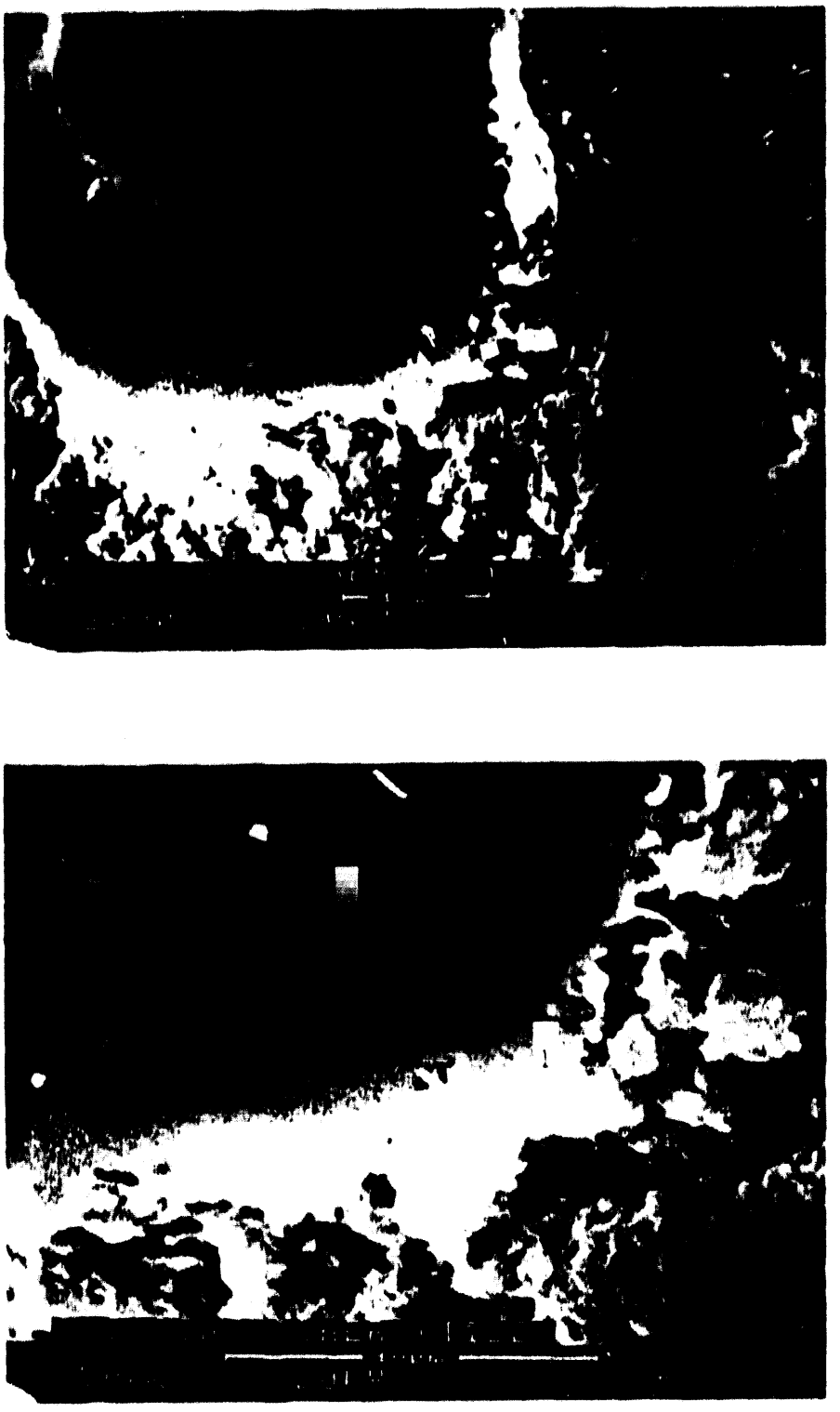

Figure 6.66 - Micrographs Detailing The Morphology Of The Agglomerated Binder Surface Phase Along Both The Grains And Interconnect Channel Areas

as along the surface of the binder interconnect areas. The agglomerates were a surface phenomena which extended to depths of ~5 μm into the binder interconnect areas. Area 1 of Photo 18 in Figure 6.66 consisted of oxygen, silicon, aluminum, sodium, potassium, and sulfur. Alternately Area 2 in Photo 18 of Figure 6.66 consisted of oxygen, silicon, aluminum, sodium, and potassium. Sulfur was absent in the interior of the binder interconnect material. Again note the absence of calcium, and the low sulfur concentration in these areas. Water leaching of the calcium sulfate phase may have resulted during C-ring sample preparation.

6.6 ELEMENTAL MICROPROBE ANALYSIS OF THE 500 HOUR PFBC EXPOSED CLAY BONDED SILICON CARBIDE MATRIX

Elemental microprobe analysis (EMA) was performed along a fractured cross-section of the clay bonded silicon carbide matrix that had been exposed for 500 hours to the PFBC oxidising environment. Figure 6.67 shows the morphology of the mounted, polished, and gold coated cross-section of material that was used in this effort. Note the variation in the thickness of the clay binder phase that coated the silicon carbide grains (i.e., BSE (back-scatter electron) micrograph, silicon-, aluminum-, and oxygen-enriched areas).

We attempted to qualitatively track the presence of silicon, carbon, aluminum, oxygen, and sulfur through a binder interconnect area (i.e., between two adjacent grains) in the PFBC exposed clay bonded silicon carbide matrix. As shown in Figure 6.68, oxygen, aluminum, and silicon were present in the binder interconnect area, while silicon and carbon were present in the adjoining silicon carbide grains. Line traces across the area indicated in the upper right micrograph detail the relative concentration of each element. The concentration of aluminum significantly increased near the mid-section of the binder interconnect phase, and was depleted close to each adjoining silicon carbide grain. At this magnification, the presence of an oxide formation along the silicon carbide grains, at the grain-binder interface was not apparent. Higher resolution micrographs and line traces are needed to resolve this concern.

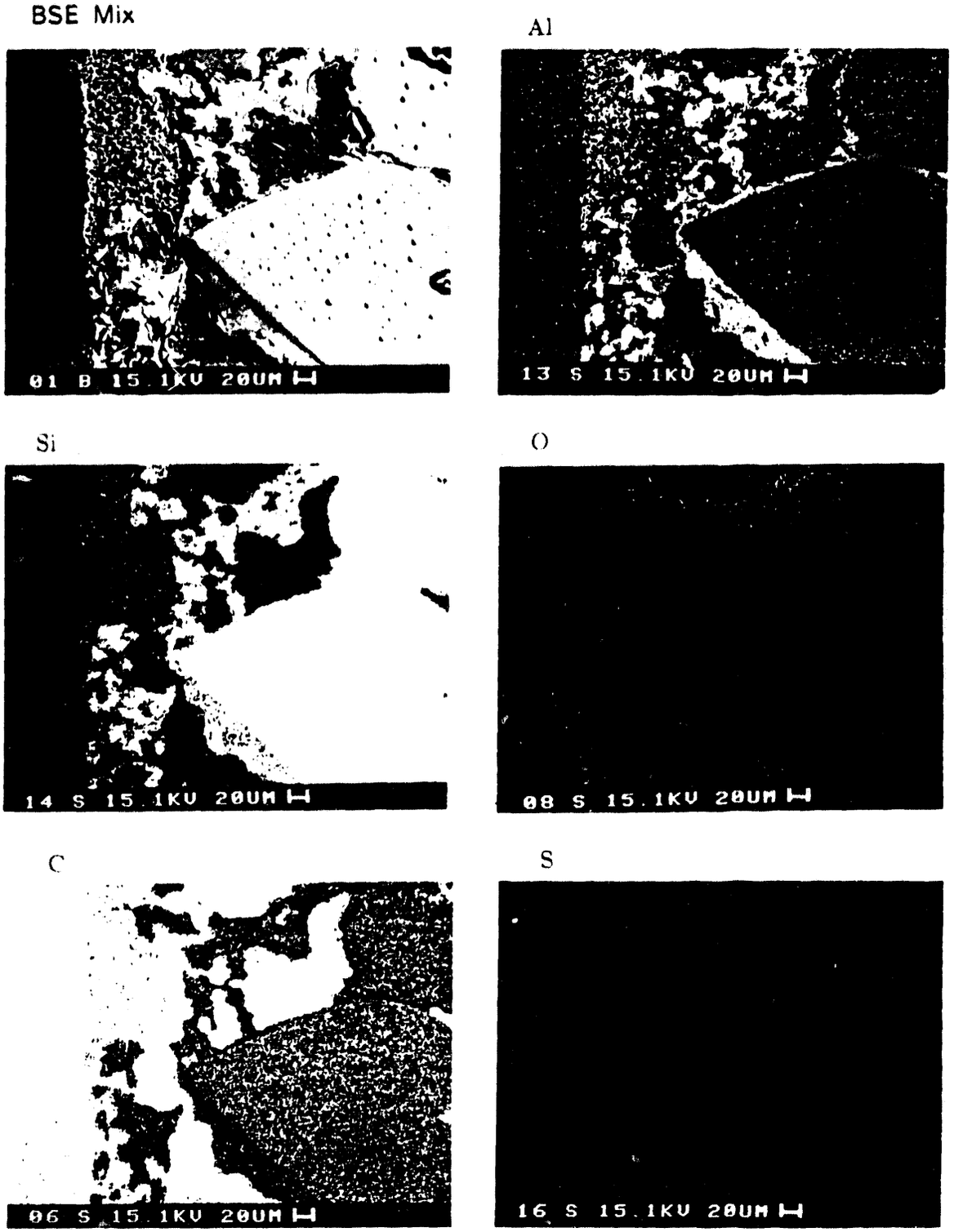

Figure 6.67 - Elemental Microprobe Analysis Across A Polished Section Of The 500 Hour PFBC Exposed Clay Bonded Silicon Carbide Matrix

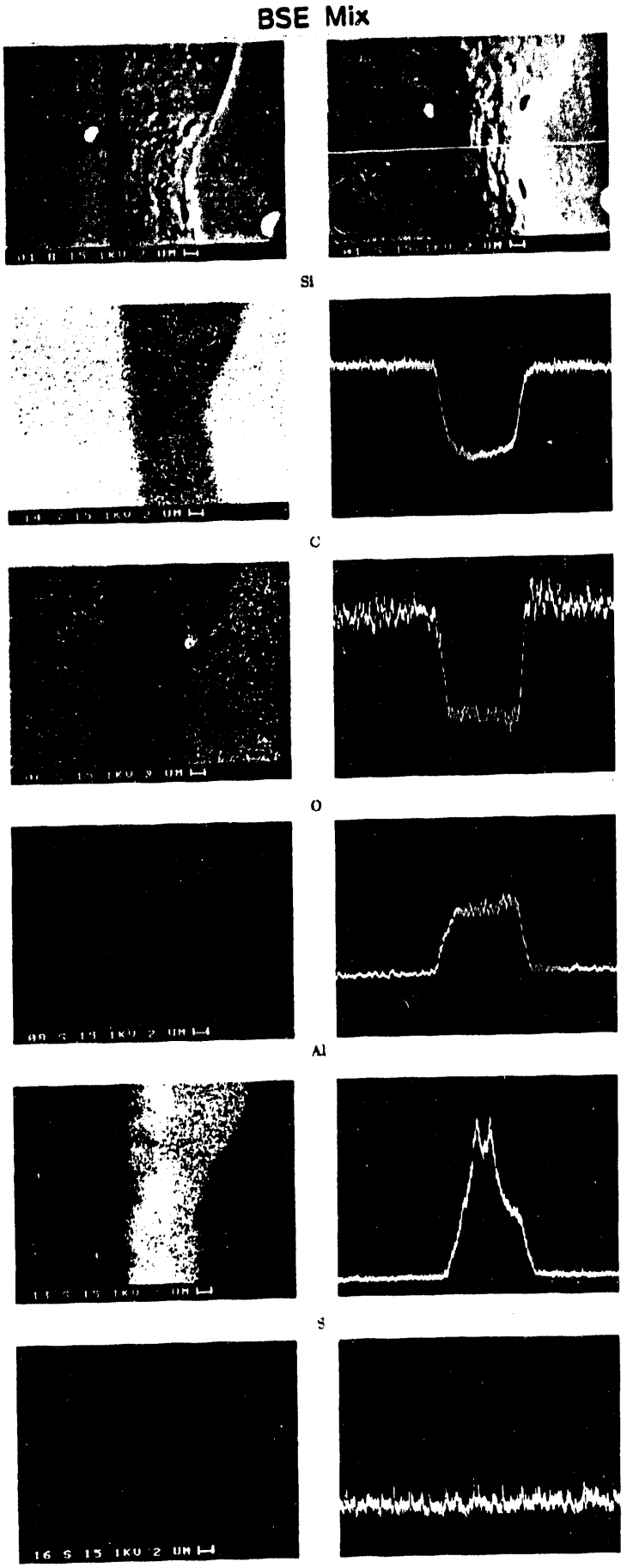

Figure 6.68 - Elemental Microprobe Analysis And Line Traces Across A Polished Section Of The 500 Hour Exposed PFBC Clay Bonded Silicon Carbide Matrix

RM-29897

7. CLAY BONDED SILICON CARBIDE MATERIAL CHARACTERIZATION

In this section we will discuss several aspects of the as-manufactured material properties of the clay bonded silicon carbide filter matrix. We will also identify whether changes in the hot strength of the filter matrix resulted after 500 hours of operation in the high temperature oxidizing environment. Data will be presented which detail the hot strength C-ring compression results for failed candle sections, as well as intact candle filters that survived 500 hours of operation at Tidd. Room temperature burst strength data are also presented for sections of material that were removed from actual intact candle filters.

7.1 AS-MANUFACTURED STRENGTH OF THE CLAY BONDED SILICON CARBIDE MATRIX

A full length candle filter was sectioned for C-ring compression strength analysis. Typically the 9 to 10 mm thick C-ring sections were prepared without chamfering along the edge of the coarse clay bonded silicon carbide structure. Between 5 and 10 C-rings were tested at temperatures ranging between 25 and 1000°C. As shown in Table 7.1 and Figure 7.1, strength appears to increase between room temperature and 400°C (70 and 752°F). Thereafter, the strength of the clay bonded silicon carbide matrix decreases as temperature increases. Note that an ~10% 1σ variation results in the reported strength values.

The operating temperature of the Westinghouse APF system was between 730 and 850°C (1346°F and 1562°F; Table 3.4). Notice that the hot strength of the clay bonded silicon carbide matrix at 800°C (1472°F) is nearly comparable to the as-manufactured room temperature strength of the material. During relatively short operating periods of time when the Westinghouse APF system was operated at higher temperatures, the candles would be expected to be somewhat weaker in their overall

TABLE 7.1

C-RING COMPRESSION STRENGTH OF THE AS-MANUFACTURED FILTER MATRIX AS A FUNCTION OF TEMPERATURE

Temperature, °C (°F)	Strength, psi	
Room Temperature	1285.57 ± 197	(10)*
200 (392)	1287.02 ± 117.58	(5)
400 (752)	1478.75 ± 54.79	(5)
600 (1112)	1443.65 ± 221.25	(5)
700 (1292)	1385.93 ± 139.01	(5)
730 (1346)	1387.09 ± 120.03	(5)
800 (1472)	1246.97 ± 151.34	(5)
850 (1562)	1139.66 ± 105.45	(5)
900 (1652)	1093.84 ± 174.45	(5)
1000 (1832)	517.77 ± 51.73	(5)

* Number In Parentheses Indicate The Number Of C-Rings Tested.

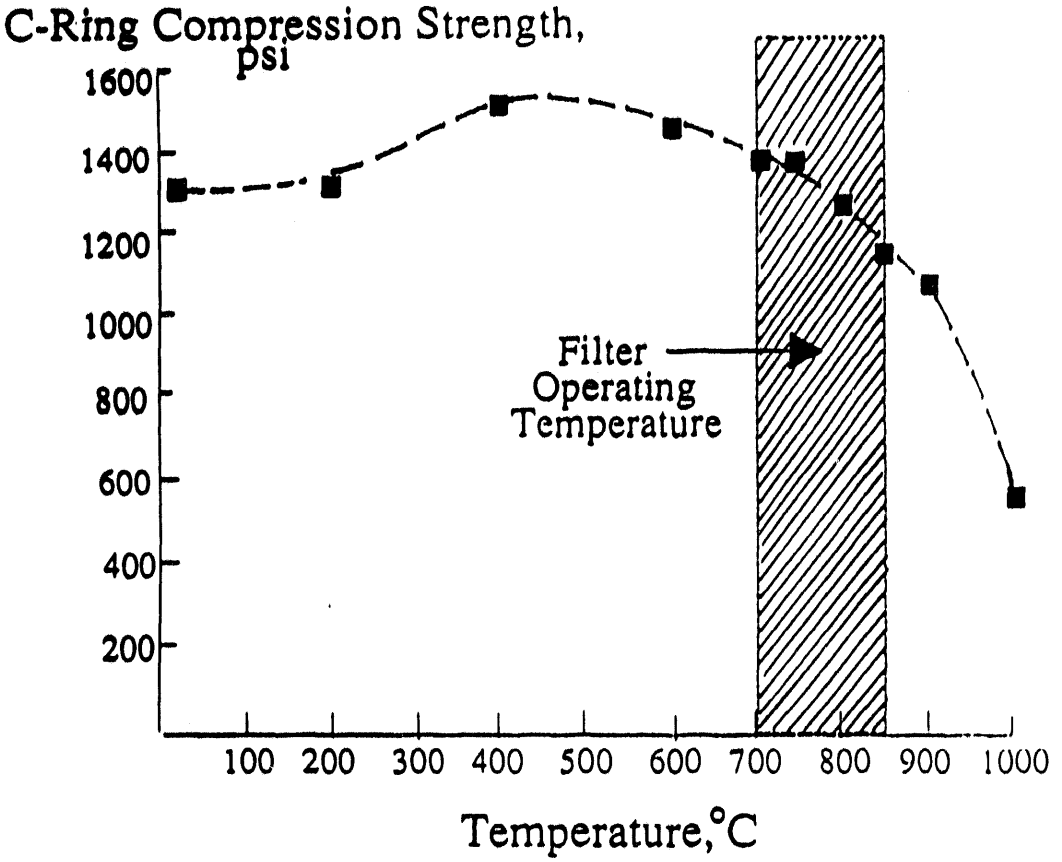

Figure 7.1 - C-Ring Compression Strength Of An As-Manufactured Clay Bonded Silicon Carbide Schumacher Dia Schumalith F40 Candle As A Function Of Temperature

material strength in comparison to their as-manufactured room temperature strength. As shown in Figure 7.2, the brittle characteristics of the clay bonded silicon carbide matrix are retained to temperatures of 900°C. The material exhibits a plastic characteristic at temperatures between 900°C (1652°F) and 1000°C (1652°F and 1832°F).

7.2 STRENGTH OF A FRACTURED CLAY BONDED SILICON CARBIDE FILTER SEGMENT

A section of the clay bonded silicon carbide filter that had been removed from the Westinghouse APF ash hopper was subjected to strength characterization. We are not able to identify the total length of operating time that the ~305 mm (~12 inch) candle filter segment had experienced, prior to the candle breaking. Table 7.2 and Figure 7.3 present the room temperature and hot strength (730°C; 1346°F) data for the as-manufactured matrix, as well as comparable strength data for the fractured candle filter segment. After 500 hours of exposure in the PFBC gas environment, a 25-27% reduction in strength of the candle filter matrix was observed at both room temperature and at process operating temperatures of 730°C (1346°F).

Note in Table 7.2 and Figure 7.3 that the strengths of the as-manufactured and failed candle section at 730°C (1346°F) were somewhat higher than their corresponding room temperature strengths. We suspect that the phase changes and/or crystallization which occurred along the pore cavity wall (Discuss in Section 6) enhanced the hot strength of the PFBC exposed filter material over its room temperature strength. Figure 7.4 provides the load versus deflection curves for the clay bonded silicon carbide matrix after exposure in the PFBC gas environment. Brittle fracture characteristics of the exposed matrix resulted during C-ring compression testing.

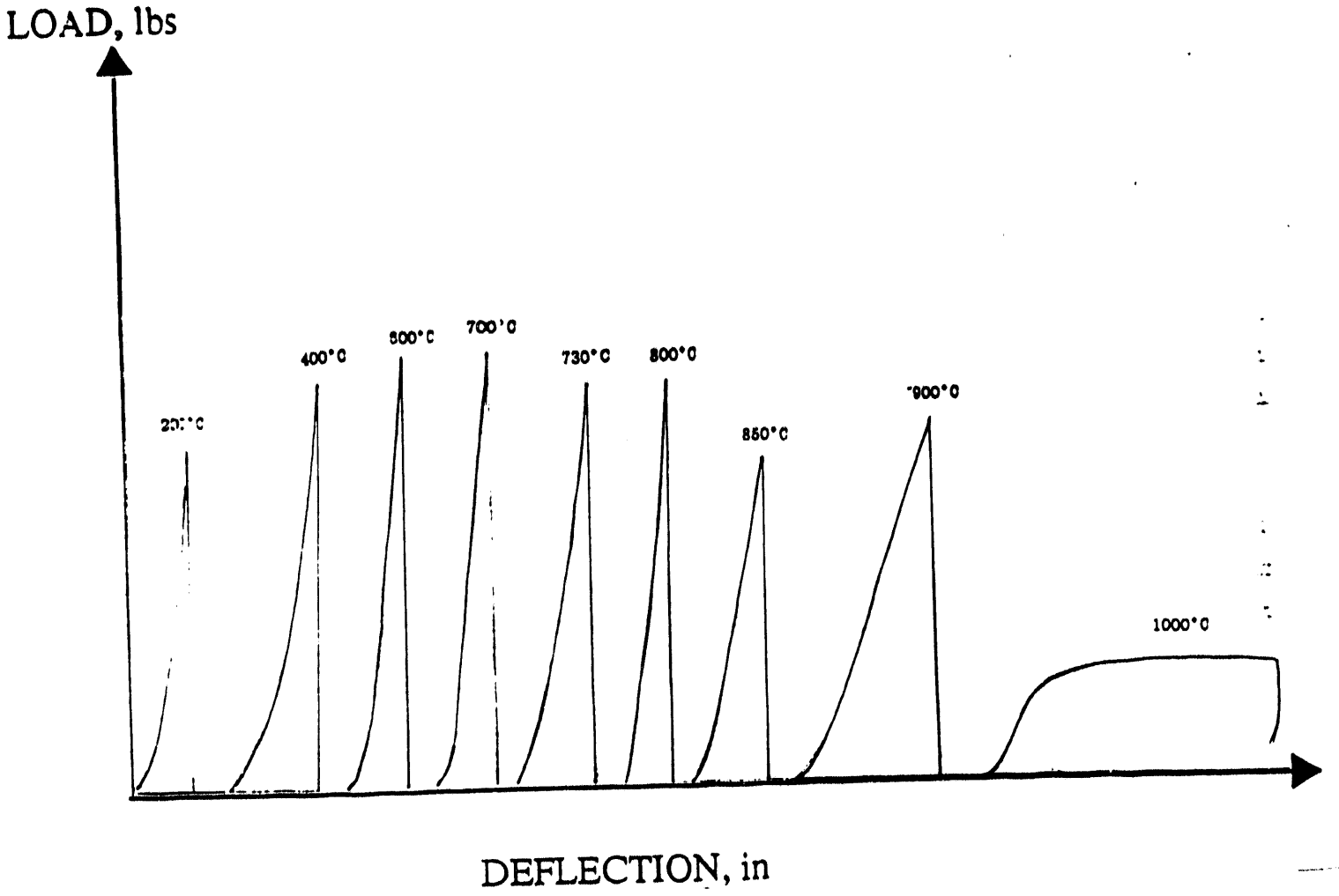

Figure 7.2 - C-Ring Compression Load Versus Deflection Curves For The Schumacher Dia Schumalith As-Manufactured Matrix As A Function Of Temperature

TABLE 7.2

COMPARISON OF AS-MANUFACTURED AND 500 HOUR PFBC EXPOSED CLAY BONDED SILICON CARBIDE MATERIAL STRENGTH

As-Manufactured Clay Bonded Silicon Carbide Matrix

Temperature	Strength, psi	Fracture Characteristics
Room Temperature	1285.57 ± 197.20	Brittle
730°C (1346°F)	1387.09 ± 120.03	Brittle

Fracture Candle Segment Removed From The Ash Hopper

Temperature	Strength, psi	Fracture Characteristics
Room Temperature	965.7 ± 120.0	Brittle
730°C (1346°F)	1018.1 ± 113.7	Brittle

Percent Strength Loss

Room Temperature	25%
730°C (1346°F)	27%

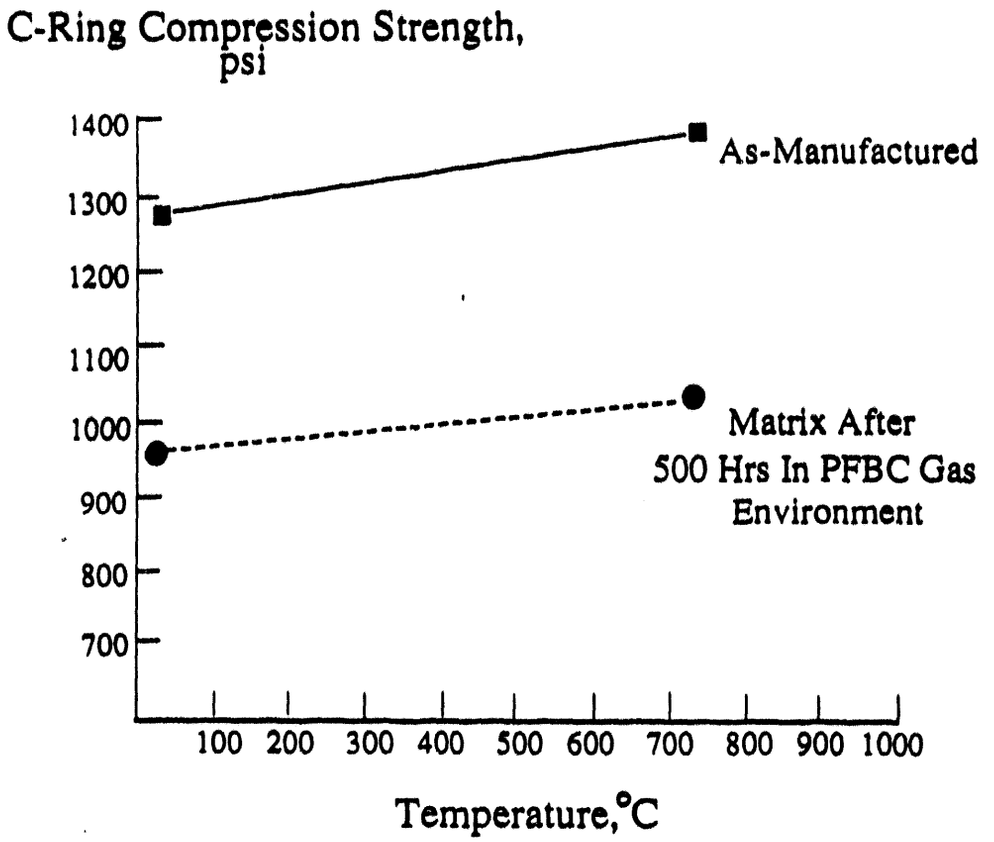

Figure 7.3 - Comparison Of The As-Manufactured And 500 Hour PFBC Gas Exposed Clay Bonded Silicon Carbide Filter Material Strengths

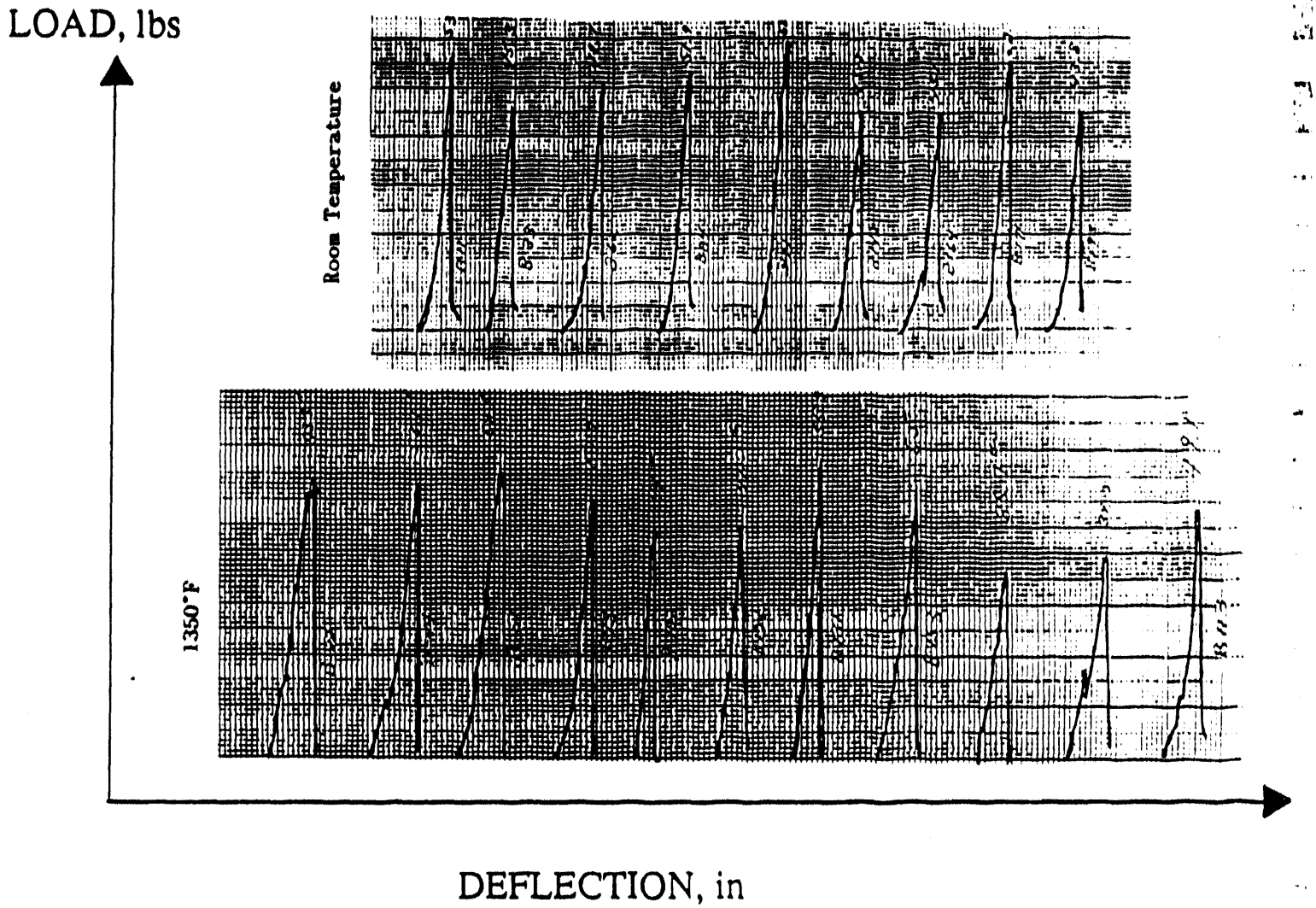

Figure 7.4 - Load Versus Deflection Curves For The Clay Bonded Silicon Carbide Matrix That Was Removed From The Ash Hopper

7.8 STRENGTH OF INTACT CLAY BONDED SILICON CARBIDE CANDLE FILTERS AFTER 500 HOURS OF EXPOSURE IN THE PFBC GAS ENVIRONMENT

Five candles were selected for C-ring compression and burst strength characterization. These included four surveillance candles (B/T-1 #504; B/M-1 #436; B/B-1 #193; and A/B-6 #065), and one additional candle that was visibly bowed (A/B-6 #065; 6.35 mm bow). Table 7.3 summarizes the C-ring compression results for each of these candle filters at room temperature, 732°C (1350°F), and 843°C (1550°F). Between nine and eleven C-rings were tested at each temperature. The 1σ variation of the reported C-ring compression data is ~10%.

Strength data for the intact candle filters are presented in Table 7.3. Note that the strength of the intact candle filters was higher both at room temperature, as well as at 732°C (1350°F) in comparison to candle filter segment that had fallen into the ash hopper. The strength of the candle filters appeared to be uniform throughout the top, middle, and bottom plenums, as shown by the data presented in Table 7.3 for Cluster B. The bottom plenum candle #065 in Cluster A (A/B-6) had a strength comparable to that of the fractured candle filter section that had fallen into the ash hopper. This candle was in close proximity to the section of candles that had fractured during hot gas filtration testing.

What was surprising in the data presented in Table 7.3 was that the room temperature strength of the bowed candle was higher than any other room temperature C-ring compression strength value. The bowed candle also exhibited the smallest increase in strength from room temperature to 732°C (1350°F) in comparison to the "straighter" candle filters. The bowed candle also exhibited a relatively large loss in strength between 732°C (1350°F) and 843°C (1550°F) in comparison to the other candle filters.

TABLE 7.3

C-RING COMPRESSION STRENGTH OF INTACT CANDLE FILTERS, psi

Candle Location	Candle ID	Room Temperature	732°C (1350°F)	843°C (1550°F)
B/T-1	504	1120.23 ± 123.13	1226.11 ± 115.88	1013.49 ± 98.48
B/M-1	436	1096.30 ± 116.17	1172.01 ± 133.87	1041.91 ± 135.17
B/B-1	193	1147.21 ± 111.82	1245.11 ± 107.76	1044.23 ± 106.60
A/B-6	065	940.54 ± 59.46	1056.27 ± 130.82	899.06 ± 98.04
B/B-45 *	106	1180.42 ± 98.04	1229.88 ± 127.05	1075.27 ± 94.13

* Bowed Candle.
RT: 15 Samples; 1350°F: 10-11 Samples; 1550°F: 9-10 Samples.
Note All Brittle Fractures Resulted Under Load.

Burst strength measurements were performed at Schumacher on the 254 mm (12 inch) sections of candle filter that were removed from each of the five intact candles (Table 7.4). Initially testing at Schumacher indicated a burst strength of 1035 ± 63 psi (28 candle filters) for the 450 clay bonded silicon carbide candle filter production lot. The burst strength for the clay bonded silicon carbide production lot exceeded the original manufacturing specification of >870 psi (>60 bar) for the individual candle filter elements. The reported burst strength for the five candles that were exposed to the PFBC gas environment ranged between 986 and 1261 psi (1128.1 ± 115.7 psi) which is clearly greater than the original burst strength specification, and generally comparable to the initial burst strength of the as-manufactured candle filters.

A direct correlation between room temperature C-ring compression and burst strength of the 500 hours PFBC exposed clay bonded silicon carbide matrix was indicated for candles that were located in a common cluster or location within the Westinghouse APF vessel (Figure 7.5). What was also interesting to note was that as the candle TOF value increased, the room temperature C-ring compression strength of the clay bonded silicon carbide matrix decreased, again for candle filters that were located within a common cluster or location within the Westinghouse APF vessel. Cluster A candles and the bowed Cluster B candle tended to deviate from the TOF/C-ring compression and burst strength/C-ring compression relationship.

Note that the C-ring compression strength tests detail any changes or flaws that have been introduced along the candle OD surface during process operation. In contrast the burst strength data provide information with regard to more typically macroscopic changes that have occurred along the candle ID surface. Based on the limited strength data that have been generated to date, as well as the physical characteristics of the primary fracture along each failed candle filter element, thermal fatigue due to pulse cycling does not appear to significantly contributed to changes within the clay bonded silicon carbide candle filter matrix. C-ring

TABLE 7.4

500 HOURS PFBC EXPOSED MATERIAL PROPERTIES FOR THE CLAY BONDED SILICON CARBIDE CANDLE FILTERS

Candle Location	Candle ID	TOF, μsec Initial	TOF, μsec Final	Room Temperature C-Ring Compression Strength, psi	Burst Strength, psi *
B/T-1	504	332	339	1120.23 ± 123.13	1087.5
B/M-1	436	336	343	1096.30 ± 116.17	1073.0
B/B-1	193	323	335	1147.21 ± 111.82	1261.5
A/B-6	065	348	362	940.54 ± 59.46	986.0
B/B-45	106	331**	348	1180.41 ± 98.04	1232.5

* Schumacher Burst Strength Data; Average Burst Strength Of 1035 ± 63 psi Determined For 28 Candle Filters.

** Schumacher TOF Data.

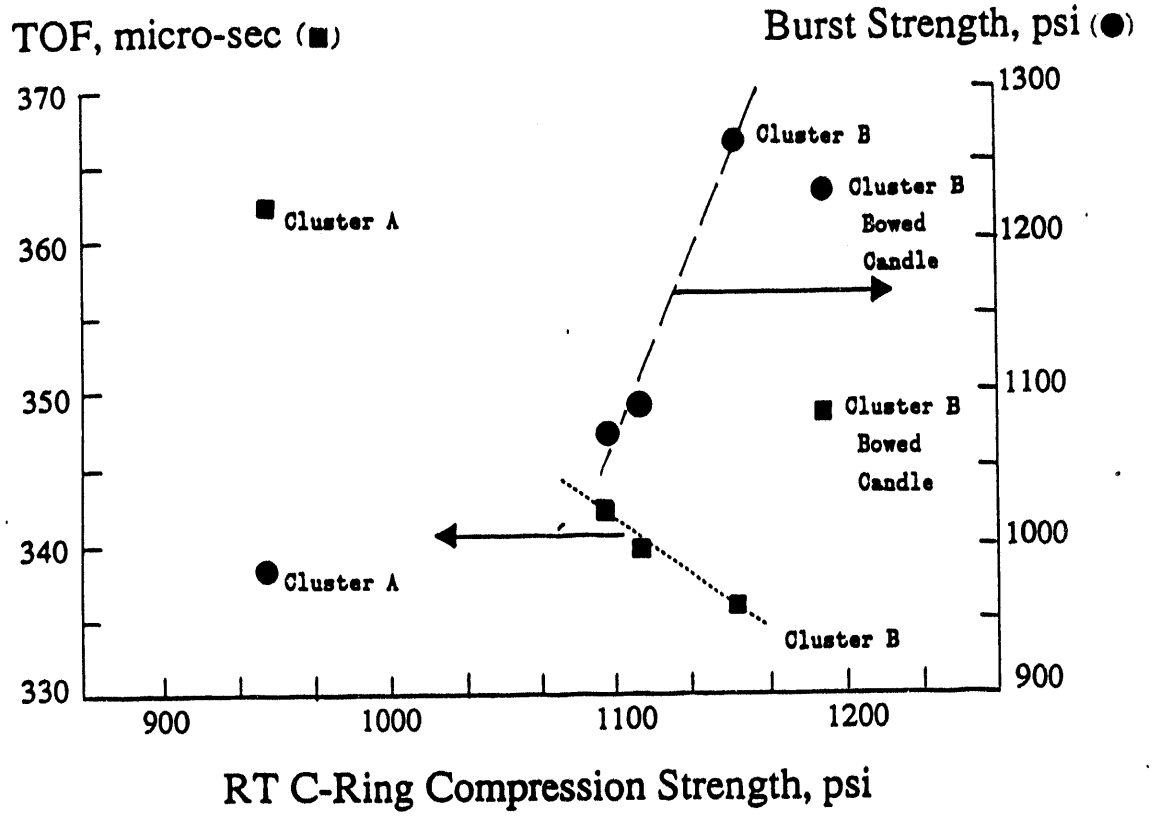

Figure 7.5 - Correlation Of TOF And Burst Strength Data With Room Temperature C-Ring Compression Strength Data For Candle Filters That Have Been Exposed To 500 Hours Of PFBC Gas Environment

tension strength testing will be performed to identify whether change has occurred within the matrix along the candle ID, which may be indicative of thermal fatigue.

7.4 HF DISSOLUTION OF THE CLAY BONDED SILICON CARBIDE MATRIX

An attempt was made to acid leach a section of the as-manufactured clay bonded silicon carbide candle filter material, as well as a section from a candle that experienced 500 hours of operation in the PFBC gas environment. This approach was expected to provide insight into the possible oxidation that may have resulted along the silicon carbide grains after long-term exposure in the oxidizing flue gas slipstream. Initially each sample was crushed and weighed in a platinum crucible. A dilute HF solution was added to both samples. Each were then heated on a hot plate for three days until they were completely dry. As a result of this procedure, all SiO_2 that is present in the matrix is expected to react with HF and form volatile SiF_4, leaving the residual silicon carbide grain intact. After HF dissolution and drying, each sample was reweighed, washed to remove any residual soluble fluoride compounds, and then once again reweighed. The total silicate content was based on the change in material weight that resulted from this procedure.

Note that the filter membrane had not been removed from either the as-manufactured or from the 500 hour PFBC exposed candle matrix. The filter membrane consists predominantly of an aluminosilicate fibrous layer and the silicon-rich binder phase which is typically used throughout the coarse grain structure. The total silicate content in the as-manufacture candle filter matrix was determined to be 13.07%, while the 500 hour PFBC sample contained a total silicate content of 13.25%. Based on these data, negligible oxidation was expected to have resulted along the silicon carbide grains in the Schumacher Dia Schumalith F40 matrix after 500 hours of exposure in the PFBC gas environment.

7.5 AUGER ANALYSIS OF THE CLAY BONDED SILICON CARBIDE MATRIX

Auger analysis was performed along the section of the candle filter matrix that had fallen into the ash hopper. Table 7.5 and Figure 7.6 detail the results of the Auger analysis along the binder coated silicon carbide grains that experienced PFBC gas conditions. Through a depth of ~4000A (~4 μm) we noted that considerable change had occurred within the binder phase. Along the external binder surface (i.e., pore cavity wall), oxygen (O), silicon (Si), and aluminum (Al) were detected. Along this area sulfur (S) was not detected until 860A (0.860 μm) had been sputtered away. Carbon (C) was also detected in this layer, while the concentration of silicon and oxygen decreased, and aluminum became virtually absent in the binder matrix. The carbon and sulfur content continued to increase as the sputtering depth increased, while the oxygen and silicon concentration continued to decrease. Deeper into the binder coated grains, the concentration of carbon increased in parallel with silicon, implying that the silicon carbide grain had been located. Note the low concentration of oxygen which also existed in this area (2060A or 2 μm). Further sputtering slightly enhanced the carbon and silicon atomic concentration, while oxygen was present at ~6 atomic percent. The low concentration of oxygen in the silicon- and carbon-enriched matrix implied that a very thin oxide coating existed between the binder and the silicon carbide grain. Additional analyses are needed to further substantiate these results.

TABLE 7.5

ELEMENT CONCENTRATION THROUGH THE BINDER PHASE OF THE
PFBC GAS EXPOSED CLAY BONDED SILICON CARBIDE CANDLE FILTER
AS DETERMINED BY AUGER ANALYSES

Auger Depth Profile
Tidd Candle 1/8" from OD PCE 1
Atomic %

Depth (Angstroms)	Oxygen	Sulfur	Carbon	Calcium	Silicon	Aluminum	Magnesium
0	62.28	0.00	0.00	0.00	24.05	13.67	0.00
180	64.29	0.00	0.00	0.00	19.67	16.05	0.00
860	16.76	31.88	31.70	0.00	19.67	0.00	0.00
1060	7.77	39.13	35.25	0.00	17.85	0.00	0.00
1260	6.67	41.23	35.69	0.00	16.41	0.00	0.00
2060	4.80	0.00	63.41	0.00	31.79	0.00	0.00
3060	6.01	0.00	58.87	0.00	35.11	0.00	0.00
4060	6.11	0.00	59.29	0.00	34.60	0.00	0.00

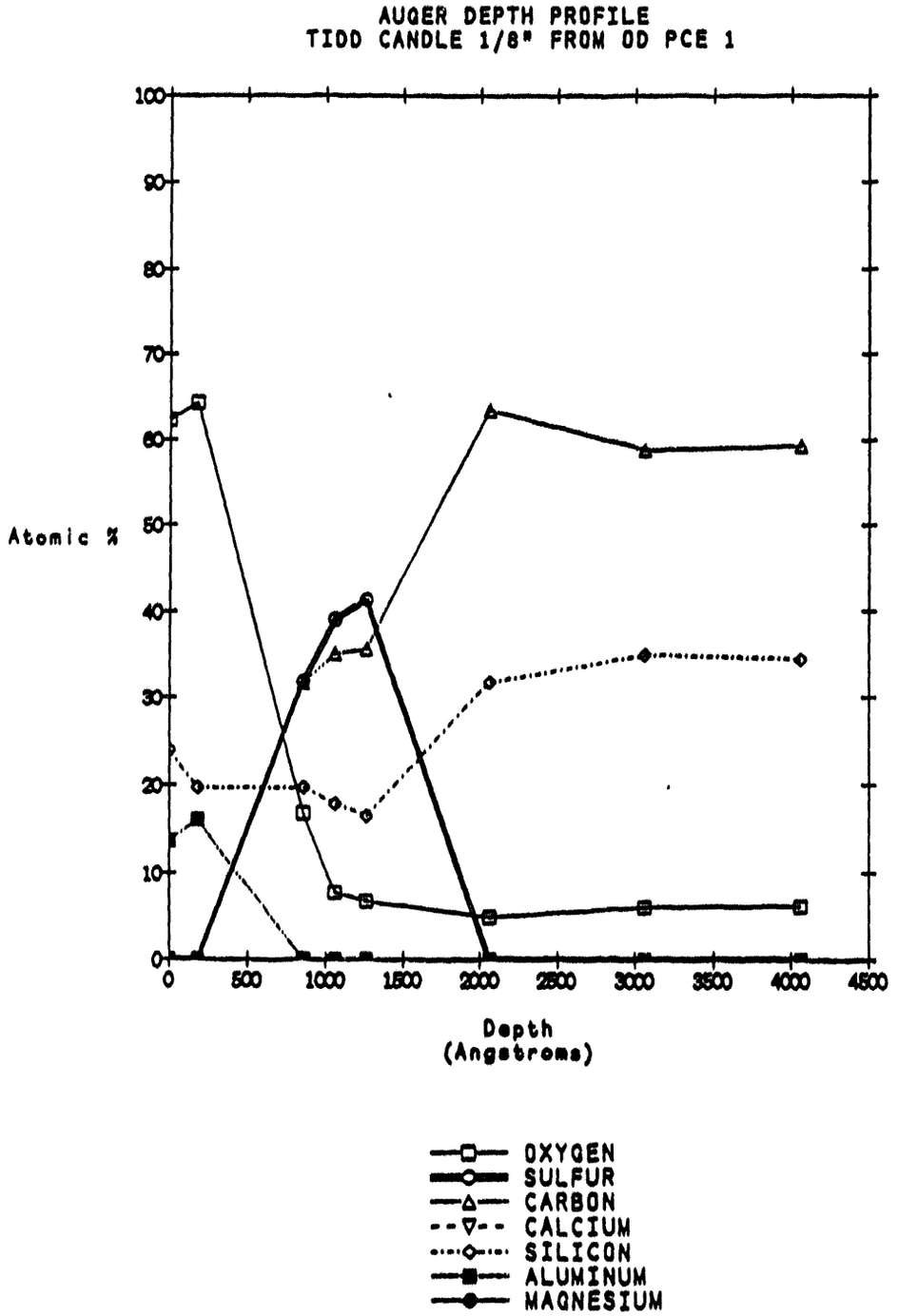

Figure 7.6 - Auger Depth Of Profile Through The Binder Phase Of The Clay Bonded Silicon Carbide Candle Filter After Exposure To The PFBC Gas Environment

8. CONCLUSIONS

- In the initial surveillance effort, general agreement resulted between the Westinghouse and Schumacher time-of-flight (TOF) data for the as-manufactured candle filters. Westinghouse continuously recalibrated the Ultran equipment during conduct of the TOF measurements, while Schumacher calibrated their Pundit TOF equipment on a daily basis. Any discrepancy between the Westinghouse and Schumacher data is considered to result primarily from equipment recalibration frequency.

- The majority of the failed candles were fractured near or below the fine-to-coarse transition section in the clay bonded silicon carbide candle filter elements. Each primary fracture contained a shear lip, typical of a beam breaking in a bending mode. There was no evidence of longitudinal cracks in the clay bonded silicon carbide matrix. Secondary fractures consisted of virtually all transverse breaks.

- Bowing was evident along the remaining intact bottom plenum candles, as well as along candle filters that were reconstructed from sections that had fallen into the ash hopper. Bowing was generally in the appropriate direction relative to the shear lip. This supported the conjecture that a sustained load was applied to the bottom of the candle(s) causing it to bend under load at temperature, and finally to fracture below or near the fine-to-coarse grain transition section.

- Post-test measurements of the candle filter indicated that within experimental tolerances (±1 mm) all candles retained their initial length after 500 hours of operation in the PFBC gas environment. Within the bottom plenums, a 1.3 to 25-fold increase in bow resulted

over the initial candle bow. Out of the original 27 surveillance candles that were located in the bottom plenums, 18 were out-of-bow tolerance (>3 mm) after exposure to the PFBC environment. Post-test characterization of the remaining bottom plenum candles indicated that a maximum bow of 23.8 mm was detected along an inner ring candle filter (B/B-28). The influence of ash bridging at temperature produced significant load on the candles to deform the clay bonded silicon carbide filter elements.

- A negligible increase in bow was detected along the candle filters located in the top plenum arrays. A slight increase in bow was observed along the candles in the middle plenum arrays, while the largest increase in bow was observed for candles located in the bottom plenum arrays. The greatest extent of bowing resulted in the bottom arrays which had significant ash bridges formed between adjacent candle filters.

- The adherence or inclusion of fines along the clay bonded silicon carbide candle filters did not influence the time-of-flight measurements. In other words, the strength of the candles can be measured directly in the as-received candle state, with or without dust cake removal, provided adequate contact is available for both TOF transducers.

- Post-test TOF characterization of the surveillance filters indicated that the candles lost strength after 500 hours of exposure in the PFBC gas environment in comparison to their as-manufactured state.

- The as-manufactured clay bonded silicon carbide Schumacher Dia Schumalith F40 matrix retain its initial strength up to temperatures of ~750-800°C. Thereafter a reduction in the as-fabricated strength of the matrix resulted. A brittle fracture characteristic of the

matrix results during C-ring compression strength testing up to temperatures of 900°C. Between 900 and 1000°C, the matrix undergoes plastic deformation.

- C-ring strength analysis of the candle filter segments removed from the ash hopper indicated that the matrix retained 75% of its as-fabricated strength at room temperature test conditions. At process temperatures of 730°C, the failed filter segments retained 73% of their as-fabricated hot strength. A 10% 1σ value was typical for all room temperature and hot strength C-ring compression strength measurements performed to date.

- After 500 hours of exposure in the PFBC gas environment, the intact candle filters had a somewhat higher room temperature and hot strength in comparison to filter segments that were removed from the ash hopper (retention of ~85-90% versus ~75% of the original as-manufactured strength, respectively).

- Uniform strength of the filter elements was identified throughout a common cluster of three candle arrays in the Westinghouse APF vessel after 500 hours of hot gas filtration.

- The minor variations in the TOF data directly corresponded to the C-ring compression strength for candles within a common cluster. Burst strength data similarly correlated with C-ring compression strength for these filters.

- Characterization of the candles removed for post-test analysis indicated that the pressure drop in the candles increased from the top to the bottom clusters, particularly along Cluster A. Bottom plenum Cluster A candles had the highest pressure drop of all candles. This plenum also had the greatest number of broken candles after 500 hours of hot gas filtration.

- After 500 hours of operation in the PFBC gas environment, the OD membrane of the Schumacher Dia Schumalith candle remained intact. The OD membrane did not permit penetration of fines into the filter wall.

- Examination of the clay bonded silicon carbide microstructure indicated that sulfur and calcium-enriched micron and submicron aerosol droplets/particles were evident along the binder phase of the grains that were directly below the OD fibrous membrane. Phase changes (i.e., mullitization) in the binder coating along the grains beneath the silicon-, sulfur- and calcium-enriched aerosol droplets/particles were evident.

- Sulfur appeared to be sorbed into the binder matrix of the 500 hour PFBC exposed clay bonded silicon carbide candle filter. The resulting sulfur-enriched phase appeared to be limited to a depth of 5 μm along the binder surface. Minimal influence through the binder interconnecting channels resulted after 500 hours of hot gas filtration.

- In the absence of calcium, a sulfur gradient was established along the cross-sectioned candle filter wall. The highest concentration of sulfur appeared along the silicon carbide binder phase near the candle ID surface. Complete pore plugging was evident along the ID wall of the clay bonded silicon carbide matrix, as a result of fines penetration during pulse cleaning after an initial candle failure.

- Auger analysis has the capabilities to determine the location of the binder and subsurface silicon carbide grain. The outer surface of the Schumacher Dia Schumalith clay bonded binder phase consisted of oxygen (O), silicon (Si), and aluminum (Al). Beneath the binder surface phase, an oxygen, sulfur (S), carbon (C), and silicon layer formed. As oxygen was depleted at the binder/grain interface, the

atomic percent of sulfur and carbon increased. Silicon and carbon were not in a 1:1 atomic percent ratio which indicated that a layer formed above the silicon carbide grain. Sublayers contained low concentrations of oxygen along the silicon carbide grain.

- Negligible oxidation of the silicon carbide matrix was detected over background in an acid leach of the 500 hour PFBC exposed filter matrix. Although extensive changes in the matrix were not evident via this test, Auger analysis indicated that subtle oxidative changes may have actually occurred.

- Post-test examination of the candle segments which were removed from the ash hopper indicated that a white layer of sulfated dolomite coated the candle OD surface, below the ash cake layer. To date we have not been able to confirm whether a thin ash/dust cake layer was initially deposited uniformly below the sulfated sorbent layer (i.e., conditioned layer).

- Thick ash-sorbent dumpling-like deposits, as well as an ash-scale layer remained along the 500 hour PFBC exposed intact candle filters. The dumpling-like deposits extended between 5 and 15 mm above the candle OD surface, while the scale-like deposits were <5 mm thick. Both dumplings and scale were easily removed, and virtually retained the contour of the candle wall. Both materials consisted of PFBC ash and sulfated dolomitic fines. The dumplings and scale-like deposits were relatively porous. Sulfated dolomitic fines were somewhat smaller in comparison to the particle size of the ash fines.

- Fractured candle filter segments typically contained a layer of sulfated dolomitic sorbent material along their ID surface. This implied that at test termination, sorbent from the primary cyclone was carried through the Westinghouse APF system.

- A very hard, white cement-like ash was removed from the bottom of the ash hopper, as well as from the ID of the candles that were found in this area. The cement-like deposit was extremely dense (i.e., negligible porosity), and consisted of either isolated islands of magnesium sulfate hydrate (kiersite), or was a combination of kiersite and anhydrite (calcium sulfate). Alternately the pinkish-orange dense areas of ash included both of these constituents, as well as hematite (iron oxide). The white areas were identified by EDAX analysis to be enriched with magnesium.

- At least three candle failure events transpired during the 500 hours of hot gas filtration in the Westinghouse APF system. These included:

  - An initial candle(s) failure which released dust into the various plenums. Dust was then redistributed along the ID surface of intact candles during pulse cleaning.

  - Sections from the intact candles then fell into the dust hopper at various times. The location in the hopper and contents in their ID may track the coarse of failure during hot gas filtration. For example, early on, candle sections may have fallen into the bottom of the hopper which ultimately contained the cement-like sorbent/ash deposit. Alternately, candle sections may have fallen into the ash hopper but had not dropped to the depth of the resulting cement-like sorbent/ash deposit. One fractured surface of the candle segment would have been heavily coated with ash which accumulated on this surface while the candle section remained rigidly supported in the filter holder. Ash then packed along the second fractured surface of these candle segments during continued ash accumulation in the filter vessel. Additional failure continued as candles continued to sever and

drop into the hopper ash. In this case a caked fractured end and a somewhat fresh fractured surface would have resulted either above or slightly below the ash hopper level (i.e., near test termination).

- Failure of candles at test termination causing a fresh fracture along the candle cross-sectioned wall that was virtually free of dust.

- Failure of the candles during removal of the cluster arrays from the Westinghouse APF vessel and transport to its structural holder. These fractures may have already occurred, but due to ash bridging, the fractures were tightly held in position. Vibration, etc., during the lift and transport of the array may have ultimately caused separation of the fractured sections. Similarly contact of the bottom plenum candles (i.e., outer ring candles) with the filter vessel may be responsible for the two fresh fractured, long candles that remained in the filter holders at test termination.

9. RECOMMENDATIONS

- In the event of candle failure(s) within the hot gas filtration system, incorporation of a membrane along the ID wall of the coarse grained candle filters would prevent penetration of fines into the ceramic matrix during pulse gas cleaning.

- Development of an initially higher strength clay bonded silicon carbide matrix is recommended in order to mitigate candle failure under sustained load in the event that ash bridging or cascading results.

- Development of a more stable, chemically inert binder phase would mitigate loss of material strength in the matrix during long-term exposure to PFBC gas conditions. Alternately process modifications during filter production may also minimise the typical initial loss of material strength which resulted within the first several hundred hours of exposure to advanced coal fired process environments.

- Identify the role of sulfur and various trace contaminant phases in the actual PFBC gas environment that are in contact with the clay binder and ceramic filter matrix. Assess actual concentrations of these species within the gas phase, and the resulting phases in the ceramic filter matrix after long-term exposure.

- Replace and/or omit full length candles in position that are closest to the vessel wall. This would prevent bowing and/or fracturing of these candles in the event that ash accumulates at these locations during filter operation.

10. ACKNOWLEDGMENTS

We wish to acknowledge the efforts of Mr. Thomas Mullen and Mr. Robert Palmquist for performing the scanning electron microscopy/energy dispersive x-ray analyses (SEM/EDAX) and elemental microprobe analyses (EMA) on the ceramic filter and ash materials. The results of their effort identified significant phase changes that occurred along the surface of the binder phase after exposure of the clay bonded silicon carbide matrix to 800 hours of pressurized fluidized-bed combustion gas conditions. Similarly SEM/EDAX analyses were used to define the morphology and compositional changes in the ash materials that were formed throughout the Westinghouse APP system.

The efforts of Dr. Richard Tressler at Penn State are acknowledged for conducting the fracture analyses on the failed candle filters, as well as overseeing the preliminary acid leach oxidative testing of the ceramic matrix in an attempt to define the stability of the silicon carbide grains under pressurized fluidized-bed combustion conditions.

Dr. Arthur Byers and Mr. David Dotar are acknowledged for performing the Auger analyses which provided a unique insight into the composition of possible binder-grain interface phases. Both Dr. Byers and Mr. Dotar are also acknowledged for their effort in performing the x-ray diffraction (XRD) analyses which identified the composition of the isolated sorbent/ash cement-like phase that formed in the bottom of the ash hopper.

Mr. Mostan Attaar, Mr. Fran Gradich, and Mr. Ben Sauka are acknowledged for their efforts in conducting the initial and post-test nondestructive time-of-flight (TOF) measurements. The results of these analyses complement the data that were initially generated at Schumacher on the original candle filters, as well as support the strength data generated by destructive analyses. A special thanks is extended to Mr. James Prohaska, Mr. Samuel Withrow, and Mr. Edward Dias for the expediency of obtaining the C-ring compression strength information. Mrs. Astrid Wagner is acknowledged for providing the burst strength information at Schumacher for select candle filter sections.

Mr. Frank Cassic and Mr. Eugene Smeltzer are acknowledged for their efforts in performing the candle permeability testing, and similarly Mr. Richard Runkle and Mr. John Meyer are acknowledged for determining the extent of bowing of the full length candle filters after exposure in the pressurized fluidized bed combustion gas environment.

Expressed thanks are also extended to Mr. Forest Walker at the Geochemical Testing Laboratories for performing the ash fusion, and proximate and ultimate analyses, and to Mr. Arthur Wolfe and Mr. Richard Runkle for their on-going efforts in detailing the elemental compositions of the ash materials.

Mr. William Dilmore is acknowledged for providing the detailed filter location drawings which are beneficial in continuously tracking the location of each filter element in the Westinghouse APP vessel, as well as tabulating the specific material characterization results that were generated for each filter element.

In addition, the efforts of Mr. William Marks, Mr. Stephen Jaraffa, and Mrs. Rose Rouse are acknowledged for their assistance in the final production of this report.

END DATE

10-26-93